Faculty of Aerospace Engineering

Helicopter Nonlinear Flight Control

An Acceleration Measurements-based Approach using Incremental Nonlinear Dynamic Inversion

Pedro V. M. Simplício

August 23, 2011

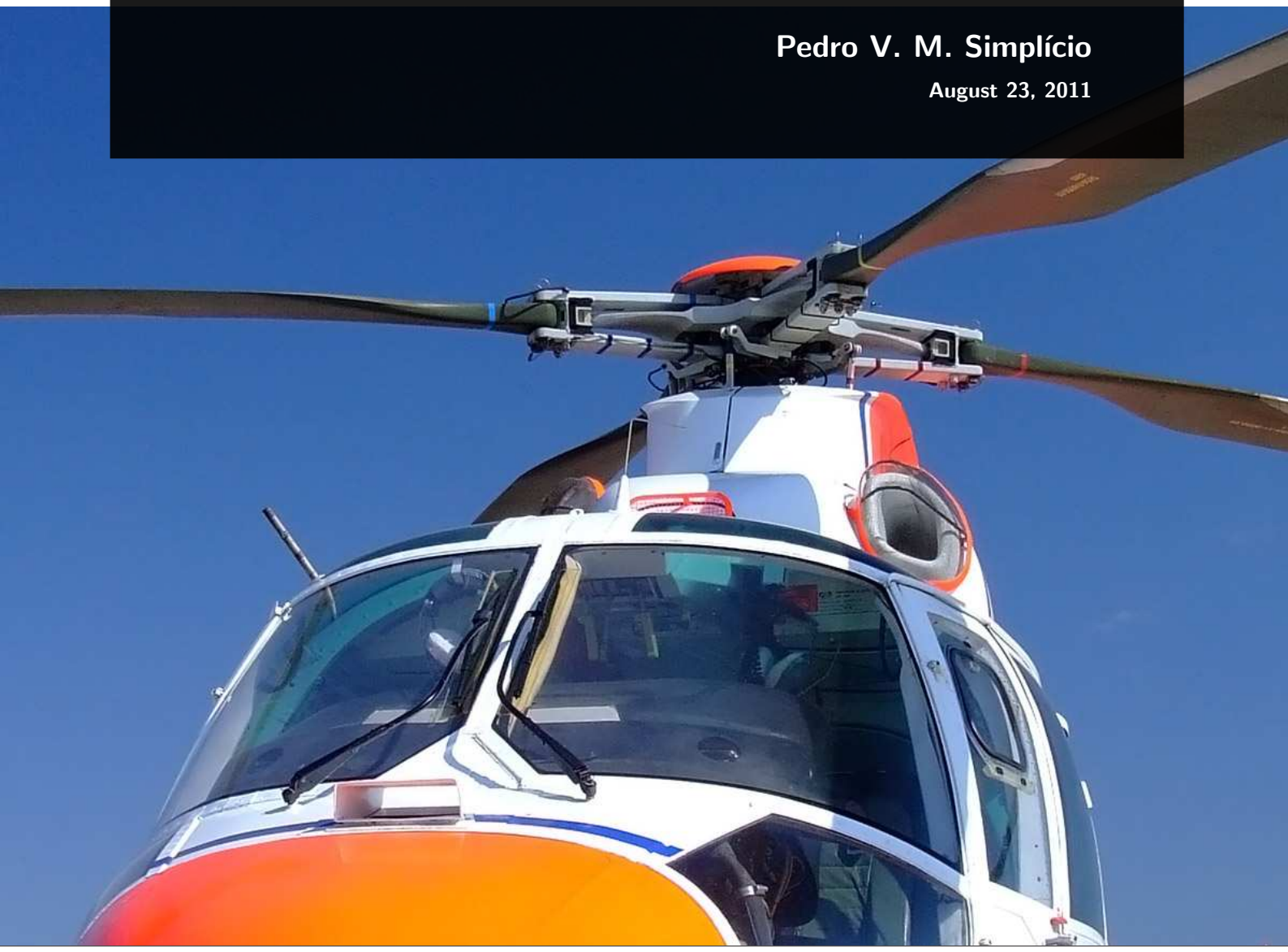

TU Delft Delft University of Technology

Challenge the future

Helicopter Nonlinear Flight Control

An Acceleration Measurements-based Approach using Incremental Nonlinear Dynamic Inversion

Master of Science Thesis

For obtaining the degree of Master of Science in Aerospace Engineering
at Delft University of Technology

Pedro V. M. Simplício

August 23, 2011

Faculty of Aerospace Engineering · Delft University of Technology

Delft University of Technology

Delft University Of Technology
Department Of
Control and Simulation

The undersigned hereby certify that they have read and recommend to the Faculty of Aerospace Engineering for acceptance a thesis entitled **"Helicopter Nonlinear Flight Control"** by **Pedro V. M. Simplício** in partial fulfillment of the requirements for the degree of **Master of Science**.

Dated: August 23, 2011

Readers:

prof. dr. ir. J.A. Mulder

dr. Q.P. Chu

dr. M.D. Pavel

dr. ir. E. van Kampen

Abstract

Accurate helicopter flight control is always a challenging problem due to the inherent instabilities and nonlinearities of rotorcraft dynamics, its changing properties with flight condition and the engineering difficulties to predict the aerodynamics of the rotors with high levels of fidelity. These characteristics justify the need for a control system that is able to efficiently cope with the nonlinearities and cross-couplings of the helicopter model, assuring simultaneously robustness in the presence of model inaccuracies and changes in configuration.

When compared to fixed-wing aircraft, helicopters present a distinct advantage in terms of maneuverability, conferring to this type of vehicle the capability to perform a wide range of tasks that are not possible with other aircraft. The achievement of enhanced performances during rotorcraft operation clearly motivates the development of improved flight control laws. The research performed in this area for the past few years normally concerns a controller architecture based on an approximate model inversion, together with a robust control synthesis or adaptive elements to compensate for the inversion error. Robust control results sometimes in too conservative control laws. On the other hand, adaptive strategies are not only associated with complex control structures, they are also particularly problematic in terms of flight certification.

In this master thesis, a novel approach for nonlinear flight control using an incremental model inversion is adopted to stabilize and control a single main and tail rotor helicopter, with the main objective of being insensitive to most of the uncertainties often found in helicopters. This technique is generally known as Incremental Nonlinear Dynamic Inversion (INDI). Its main advantage is that it employs the feedback of acceleration measurements to extract the information relative to any aerodynamic change in the aircraft. As a consequence, the control system does not need any model data that depends exclusively on the states of the system, enhancing significatively the robustness of the control law to model uncertainties or disturbances. Moreover, the fact that the INDI-based control loops require less information about the model also contributes to a considerable simplification of the control laws, which is very useful when the mathematical model of the system is rather complex, as in the case of a helicopter.

This research can be seen as a feasibility study of the practical applicability of the control laws derived to advanced helicopter flight control systems for a project between Delft University of Technology and the Boeing Company. It starts with one chapter fully dedicated to nonlinear rotorcraft modelling. After implementing the developed model, a three-loop architecture

that relies on the existence of a time scale separation between loops is designed to provide navigational control of the vehicle. The three referred loops are able to assure tracking of commanded signals in terms of angular rate, attitude of the aircraft and ground velocities. Furthermore, a technique known as Pseudo-Control Hedging (PCH) is also introduced in order to alleviate the requirements associated with the multiple time scale separations and to cope with saturation effects due to the dynamics of the actuators.

The overall flight control system is tested by performing several maneuvers with distinct agility levels commonly used for rotorcraft flying qualities analysis: a bob-up and bob-down, a slalom maneuver, a transient turn and also a pirouette. In addition, several simulations are carried out in order to investigate the influence of certain non-idealities in the tracking performance and control demands of the system. The factors analyzed are the existence of rotor aerodynamic uncertainties, changes in the inertia of the vehicle, a malfunction of the tail rotor, sensor dynamics, actuator delays, wind effect and different controller sampling frequencies.

The results obtained show that the suggested control strategy is able to decouple the responses associated with the different control channels and to directly enforce the desired handling qualities in the evolution of the control variables. It allows then to achieve an efficient tracking of the commanded ground velocities and heading angle of the helicopter with the overall control system. Furthermore, it is verified that the controller is perfectly robust to model uncertainties within the range of inaccuracies expected to find in reality and that, despite being slightly noticeable, the effects of sensor dynamics and actuator delays are still admissible for a potential practical implementation. In conclusion, due to the robustness properties of this flight control system, only a simplified model of the helicopter as the one presented in this thesis may be enough to assure an effective control of the vehicle.

Acknowledgements

First of all, I would like to express my thanks to my supervisors, Dr. Ping Chu and Dr. Marilena Pavel, from Delft University of Technology, and Prof. José Azinheira, from Instituto Superior Técnico, for sharing with me their knowledge and enthusiasm throughout the development of my research. Their permanent support and valuable feedback were crucial for the success of the project. I am also very grateful that Prof. Bob Mulder and Dr. Erik-Jan van Kampen accepted to join the examination committee for my thesis.

I want to thank my Portuguese friends and fellow students Guilherme, Hugo, João, Nuno, Pedro and Tiago for helping each other out during our time in Delft and for the fruitful technical discussions we had. My word of thanks goes also to the SIM 0.04 and 0.08 community, in particular to Auke, Gwan, Jeroen, Joris, Koen and Martin, for their very useful suggestions regarding my thesis and for the pleasant and relaxed working environment of our student rooms.

Last but not least, I am most grateful to my parents and grandparents who always supported and encouraged me in all possible ways during my studies. My gratitude goes also to Ana for her patience and support while I stayed abroad.

Delft, University of Technology — Pedro V. M. Simplício
August 23, 2011

Contents

List of Figures

List of Tables

Acronyms

ACAH	Attitude Command/Attitude Hold
ADI	Approximate Dynamic Inversion
AFCS	Automatic Flight Control System
ANDI	Adaptive Nonlinear Dynamic Inversion
BIBO	Bounded-Input Bounded-Output
CA	Control Axis
CG	Center of Gravity
DA	Disc Axis
DOF	Degrees Of Freedom
EOM	Equations Of Motion
FBW	Fly-By-Wire
FDI	Failure Detection and Isolation
GPS	Global Positioning System
GVE	Good Visual Environment
IMU	Inertial Measurement Unit
INDI	Incremental Nonlinear Dynamic Inversion
ISA	International Standard Atmosphere
LPF	Low-Pass Filter
LQR	Linear-Quadratic Regulator
MCP	Mode Control Panel
MIMO	Multiple Input Multiple Output
MR	Main Rotor
MRAC	Model Reference Adaptive Control
NDI	Nonlinear Dynamic Inversion
NED	North-East-Down
NN	Neural Network
P	Proportional

PCH	Pseudo-Control Hedging
PD	Proportional-Derivative
PI	Proportional-Integrative
PID	Proportional-Integrative-Derivative
PINDI	Predictive Incremental Nonlinear Dynamic Inversion
RCAH	Rate Command/Attitude Hold
RM	Reference Model
RMSE	Root-Mean-Square Error
RPM	Rotations Per Minute
SA	Shaft Axis
SAS	Stability Augmentation System
SIMONA	SImulation, MOtion and NAvigation
SISO	Single Input Single Output
TR	Tail Rotor
TRCPH	Translational Rate Command/Position Hold
UAV	Unmanned Air Vehicle
VTOL	Vertical Take-Off and Landing

List of Symbols

Greek Symbols

α_{ef}	Effective angle of attack, [rad]
$\alpha_{fus_{M=0}}$	Incidence angle of the fuselage for zero pitch moment, [rad]
α	Angle of attack, [rad]
β	Sideslip angle, [rad]
β	Blade flapping angle, [rad]
γ_s	Rotor shaft tilt angle, [rad]
γ	Flight path angle, [rad]
γ	Lock number, [-]
δ_a	Ailerons deflection, [rad]
δ_e	Elevator deflection, [rad]
δ_r	Rudder deflection, [rad]
δ	Sweep correction to account for non-steady flow around the airfoil, [-]
Δt	Time step, [s]
ε	Aerodynamic relative error, [-]
ε_β	Flapping hinge offset ratio, [-]
ϵ_0	Average downwash angle at the fuselage, [rad]
ϵ	Singular perturbation, [-]
ϵ	Angular accelerations predictive error, [rad/s^2]
ζ	Damping ratio, [-]
θ_0	Collective pitch of the main rotor, [rad]

θ_{1c}	Lateral cyclic pitch of the main rotor (positive for a right stick deflection), [rad]
θ_{1s}	Longitudinal cyclic pitch of the main rotor (positive for a forward stick deflection), [rad]
θ_{0tr}	Collective pitch of the tail rotor, [rad]
$\underline{\theta}$	Angular orientation of the vehicle, [rad]
θ_{tw}	Linear blade twist, [rad]
θ	Attitude pitch angle, [rad]
θ	Blade pitch angle, [rad]
λ_0	Induced inflow ratio, [-]
$\underline{\lambda}$	Vector with the induced inflow ratios of both rotors, [-]
λ	Rotor permeability, [-]
μ_x	Rotor advance ratio, [-]
μ_z	Normalized component of the airspeed perpendicular to the rotor, [-]
μ	Normalized airspeed, [-]
ν_0	Induced downwash velocity, [m/s]
ν_β	Normalized flapping frequency, [-]
$\underline{\nu}_h$	Vectorial pseudo-control hedge
ν_h	Scalar pseudo-control hedge
ν_∞	Induced downwash velocity infinitely far downstream, [m/s]
$\underline{\nu}$	Generic virtual control vector
ν	Generic virtual control input
ρ_{bl}	Blade mass per unit length, [kg/m]
ρ	Air density, [kg/m^3]
σ	Rotor solidity, [-]
σ	Standard deviation
τ	Finite differences perturbation
τ	Generic time constant, [s]
$\underline{\Phi}$	Diffeomorphism transformation
ϕ	Blade inflow angle, [rad]
ϕ	Attitude roll angle, [rad]
χ	Heading angle, [rad]
Ψ	Blade azimuth, [rad]
ψ	Attitude yaw angle, [rad]

$\underline{\Omega}$	Transformation matrix between $\underline{\omega}$ and $\underline{\dot{\theta}}$, [-]
Ω	Rotor rotational speed, [rad/s]
$\underline{\omega}$	Angular rate vector in the body-fixed reference frame, [rad/s]
ω_n	Natural frequency, [rad/s]

Roman Symbols

$\underline{A}$	Generic state matrix
A	Rotor disc area, [m^2]
a_0	Rotor coning angle, [rad]
a_{1R}	Longitudinal disc-tilt angle relative to the shaft axis, [rad]
a_1	Longitudinal disc-tilt angle (positive for a backward disc-tilt), [rad]
$\underline{a}_B$	Linear acceleration vector in the body-fixed reference frame, [m/s^2]
$\underline{a}$	Generic vector function
a	ISA temperature gradient, [K/m]
a	Generic scalar function
$\underline{B}$	Input dependency matrix
b_{1R}	Lateral disc-tilt angle relative to the shaft axis, [rad]
b_1	Lateral disc-tilt angle (positive for a right disc-tilt), [rad]
b	Generic scalar function
C_D	Drag force coefficient, [-]
C_H	Rotor longitudinal drag force coefficient, [-]
C_{L_α}	Blade lift curve slope, [rad^{-1}]
C_{L_m}	Medium lift force coefficient, [-]
C_L	Lift force coefficient, [-]
$C_{M_{fus}}$	Fuselage pitch moment coefficient, [-]
$C_{N_{fus}}$	Fuselage yaw moment coefficient, [-]
C_Q	Rotor torque moment coefficient, [-]
C_S	Rotor lateral drag force coefficient, [-]
C_T	Thrust force coefficient, [-]
c_e	Equivalent blade chord, [m]
$\underline{c}$	Predictive filter coefficients vector, [s^{-1}]
D_1	Aerodynamic force tangential to the control plane, [N]
D	Drag force, [N]
e_β	Flapping hinge offset, [m]

e	Generic tracking error
F_0	Parasite drag area of the fuselage, [m^2]
F_{tr}	Fin blockage factor, [-]
F	Generic reference frame, [-]
$f_{control}$	Controller sampling frequency, [Hz]
f_{GPS}	GPS processing frequency, [Hz]
$\underline{f}$	Generic force vector, [N]
$\underline{f}$	Generic vector function
f	Generic scalar function
$\underline{G}$	Control effectiveness matrix
$\underline{g}$	Generic vector function
g	Earth's gravitational acceleration, [m/s^2]
g	Generic scalar function
$\underline{H}$	Predictive filter regressor function
$\underline{H}$	Generic transfer matrix
H	Generic transfer function
H	Rotor longitudinal drag force, [N]
$\underline{h}$	Generic vector function
h	Generic scalar function
h	Altitude, [m]
h	Vertical position with respect to the helicopter CG, [m]
I_β	Blade moment of inertia about its flapping hinge, [$kg.m^2$]
$\underline{I}_{n\times n}$	$n \times n$ identity matrix, [-]
$\underline{J}$	Inertia tensor of the helicopter, [$kg.m^2$]
J	Predictive cost function, [rad^2/s^4]
K_D	Derivative gain
K_I	Integral gain
K_P	Proportional gain
K_{corr}	Correction factor for the lateral disc-tilt angle, [-]
K_{fus}	Correction coefficient for the pitch moment of the fuselage, [-]
K_{ht}	Correction coefficient for the pitch moment of the horizontal tail, [-]
K_{tr}	Main rotor downwash factor at the tail rotor, [-]
$\underline{K}$	Generic transfer matrix

K	Linear controller transfer function
k	Generic proportional gain
L	Aerodynamic moment around the body x-axis, [N.m]
L_*	Control derivative of the L moment with respect to variable $*$
L	Lift force, [N]
l_1	Lateral position with respect to the helicopter CG, [m]
l	Longitudinal position with respect to the helicopter CG, [m]
M_A	Flapping aerodynamic moment, [N.m]
M_*	Control derivative of the M moment with respect to variable $*$
M	Aerodynamic moment around the body y-axis, [N.m]
m	Number of outputs (and inputs) of the system, [-]
m_{bl}	Blade mass, [kg]
$\dot{m}$	Mass flux of the rotor wake, [kg/s]
$\underline{m}$	Generic moment vector, [N.m]
m	Total mass of the helicopter, [kg]
N	Aerodynamic moment around the body z-axis, [N.m]
N_*	Control derivative of the N moment with respect to variable $*$
N	Rotor number of blades, [-]
n	Order of the system, [-]
$\underline{p}$	Position vector in the NED frame, [m]
p	Air pressure, [Pa]
p	Rotational rate around the body x-axis, [rad/s]
Q	Rotor torque moment, [N.m]
q	Rotational rate around the body y-axis, [rad/s]
R_{fus}	Fuselage drag resultant force, [N]
$\underline{R}$	Generic rotation matrix, [-]
r	Relative degree of the system, [-]
R	Ideal gas constant, [J/(kg.K)]
R	Rotor radius, [m]
r_{bl}	Radial position of a blade element, [m]
r	Rotational rate around the body z-axis, [rad/s]
S	Surface area, [m^2]
S	Rotor lateral drag force, [N]

s	Laplace domain variable
T_1	Component of the aerodynamic force normal to the control plane, [N]
T_2	Component of the thrust force tangential to the control plane, [N]
$\underline{T}$	Generic transformation matrix, [-]
T	Thrust force, [N]
T	Air temperature, [K]
t	Time variable, [s]
U	Normalized resultant flow velocity in each blade element, [-]
u	Generic system input
u_P	Normalized velocity perpendicular to the control plane, [-]
u_R	Normalized velocity along a blade axis, [-]
u_T	Normalized velocity tangential a blade element, [-]
u	Airspeed component along the body x-axis, [m/s]
$\underline{u'}$	Helicopter input vector excluding the collective of the main rotor, [rad]
$\underline{u}$	Generic system input vector
V_{fus_M}	Equivalent volume of the fuselage in the horizontal plane, [m^3]
V_{fus_N}	Equivalent volume of the fuselage in the lateral plane, [m^3]
V	Total airspeed, [m/s]
$\underline{v}_E$	Linear velocity vector in the NED frame, [m/s]
$\underline{v}$	Velocity vector in the body axes, [m/s]
v	Airspeed component along the body y-axis, [m/s]
$\underline{W}$	Generic weighting matrix, [-]
W	Total weight of the helicopter, [N]
w	Airspeed component along the body z-axis, [m/s]
X	Aerodynamic force in the body x-axis, [N]
$\underline{x}$	Generic state vector
x	Generic state variable
x	Position x coordinate in the NED frame, [m]
Y	Aerodynamic force in the body y-axis, [N]
$\underline{y}$	Generic system output vector
y	Generic system output
y	Position y coordinate in the NED frame, [m]
Z_*	Stability derivative of the Z force with respect to variable $*$

Z	Aerodynamic force in the body z-axis, [N]
z^{-1}	Unit delay operator
$\underline{z}$	Generic state vector
z	Position z coordinate in the NED frame, [m]

Subscripts and superscripts

0	Current state/ISA sea level/Built-in parameter
att	Attitude loop
b	Body-fixed reference frame
com	Commanded
cp	Control plane
des	Desired
dp	Disc plane
e	Eccentricity
f	Fast dynamics
fus	Fuselage
Gl	Glauert theory
ht	Horizontal tail
mr	Main rotor
nav	Navigational loop
n	Nominal conditions
ol	Open-loop
o	NED reference frame
rm	Reference model
rot	Rotational loop
sat	After saturation
s	Slow dynamics
sp	Shaft plane
$trim$	Trim value
tr	Tail rotor
v	Velocity reference frame
vt	Vertical tail
x	x-axis component
y	y-axis component
z	z-axis component

Other Notations

$\dot{x}$	First time derivative of x
$\ddot{x}$	Second time derivative of x
$x^{(n)}$	n-th time derivative of x
$\mathrm{d}x$	Elementary perturbation of x
∇x	Gradient of x
$\underline{D}(\underline{x})$	Jacobian of $\underline{x}$
$L_y x$	Lie derivative of y with respect to $\underline{x}$
x_i	i-th component of vector $\underline{x}$
X_i	ii-th component of matrix $\underline{X}$
$\bar{x}$	Normalized (dimensionless) value of x
$\hat{x}$	Estimated value of x
Δx	Deviation of x from its nominal condition or from its trim value
c_x	Cosine of x
s_x	Sine of x

Conversion factors

1 feet (ft)	0.3048 m
1 knot (kt)	0.5144 m/s

Chapter 1

Introduction

This chapter presents an introduction to the research work entitled "Helicopter Nonlinear Flight Control: An Acceleration Measurements-based Approach using Incremental Nonlinear Dynamic Inversion". This Master of Science thesis was developed at the Faculty of Aerospace Engineering of the Delft University of Technology. It is integrated in a Double Degree Diploma on Flight Dynamics, Control and Avionics between the referred university and Instituto Superior Técnico, part of the Technical University of Lisbon.

1-1 Project Motivation

When compared to fixed-wing aircraft, helicopters present a distinct advantage in terms of maneuverability: they can hover for extended periods of time, describe vertical flight trajectories like Vertical Take-Off and Landing (VTOL), they are able to fly backwards, sideways and perform extreme agile maneuvers at high and low airspeeds. These characteristics allow helicopters to perform a wide range of tasks that were not previously possible with other aircraft. These tasks include for example military missions, search and rescue, firefighting, transportation and construction, often carried in urban environments.

Nevertheless, helicopters are highly nonlinear and complex systems, inherently unstable by nature. This is mainly due to an extremely coupled rotor-body interaction, which gives rise to a variety of inter-axis couplings in their response. This behavior makes helicopter piloting a very demanding job, with an incredible workload for the pilot, especially in situations of rapid combat, high crosswinds or low light. For this reason, the implementation of Stability Augmentation Systems (SASs) (which can go from mechanical stabilization devices to Automatic Flight Control Systems (AFCSs)) is crucial to assure safety and effectiveness in helicopter operation. A chronological description of most of these systems is presented in (Stiles, Mayo, Freisner, Landis, & Kothmann, 2004). The capabilities mentioned above clearly justify the expenses needed to develop mathematical models and control strategies for these highly complex systems.

As every technology, helicopters do also have some disadvantages when compared to fixed-wing aircraft. They are noisier, less safe, considerably more difficult to fly and extremely vibrating systems. Probably because of these aspects, the aeronautical community is substantially more devoted to fixed-wing research rather than their rotary-wing counterparts. In fact, while commercial airplanes and military fighters have been flying with Fly-By-Wire (FBW) technology onboard for several years and even despite the extensive research done by excellency institutes in this filed, it was only in 2008 that the first flight of the only fully FBW rotary-wing aircraft currently in flight test development, the Sikorsky's UH-60M Upgraded Black Hawk, took place (Deagel, n.d.).

In a FBW system, the pilot's stick movements, instead of being directly transmitted to the actuators, are converted to electronic signals that are sent to computers featuring digital advanced flight control laws. The actions required to perform the pilot's commands are then electronically supplied to the helicopter actuators. Furthermore, the elimination of traditional mechanical linkages brings several technical advantages since it saves weight, reduces maintenance costs, improves reliability and enhances performance.

The flight control systems mentioned above are of crucial relevance for the maneuverability of the aircraft. The achievement of enhanced performances clearly motivates the aerospace industry to develop more optimal flight control laws. They not only have to provide the tracking of the references inputted by the pilot, they also have to assure the stabilization of the helicopter and the effectiveness of the flight. Furthermore, inadequate control laws may result in a necessary reduction of their flight envelope due to problems associated with the saturation of actuators during aggressive maneuvers.

Having in mind the important role of helicopters nowadays and the continuous need for advanced research and development in the area of rotorcraft dynamics and control, Delft University of Technology is expanding their high-fidelity motion-based flight simulator, the SImulation, MOtion and NAvigation (SIMONA) Research Simulator depicted in Figure 1-1, from a fixed-wing platform to encompass a rotary-wing environment. With this improvement, the Boeing Company is offering opportunities to SIMONA for future tests and scenarios in order to create a collaborative project with the university. Comparison of the results of the experiments will not only be used to develop the rotary-wing platform and improve its fidelity, but also to correlate the SIMONA against Boeing's AH-64 Apache fixed-based simulator for specific flying and handling qualities evaluations.[1]

The work packages delivered by Boeing to the university consist basically in the following tasks:

- Modification of the SIMONA flight deck to support helicopter controls, instruments and outside visuals;
- Integration and validation of the flight simulation model of Boeing's AH-64 Apache advanced attack helicopter;
- Definition, implementation and execution of handling qualities experiments;

[1] Flying and handling qualities basically describe the ease and effectiveness with which an aircraft responds to pilots commands.

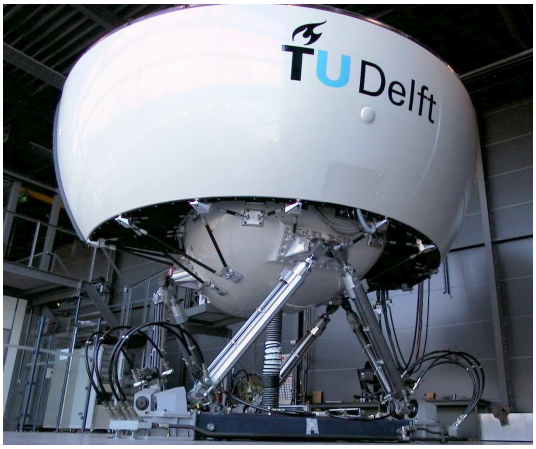

Figure 1-1: The SIMONA Research Simulator. [source: `http://www.simona.tudelft.nl`]

- Development of advanced helicopter control laws. In particular, it is desirable that these laws yield significant improvements in terms of handling qualities and an increased flight envelope for full-authority controllers.

This last point corresponds then to the main motivation behind this thesis. Its specific objectives are established in Section 1-3, after a summarized background in Helicopter Nonlinear Flight Control, presented in the next section.

1-2 Background

For further clarity, this section related to the state of the art in Helicopter Nonlinear Flight Control is divided in two subsections, each one presenting the most relevant developments in terms of nonlinear control strategies and helicopter flight control, respectively.

1-2-1 Nonlinear Control Strategies

Flight control systems have evolved dramatically over the past decades, starting as limited-authority analogue systems to provide a bit of stability augmentation until full-authority digital systems, critical to assure full envelope performance (Enns, Bugajski, Hendrick, & Stein, 1994).

Linear controllers represent the simplest form to control a system. The beginning of the formal analysis of these techniques dates back to the end of the nineteenth century and, since then, linear controllers have been used for many different types of applications and several powerful tools to project them have been developed. However, as the name indicates, linear controllers are derived based on the feedback of a linear system or on a linearization of a nonlinear system with respect to a certain solution. This linearization only works as a good representation of the true nonlinear system near the referred solution and, as the condition of the system deviates from it, the accuracy of the linear approximation decreases and the performance of the controller is degraded.

If the tasks of the control system involve a large range or high-speed motions, nonlinear effects will become significant in the dynamics and the closed-loop system may become unstable. Helicopters and other modern military aircraft are notable examples of highly nonlinear systems, inherently unstable and designed for large operating envelopes.

As explained in (Slotine & Li, 1991), the main advantage of designing linear controllers lies in the fact that the desired behavior of linear control systems can be systematically specified, either in the time or frequency domain. Unfortunately, general methods do not exist for designing nonlinear controllers, but several different approaches can be adopted. For nonlinear systems, concepts like impulsive response or transfer function do not exist and one looks instead for some qualitative specifications like accuracy and speed of response in the operating region of interest.

Gain-scheduling

To overcome the shortcoming associated with the limited validity of a single linear controller for a nonlinear system, a technique known as gain-scheduling was intuitively developed (Slotine & Li, 1991). It consists of selecting multiple operating (equilibrium) points which cover the whole range of the system operation and, for each one, make a linear approximation of the nonlinear system and design a linear feedback control law. Each of these laws is applicable in the neighborhood of a specific point. Between operating points, the parameters of the different controllers are interpolated (scheduled), originating a global control system.

The main limitations associated with this technique are the complexity in deriving a formal proof of stability for this kind of control and the fact that its design is fixed and inflexible. Any mismatch between the model and the true system will cause performance degradation. Besides that, the choice of the operating points and the individual controller design is a tedious and time consuming process. Furthermore, the resulting controller has still to be verified with extensive nonlinear simulations to assure that the global control law possesses the desired local properties introduced for its operating points.

Gain-scheduling is a conceptually simple and well-established approach, with successful application to many complex systems, like military aircraft (Stevens & Lewis, 2003). It is still the prevailing strategy to control most of the aircraft. Nevertheless, the desire for enhanced agility of modern aircraft demands that they perform over an increased range of operation conditions, even sacrificing their own static stability. As stated in (Goman & Kolesnikov, 1998), this expansion involves not only radical changes in their configuration but also the replacement of conventional control strategies by more advanced alternate methodologies based on pure nonlinear controllers. Above all, these techniques have the ability to cope with a much higher range of conditions of intrinsic nonlinear systems.

Nonlinear Dynamic Inversion

The basic idea behind the Nonlinear Dynamic Inversion (NDI), also referred to as feedback linearization, is to first transform a nonlinear system into an equivalent linear system and then use the well-known classical linear methods like Proportional-Integrative-Derivative (PID) controllers or Linear-Quadratic Regulators (LQRs) to complete the design. The referred transformation is obtained through a combination of a state feedback and a coordinate

transformation that reduces the dynamics of the controlled variables to simple integrators. Since after this transformation the system is linearized, a single linear controller suffices to assure control over the entire envelope and therefore no gain-scheduling is needed.

Mainly because of this benefit, the NDI is one of the most powerful and common techniques on nonlinear control. After some years of experience with this type of design, control engineers now believe that the NDI will eventually replace the gain-scheduling as the prevailing flight control technique. This statement is supported by the example of the Lockheed Martin F-35 Lightning II, a multirole fighter that started flying in 2006 with a set of flight control laws based on NDI (Wedershoven, 2010).

The application of the NDI to aerospace systems is especially useful because it allows to enforce the desired flying qualities directly in the closed-loop response, as shown in (Brinker & Wise, 1996). This control methodology has a wide range of successful applications that encompass, among many others, fighter jets (Enns et al., 1994) and reentry vehicles (Costa, Chu, & Mulder, 2003).

The major drawback of the NDI is associated with the fact that it relies on the exact cancellation of the nonlinearities of the system. Nevertheless, in complicated systems like aircraft, model uncertainties[2] or changes on its parameters often occur (Sonneveldt, Oort, Chu, & Mulder, 2009). Due to these inaccuracies (differences between the mathematical model and the actual physical system), the exact cancellation of the nonlinearities becomes impossible and the performance of the controller is degraded. Furthermore, the NDI method is only applicable to systems that can be transformed into the linearizable form. This class of systems is known as feedback linearizable.

Backstepping

For systems that are not feedback linearizable or as a mean to acquire more flexibility in the controller design, a technique known as backstepping can be applied instead of the NDI. This technique is very well explained in (Oort, 2011). The name backstepping indicates the existence of a recursive method which starts with the differential equations of the nonlinear system and steps back towards the control inputs that are separated from them by the largest number of integrators.

The design procedure is similar to that of the NDI but, instead of first transforming the nonlinear system into an equivalent linear one directly, a stabilizing feedback is constructed for each step of the recursive method mentioned above. This feedback is achieved through a change of coordinates to an error system, in which the control law is established using a control Lyapunov function. According to Lyapunov's theory, this type of function works as a measure of the energy in the error system. As it represents a quantification of energy, the control Lyapunov function can never be negative definite and can only be zero in the zero state. The control input shall thus render the derivative of the control Lyapunov function negative semidefinite, dissipating the energy of the error and stabilizing the system.

A very interesting application of backstepping to flight control can be found in (Farrell, Sharma, & Polycarpou, 2005).

[2]Model uncertainties can result from parametric uncertainties, which limit the operational envelope of the vehicle, or unmodeled dynamics, which limit the achievable bandwidth of the system.

Robust Control

As mentioned in (Slotine & Li, 1991), pure model-based nonlinear controllers like NDI or backstepping are designed based on a nominal model of the physical system, guaranteeing stability for that model. In order to assure robustness of the controller in the presence of effects which are not considered in the design such as relatively small disturbances, measurement noise or unmodeled dynamics, the so-called robust controllers can be designed by considering both the nominal model and some characterization of the model uncertainties.

The referred improvement can be combined with a nonlinear controller, for example, by using a robust control law (of which the H_∞ and μ synthesis are the most common ones) to design the additional linear controller. One example of this kind of approach to flight control is given in (Goman & Kolesnikov, 1998).

When the model uncertainties mentioned above become larger or if their characterization is unknown, a robust control strategy may result in a too conservative approach or it may not suffice to provide an adequate response of the system (Calise & Rysdyk, 1998). In this case, in order not to sacrifice the achievable performance of the system, a more complex control strategy is required.

Adaptive Control

To overcome the limitations of robust control, adaptive control architectures were developed as alternative approaches to deal with uncertain or time-varying systems. They can be interpreted as dynamic feedback laws which, by increasing the order of the controller, allow its adaptation to changes in the controlled system. Artificial Neural Networks (NNs) are normally used in this process since they have the ability to mimic continuous nonlinear functions within the desired accuracy. In general, two types of adaptive control exist.

In direct adaptive control the system itself is not identified, but an adaptation mechanism is designed to update the parameters of some controller that will stabilize the system and assure the desired closed-loop response. The referred controller is normally composed of a nonlinear control law and an online NN or disturbance observers to compensate for the error associated with its inaccuracies. The nonlinear controller can also be composed of a single NN or it can be used in parallel with another control law.

On the other hand, indirect adaptive control makes use of an adaptive element (normally a NN) to identify the unknown system dynamics online by estimating some model parameters and a controller to provide control assuming that model is correct. When the NN is trained properly, it will correspond to a perfect copy of the model. The controller is tuned until the output of the NN is the same as the references commanded to the system.

Two very recent works in which adaptive control is used in flight control systems are (Lombaerts, 2010) and (Oort, 2011). The first one applies adaptive elements to improve a NDI-based controller, while the latter uses them in combination with a backstepping scheme.

Adaptive controllers are however particularly troublesome when it comes to the issue of flight certification. Firstly, it is inherently difficult to prove that the adaptive element will rarely "learn" incorrectly and thus causing harm to the vehicle. In addition, it is also very hard to

show formally that, in case of a failure in adaptation to an extreme level, the adaptive element is still able to recover, assure stability and control of the system. Civil and military applications have also proven the benefits of the ability to accommodate changing dynamics and payload configurations without having to rely on substantial adaption efforts (E. N. Johnson & Kannan, 2005).

Incremental Control

Over the past decade, the literature concerning practical implementations of the NDI (or backstepping) in critical flight conditions is typically based on augmentations of the standard versions of these methodologies with robust or adaptive control (Chen & Zhang, 2008). This yields therefore complex control structures or high degree controllers.

A more intuitive, yet innovative, approach consists of modifying the architecture of a nonlinear controller in such a way that acceleration feedback is employed to extract the information relative to any aerodynamic change in the aircraft. Furthermore, in this approach, instead of computing the total control inputs to obtain the desired response, only the incremental changes with respect to the previous conditions are calculated. In fact, this type of action is much more similar to the one provided by a human pilot.

This strategy can be applied for both NDI and backstepping methodologies. In the first case, it acquires the designation of incremental, modified or simplified NDI. The main advantage of the Incremental Nonlinear Dynamic Inversion (INDI) lies in the fact that, due to its incremental derivation, the controller does not need any model data that depends exclusively on the states of the system. This allows to enhance significatively the robustness of the control law to model uncertainties or disturbances.

Incremental control has also been a relevant object of study in the division of Control and Simulation of the Delft University of Technology, with two master thesis in the last two years. The first one (Sieberling, 2009) considers a prototype Unmanned Air Vehicle (UAV) model and develops a robust control law to further increase the robustness of the INDI design methodology. The second one (Wedershoven, 2010) regards the model of a F-16 jet fighter and performs detailed analysis and simulations to investigate the differences between the NDI and the INDI approaches, as well as the particular factors on which they depend.

1-2-2 Helicopter Flight Control

Two of the first most relevant designs of nonlinear controllers for helicopters are presented in (Prasad & Lipp, 1993) and (Njaka, Menon, & Cheng, 1994), both of them using some kind of feedback linearization. It was not properly a nonlinear dynamic inversion since, due to the extreme nonlinearities and couplings of helicopters, a direct inversion of its dynamics is not possible. The feedback linearization was only made assuming an affine model constructed with the stability and control derivatives associated with linearizations of the model at pre-specified trim conditions. Hence, the dynamic inversion achieved is not exact, but an approximate inverse of the helicopter system instead. This fact contributed therefore to a limited performance of the control systems obtained. Nevertheless, very important strategies were already introduced in the designs proposed: the first reference derives an approximate

model inversion to provide navigational control of the helicopter and the second one uses an approach based on time scale separation to simplify the implementation of the controller.

In order to reduce the effects of an inaccurate feedback linearization, several works were carried out with increased successful results in the following years (Leitner, Calise, & Prasad, 1998; Calise & Rysdyk, 1998; Hovakimyan, Kim, Calise, Prasad, & Corban, 2001; Lee, Ha, & Kim, 2005). In all these references, online NNs are employed to approximate the inversion error and provide an additional adaptive control to compensate for it. The adaptation mechanism of the NNs is normally based on the dynamics of the tracking error of the model states. This type of control architecture became quite common in helicopter flight control and it is known as Adaptive Nonlinear Dynamic Inversion (ANDI). In general, further developments considered also this type of architecture, but added some improvements in the structure of the dynamic inversion itself or in the design of the adaptive element. (E. N. Johnson & Kannan, 2005) is a good example of the first case, in which the author developed a time scale separated dynamic inversion for an autonomous UAV helicopter and included a method to protect the adaptation process from actuator limits and dynamics. Regarding the second case, in (Zeng & Zhu, 2006) an interesting adaptive compensator is presented as an effective alternative to NNs, more intuitive and less complex.

The application of an exact feedback linearization to rotorcraft flight control can be found in (Howitt, 2005). In this case, the incremental version of the NDI was implemented and thus no adaptive element was needed. The control strategy includes the concept of rotor state feedback to counter air resonance and to allow for intrinsic carefree handling protection of hub moment limits. Nevertheless, the theoretical development and practical simulations were performed for a rig rotor. Consequently, since no tail rotor or yaw control exists, this approach is still too simplified for real helicopters application. This article was then referred in (Bradley & Thomson, 2005) as a promising method to implement helicopter and tilt-rotor inverse simulation.[3]

With respect to the research carried out in the division of Control and Simulation of the Delft University of Technology, four master thesis were developed in helicopter flight control for the past few years. (Bijnens, 2005) and (Klamer, 2007) attempted to design helicopter autopilots for 2-D models, both of them with only limited success. The first one adopted an adaptive backstepping approach while the other one implemented a controller based on adaptive nonlinear dynamic inversion, both using NNs as adaptive element. The development of autopilots for 3-D helicopter models was tackled by (Jong, 2004) and (Moelans, 2008). The control system designed by the former was based on gain-scheduling and thus it was only valid in a limited region of the flight envelope. The second one was already able to provide proper tracking of the desired reference trajectories for a wider range of conditions since it used, once again, an approach based on adaptive nonlinear dynamic inversion.

1-3 Objectives

It is now possible to define very clearly the research objectives behind this master thesis. The main goal is to develop alternative advanced flight control laws for a 3-D helicopter model that allow improvements in terms of:

[3] In this context, inverse simulation is defined as the prediction of the control actions needed to pilot a vehicle through a given maneuver.

- Flight envelope, increasing the operational range of rotorcraft by coping more efficiently with their nonlinear effects and inter-axis couplings;
- Practical applicability, avoiding the complex structures and the flight certification problems associated with adaptive controllers;
- Robustness, providing an adequate behavior in the presence of model inaccuracies, changes in configuration and external disturbances.

According to this, the basis nonlinear control strategy selected to fulfil these requirements is the INDI. This choice is also strongly motivated by the innovative character associated with it. To the author's knowledge, an approach based on INDI for helicopter flight control has never been presented. This research can then be seen as a feasibility study to analyze the application of INDI to helicopter control and identify the improvements it brings, as well as its drawbacks.

In the end, it is desirable to have an autopilot for a generic helicopter that not only assures the complete stabilization of the vehicle, but that also tracks efficiently velocity references commanded to the system. To analyze the performance of the overall controller, several trials based on real handling qualities assessment for rotorcraft will have to be carried out. In addition to these trials, a series of tests will also have to be performed to investigate carefully if the robustness properties of the controller are adequate for a potential practical implementation.

Unfortunately, in the beginning of this research, the AH-64 Apache flight simulation model had not been delivered by the Boeing Company yet. Because of this, a mathematical nonlinear helicopter model with an adequate fidelity had to be developed for the derivation of the flight control system and for the subsequent tests and simulations. This task turned out to be a very important part of the research project.

Due to the public availability of its specific data, the rotorcraft model analyzed throughout the present work is the Bölkow Bö-105, shown in Figure 1-2.

Figure 1-2: An aerobatic Bölkow Bö-105. [source: `http://profefeito.blogspot.com`]

The Bö-105 was the first light helicopter to enter commercial service. Its production began in 1971 under Messerschmitt-Bölkow-Blohm (MBB) and presented an innovative rotor with reinforced blades made of composite materials. This vehicle displays an excellent maneuverability, reason why it serves in the civil and military sectors for all the tasks that a helicopter

can perform (Eurocopter, n.d.). Nearly 1,500 Bö-105's were built in 25 different versions. In 1991, MBB became a part of Eurocopter and, ten years later, the Bö-105 was replaced by the Eurocopter EC-135.

1-4 Thesis Outline

The scientific research reported here begins with one chapter (Chapter 2) fully dedicated to helicopter modelling. In this chapter, the working principle and configuration of a general helicopter is described, followed by the derivation of a mathematical system to model it and by the respective open-loop analysis.

Afterwards, throughout Chapters 3 and 4, all the control theory necessary for the development of the helicopter advanced control laws analyzed in this thesis is presented. The former chapter deals with the formal theory behind the Nonlinear Dynamic Inversion and the later one is relative to the Pseudo-Control Hedging technique.

Once all the required control theory is presented, the following chapters describe the design methodology adopted for the three control loops developed in this thesis: an angular rate controller in Chapter 5, an attitude angles controller in Chapter 6 and a navigational controller in Chapter 7. In each one of these chapters, the corresponding control architecture is shown and the results obtained from its application to the helicopter nonlinear model are discussed.

Chapter 8 presents the results obtained from tests made to the overall flight control system when different uncertainties and disturbances are introduced. Finally, Chapter 9 includes a brief discussion on the practical applicability of the control system implemented and on the advantages and shortcomings of applying Incremental Nonlinear Dynamic Inversion to both fixed-wing and rotary-wing aircraft.

The thesis ends with the most relevant conclusions and recommendations of this work in Chapter 10. In addition, a set of five appendices is also available as a complement to some particular subjects analyzed during the research.

Chapter 2

Helicopter Modelling

"*The helicopter is an aircraft that uses rotating wings to provide lift, propulsion and control.*" (W. Johnson, 1980). In opposition to a fixed-wing aircraft, in which the lift, propulsion and control forces and moments are produced by separate aerodynamic surfaces, in an helicopter, all these contributions are generated by its rotor. The conventional helicopter rotor consists of two or more identical blades attached to a central hub. A shaft torque from the engine provides a uniform rotational motion to these blades with respect to the air and the aerodynamic forces generated from this interaction produces the torque, thrust and other forces and moments of the rotor.

As already mentioned, the main characteristic of the helicopter is that it can produce all the referred forces even when its translational velocity is zero, allowing this vehicle to perform vertical flight. When compared to fixed-wing aircraft, the price for vertical flight includes however a higher power requirement and a more complex mechanical system, factors that are directly translated in operational and maintenance costs. Furthermore, the rotor is a source of vibration and the stability characteristics of the vehicle are often marginal, meaning that piloting a helicopter is a very demanding task and thus the development of AFCSs is crucial.

The first step to design and test a control system is to develop a model of the system to be controlled. With this in mind, this chapter deals with the derivation of a nonlinear model that allows to simulate the dynamics and kinematics of a helicopter with a satisfactory fidelity to the real vehicle. Firstly, the configuration of a conventional helicopter is presented in Section 2-1, together with a description of its control systems. Then, the parameters and systems of reference necessary to carry out the mathematical derivation of the model are introduced and the sign conventions established in Section 2-2. In Section 2-3, the model adopted for the helicopter is presented, highlighting the modular structure that composes it. Finally, in Section 2-4, the results of a test to the model in open-loop are shown, proving that the model is highly unstable, even around hover conditions.

2-1 Helicopter Configuration

The first rotary-wing aircraft to reach substantial forward velocities was the Cierva autogyro (Prouty & Curtiss, 2003). It was built in 1923 and consisted of an airplane modified with rotating wings that would not stall. Being an autogyro, no power was needed to rotate its blades and, since the pilot had no control over them, the aircraft was piloted with the conventional airplane surfaces.

One of the main problems encountered by rotary wing inventors was the asymmetrical velocity field in the rotor during forward flight. This phenomenon is illustrated for a rotor with an anticlockwise rotation in Figure 2-1.

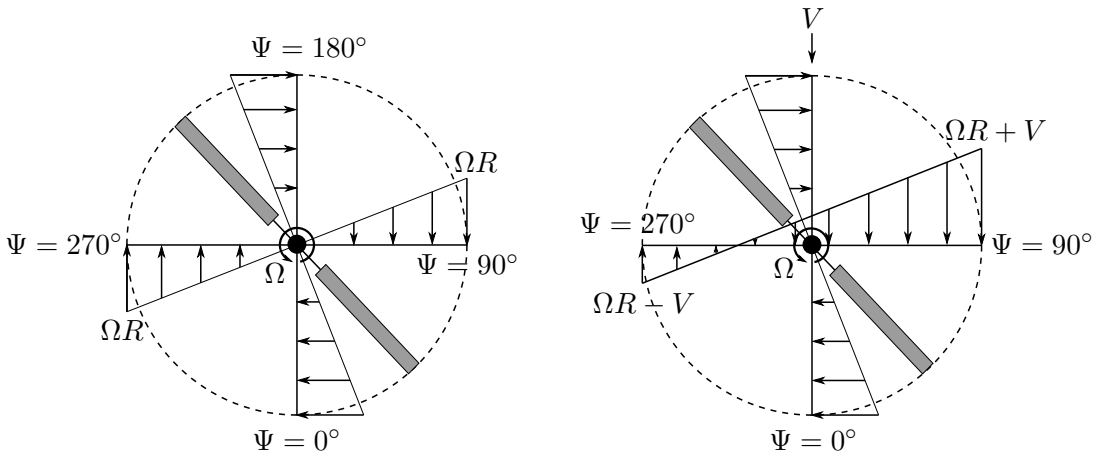

(a) Hovering flight. **(b)** Forward flight.

Figure 2-1: Profile of the velocity normal to the leading edge in hover and forward flight.

In this figure, Ω is the angular velocity (or Rotations Per Minute (RPM)) of the rotor, R is its radius, V is the forward velocity of the vehicle and Ψ is called the azimuth of one blade. In hovering flight, the distribution of the incident velocities is always symmetrical with respect to the rotor hub. However, during forward flight, while for the advancing side ($0° < \Psi < 180°$) the normal velocities are higher than in the hover situation, in the retreating side ($180° < \Psi < 360°$) the referred velocities are smaller and even a reverse flow region exists near the hub. This dissymmetry of velocities generates a lift gradient that yields a roll moment in the rotorcraft. The introduction of hinges in the blade roots allowed Cierva to overcome this problem, since they enabled a flapping motion of the blades such that the local angles of attack are changed to compensate for the asymmetrical lift distribution.

Due to Coriolis effects, when the rotor blades flap, a corresponding in-plane vibration appears at the blade root, usually known as lag (or lead-lag) motion. To cope with this vibration, also lag hinges have to be introduced in the connection with the rotor hub. This motion is also responsible for the so-called ground (or air) resonance, one of the main dynamic problems of rotorcraft. Because of this, dampers for the lag motion have normally to be introduced in order to attenuate the frequency of this vibration.

Besides the flapping and the lag motion, the blades can also be feathered about an axis parallel to the blade span. As it will be seen later on, this rotation is very useful to provide control of

the whole helicopter, since it allows to change the pitch of the blades. The three fundamental blade motions and the hinge associated with each one are illustrated in Figure 2-2.

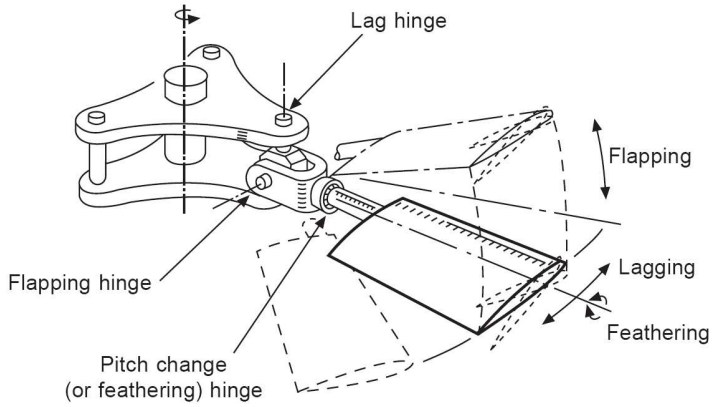

Figure 2-2: Fundamental blade motions. [source: (Bramwell et al., 2001)]

These motions produce high stresses in the blades and thus large moments are transmitted through the hub to the helicopter. The mechanical arrangement of these parts must be carefully designed to accommodate the blade motions and to keep the referred loads low. The choice made for the connection of the blades to the shaft provides a fundamental classification of the rotor. In (Hohenemser, 1974) the different types of hinge arrangements are described, of which the most common ones are:

- The articulated rotor which, as already mentioned, uses feathering, flap and lag hinges to attach the blades to the hub. As mentioned above, these hinges operate under very high loads and therefore they require frequent maintenance. Additionally, a hinged hub has also the disadvantage of becoming considerably bulky for a large number of blades, increasing its contribution to the total drag of the helicopter;
- The semi-hingeless rotor, in which the use of lag hinges was replaced by an attachment made with cantilever root restraint, allowing blade lagging through bending at the rotor;
- The hingeless (or rigid) rotor, containing only feathering hinges since the flap hinges were removed by providing the blades with a larger bending flexibility (soft flapwise) and by using tension-torsion straps to carry the centrifugal load. The main advantages of hingeless rotors are reduced maintenance, fewer hub parts and improved control response;
- The bearingless rotor, which is truly hingeless since all the hinges are omitted in the attachment. As is it based on composite materials with elastomeric elements, the development of this type of rotor started more recently;
- The teetering rotor, a special arrangement in which a pair of blades is mounted as a single unit, attached to the rotor shaft as in a semi-hingeless rotor.

For more details with respect to this classification, the reader is referred to (W. Johnson, 1980) or (Bramwell et al., 2001).

Returning to the history, soon after the development of the Cierva autogyro, it became clear that the effectiveness of the airplane control surfaces was less than desirable, especially when flying at low airspeeds. Inspired by the way people tilt their umbrellas to protect themselves during a windy rainstorm, he came out with the idea of the so-called "direct control" system. With this system, the rotor is mounted on a gimbal that can be tilted longitudinally and laterally by a control stick. As the rotor thrust vector is always practically perpendicular to its tip-path plane (the plane described by the tips of the rotation blades), the rotorcraft is accelerated in the direction of the tilt, generating roll and pitch moments around its Center of Gravity (CG).

However, in opposition to autogyros, helicopters do need torque provided by the engine and it was found that direct control is not practical for this type of vehicle. The system adopted to provide roll and pitch control for a helicopter while accounting for the unequal aerodynamics on the rotor is known as cyclic pitch and it was spontaneously proposed in 1906 by Crocco (Prouty & Curtiss, 2003). As the name indicates, it makes use of the pitch motion of the blades and is currently one of the main control systems of a helicopter.

2-1-1 Cyclic Pitch

The key to cyclic pitch is the swashplate, the assembly that allows to control the pitch angle of the blades. An example of this system is given in Figure 2-3, where the generic control system of a helicopter is shown.

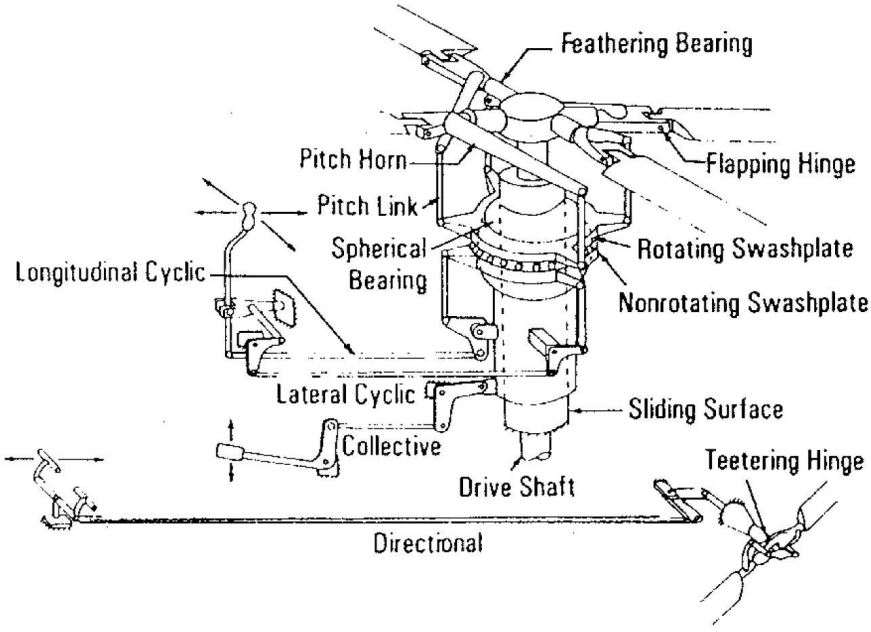

Figure 2-3: Generic helicopter control system. [source: (Prouty & Curtiss, 2003)]

As it can be seen in the figure, the swashplate assembly consists of a rotating and a nonrotating plate. The rotating plate rotates with the drive shaft and with the blades due to link that connects them. The angle and position of the fixed plate is changed by control rods that

are controlled by the pilot. This angle is transmitted to the rotating plate (and thus to the blades), which rotates on top of the fixed plate because of the spherical bearings between them.

The cyclic pitch control allows to tilt the swashplate and, consequently, the rotor tip-path plane, by introducing a cyclic change in the pitch of the blades. As already explained, since the thrust vector is almost perpendicular to this plane, the desired displacement of the helicopter can be achieved by tilting this vector into the desired direction. This tilt is controlled by the pilot with a stick, as shown in Figure 2-3.

When the stick is moved forward or backward, the tip-path plane tilts longitudinally and the helicopter pitches the nose down or up, respectively. Similarly, when the stick is moved to the right or to the left, the tip-path plane tilts laterally and the helicopter rolls to the right or to the left. Obviously, a combined movement can always be decomposed into longitudinal and lateral contributions. In addition, the cyclic stick has normally a trim switch that can be used to neutralize the stick forces. When activated, it controls the tension on a spring in order to hold the stick in a desired position, reducing the workload of the pilot when the helicopter is flying in steady conditions (Moelans, 2008).

2-1-2 Collective Pitch

While the cyclic control changes the pitch of the blades cyclicly, a collective control also exists that allows to vary the pitch of all the blades with the same amount. This is possible due to the vertical movement of the swashplate with a sliding surface around the rotor shaft which, as indicated in Figure 2-3, is controlled by a lever located on the left side of the pilot. When the pilot pulls this lever up, the pitch of the blades increases, more lift is generated and thus the thrust produced by the rotor will also increase (if the blades do not stall). Similarly, the thrust produced decreases when the collective lever is lowered. This type of control is therefore used for climbing and descending, but also to accelerate and decelerate the horizontal motion when the helicopter.

An important remark has also to be made with respect to the use of the collective pitch. When the pitch of the blades is increased, not only more lift, but also more drag will be generated, causing the RPM of the engine to drop. In this situation, to keep the RPM constant, more power has to be applied to the engine. This is done by twisting the handle of the collective lever simultaneously with the application of the collective pitch. In most of the modern helicopters, this compensation is automatically achieved with a device called "the governor" (Moelans, 2008).

2-1-3 Anti-torque Pedals

Another major problem that helicopter designers had to solve was the counteraction of the torque produced by the engine. As the rotor is mounted on the fuselage, according to the principle of conservation of the angular momentum, its torque moment generates an equal and opposite moment on the fuselage, making it spin. In a conventional single main rotor helicopter, this moment is counteracted by the force (thrust) generated by a small auxiliary rotor, located on a tail boom at the rear of the fuselage. The thrust produced by this rotor

is again controlled by varying the collective pitch of its blades, which is done by means of the application of two pedals, as depicted in Figure 2-3. The left pedal increases the yaw moment of the helicopter to the left and the other one is used to turn to the right. This moment can therefore be used not only to balance the main rotor torque, but also to provide directional control of the vehicle by changing its heading. The tail rotor has no cyclic pith system, adjusting itself by flapping, as Cierva's original rotor did (Prouty & Curtiss, 2003). Due to its high rotational speed and small radius, this flapping motion is often neglected.

Besides this classic single main rotor and tail rotor configuration, alternative strategies also exist to provide the torque balance. These are normally based on a twin main rotor configuration that uses two contrarotating rotors of equal size and loading, so that their torques are equal and opposing. The fact that they do not require a power-absorbing auxiliary rotor represents an advantage of this configuration but, on the other hand, the aerodynamic interferences between the two rotors may result in the loss of approximately the same amount of power. Some examples of twin rotor arrangements are presented in Figure 2-4. From the left to the right, these correspond respectively to a tandem configuration, a side-by-side placement and a coaxial arrangement of the two rotors.

(a) CH-47 Chinook. **(b)** V-22 Osprey. **(c)** Ka-50 Kamov.

Figure 2-4: Examples of twin rotors arrangements. [source: Google Images]

Due to its wide adoption, only the single main rotor and tail rotor configuration is analyzed in this research thesis. As it was seen, the three control inputs described throughout this section are associated with four angular deflections: the collective pitch, often represented by θ_0, the longitudinal and lateral cyclic pitch, θ_{1s} and θ_{1c}, respectively, and the collective pitch of the tail rotor θ_{0tr}.

2-1-4 From Mechanical Stabilization to Automatic Control Systems

The intense instabilities associated with helicopters and the consequent need for being constantly acting on the different controls at the same time represent the main reasons for an intensive workload of the pilot, making helicopter control a very challenging task. In the early years, mechanical stabilizing systems were implemented in rotary-wing aircraft to help with this task (Prouty & Curtiss, 2003). These systems, of which the Bell Stabilizing Bar and the Hiller Servo Rotor are important examples, are mainly based on external gyros.

In addition, on the first small helicopters, all of the control forces were modest and the pilot could act directly on the control mechanisms as depicted is Figure 2-3. Nevertheless, as helicopters got bigger, so did the forces and hydraulic boosted actuators had to be installed to help the pilot handling the helicopter by providing extra strength in the control deflections.

With the development of electronics, the hydraulic control actuators began to incorporate an electrohydraulic servovalve that can be operated by electric signals coming from a computer. With this configuration, the integration of automatic control laws became possible and Stability Augmentation Systems (SASs) with limited authorities around 10% of the actuator travel started being implemented to enhance the flying qualities of rotorcraft.

Once this system is incorporated and with the further development of flight control laws, full authority flight controllers became possible and the first helicopter autopilots were implemented. In this case, instead of controlling directly the control deflections, the pilot simply sends his intentions to the flight computer on board, which computes the required actions of the actuators to perform the desired maneuvers. The references commanded to the computer are normally supplied in terms of angular rates or attitude angles that correspond to the displacement of the conventional control interfaces in the cockpit which, in alternative, can be replaced by simple side-arm sticks. This type of configuration is the basis for Fly-By-Wire (FBW) systems and it is schematized in Figure 2-5.

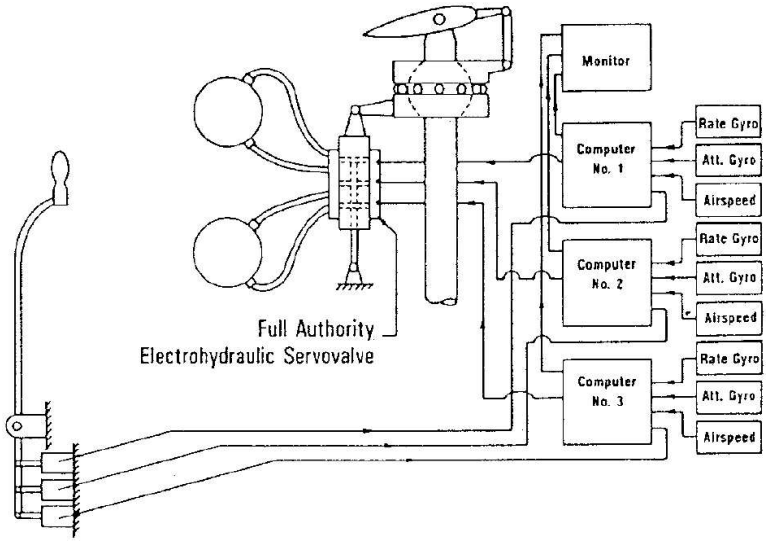

Figure 2-5: Fly-by-wire configuration in a helicopter. [source: (Prouty & Curtiss, 2003)]

As it can be seen, besides receiving the signals commanded from the pilot, the control computers also receive information from the helicopter sensors and monitors to provide an improved interface may also be included. Furthermore, to make these systems safe, they must be triply or even quadruply redundant (Prouty & Curtiss, 2003). By eliminating the mechanical linkages between the cockpit and the actuators, a reduction in the weight of the vehicle and in the complexity of its mechanical systems is achieved.

The behavior of the helicopter depends strongly on the performance of the flight control systems implemented in the computers. The work presented in the following chapters aims to develop a new approach to these laws and to assess the main advantages and drawbacks it brings when compared to the current technology. From now on, the dynamics of the actuators associated with the control inputs of the helicopter is assumed to be constrained by saturation and rate limits only.

2-2 Rotor Parameters and Systems of Reference

In the previous section, some concepts such as flapping motion and tip-path plane were introduced. In order to further clarify these concepts and to introduce all the definitions required to understand the development of the model adopted for the rotor, this section presents the necessary systems of reference and sign conventions. It in mainly based on (Pavel, 1996).

Appendix A contains information about the most common and well-known reference frames used in aircraft simulation. To study the rotor motion, it is however useful to define three more planes of reference as follows:

- The shaft (or hub) plane. As the name indicates, it is always perpendicular to the rotor shaft and it is therefore more simple and convenient to deduce the forces equilibrium with respect to it;
- The disc (or tip-path) plane. Again, as the name indicates, it is defined by the path described by the tip of the blades during their rotation. The thrust produced by the rotor is practically perpendicular to this plane;
- The control (or no-feathering) plane is actually a fictive plane. It would correspond to the disc plane if no rotor flapping motion existed and, for this reason, it is useful to measure the flapping angles relatively to it.

While in hovering flight these three planes coincide, in a more generic situation their relative positions are shown in Figure 2-6.

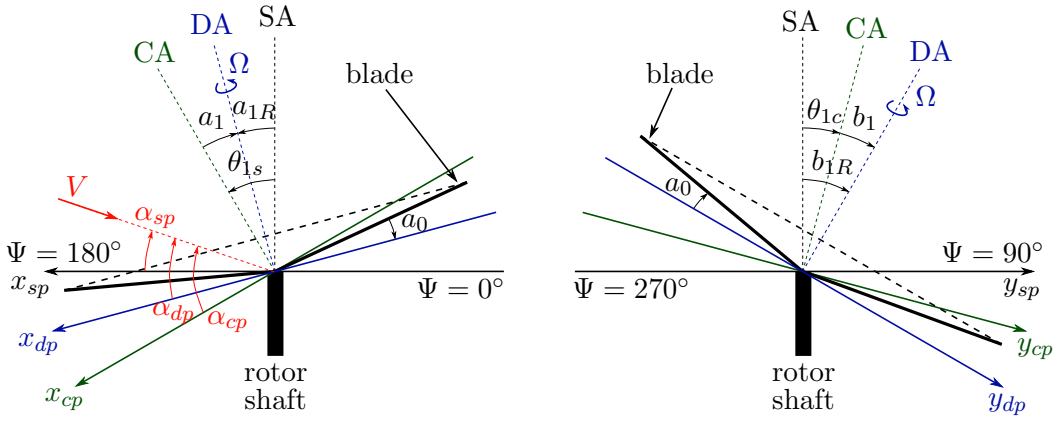

(a) Left view. **(b)** Aft view.

Figure 2-6: Rotor systems of reference and tilt angles.

Two orthogonal axes x and y can be defined coplanar with each plane, both with the origin at the center of the rotor hub. These axes are also depicted with different colors in the mentioned figure where the subscripts *sp*, *dp* and *cp* stand for shaft, disc and control plane, respectively. Additionally, with each plane there is an axis defined perpendicularly to it: Shaft Axis (SA), Disc Axis (DA) and Control Axis (CA). With them, a third coordinate z

can be associated in such a way that the 3-D frames are right-handed reference systems. For clarity of the figure under analysis, these are not represented. It is important to note that the three reference frames defined here do not rotate with the rotor blades. Also in this figure, some very important angles are presented, together with the arrows that indicate the sense in which they are defined positive. The physical meaning of these angles is now to be explained.

Despite the considerable flexibility of rotor blades, much of the helicopter theory can be derived regarding them as rigid bodies. With this assumption, in steady-state operation, blade motion is periodic around the azimuth Ψ. Hence, in these conditions, the flapping motion can be expanded as a Fourier series:

$$\beta(\Psi) = a_0 - a_1 \cos\Psi - b_1 \sin\Psi - a_2 \cos 2\Psi - b_2 \sin 2\Psi - ... \tag{2-1}$$

where β is the flapping angle, defined positive for upward deflections. For performance analysis and helicopter control, only its mean (a_0) and first harmonics (a_1 and b_1) are of primary importance for the rotor motion. In fact, it is demonstrated that the remaining harmonics have the same order as the elastic deflections of the blades and, for consistency with the rigid body assumption, they can be neglected. a_0 is known as the coning angle, a_1 is the longitudinal disc-tilt angle and b_1 is the lateral disc-tilt angle. Recalling the physical meaning of the flapping angles and taking into account that these are measured with respect to the control plane, the validity of expression (2-1) can also be checked from the analysis of Figure 2-6. For example, for $\Psi = 0^\circ : \beta \approx a_0 - a_1$, for $\Psi = 90^\circ : \beta \approx a_0 - b_1$, etc.

It is now possible to define the rotation to transform the reference system associated with the control plane into the disc plane $\underline{T}_{dp}^{cp}$. Using the rotor disc-tilt angles and the rotation matrices defined in Appendix A, it is easy to visualize that:

$$\underline{T}_{dp}^{cp} = \underline{R}_y(a_1)\underline{R}_x(b_1) = \begin{bmatrix} \cos a_1 & \sin a_1 \sin b_1 & -\sin a_1 \cos b_1 \\ 0 & \cos b_1 & \sin b_1 \\ \sin a_1 & -\cos a_1 \sin b_1 & \cos a_1 \cos b_1 \end{bmatrix} \tag{2-2}$$

Similarly to the flapping motion, also the pitch motion can be described by a Fourier series in steady-state conditions. Assuming that the blades present a linear twist θ_{tw}, the pitch angle is given by:

$$\theta(\Psi) = \theta_0 + \theta_{tw}\bar{r}_{bl} - \theta_{1c} \cos\Psi - \theta_{1s} \sin\Psi - \theta_{2c} \cos 2\Psi - \theta_{2s} \sin 2\Psi - ... \tag{2-3}$$

where $\bar{r}_{bl} = r_{bl}/R$ is the normalized value of the radial position of a blade element r_{bl}. Once again, the harmonics of second and higher order can be neglected and the angles θ_0, θ_{1c} and θ_{1s} are already known as collective pitch, lateral cyclic pitch and longitudinal cyclic pitch, respectively. For simplicity, the effect of the blade twist is not represented in Figure 2-6.

As depicted in the figure, it is also possible to define the flapping angles relatively to the shaft axis by making use of the cyclic pitch angles: $a_{1R} = a_1 - \theta_{1s}$ and $b_{1R} = b_1 + \theta_{1c}$. These are very useful to transform the forces generated by the rotor into the body-fixed reference frame of the helicopter. The only difference between the orientation of this system of reference and the shaft plane is a small forward tilt angle γ_s. Once again, applying the matrices presented in Appendix A, the transformation from the frame associated with the disc plane to the body

axes $\underline{T}_b^{dp}$ is defined by the rotation:

$$\begin{aligned}\underline{T}_b^{dp} &= \underline{R}_y(-a_{1R}-\gamma_s)\underline{R}_x(-b_{1R}) = \\ &= \begin{bmatrix} \cos(a_{1R}+\gamma_s) & \sin(a_{1R}+\gamma_s)\sin b_{1R} & \sin(a_{1R}+\gamma_s)\cos b_{1R} \\ 0 & \cos b_{1R} & -\sin b_{1R} \\ -\sin(a_{1R}+\gamma_s) & \cos(a_{1R}+\gamma_s)\sin b_{1R} & \cos(a_{1R}+\gamma_s)\cos b_{1R} \end{bmatrix}\end{aligned} \tag{2-4}$$

The lag motion in steady-state operation of the rotor may also be expanded as a Fourier series. Nevertheless, it will not be considered in the model to be developed since this is out of the scope of this thesis. Furthermore, the remaining blade motions can be analyzed with sufficient accuracy by treating them separately.

Also represented in Figure 2-6 are several angles of attack α between the different planes and the velocity of the airspeed of the helicopter in forward flight. The shaft plane angle of attack α_{sp} can be determined directly from the longitudinal and vertical components of the helicopter airspeed. The angle of attack relative to the control plane is then given by $\alpha_{cp} = \alpha_{sp} + \theta_{1s}$ and the disc plane angle of attack is $\alpha_{dp} = \alpha_{cp} + a_1$.

The resultant velocity seen by the rotor can therefore be resolved into components parallel and normal to the control plane and made dimensionless with the rotor tip speed ΩR. The parallel component corresponds simply to $V\cos\alpha_{cp}$, being quantified by the rotor advance ratio:

$$\mu_x = \frac{V\cos\alpha_{cp}}{\Omega R} \tag{2-5}$$

The normal component depends on the velocity of the vehicle and on the induced velocity ν_0 of the airflow that passes through the disc due to the production of lift. It is given by the rotor permeability:

$$\lambda = \mu_z - \lambda_0 = \frac{V\sin\alpha_{cp}}{\Omega R} - \frac{\nu_0}{\Omega R} \tag{2-6}$$

The calculation of the induced inflow ratio λ_0 is therefore of great importance and will be presented when the mathematical model of the helicopter rotor is deduced. For the aerodynamic calculations concerning the main rotor, the lateral inflow (due to the lateral component of the velocity) and thus the sideslip angle can normally be neglected. The effect of the lateral velocity is however contained in the absolute value of V.

Besides the parameters presented above, there are others very useful to characterize a rotor. The first one is the rotor disc area, given intuitively by:

$$A = \pi R^2 \tag{2-7}$$

Another one is the rotor solidity, defined as the ratio between the total blade area and the rotor disc area. If the rotor is composed by N blades with an equivalent chord c_e, this parameter is given by:

$$\sigma = \frac{Nc_e}{\pi R} \tag{2-8}$$

The equivalent chord corresponds to the chord of a rectangular blade that presents the same aerodynamic properties of the real (non-rectangular) blade. The last important parameter is the Lock number, which represents the ratio of the aerodynamic and inertial forces on a blade:

$$\gamma = \frac{\rho C_{L_\alpha} c_e R^4}{I_\beta} \tag{2-9}$$

where ρ is the air density, C_{L_α} is the blade lift curve slope and I_β is the moment of inertia of the blade about its flapping hinge.

These parameters will be very useful throughout the next section. They can also be defined for the tail rotor, being identified by the subscript tr in this case.

2-3 The 8 Degrees of Freedom Nonlinear Model

One of the most important issues in helicopter modelling is the choice of how much detail is required in terms of the number of mechanical Degrees Of Freedom (DOF) and the detail level of aerodynamic models. While accounting for a large number of DOF associated with the rotor dynamics results in a highly complex system, incorrect simplifications of the model may lead to the existence of important unmodeled dynamics. The key is to keep the essential effects and discard insignificant contributions of the system dynamics in the operating range of interest. Examples of simple helicopter modelling for small UAVs can be found in (Cunha & Silvestre, 2003) or (Vilchis, Brogliato, Dzul, & Lozano, 2003).

In (Pavel, 2001), a literature survey on helicopter simulation and modelling is presented and shows that, depending on the specific application, the number of DOF considered in the development of 3-D mathematical models varies typically from the most simple 6-DOF of the body only to a 16-DOF model that includes complex descriptions of the rotor dynamics and nonlinear aerodynamics. In a typical 6-DOF model, the motion of the rigid body in space is represented by three degrees of translation (u, v, w) and three degrees of rotation (p, q, r).

Furthermore, the required accuracy of the model also depends on the helicopter characteristics. For example, while a 6-DOF model usually suffices to determine natural aircraft behavior of an articulated helicopter, this approximation in no longer applicable to hingeless rotorcraft. This was explained in (Curtiss, 1986) as follows: "*the dynamics of the fuselage and rotor of an articulated helicopter can usually be seen as a cascade problem, a rapid rotor response followed by a slower fuselage response. For hingeless configurations, the body motion speeds up and the rotor dynamics enter into the body dynamics*". This type of influence is also strongly affected by the stiffness of the blades flapwise. According to (Hohenemser, 1974), the stiffer they are, the more the attitude of the rotor is "frozen" with respect to the fuselage and the larger are the fuselage attitude changes between hovering and cruising flight. From these examples, it can be seen that helicopter modelling is indeed a very complex process.

Also in the referred literature survey, it is concluded that, for the purpose of designing AFCSs to hingeless helicopters without using rotor feedback, the models adopted more often consist of the 6-DOF body simulation plus 2-DOF to account for the quasi-dynamic inflow of the main and tail rotors plus a quasi-steady or a first-order description of the rotor disc-tilt dynamics. For simplicity, in this research thesis only the steady-state rotor disc-tilt angles

are considered, but quite some effort is put on the determination of the disc-tilt angles (a_0, a_1, b_1) as accurately as possible, as it will be seen in the next subsection.

Extended models are normally used for handling qualities analysis and result from the expansion of the 8-DOF model in the following areas:

- Rotor disc-tilt dynamics. Second-order dynamics are included in the model instead of the first-order description or the simple steady-state angles;
- Rotor lag dynamics. As already mentioned, these dynamics are not considered in the 8-DOF model. They are mostly of primary importance for aeroelastic stability purposes and only during the 1980's more attention was paid to the study of their influence on flying qualities and controller design;
- Inflow dynamics. Instead of the quasi-dynamic description of the inflow induced by the rotors, a dynamic formulation that considers longitudinal and lateral variations of the inflow allows to obtain even more realistic results. These descriptions are based on different sets of coefficients and several methods exist to determine them. The one developed in (Pitt & Peters, 1981) is normally found to give the best representation of the inflow gradient;
- Engine dynamics. As explained in (Rohlfs, 1998), the helicopter yaw response, when considered as coupling response, is influenced by the dynamic engine and drive train torque. This means that, instead of assuming the rotor RPM constant ($\dot{\Omega} = 0$), a first-order differential equation can be used for the rotor speed of rotation. This consideration is often made when the scenario of the engine loss is simulated.

In this research thesis, the helicopter is modeled by subdividing it into its main components (main rotor, tail rotor, fuselage, horizontal and vertical tails) and adding the contribution of each part to the general system of forces and moments. The model adopted is mainly based on (Pavel, 2001). The flow is assumed incompressible, no reverse flow regions are considered and the tails and the fuselage are modeled with linear aerodynamics. The angular velocity of the main rotor is assumed constant and anticlockwise and, according to this assumption, the senses in which the control deflections and the disc-tilt angles are defined positive correspond to those indicated in Figure 2-6. Further assumptions associated with the rotor aerodynamics will be presented in more detail throughout the next subsection.

As mentioned in Chapter 1, the rotorcraft model analyzed throughout the present work is the Bölkow Bö-105, a light, multi-purpose utility helicopter. It is characterized by its hingeless rotor (Hohenemser, 1974) and all the parameters needed to simulate its dynamics are listed in Appendix B. To calculate the air density ρ, an atmospheric model had also to be implemented and its mathematical formulation is available in Appendix C. Figure 2-7 allows to more clearly understand the mathematical development carried out in the next subsections.

2-3-1 Main Rotor

The standard approach for the main rotor description is the blade element formulation in which each blade is discretisized into several sections and the local aerodynamic and inertia

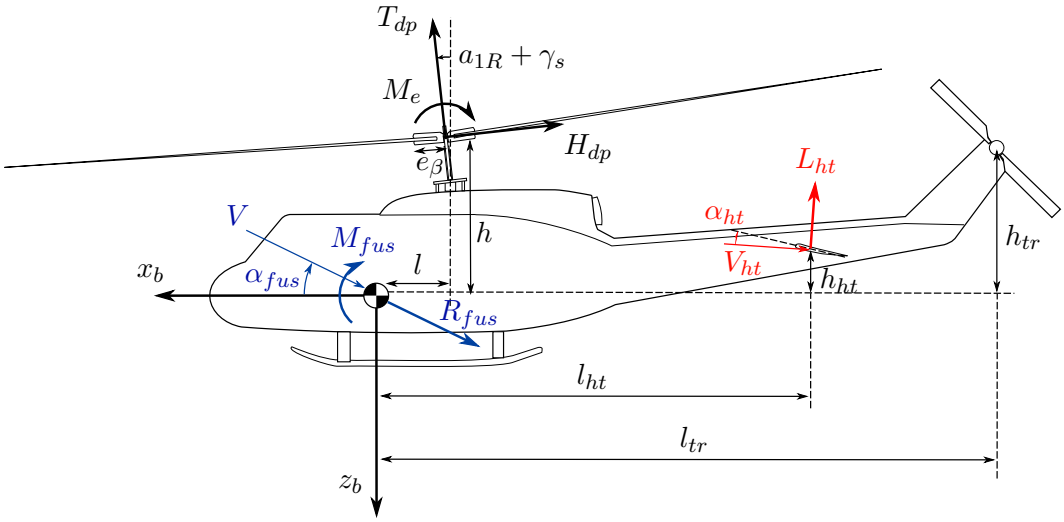

(a) Left view.

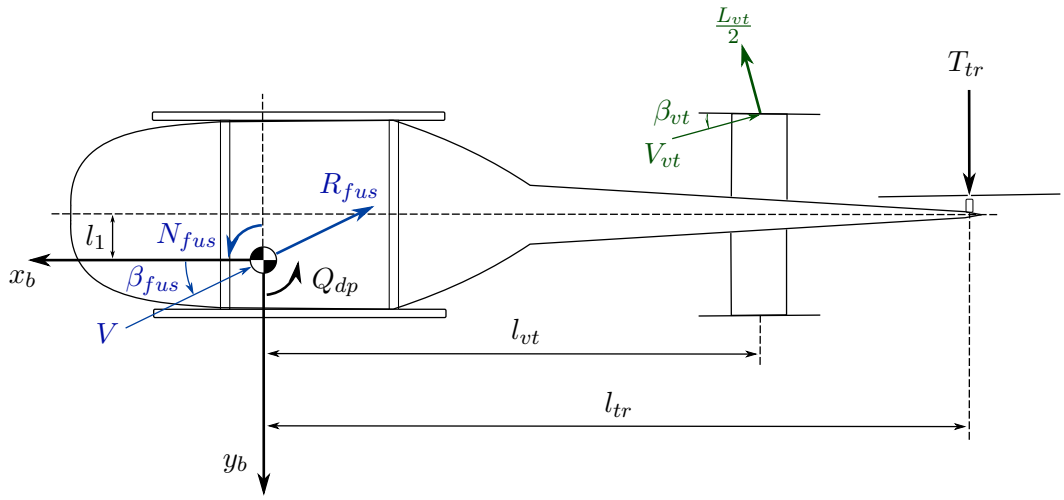

(b) Bottom view.

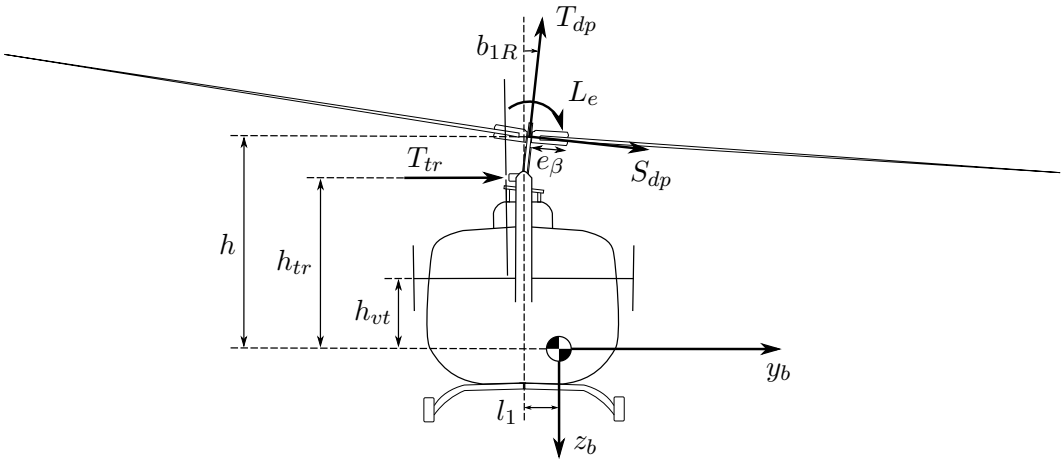

(c) Aft view.

Figure 2-7: Helicopter model.

forces are then summed up to determine the total rotor forces and moments. Each section acts as a two-dimensional airfoil. The validity of the blade element theory only holds for blades with high aspect ratio, which is normally true for rotary wings.

As it can be seen in Figure 2-8, the velocity of the air relative to the blade can be divided into a tangential u_T and a radial u_R component.

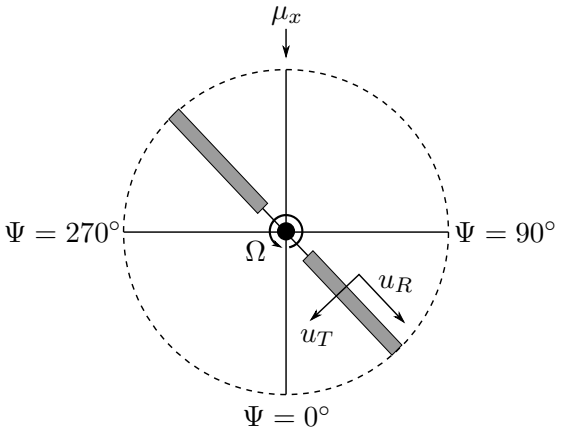

Figure 2-8: In-plane components of the air velocity relative to the blade.

At this point, the angular velocities of the helicopter are assumed to be null, meaning that the mentioned components have only to account for its forward speed and for the rotor rotation. They can be made dimensionless by dividing them by ΩR, yielding:

$$u_T = \bar{r}_{bl} + \mu_x \sin\Psi \tag{2-10}$$

$$u_R = \mu_x \cos\Psi \tag{2-11}$$

Furthermore, as depicted in Figure 2-9, there is also a component of the velocity perpendicular to the control plane, which depends on the permeability of the rotor, on the angular velocity of the blade due to the flapping motion $\dot{\beta}$ and on the influence of u_R when the blade is flapped up by the angle β.

The components associated with the flapping motion are schematized in Figure 2-10, in which the small angle assumption was made ($\cos\beta \approx 1$, $\sin\beta \approx \beta$). For hingeless helicopters, the substantial effect of blade bending flexibility in the rotorcraft flight dynamics can be taken into account by assuming rigid blades with root flexures at an equivalent hinge offset. This offset has a length $e_\beta = \varepsilon_\beta R$, where ε_β is the flapping hinge offset ratio, and it is also depicted in the referred figure.

According to this, the dimensionless perpendicular velocity in the blade is then given by:

$$u_P = -\lambda - (\bar{r}_{bl} - \varepsilon_\beta)\dot{\beta} - \beta\mu_x \cos\Psi \tag{2-12}$$

The resultant velocity U in each section of the blade is therefore influenced by the tangential and perpendicular components of the velocity. It defines an angle of attack α with the chord

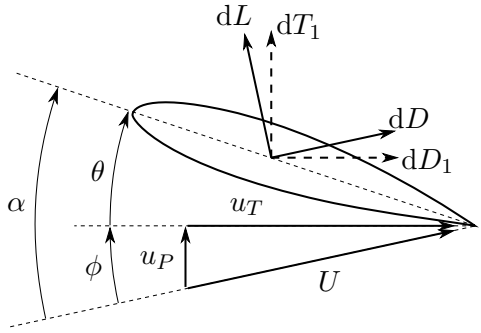

Figure 2-9: Aerodynamics of the rotor blade section.

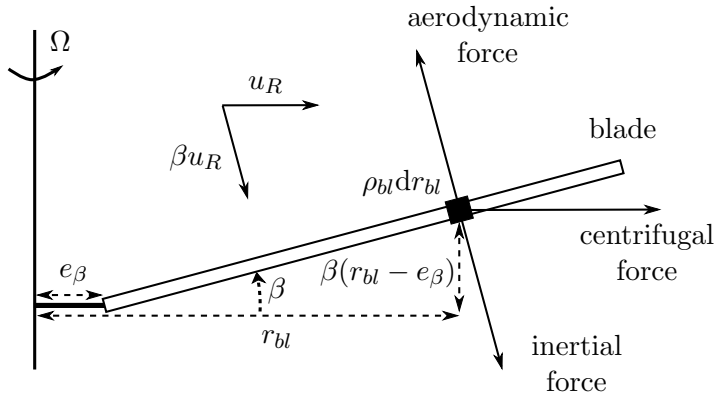

Figure 2-10: Air velocity and forces on a rotor blade for small flapping angles.

of the airfoil and an inflow angle ϕ with the control plane. If this angle is assumed small: $\phi \approx u_P/u_T$ and $U \approx u_T$. The pitch of the blade section is also related with these two angles: $\theta = \alpha - \phi$.

The aerodynamic elementary lift $\mathrm{d}L$ and drag $\mathrm{d}D$ forces are respectively normal and parallel to the velocity U and they can be expressed as:

$$\mathrm{d}L = \frac{1}{2}\rho\left(\Omega R u_T\right)^2 C_L c_e \mathrm{d}r_{bl} \tag{2-13}$$

$$\mathrm{d}D = \frac{1}{2}\rho\left(\Omega R u_T\right)^2 C_D c_e \mathrm{d}r_{bl} \tag{2-14}$$

and, when stall and compressibility effects are neglected, the two coefficients can be given by (W. Johnson, 1980):

$$C_L = C_{L_\alpha}\alpha \tag{2-15}$$

$$C_D = 0.0087 - 0.0216\alpha_{ef} + 0.4\alpha_{ef}^2 \tag{2-16}$$

In the expressions above C_{L_α} is the blade lift curve slope and α_{ef} is an effective angle of attack which, according to (Pavel, 1996), can be determined from a medium lift coefficient defined as:

$$C_{L_m} = C_{L_\alpha}\alpha_{ef} = \frac{6}{1+\mu_x^2/18}\frac{C_T}{\sigma} \tag{2-17}$$

The equation to compute the thrust coefficient C_T will be derived later on this subsection.

Furthermore, the aerodynamic forces can be resolved into a normal and an in-plane force, respectively, $\mathrm{d}T_1$ and $\mathrm{d}D_1$. Once again, making the small angles assumption and for $C_L \gg C_D$:

$$\mathrm{d}T_1 = \mathrm{d}L\cos\phi + \mathrm{d}D\sin\phi \approx \mathrm{d}L \tag{2-18}$$

$$\mathrm{d}D_1 = -\mathrm{d}L\sin\phi + \mathrm{d}D\cos\phi \approx -\mathrm{d}L\phi + \mathrm{d}D \tag{2-19}$$

where $\mathrm{d}T_1$ is the contribution of each blade element to the rotor thrust, the first component of $\mathrm{d}D_1$ is the induced drag and the second component is the profile drag. If the expressions obtained so far are used for these forces, the following results are obtained:

$$\mathrm{d}T_1 = \frac{1}{2}\rho\left(\Omega R\right)^2 c_e C_{L_\alpha}\left(\theta u_T^2 + u_T u_P\right) \tag{2-20}$$

$$\mathrm{d}D_1 = \frac{1}{2}\rho\left(\Omega R\right)^2 c_e\left[u_T^2 C_D - C_{L_\alpha}\left(\theta u_T u_P + u_P^2\right)\right] \tag{2-21}$$

Flapping Motion

Now consider the equilibrium of the inertial and aerodynamic moments about the equivalent flapping hinge acting on a mass element $\rho_{bl}\mathrm{d}r_{bl}$, where ρ_{bl} is the blade mass per unit length (assuming a uniform distribution along the blade) and $\mathrm{d}r_{bl}$ is the infinitesimal blade element, as shown in Figure 2-10. Here it is again assumed that the flapping angles are small and that the gravitational forces are also small when compared to the remaining ones. The aerodynamic force $\mathrm{d}T_1$ with moment arm $(r_{bl} - e_\beta)$ has therefore to be balanced by the inertial force $\rho_{bl}(r_{bl} - e_\beta)\ddot{\beta}$ with moment arm $(r_{bl} - e_\beta)$ and by the centrifugal force $\rho_{bl}\Omega^2 r_{bl}$ with moment arm $(r_{bl} - e_\beta)\beta$. To account for the total moments on the blade, the infinitesimal elements have to be integrated over its span, yielding:

$$\int_{e_\beta}^{R} \mathrm{d}T_1(r_{bl} - e_\beta)\,\mathrm{d}r_{bl} = \int_{e_\beta}^{R} \rho_{bl}(r_{bl} - e_\beta)^2\ddot{\beta}\,\mathrm{d}r_{bl} + \int_{e_\beta}^{R} \rho_{bl}\Omega^2 r_{bl}(r_{bl} - e_\beta)\beta\,\mathrm{d}r_{bl} \tag{2-22}$$

The left-hand side of the expression corresponds to the aerodynamic moment M_A and the equation can be rearranged as follows:

$$\begin{aligned} M_A &= \ddot{\beta}\int_{e_\beta}^{R} \rho_{bl}(r_{bl} - e_\beta)^2\,\mathrm{d}r_{bl} + \Omega^2\beta\left(\int_{e_\beta}^{R} \rho_{bl} r_{bl}^2\,\mathrm{d}r_{bl} - \int_{e_\beta}^{R} \rho_{bl} r_{bl} e_\beta\,\mathrm{d}r_{bl}\right) = \\ &= \ddot{\beta}\int_{e_\beta}^{R} \rho_{bl}(r_{bl} - e_\beta)^2\,\mathrm{d}r_{bl} + \Omega^2\beta\left(\int_{e_\beta}^{R} \rho_{bl}(r_{bl} - e_\beta)^2\,\mathrm{d}r_{bl} + \int_{e_\beta}^{R} \rho_{bl} e_\beta(r_{bl} - e_\beta)\,\mathrm{d}r_{bl}\right) = \\ &= \ddot{\beta}\int_{0}^{R-e_\beta} \rho_{bl} r_{bl}^2\,\mathrm{d}r_{bl} + \Omega^2\beta\left(\int_{0}^{R-e_\beta} \rho_{bl} r_{bl}^2\,\mathrm{d}r_{bl} + e_\beta\int_{0}^{R-e_\beta} \rho_{bl} r_{bl}\,\mathrm{d}r_{bl}\right) \end{aligned} \tag{2-23}$$

The integral $\int_0^{R-e_\beta} \rho_{bl} r_{bl}^2\,\mathrm{d}r_{bl}$ was already introduced as the blade flapping moment of inertia I_β. If the expression above is divided by this parameter, the following equation is obtained for the blade flapping motion:

$$\ddot{\beta} + \Omega^2\nu_\beta^2\beta = \frac{M_A}{I_\beta} \tag{2-24}$$

where, for blades with a uniform mass distribution and recalling that $e_\beta = \varepsilon_\beta R$:

$$\nu_\beta^2 = 1 + e_\beta \frac{\int_0^{R-e_\beta} \rho_{bl} r_{bl}\, \mathrm{d}r_{bl}}{\int_0^{R-e_\beta} \rho_{bl} r_{bl}^2\, \mathrm{d}r_{bl}} = 1 + \frac{3}{2}\frac{e_\beta}{R-e_\beta} = 1 + \frac{3}{2}\frac{\varepsilon_\beta}{1-\varepsilon_\beta} \tag{2-25}$$

It can be concluded that the left-hand side of equation (2-24) describes a mass-spring system with flapping natural frequency $\Omega\nu_\beta$. When there is no hinge offset ($\varepsilon_\beta = 0$), the later frequency matches the rotational speed of the rotor, which produces the centrifugal force that acts as a spring, opposing the blade flap motion. The primary effect of the existence of an equivalent hinge offset is primarily a small increase in the natural frequency of the flapping motion. The equivalent hinge offset ratio is then defined so that the theoretical natural frequency of the flapping motion matches its actual value. For the Bö-105, the physical flapping natural frequency is 1.12Ω (Hohenemser, 1974) and hence, from (2-25), $\varepsilon_\beta = 0.14$.

According to (2-22) and by making use of (2-20), it is possible to write the flapping aerodynamic moment as a function of the components of the velocity in a blade element:

$$M_A = \int_{e_\beta}^{R} \mathrm{d}T_1 (r_{bl} - e_\beta)\, \mathrm{d}r_{bl} = \frac{1}{2}\rho\,(\Omega R)^2\, c_e C_{L_\alpha} \int_{e_\beta}^{R} (\theta u_T^2 + u_T u_P)(r_{bl} - e_\beta)\, \mathrm{d}r_{bl} \tag{2-26}$$

At this point, some important remarks have to be made:

- Even without a hinge spring, the flapping motion is aerodynamically damped because of the presence of $\dot{\beta}$ in u_P (see (2-12));
- The computation of the integral above is quite complex (recall the expressions for u_T, u_P and θ, in the previous section);
- The fidelity of the equation (and its complexity) increases when more contributions (for example, the angular velocities of the helicopter) are accounted in u_T and u_P.

According to (Pavel, 2001), the flapping motion, as seen from a frame of reference rotating with the blades, can be divided into three time scales:

- Fast motions, corresponding to transients associated with the eigenfrequency of the blades;
- Intermediate fast motions, corresponding to the steady-state response of the blades to control inputs and body rotations;
- Slow motions, corresponding to the steady-state response of the blade to variations of the helicopter speed.

For simulation modelling, only the steady-state flapping motions of the blades are normally considered, meaning that the fast time scales are neglected. This can be intuitively explained from the fact that, for this type of application, one is not interested in the free motion of the blades, but on how their motion is transmitted to the airframe. Furthermore, the blades are assumed to respond instantaneously to control inputs, pitch motion and helicopter

velocity, resulting in an asymptotic approximation of the complete flapping behavior. This assumption is coherent with the truncation of the Fourier series (2-1) so that only the mean and first harmonics are of relevance.

One possible method to obtain these disc-tilt angles is explained in (W. Johnson, 1980). It involves the application of the operators $\frac{1}{2\pi}\int_0^{2\pi}(...)\,\mathrm{d}\Psi$, $\frac{1}{\pi}\int_0^{2\pi}(...)\cos\Psi\,\mathrm{d}\Psi$ and $\frac{1}{\pi}\int_0^{2\pi}(...)\sin\Psi\,\mathrm{d}\Psi$ to (2-24) and the definitions of the harmonics to replace the integrals of the blade motion by the Fourier coefficients. With this, the linear differential equations are reduced to linear algebraic equations for the harmonics. As stated in (Aalst & Pavel, 2002), one of the most simple and used solutions to express the disc-tilt angles from the referred equation is given by the so-called "Bramwell flapping angles":

$$a_0 = \frac{\gamma}{8}\left[\theta_0(1+\mu_x^2)+\frac{4}{3}\lambda+\frac{2}{3}\mu_x\bar{p}\right] \tag{2-27}$$

$$a_1 = \frac{\frac{8}{3}\mu_x\theta_0+2\mu_x\lambda+\bar{p}-\frac{16}{\gamma}\bar{q}}{1-\frac{1}{2}\mu_x^2} \tag{2-28}$$

$$b_1 = \frac{\frac{4}{3}\mu_x a_0+\bar{q}-\frac{16}{\gamma}\bar{p}}{1+\frac{1}{2}\mu_x^2} \tag{2-29}$$

where $\bar{p}=p/\Omega$ and $\bar{q}=q/\Omega$ are the dimensionless roll and pitch rates of the helicopter.

These expressions still do not account for some very important influences such as the blade twist or the hinge offset. To overcome this shortcoming, in (Pavel, 2001) the following expressions are suggested:

$$a_0 = \frac{\gamma}{8\nu_\beta^2}\left[\theta_0(1+\mu_x^2)+\frac{4}{3}\lambda+\frac{2}{3}\mu_x\bar{p}+\theta_{tw}\left(\frac{4}{5}+\frac{2}{3}\mu_x^2\right)-\frac{4}{3}\mu_x\theta_{1s}\right] \tag{2-30}$$

$$a_1 = \frac{8}{\gamma}\frac{\nu_\beta^2-1}{1-\frac{1}{2}\mu_x^2}b_1+\frac{\frac{8}{3}\mu_x\theta_0+2\mu_x\lambda+\bar{p}-\frac{16}{\gamma}\bar{q}+2\theta_{tw}\mu_x-\left(1+\frac{3}{2}\mu_x^2\right)\theta_{1s}}{1-\frac{1}{2}\mu_x^2} \tag{2-31}$$

$$b_1 = -\frac{8}{\gamma}\frac{\nu_\beta^2-1}{1+\frac{1}{2}\mu_x^2}a_1+\frac{\frac{4}{3}\mu_x a_0+\bar{q}-\frac{16}{\gamma}\bar{p}+\left(1+\frac{1}{2}\mu_x^2\right)\theta_{1c}}{1+\frac{1}{2}\mu_x^2} \tag{2-32}$$

In (Voskuijl, Pavel, Walker, Gubbels, & Manimala, 2009), another set of equations for the flapping blade is derived, including many higher-order coupling terms that are usually neglected in the classical formulations. Nevertheless, the effect of those terms is often quite small when compared to the classical formulations.

The expressions shown so far are derived assuming that the distribution of the induced velocity is uniform along the rotor disc. According to (Pavel, 1996), in order to account for non-uniformity effects, a correction factor:

$$K_{corr}=\frac{1.33\mu_x/|\lambda|}{1.2+\mu_x/|\lambda|} \tag{2-33}$$

is usually included in the formula of the lateral disc-tilt angle, yielding:

$$b_1 = -\frac{8}{\gamma}\frac{\nu_\beta^2-1}{1+\frac{1}{2}\mu_x^2}a_1+\frac{\frac{4}{3}\mu_x a_0+\bar{q}-\frac{16}{\gamma}\bar{p}+\left(1+\frac{1}{2}\mu_x^2\right)\theta_{1c}+K_{corr}\lambda_0}{1+\frac{1}{2}\mu_x^2} \tag{2-34}$$

Also in (Voskuijl et al., 2009), the influence of a sweep correction factor in the disc-tilt angles to account for the effects of non-steady flow around the airfoil is analyzed. This correction is given by:

$$\delta = \frac{4}{6}\frac{\mu_x \pi \sigma}{N} \ln\left(\frac{4}{3}\frac{\mu_x \pi \sigma}{N}\right) \tag{2-35}$$

It was concluded that, with respect to trim calculations of the Bö-105, this sweep effect provides an increased accuracy in the prediction of the lateral tilt of the rotor at low flight velocities, but a considerable degradation of the prediction at higher velocities. For this reason, it was decided not to use this correction factor in the model adopted and the rotor disc-tilt angles are therefore obtained with (2-30), (2-31) and (2-34).

Rotor Forces and Torque Moment

As depicted in Figure 2-11, due to the flapping angle β, the elementary aerodynamic force $\mathrm{d}T_1$ (see Figure 2-9) decomposes in an elementary force $\mathrm{d}T_2$ parallel to the control plane and in the elementary thrust of the rotor $\mathrm{d}T$, perpendicular to the referred plane.

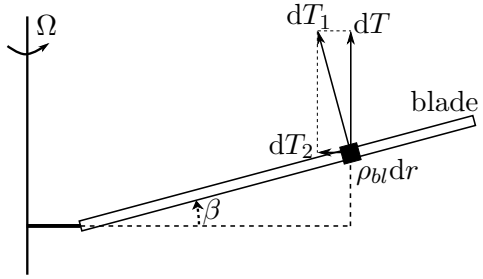

Figure 2-11: Out-of-plane forces acting on the rotor.

Assuming the small angle approximation for β and making use of (2-18):

$$\mathrm{d}T_2 = \mathrm{d}T_1 \sin\beta \approx \beta \mathrm{d}L \tag{2-36}$$

$$\mathrm{d}T = \mathrm{d}T_1 \cos\beta \approx \mathrm{d}L \tag{2-37}$$

Together with $\mathrm{d}D_1$ (see Figure 2-9), due to the flapping angle, $\mathrm{d}T_2$ also acts on the rotor as an in-plane force, as indicated in Figure 2-12. Depending on the azimuth angle, the resultant of these two forces can be decomposed in an elementary longitudinal drag force $\mathrm{d}H$ (opposing to the movement of the helicopter) and a lateral force $\mathrm{d}S$ (oriented from the regressing to the advancing side of the rotor).

Repeating the same procedure as before:

$$\mathrm{d}H = \mathrm{d}D_1 \sin\Psi - \mathrm{d}T_2 \cos\Psi \approx \mathrm{d}D \sin\Psi - \mathrm{d}L(\phi \sin\Psi + \beta \cos\Psi) \tag{2-38}$$

$$\mathrm{d}S = -\mathrm{d}D_1 \cos\Psi - \mathrm{d}T_2 \sin\Psi \approx -\mathrm{d}D \cos\Psi + \mathrm{d}L(\phi \cos\Psi - \beta \sin\Psi) \tag{2-39}$$

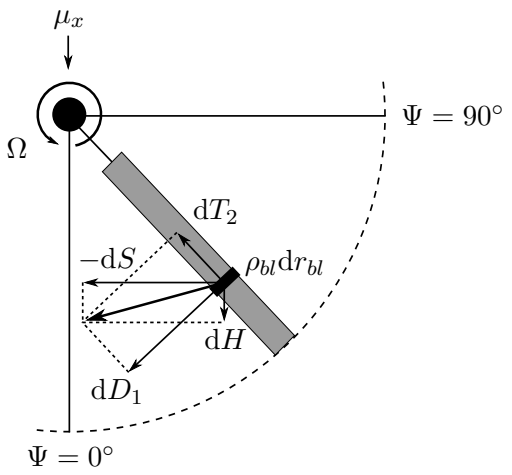

Figure 2-12: In-plane forces acting on the rotor.

Additionally, the torque moment Q of the rotor is simply due to the force D_1 times the arm r_{bl}, meaning that:

$$\mathrm{d}Q = r_{bl}\mathrm{d}D_1 \approx r_{bl}(\mathrm{d}D - \phi \mathrm{d}L) \tag{2-40}$$

The steady-state forces and moment acting on the rotor (T, H, S and Q) are then obtained from the integration of equations (2-37), (2-38), (2-39) and (2-40) over the blade span, averaging them over the azimuth and multiplying by the number of blades N. They can also be defined dimensionless with $T = \rho A\left(\Omega R\right)^2 C_T$, $H = \rho A\left(\Omega R\right)^2 C_H$, $S = \rho A\left(\Omega R\right)^2 C_S$ and $Q = \rho A\left(\Omega R\right)^2 R C_Q$, where:

$$C_T = \frac{N}{2\pi\rho A\left(\Omega R\right)^2}\int_0^{2\pi}\int_0^R \mathrm{d}L\,\mathrm{d}\Psi = \frac{\sigma}{4\pi}\int_0^{2\pi}\int_0^1 u_T^2 C_L\,\mathrm{d}\bar{r}_{bl}\mathrm{d}\Psi \tag{2-41}$$

$$\begin{aligned} C_H &= \frac{N}{2\pi\rho A\left(\Omega R\right)^2}\int_0^{2\pi}\int_0^R \left[\mathrm{d}D\sin\Psi - \mathrm{d}L(\phi\sin\Psi + \beta\cos\Psi)\right]\,\mathrm{d}\Psi = \\ &= \frac{\sigma}{4\pi}\int_0^{2\pi}\int_0^1 u_T^2\left[C_D\sin\Psi - C_L(\phi\sin\Psi + \beta\cos\Psi)\right]\,\mathrm{d}\bar{r}_{bl}\mathrm{d}\Psi \end{aligned} \tag{2-42}$$

$$\begin{aligned} C_S &= \frac{N}{2\pi\rho A\left(\Omega R\right)^2}\int_0^{2\pi}\int_0^R \left[-\mathrm{d}D\cos\Psi + \mathrm{d}L(\phi\cos\Psi - \beta\sin\Psi)\right]\,\mathrm{d}\Psi = \\ &= \frac{\sigma}{4\pi}\int_0^{2\pi}\int_0^1 u_T^2\left[-C_D\cos\Psi + C_L(\phi\cos\Psi - \beta\sin\Psi)\right]\,\mathrm{d}\bar{r}_{bl}\mathrm{d}\Psi \end{aligned} \tag{2-43}$$

$$\begin{aligned} C_Q &= \frac{N}{2\pi\rho A\left(\Omega R\right)^2 R}\int_0^{2\pi}\int_0^R \left[r_{bl}(\mathrm{d}D - \phi\mathrm{d}L)\right]\,\mathrm{d}\Psi = \\ &= \frac{\sigma}{4\pi}\int_0^{2\pi}\int_0^1 \left[\bar{r}_{bl}u_T^2(C_D - \phi C_L)\right]\,\mathrm{d}\bar{r}_{bl}\mathrm{d}\Psi \end{aligned} \tag{2-44}$$

As already mentioned, these coefficients are related to forces and moments represented in the control plane. Recalling the direction of these forces and the orientation of the axes associated with the latter plane, the force vector $\underline{f}$ generated by the main rotor is written in the system of reference associated with the control plane as $\underline{f}_{mr,cp} = [-H \ S \ -T]^T$, but it can also be defined in the frame related to the disc plane $\underline{f}_{mr,dp} = [-H_{dp} \ S_{dp} \ -T_{dp}]^T$. Moreover, the transformation between these two systems of reference was introduced in Section 2-2 and, from its application results:

$$\underline{f}_{mr,dp} = \underline{T}_{dp}^{cp} \underline{f}_{mr,cp} \Leftrightarrow \begin{bmatrix} -H_{dp} \\ S_{dp} \\ -T_{dp} \end{bmatrix} = \begin{bmatrix} \cos a_1 & \sin a_1 \sin b_1 & -\sin a_1 \cos b_1 \\ 0 & \cos b_1 & \sin b_1 \\ \sin a_1 & -\cos a_1 \sin b_1 & \cos a_1 \cos b_1 \end{bmatrix} \begin{bmatrix} -H \\ S \\ -T \end{bmatrix} \quad (2\text{-}45)$$

Using this equation, it is possible to obtain the coefficients of the forces in the disc plane from the ones in the control plane. Once again, using the small angle assumption for the rotor disc-tilt and, for the normal case in which $T \gg H, S$:

$$C_{T_{dp}} \approx C_T \quad (2\text{-}46)$$

$$C_{H_{dp}} \approx C_H - C_T a_1 \quad (2\text{-}47)$$

$$C_{S_{dp}} \approx C_S - C_T b_1 \quad (2\text{-}48)$$

Similarly, it can be concluded that the rotor torque moment in the control axis corresponds approximately to the torque about the disc axis and that the remaining components that are originated in this reference frame are null. Hence:

$$C_{Q_{dp}} \approx C_Q \quad (2\text{-}49)$$

These coefficients can therefore be determined once the integrals (2-41) to (2-44) are solved. Nevertheless, it is important to have in mind that:

- As explained for the flapping equation of motion, the integrals are extremely complex to compute since they depend directly on u_T, but also on u_P through the influence of the angle of attack α on $\mathrm{d}C_L$ and $\mathrm{d}C_D$. Furthermore, α also depends on the pitch of the blades θ which, as already seen, is described by a truncated Fourier series on Ψ;
- As it was already mentioned, the expressions for the dimensionless velocities can become rather complex when more influences (for example, the angular velocities of the helicopter) are considered;
- The effects of root cutout and tip loss can be simply introduced by changing the lower and upper limits of integration, respectively.

The equations adopted for the coefficients in this research thesis correspond to a simplified version of the formulae available in (Pavel, 2001):

$$C_{T_{dp}} = \frac{\sigma C_{L_\alpha}}{2} \left[\left(\frac{1}{3} + \frac{\mu_x^2}{2} \right) \theta_0 + \frac{1 + \mu_x^2}{8} \theta_{tw} + \frac{\mu_x \bar{p}}{4} + \frac{\lambda}{2} \right] \quad (2\text{-}50)$$

$$C_{H_{dp}} = \sigma C_D \frac{\mu_x}{4} + \frac{\sigma C_{L_\alpha}}{4}\left[\left(a_1\frac{\mu_x^2}{2} + \mu_x\lambda\right)\theta_0 + \frac{\mu_x\lambda}{2}\theta_{tw} + \right.$$
$$\left. + \bar{q}\left(\frac{b_1\mu_x}{4} - \frac{a_0}{3}\right) - \frac{a_0 b_1}{3} + (a_0^2 + a_1^2)\frac{\mu_x}{2} + \frac{\bar{p}\lambda}{2}\right] \quad (2\text{-}51)$$

$$C_{S_{dp}} = \frac{\sigma C_{L_\alpha}}{4}\left[-\frac{1}{2}\mu_x a_0\theta_0 + \left(-a_0\frac{\mu_x}{3} + b_1\frac{\mu_x^2}{4} - \frac{\bar{q}}{4}\right)\theta_{tw} - \right.$$
$$\left. - 3a_0\mu_x\left(\mu_x a_1 - \lambda\right) + b_1\frac{\mu_x a_1 - \lambda}{2} + a_0 a_1\frac{\mu_x^2 + 1}{3}\right] \quad (2\text{-}52)$$

According to (Pavel, 1996), the torque coefficient can be approximated as a function of the remaining ones:

$$C_{Q_{dp}} = \sigma\left[\frac{C_D}{8}\left(1 + 4.7\mu_x^2\right) - C_{T_{dp}}\lambda_{dp} - C_{H_{dp}}\mu_x\right] \quad (2\text{-}53)$$

in which $\lambda_{dp} = \frac{V}{\Omega R}\sin\alpha_{dp} - \lambda_0$ is the rotor permeability relative to the disc plane.

Global Contribution

After the calculation of the forces and torque moment generated by the main rotor from the coefficients above, the computation of their contribution to the motion on the helicopter is very easy to obtain. The contribution of the forces corresponds simply to the transformation of the vector relative to the disc plane $\underline{f}_{mr,dp}$ into the body axes using (2-4):

$$\underline{f}_{mr} = \begin{bmatrix} X_{mr} \\ Y_{mr} \\ Z_{mr} \end{bmatrix} = \underline{T}_b^{dp}\,\underline{f}_{mr,dp} =$$
$$= \begin{bmatrix} \cos\left(a_{1R} + \gamma_s\right) & \sin\left(a_{1R} + \gamma_s\right)\sin b_{1R} & \sin\left(a_{1R} + \gamma_s\right)\cos b_{1R} \\ 0 & \cos b_{1R} & -\sin b_{1R} \\ -\sin\left(a_{1R} + \gamma_s\right) & \cos\left(a_{1R} + \gamma_s\right)\sin b_{1R} & \cos\left(a_{1R} + \gamma_s\right)\cos b_{1R} \end{bmatrix} \begin{bmatrix} -H_{dp} \\ S_{dp} \\ -T_{dp} \end{bmatrix} \quad (2\text{-}54)$$

In addition, the contribution of the moments $\underline{m}$ corresponds not only to the torque generated by the rotor Q_{dp}, acting practically along the z-axis, but also to supplementary roll L_e and pitch M_e moments due to the blade hinge offset and to the effect of the arm between the point of application of the forces and the helicopter CG. The coordinates of the referred point in the body-fixed reference system are, as indicated in Figure 2-7, $[-l \;\; -l_1 \;\; -h]^T$ and the contribution of the moments is therefore:

$$\underline{m}_{mr} = \begin{bmatrix} L_{mr} \\ M_{mr} \\ N_{mr} \end{bmatrix} = \begin{bmatrix} L_e \\ M_e \\ Q_{dp} \end{bmatrix} + \begin{bmatrix} -l \\ -l_1 \\ -h \end{bmatrix} \times \underline{f}_{mr} = \begin{bmatrix} L_e + hY_{mr} - l_1 Z_{mr} \\ M_e - hX_{mr} + lZ_{mr} \\ Q_{dp} + l_1 X_{mr} - lY_{mr} \end{bmatrix} \quad (2\text{-}55)$$

The moments L_e and M_e result from the centrifugal forces introduced by the eccentricity due to the blade hinge offset. These supplementary roll and pitch moments are derived in (Pavel, 2001) and given respectively by:

$$L_e = (\Omega R)^2 \varepsilon_\beta m_{bl} \sin b_{1r} \tag{2-56}$$

$$M_e = (\Omega R)^2 \varepsilon_\beta m_{bl} \sin(a_{1r} + \gamma_s) \tag{2-57}$$

Quasi-dynamic Inflow

In the blade element theory, it is assumed that the induced velocity is uniform over the rotor disc. While this is a good assumption at high forward speeds, at low speeds the order of magnitude of this inflow velocity approaches the other velocity components at the rotor blade. On the other hand, a different type of analysis was proposed by Glauert and it is based on the momentum theory. This approach regards the rotor as an actuator disc. An actuator disc is simply a circular surface of zero thickness that can support a pressure difference and thus accelerate the air through it. The loading is assumed to be steady, but in general it may vary over its surface. It is important to note that this model represents simply an ideal approximation of the actual rotor, which would be equivalent to considering an infinite number of blades. Obviously, since this imposes a limitation in the applicability of this theory, it is mainly used to obtain a first estimate of the wake-induced flow (W. Johnson, 1980).

Consider first an actuator disc of area A and total thrust T in hover, as the one depicted in Figure 2-13. Let ν_0 be the induced velocity at the rotor disc and ν_∞ the wake-induced velocity infinitely far downstream, where the pressure is at the ambient level p_0. Assume also that the rotational energy in the wake due to the rotor torque is neglected and that the fluid is incompressible and inviscid.

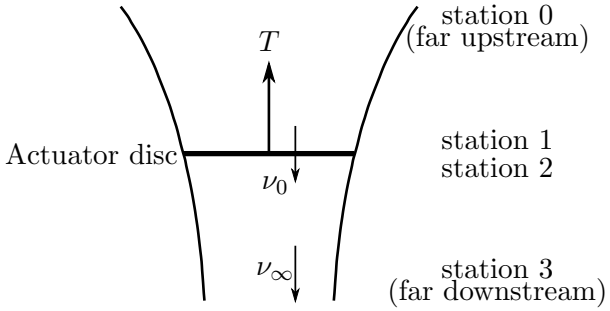

Figure 2-13: Momentum theory flow model for hover.

By conservation of mass, the mass flux is constant all along the wake, corresponding to $\dot{m} = \rho A \nu_0$. Momentum conservation states that the thrust of the rotor imposes a rate of change of the flow momentum. Since the flow far upstream is at rest for the hovering rotor, this results in:

$$T = \dot{m}\nu_\infty = \rho A \nu_0 \nu_\infty \tag{2-58}$$

Applying Bernoulli's equation between stations 0 and 1 and stations 2 and 3 yields:

$$p_0 = p_1 + \frac{1}{2}\rho \nu_0^2 \tag{2-59}$$

$$p_2 + \frac{1}{2}\rho\nu_0^2 \;=\; p_0 + \frac{1}{2}\rho\nu_\infty^2 \tag{2-60}$$

and, combining these equations:

$$p_2 - p_1 = \frac{1}{2}\rho\nu_\infty^2 \tag{2-61}$$

The increase in total pressure from stations 1 to 2 is due to the disc loading T/A, hence:

$$p_2 - p_1 = \frac{T}{A} \Leftrightarrow \frac{1}{2}\rho\nu_\infty^2 = \rho\nu_0\nu_\infty \Leftrightarrow \nu_\infty = 2\nu_0 \tag{2-62}$$

confirming that the wake is indeed contracting, as shown in the figure. If this result is applied in (2-58), the following expression for the rotor thrust is obtained:

$$T = 2\rho A\nu_0^2 \tag{2-63}$$

Now consider the actuator disc is operating at a velocity V with an angle of attack α_{dp}. This situation is illustrated in Figure 2-14.

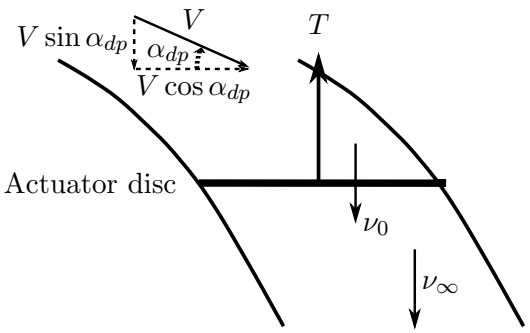

Figure 2-14: Momentum theory flow model for forward flight.

The velocity of the flow in the wake far downstream is still $\nu_\infty = 2\nu_0$, since it is assumed to be parallel to the rotor thrust vector, but the velocity of the flow that passes through the disc is now $\sqrt{(V\cos\alpha_{dp})^2 + (V\sin\alpha_{dp} + \nu_0)^2}$ instead of simply ν_0. Applying the same considerations as before, the thrust force is given by:

$$T = \dot{m}\nu_\infty = 2\rho A\nu_0\sqrt{(V\cos\alpha_{dp})^2 + (V\sin\alpha_{dp} + \nu_0)^2} \tag{2-64}$$

and using the dimensionless quantities $\mu = V/\Omega R$ and $\lambda_0 = \nu_0/\Omega R$, the thrust coefficient $C_T = T/\rho A\,(\Omega R)^2$ obtained from the Glauert theory is:

$$C_T^{Gl} = 2\lambda_0\sqrt{(\mu\cos\alpha_{dp})^2 + (\mu\sin\alpha_{dp} + \lambda_0)^2} \tag{2-65}$$

The dynamic inflow of the main rotor λ_0 is included in the model as a state variable and can be described by a quasi-dynamic inflow by means of the time constant τ_{λ_0}. Its time derivative is proportional to the difference between the thrust coefficients calculated with the blade element method C_T and with Glauert theory C_T^{Gl}. Note that, in steady operation, both thrust coefficients shall coincide. The differential equation that describes the quasi-dynamic inflow of the main rotor in then given by:

$$\tau_{\lambda_0}\dot{\lambda}_0 = C_T - C_T^{Gl} \tag{2-66}$$

2-3-2 Tail Rotor

The modelling of the tail rotor is similar to the main rotor, but it results in a much simpler description since it has no cyclic pitch and, as already mentioned, its flapping motion can be neglected. In this case, the three rotor planes coincide. Additionally, the torque moment produced by the tail rotor can also normally be neglected. This means that this rotor only contributes to the global system with the thrust force it generates. It is also assumed that the blades of this rotor do not present any twist angle. For the following derivation and as it was done for the main rotor in Section 2-2, it is convenient to define dimensionless quantities associated with the airspeed at the tail rotor. Hence, the advance ratio and the permeability of this rotor are respectively given by:

$$\mu_{x_{tr}} = \frac{\sqrt{u^2 + (w + K_{tr}\Omega R\lambda_0 + q l_{tr})^2}}{\Omega_{tr} R_{tr}} \tag{2-67}$$

$$\lambda_{tr} = -\frac{v - r l_{tr} + p h_{tr}}{\Omega_{tr} R_{tr}} - \lambda_{0_{tr}} \tag{2-68}$$

where K_{tr} is the main rotor downwash factor at the tail rotor and $\lambda_{0_{tr}}$ is the tail rotor inflow ratio. The dimensions l_{tr} and h_{tr} are depicted in Figure 2-7.

Rotor Force

Using the dimensionless parameters introduced, the thrust coefficient of the tail rotor based on the blade element method is simply given by:

$$C_{T_{tr}} = \frac{\sigma_{tr} C_{L_{\alpha,tr}}}{2}\left[\left(\frac{1}{3} + \frac{\mu_{x_{tr}}^2}{2}\right)\theta_{0tr} + \frac{\lambda_{tr}}{2}\right] \tag{2-69}$$

Note the similarity of this expression with (2-50). The tail rotor thrust force is then defined as $T_{tr} = \rho A_{tr}(\Omega_{tr} R_{tr})^2 C_{T_{tr}}$.

Global Contribution

The force calculated above only contributes to the y component of the global force acting on the helicopter. Furthermore, the aerodynamic interference caused by the vertical tail is accounted by a fin blockage factor suggested in (Padfield, 1996): $F_{tr} = 1 - 3S_{vt}/(4\pi R_{tr}^2)$. The total force is therefore given by:

$$\underline{f}_{tr} = \begin{bmatrix} X_{tr} \\ Y_{tr} \\ Z_{tr} \end{bmatrix} = \begin{bmatrix} 0 \\ T_{tr} F_{tr} \\ 0 \end{bmatrix} \tag{2-70}$$

In addition, this force also generates two moments with arms h_{tr} and l_{tr} that have to be accounted for:

$$\underline{m}_{tr} = \begin{bmatrix} L_{tr} \\ M_{tr} \\ N_{tr} \end{bmatrix} = \begin{bmatrix} h_{tr} Y_{tr} \\ 0 \\ -l_{tr} Y_{tr} \end{bmatrix} \tag{2-71}$$

Quasi-dynamic Inflow

As for the main rotor, the dynamic inflow of the tail rotor $\lambda_{0_{tr}}$ is included in the model as a state variable, being described by a quasi-dynamic inflow with a time constant $\tau_{\lambda_{0,tr}}$:

$$\tau_{\lambda_{0,tr}}\dot{\lambda}_{0_{tr}} = C_{T_{tr}} - C_{T_{tr}}^{Gl} \tag{2-72}$$

The expression for the thrust coefficient obtained with Glauert theory for this case is simply:

$$C_{T_{tr}}^{Gl} = 2\lambda_{0_{tr}}\sqrt{\mu_{x_{tr}}^2 + \lambda_{tr}^2} \tag{2-73}$$

2-3-3 Fuselage

The main influence of the fuselage can be represented by the production of a drag force R_{fus}, aligned with the velocity vector and given approximately by:

$$R_{fus} = \frac{1}{2}\rho V^2 F_0 \tag{2-74}$$

where the parasite drag area F_0 corresponds to the area of a flat-plate plane that would generate a drag force equivalent to the fuselage. Note that this force can be represented in the velocity reference frame simply as $[-R_{fus}\ 0\ 0]^T$. In addition, due to the aerodynamic angles between the velocity and the body-fixed reference frame, a pitch and a yaw moment will also appear.

The pitch moment is associated with the coefficient:

$$C_{M_{fus}} = \left(\frac{V}{\Omega R}\right)^2 \frac{1}{AR} K_{fus} V_{fus_M} \left(\alpha_{fus} - \alpha_{fus_{M=0}} - \epsilon_0\right) \tag{2-75}$$

In this equation, K_{fus} is a correction coefficient that depends on the dimensions of the fuselage, V_{fus_M} is the volume of a body equivalent to the fuselage with the same view in the horizontal plane but having circular sections, $\alpha_{fus} = -\arctan(w/u)$ is the fuselage incidence (see Figure 2-7), $\alpha_{fus_{M=0}}$ is the value of the latter angle for which $M_{fus} = 0$ and ϵ_0 is the average downwash angle. In this research thesis, the effect of this angle will not be considered but, for high velocities, it could be approximated as $\epsilon_0 = \nu_0/V$.

For the yaw moment, the following coefficient can be defined as:

$$C_{N_{fus}} = \left(\frac{V}{\Omega R}\right)^2 \frac{1}{AR} K_{fus} V_{fus_N} \beta_{fus} \tag{2-76}$$

where V_{fus_N} is the volume of a body equivalent to the fuselage with the same lateral view but having circular sections and $\beta_{fus} = \arcsin(v/V)$ is the sideslip angle.

The contribution of the forces to the overall system has to be expressed in the body-fixed reference frame, which can be achieved with two rotation matrices (see Appendix A):

$$\underline{f}_{fus} = \begin{bmatrix} X_{fus} \\ Y_{fus} \\ Z_{fus} \end{bmatrix} = \underline{R}_y(\alpha_{fus})\underline{R}_z(-\beta_{fus}) \begin{bmatrix} -R_{fus} \\ 0 \\ 0 \end{bmatrix} = -R_{fus} \begin{bmatrix} \cos\beta_{fus}\cos\alpha_{fus} \\ \sin\beta_{fus} \\ \cos\beta_{fus}\sin\alpha_{fus} \end{bmatrix} \tag{2-77}$$

The moments are simply given by:

$$\underline{m}_{fus} = \begin{bmatrix} L_{fus} \\ M_{fus} \\ N_{fus} \end{bmatrix} = \rho A(\Omega R)^2 R \begin{bmatrix} 0 \\ C_{M_{fus}} \\ C_{N_{fus}} \end{bmatrix} \tag{2-78}$$

2-3-4 Horizontal Tail

The horizontal tail is used to increase flight efficiency and acts as a wing in forward flight. Its influence can be considered only by the lift force it produces, since its drag can normally be neglected when compared to the latter. The lift force is then given by:

$$L_{ht} = \frac{1}{2}\rho V_{ht}^2 S_{ht} C_{L_{\alpha,ht}} \alpha_{ht} \tag{2-79}$$

where S_{ht} is the area of this surface and $C_{L_{\alpha,ht}}$ is the lift curve slope of its airfoil. The air velocity at this tail V_{ht} depends on the longitudinal and vertical velocity of the helicopter, but also on its pitch rate:

$$V_{ht} = \sqrt{u^2 + (w + q l_{ht})^2} \tag{2-80}$$

The most important contributions to the incidence of the horizontal tail α_{ht} are the angle of attack between the velocity above and the surface under analysis, the built-in horizontal tail incidence α_{ht_0} and the average downwash angle at this tail $K_{ht}\epsilon_0$. Regarding the later, K_{ht} is a correction coefficient that depends mainly on the location of the tail and ϵ_0 can again be approximated by ν_0/V. As for the fuselage, this angle will not be considered in the simulation. Combining all the influences, the incidence of the horizontal tail is then given by:

$$\alpha_{ht} = \arctan\left(\frac{w + q l_{ht}}{u}\right) + \alpha_{ht_0} - K_{ht}\epsilon_0 \tag{2-81}$$

Assuming a small angle of attack α_{ht}, the contribution of this surface to the global forces acting on the helicopter is simply:

$$\underline{f}_{ht} = \begin{bmatrix} X_{ht} \\ Y_{ht} \\ Z_{ht} \end{bmatrix} = \begin{bmatrix} 0 \\ 0 \\ -L_{ht} \end{bmatrix} \tag{2-82}$$

Due to the distance l_{ht} between the horizontal tail and the helicopter CG (see Figure 2-7), also a pitch moment is generated, yielding:

$$\underline{m}_{ht} = \begin{bmatrix} L_{ht} \\ M_{ht} \\ N_{ht} \end{bmatrix} = \begin{bmatrix} 0 \\ l_{ht} Z_{ht} \\ 0 \end{bmatrix} \tag{2-83}$$

2-3-5 Vertical Tail

Similarly to the previous case, the vertical tail is also considered by the lift force generated by the two surfaces when a sideslip angle exists (see Figure 2-7). The referred force is then given by:

$$L_{vt} = \frac{1}{2}\rho V_{vt}^2 S_{vt} C_{L_{\alpha,vt}} \beta_{vt} \tag{2-84}$$

where again S_{ht} is the total area of the two surfaces and $C_{L_{\alpha,vt}}$ is the lift curve slope of their airfoil. The air velocity at this tail V_{vt} depends on the longitudinal and lateral velocities of the helicopter, but also on its roll and yaw rates:

$$V_{vt} = \sqrt{u^2 + (v + ph_{vt} - rl_{vt})^2} \tag{2-85}$$

The most important contributions to the incidence of the vertical tail β_{vt} are the angle of attack between this velocity and the surfaces under analysis and the built-in vertical tail incidence β_{vt_0}. Combining these influences, the incidence of the vertical tail is then given by:

$$\beta_{vt} = \arctan\left(\frac{v + ph_{vt} - rl_{vt}}{u}\right) + \beta_{vt_0} \tag{2-86}$$

For small sideslip angles β_{vt}, the contribution of this surfaces to the global forces acting on the helicopter is approximated by:

$$\underline{f}_{vt} = \begin{bmatrix} X_{vt} \\ Y_{vt} \\ Z_{vt} \end{bmatrix} = \begin{bmatrix} 0 \\ -L_{vt} \\ 0 \end{bmatrix} \tag{2-87}$$

Due to the distance between the vertical tail and the helicopter CG, also a roll and a yaw moment are also produced, yielding:

$$\underline{m}_{vt} = \begin{bmatrix} L_{vt} \\ M_{vt} \\ N_{vt} \end{bmatrix} = \begin{bmatrix} h_{vt} Y_{vt} \\ 0 \\ -l_{vt} Y_{vt} \end{bmatrix} \tag{2-88}$$

2-3-6 Equations of Motion

The Equations Of Motion (EOM) that describe the movement of the helicopter are exactly the same used for the motion of a fixed-wing aircraft. They are therefore very well-known and widely used in the field of Aerospace Engineering, so their derivation is not shown in this research thesis. It can be found, for example, in (Etkin, 1972). Appendix A contains the definition of the reference frames adopted for their application and the transformation matrices between them. To express these equations, the following vectors shall be defined:

- The body-fixed linear velocity vector: $\underline{v} = [u\ v\ w]^T$;
- The position of the helicopter CG expressed in the North-East-Down (NED) reference frame: $\underline{p} = [x\ y\ z]^T$;

- The body-fixed angular velocity vector: $\underline{\omega} = [p\ q\ r]^T$;
- The Euler angles that parametrize the orientation of the helicopter relative to the NED reference frame: $\underline{\theta} = [\phi\ \theta\ \psi]^T$;
- The vector containing the inflow ratios of both rotors: $\underline{\lambda} = [\lambda_0\ \lambda_{0_{tr}}]^T$;
- The total force vector, containing the contributions of all the components presented in the previous subsections: $\underline{f} = \underline{f}_{mr} + \underline{f}_{tr} + \underline{f}_{fus} + \underline{f}_{ht} + \underline{f}_{vt}$;
- The total moment vector, again with the contributions of all the components of the helicopter: $\underline{m} = \underline{m}_{mr} + \underline{m}_{tr} + \underline{m}_{fus} + \underline{m}_{ht} + \underline{m}_{vt}$.

For the following equations, it is assumed that the helicopter is a rigid body with constant mass and inertia over the duration of the motion, as well as a flat and non-rotating Earth. Furthermore, the gravity field of the planet is assumed to be uniform and thus the helicopter CG coincides with its center of mass.

The first EOM corresponds to the dynamics of the translational motion and it is given by:

$$\dot{\underline{v}} = \frac{1}{m}\underline{f} + \underline{T}_b^o \begin{bmatrix} 0 \\ 0 \\ g \end{bmatrix} - \underline{\omega} \times \underline{v} = \frac{1}{m}\underline{f} + g \begin{bmatrix} -\sin\theta \\ \sin\phi\cos\theta \\ \cos\phi\cos\theta \end{bmatrix} - \begin{bmatrix} qw - rv \\ ru - pw \\ pv - qu \end{bmatrix} \tag{2-89}$$

where m and g are, respectively, the total mass of the helicopter and the gravitational acceleration, both assumed constant during the simulation.

The second EOM describes the kinematics of the translational motion of the vehicle:

$$\begin{aligned} \dot{\underline{p}} &= \underline{T}_o^b \underline{v} = \\ &= \begin{bmatrix} \cos\psi\cos\theta & \cos\psi\sin\theta\sin\phi - \sin\psi\cos\phi & \cos\psi\sin\theta\cos\phi + \sin\psi\sin\phi \\ \sin\psi\cos\theta & \sin\psi\sin\theta\sin\phi + \cos\psi\cos\phi & \sin\psi\sin\theta\cos\phi - \cos\psi\sin\phi \\ -\sin\theta & \cos\theta\sin\phi & \cos\theta\cos\phi \end{bmatrix} \underline{v} \end{aligned} \tag{2-90}$$

Analogously, there is an equation related to the dynamics of the rotational motion:

$$\dot{\underline{\omega}} = \underline{J}^{-1} \left[\underline{m} - \underline{\omega} \times \underline{J}\underline{\omega} \right] \tag{2-91}$$

in which $\underline{J}$ is the inertia matrix of the helicopter, assumed constant during the simulation.

Another equation is also needed to describe the kinematics of the rotational motion, corresponding to:

$$\dot{\underline{\theta}} = \underline{\Omega}_o^b \underline{\omega} = \begin{bmatrix} 1 & \sin\phi\tan\theta & \cos\phi\tan\theta \\ 0 & \cos\phi & -\sin\phi \\ 0 & \sin\phi/\cos\theta & \cos\phi/\cos\theta \end{bmatrix} \underline{\omega} \tag{2-92}$$

Finally, the differential equations (2-66) and (2-72) are used to simulate the quasi-dynamic inflow of the helicopter rotors:

$$\begin{aligned} \tau_{\lambda_0}\dot{\lambda}_0 &= C_T - C_T^{Gl} \\ \tau_{\lambda_{0,tr}}\dot{\lambda}_{0_{tr}} &= C_{T_{tr}} - C_{T_{tr}}^{Gl} \end{aligned} \tag{2-93}$$

Vectors $\underline{v}$, $\underline{p}$, $\underline{\omega}$, $\underline{\theta}$ and $\underline{\lambda}$ constitute the state vector $\underline{x}$ used to simulate the helicopter model presented. The number of variables it gathers indicates that this nonlinear system is of order fourteen. In addition, the control deflections of the helicopter can also be gathered into a vector form, originating the control input $\underline{u} = [\theta_0 \ \theta_{1s} \ \theta_{1c} \ \theta_{0tr}]^T$.

Figure 2-15 shows schematically how the motion of the helicopter is computed and the dependences that exist between its components. All the mathematical equations necessary to simulate each block were presented in the current section. For clarity, the Main Rotor (MR) and the Tail Rotor (TR) were divided into several blocks to compute the flapping motion, the forces and moments coefficients and their transformation into the body frame of the helicopter. Furthermore, the computations also involve specific data from the helicopter adopted (Appendix B) and the determination of the air density as a function of the altitude (Appendix C). The modular structure implemented to simulate the helicopter model allows to design and test each block (and hence each subsystem) independently from the others. Moreover, this model can be easily adapted to different helicopters by simply changing its parameters.

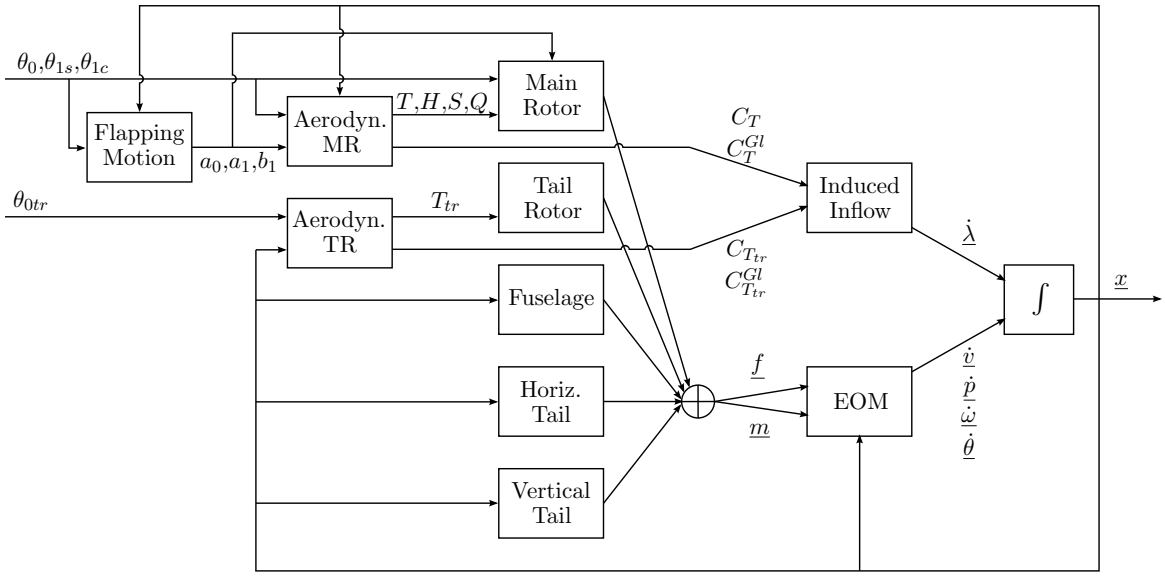

Figure 2-15: Modular structure of the helicopter model.

2-4 Open-loop System

Now that the adopted helicopter model has been developed, it is important to test whether its open-loop behavior (without the action of a control system) corresponds to what is physically expected. This can be seen as a very simple task of model validation.

The helicopter is an unstable system in open-loop. For example, the hovering flight corresponds to an unstable equilibrium point of its motion, since even a slight disturbance leads to the complete instability of the vehicle. This phenomenon is known as hover instability and it will be used in this section to analyze the open-loop response of the helicopter model.

To do so, the helicopter is trimmed in hover conditions (using the routine presented in Appendix D) and, after one second of simulation, the longitudinal cyclic is perturbed with a positive deflection of 0.5° for half a second. The result obtained is presented in Figure 2-16.

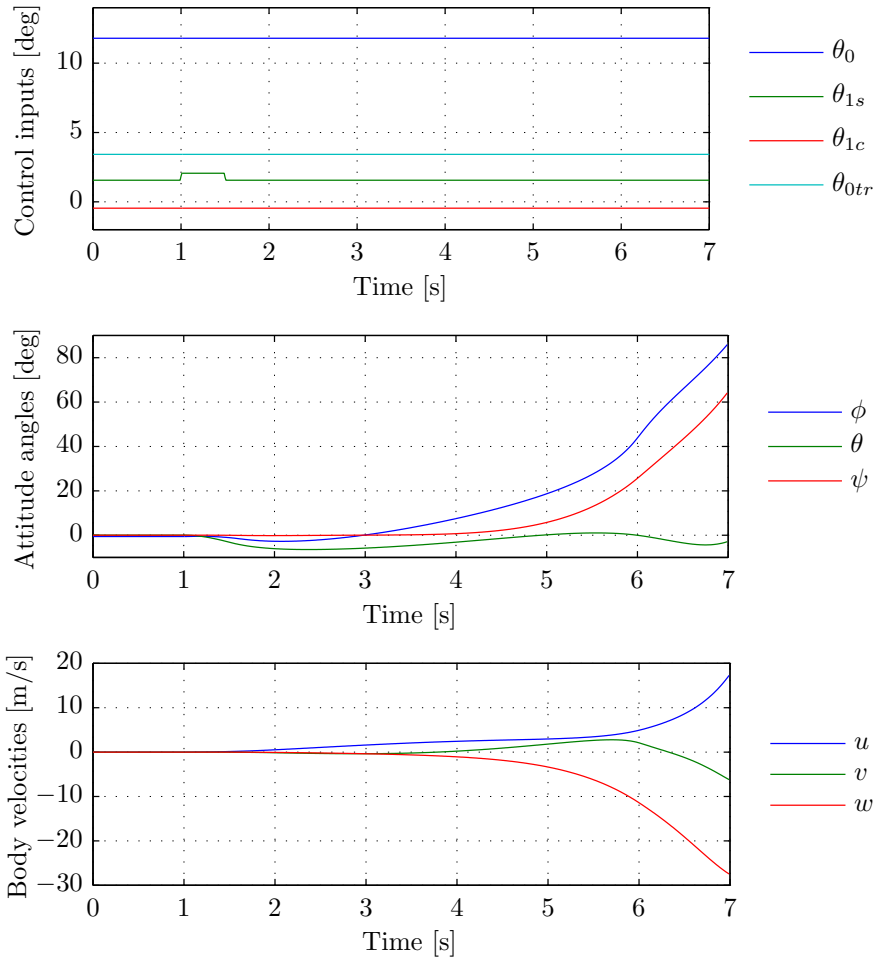

Figure 2-16: Hover instability.

Before analyzing the hover instability itself, it is important to make a remark on the values of the control inputs necessary to trim the helicopter in hover and the main dependences that influence them. Basically, the collective pitch of the main rotor θ_0 is such that the thrust produced balances the weight of the vehicle. On the other hand, the collective pitch of the tail rotor θ_{0tr} is such that the thrust generated times the distance to the helicopter CG compensates the moment torque of the main rotor. The longitudinal cyclic θ_{1s} presents a slight forward deflection, mainly to compensate the longitudinal displacement of the rotor hub with respect to the helicopter CG. Finally, since the thrust of the tail rotor acts as a lateral force pointing to the right, the thrust vector of the main rotor has to be tilted to the left, which is accomplished by a negative deflection of the lateral cyclic θ_{1c}.

Regarding now the response of the helicopter to the disturbance introduced in the longitudinal cyclic, the hover instability phenomenon occurs as follows. Due to the referred disturbance,

the main rotor tilts forward, the helicopter pitches down and a forward acceleration is produced. As the helicopter is moving forward, the rotor flaps back and generates a nose-up pitching moment about the CG. This moment damps the flapping motion, which is therefore reduced and the helicopter starts pitching down again. This originates on oscillatory movement of the helicopter with an amplitude that increases over time. Due to the complex couplings that characterize the system, this instability is also transmitted to the remaining components of the velocity vector and attitude angles, which diverge from the equilibrium point quite quickly. In conclusion, the helicopter hover instability is mainly due to the rotor's tendency to flap back when its forward velocity is increased.

Chapter 3

Nonlinear Dynamic Inversion (NDI)

The NDI control methodology was developed in the late 1970's (Brockett, 1978). In this research thesis, it is applied to the helicopter model under analysis. This chapter begins with the explanation of the main idea behind the NDI in Section 3-1, followed by the description of its working principle to generic Single Input Single Output (SISO) and Multiple Input Multiple Output (MIMO) systems in Section 3-2 and 3-3, respectively. In Section 3-4 an approach used to simplify the design of a control system is suggested and in Section 3-5, after identifying the main limitations of the NDI, its incremental form is introduced.

The theoretical development presented in this chapter is mainly based on (Enns et al., 1994; Chu, 2010; Sieberling, Chu, & Mulder, 2010; Wedershoven, 2010). For further information on the NDI technique or on another nonlinear control strategy, the reader is referred to (Slotine & Li, 1991; Isidori, 1995; Hedrick & Girard, 2010).

3-1 Fundamentals

The intuitive concept behind the NDI is quite simple. Basically, the dynamic inversion allows to generate a virtual control input ν via nonlinear feedback control and state transformation such that, when it is applied to the nonlinear system, the relation between this input and the output of the system becomes linear. Afterwards, a linear control law can be designed for ν, employing the well-known tools from the classical control theory and no gain-scheduling is needed to adapt the controller to different situations. To understand mathematically what happens, consider a n-th order nonlinear SISO system defined as:

$$\begin{aligned} \frac{\mathrm{d}^n x_1}{\mathrm{d}t^n} &= a(\underline{x}) + b(\underline{x})u \\ y &= h(\underline{x}) = x_1 \end{aligned} \tag{3-1}$$

where $\underline{x}$ is the state vector in $\mathbb{R}^n$, u is a scalar input, y a scalar output and a, b and h are scalar functions from $\mathbb{R}^n$ to $\mathbb{R}$. Let also the i-th component of vector $\underline{x}$ be denoted by x_i. In this

case, for the sake of simplicity, a linear dependence on the control input u was assumed but, as it will be seen later on, this is not a necessary condition, nor is it valid when the helicopter model is regarded. The system above can be directly recast as a space-state representation in the so-called companion form:

$$\frac{\mathrm{d}}{\mathrm{d}t}\begin{bmatrix} x_1 \\ \vdots \\ x_{n-1} \\ x_n \end{bmatrix} = \begin{bmatrix} x_2 \\ \vdots \\ x_n \\ a(\underline{x}) + b(\underline{x})u \end{bmatrix} \tag{3-2}$$

or, alternatively,

$$\begin{aligned} \frac{\mathrm{d}x_1}{\mathrm{d}t} &= \frac{\mathrm{d}y}{\mathrm{d}t} = x_2 \\ &\vdots \\ \frac{\mathrm{d}x_{n-1}}{\mathrm{d}t} &= \frac{\mathrm{d}^{n-1}y}{\mathrm{d}t^{n-1}} = x_n \\ \frac{\mathrm{d}x_n}{\mathrm{d}t} &= \frac{\mathrm{d}^n y}{\mathrm{d}t^n} = a(\underline{x}) + b(\underline{x})u \end{aligned} \tag{3-3}$$

The dependence on the control input appears explicitly and, if the virtual control input is defined as:

$$\nu = \frac{\mathrm{d}x_n}{\mathrm{d}t} = \frac{\mathrm{d}^n y}{\mathrm{d}t^n} = a(\underline{x}) + b(\underline{x})u \tag{3-4}$$

it is possible to solve for the physical control input when $b(\underline{x}) \neq 0$ as follows:

$$u = b(\underline{x})^{-1}\left(\nu - a(\underline{x})\right) \tag{3-5}$$

By introducing this expression for u into the system in the companion form, a closed-loop linear relation is obtained:

$$\frac{\mathrm{d}}{\mathrm{d}t}\begin{bmatrix} x_1 \\ \vdots \\ x_{n-1} \\ x_n \end{bmatrix} = \begin{bmatrix} x_2 \\ \vdots \\ x_n \\ \nu \end{bmatrix} \tag{3-6}$$

where all the nonlinearities have been cancelled and the system can be simply represented by a cascade of n integrators. As already mentioned, the control law for ν is obtained from a linear controller using state feedback and with the gains chosen so that the closed-loop response presents the desired characteristics. Namely, they must assure that the poles are located in the open left half-plane for exponential stability. For stabilization problems, the virtual input is given by:

$$\nu = -[k_0 \; k_1 \; \ldots \; k_{n-1}] \begin{bmatrix} y \\ \dot{y} \\ \vdots \\ y^{(n-1)} \end{bmatrix} \tag{3-7}$$

where $k_0, ..., k_{n-1}$ are simple proportional gains. With this control law, the closed loop systems becomes:

$$y^{(n)} + k_{n-1}y^{(n-1)} + \cdots + k_1\dot{y} + k_0 y = 0 \tag{3-8}$$

For tracking applications, the virtual control input depends on the state error $e = y - y_{com}$:

$$\nu - y_{com}^{(n)} = -[k_0 \; k_1 \; \ldots \; k_{n-1}] \begin{bmatrix} e \\ \dot{e} \\ \vdots \\ e^{(n-1)} \end{bmatrix} \tag{3-9}$$

and, similarly to the previous case,

$$e^{(n)} + k_{n-1}e^{(n-1)} + \cdots + k_1\dot{e} + k_0 e = 0 \tag{3-10}$$

Note that tracking problems are more difficult to solve than stabilization problems since they shall not only keep the whole state stabilized, but also drive the system output to the desired value. Moreover, stabilization problems can be regarded as a special case of tracking problems in which the desired trajectory is constant.

The component $y_{com}^{(n)}$ in (3-9) corresponds to a feedforward term that can be used to increase the speed and tracking accuracy of the response. The structure of the overall system for a tracking problem is depicted in Figure 3-1. As it can be seen, it includes an inner loop to perform the dynamic inversion (3-5) and an outer loop corresponding to the linear controller (3-9). This controller can be easily designed since the response from ν to y behaves like a cascade of n integrators. As long as the model of the system is accurately known and $b(\underline{x})$ is invertible, the gains of the outer loop assure the desired performance for a much wider range that it would be possible to obtain with a linear controller. In addition, it is important to notice that all the states that are fed back have to be known. If it is not possible to measure them directly with a sensing system, a nonlinear observer or a state estimator will have to be used for deterministic or stochastic variables, respectively.

3-2 Input-output Linearization

In the previous section, the application of the NDI was derived for systems that can be directly represented in the companion form. However, for the general case in which a system is not written in the companion form or in which the output function $h(\underline{x})$ has a nonlinear dependence on the states (and, as a consequence, is indirectly related to the controls), it is necessary to perform a state local coordinate transformation that allows to find the explicit

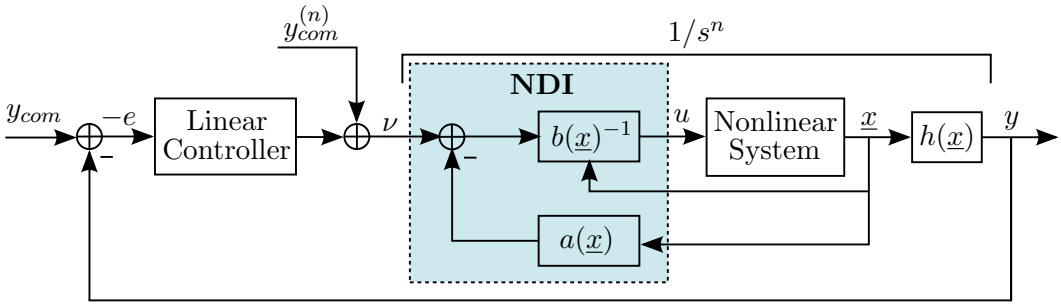

Figure 3-1: Schematic of an overall control system based on NDI.

relation between the control inputs and the outputs. This transformation is known as input-output linearization. After that, the dynamic inversion is carried out as presented before. In this section, a generic SISO system with a linear dependence on the controls is analyzed. This is represented by:

$$\begin{aligned} \dot{\underline{x}} &= \underline{f}(\underline{x}) + \underline{g}(\underline{x})u \\ y &= h(\underline{x}) \end{aligned} \tag{3-11}$$

where $\underline{x}$ is again the n-dimensional state vector, u and y are the scalar input and output, respectively, $\underline{f}$ and $\underline{g}$ are nonlinear vector fields in $\mathbb{R}^n$ and h is a nonlinear scalar function from $\mathbb{R}^n$ to $\mathbb{R}$. Since it models the effect of the control input in the response of the system, $\underline{g}$ is often referred to as control effectiveness function. To proceed with the input-output linearization, it is useful to introduce the concept of Lie derivative (Slotine & Li, 1991).

Lie derivative

Let $h(\underline{x}) : \mathbb{R}^n \to \mathbb{R}$ be a smooth scalar function and $\underline{f}(\underline{x}) : \mathbb{R}^n \to \mathbb{R}^n$ be a smooth vector field, the Lie derivative of h with respect to $\underline{f}$ is a scalar function defined by:

$$L_f h(\underline{x}) = \nabla h \underline{f}(\underline{x}) \tag{3-12}$$

where ∇ is the gradient operator. This means that the Lie derivative is simply the directional derivative of h along the direction of vector $\underline{f}$. Repeated Lie derivatives are defined recursively:

$$L_f^0 h(\underline{x}) = \nabla h(\underline{x}) \tag{3-13}$$

$$L_f^i h(\underline{x}) = L_f \left(L_f^{i-1} h(\underline{x}) \right) = \nabla \left(L_f^{i-1} h(\underline{x}) \right) \underline{f}(\underline{x}) \tag{3-14}$$

and similarly for another vector field $\underline{g}$ in $\mathbb{R}^n$:

$$L_g L_f h(\underline{x}) = \nabla \left(L_f h(\underline{x}) \right) \underline{g}(\underline{x}) \tag{3-15}$$

The procedure to obtain a linear input-output relation involves successive time-differentiations of the output, attributing each derivative to a new state variable. It stops when an explicit

dependence on the control input appears in the next time-derivative. More formally, the first order derivative of y is given by:

$$\dot{y} = \nabla h \dot{\underline{x}} = \nabla h \left(\underline{f}(\underline{x}) + \underline{g}(\underline{x})u \right) = L_f h(\underline{x}) + L_g h(\underline{x})u \tag{3-16}$$

and, if $L_g h(\underline{x}) \neq 0$:

$$u = \frac{1}{L_g h(\underline{x})} \left(\nu - L_f h(\underline{x}) \right) \tag{3-17}$$

where again a linear dependence exists for the virtual control: $\nu = \dot{y}$.

If $L_g h(\underline{x}) = 0$, an explicit relation between u and y cannot be obtained and further differentiation of the output is needed:

$$\ddot{y} = \nabla \dot{y} \dot{\underline{x}} = \nabla L_f h(\underline{x}) \left(\underline{f}(\underline{x}) + \underline{g}(\underline{x})u \right) = L_f^2 h(\underline{x}) + L_g L_f h(\underline{x})u \tag{3-18}$$

Once again, if $L_g L_f h(\underline{x}) \neq 0$, the control input can be directly determined from:

$$u = \frac{1}{L_g L_f h(\underline{x})} \left(\nu - L_f^2 h(\underline{x}) \right) \tag{3-19}$$

where the virtual control is now $\nu = \ddot{y}$.

If $L_g L_f h(\underline{x}) = 0$, the procedure is repeated until an integer number r is found such that $L_g L_f^{r-1} h(\underline{x}) \neq 0$. Hence, the generalized methodology yields:

$$u = \frac{1}{L_g L_f^{r-1} h(\underline{x})} \left(\nu - L_f^r h(\underline{x}) \right) \tag{3-20}$$

where:

$$r = \min i \in \mathbb{Z} : L_g L_f^{i-1} h(\underline{x}) \neq 0 \tag{3-21}$$

and the relation between the virtual control and the output of the system is linearized, corresponding to r integrators in cascade: $\nu = y^{(r)}$. The number r is simply the number of times that the output equation has to be differentiated until an explicit dependence on the control appears. It is known as the relative degree of the system. If the referred dependence never appears, the system is not feedback linearizable and the NDI cannot be applied to control it (Marino, 1986).

Internal and zero dynamics

For any feedback linearizable system of order n, it can be stated that $r \leq n$ always and, if $r < n$, part of the system is rendered unobservable. This part cannot be assessed from the input-output linearization and it is thus known as internal dynamics. It is also important to note that r can never be larger than n since if more differentiations of the output function were needed to appear the control influence, the order of the system would be higher than n. On the other hand, if infinite differentiations of y would never allow to obtain the control dependence, the system could not be defined as feedback linearizable.

Conceptually, internal dynamics are simply the remaining motions allowed to the system when the inverted outputs are being constrained by the NDI controller. In order to assure the effectiveness of the controller when $r < n$, the internal dynamics have to be stable (bounded) in the region of interest. Unfortunately, due to the nonlinearities and potential couplings of the whole system, the stability of internal dynamics is in general very difficult to evaluate.

Nevertheless, if the system is linear, the eigenvalues of the internal dynamics correspond to the zeros of the transfer functions of the control variables and, for that reason, they are known as zero dynamics (Enns et al., 1994). In this case, the relative degree is the excess of poles over zeros and, if there are any zeros ($r < n$), the zero dynamics are stable and well-behaved if all the zeros are located in the left half-plane (meaning that the system is minimum-phase) and have reasonable damping ratios (between 0.6 and 1.0). Internal dynamics correspond to a generalization of the same ideas, resulting in the conclusion that this behavior has to be taken into account when choosing the control variables of a system.

It is now possible to define a coordinate transformation to convert a feedback linearizable system into the companion form, characterized by the state vector $\underline{z}$. This transformation is given by the nonlinear transformation $\underline{\Phi}$, which can be classified as a diffeomorphism: a smooth bijective mapping with a smooth inverse. In this particular case, it is given by:

$$\underline{z} = \underline{\Phi}(\underline{x}) = \begin{bmatrix} \phi_1(\underline{x}) \\ \phi_2(\underline{x}) \\ \vdots \\ \phi_r(\underline{x}) \\ \phi_{r+1}(\underline{x}) \\ \vdots \\ \phi_n(\underline{x}) \end{bmatrix} \tag{3-22}$$

where the first r components correspond to:

$$\phi_i(\underline{x}) = L_f^{i-1} h(\underline{x}) \tag{3-23}$$

Furthermore, it is also verified that:

$$\dot{\phi}_i(\underline{x}) = \nabla \phi_i \dot{\underline{x}} = \nabla L_f^{i-1} h(\underline{x}) \left(\underline{f}(\underline{x}) + \underline{g}(\underline{x}) u \right) = L_f^i h(\underline{x}) + L_g L_f^{i-1} h(\underline{x}) u \tag{3-24}$$

and, according to the definition of relative degree, the second term is only different than zero for $i = r$. After this transformation, the system is expressed in the companion form presented in the previous section and, considering the inverse mapping $\underline{x} = \underline{\Phi}^{-1}(\underline{z})$, the following relations are derived by analogy:

$$\frac{\mathrm{d}^r z_1}{\mathrm{d}t^r} = a(\underline{z}) + b(\underline{z}) u \tag{3-25}$$

$$\frac{\mathrm{d}}{\mathrm{d}t}\begin{bmatrix} z_1 \\ \vdots \\ z_{r-1} \\ z_r \end{bmatrix} = \begin{bmatrix} z_2 \\ \vdots \\ z_r \\ a(\underline{z}) + b(\underline{z})u \end{bmatrix} \tag{3-26}$$

$$\nu = \frac{\mathrm{d}z_r}{\mathrm{d}t} = \frac{\mathrm{d}^r z_1}{\mathrm{d}t^r} = a(\underline{z}) + b(\underline{z})u \tag{3-27}$$

$$u = b(\underline{z})^{-1}\left(\nu - a(\underline{z})\right) \tag{3-28}$$

where:

$$a(\underline{z}) = L_f^r h(\underline{x}) \tag{3-29}$$

$$b(\underline{z}) = L_g L_f^{r-1} h(\underline{x}) \tag{3-30}$$

It is always possible to find $n - r$ more functions $\phi_i(\underline{x})$, for $r + 1 \leq i \leq n$, such that $\nabla\phi_i \underline{g}(\underline{x}) = L_g\phi_i(\underline{x}) = 0$ is verified for all the $\underline{x}$ in the region of interest. These components of the diffeomorphism $\underline{\Phi}(\underline{x})$ correspond to the internal dynamics of the systems and show that the unobservable states $z_{r+1}, ..., z_n$ do not depend explicitly on the control input u and cannot be controlled. The internal dynamics are not observable because the first r components of $\underline{z}$ do not depend on them at all.

Once again, by setting $\underline{x} = \underline{\Phi}^{-1}(\underline{z})$, the state-space description of the internal dynamics of the system is given by:

$$\frac{\mathrm{d}}{\mathrm{d}t}\begin{bmatrix} z_{r+1} \\ \vdots \\ z_n \end{bmatrix} = \begin{bmatrix} L_f^{r+1} h(\underline{x}) \\ \vdots \\ L_f^n h(\underline{x}) \end{bmatrix} \tag{3-31}$$

After the application of this transformation, the first r equations are linearized and it is possible to design a control law for ν based on the tracking error $e = y - y_{com}$ using linear control techniques, as mentioned for (3-9). It is also important to note that this control law is of order r and if it is smaller than the order n of the system, it does not account for the internal dynamics, which are unobservable to the input-output linearization. As a consequence, the effectiveness of the controller depends strongly on the stability of the internal dynamics.

3-3 Extension to MIMO Systems

The input-output linearization procedure presented in the previous section for a SISO system can be easily extended to the MIMO case. Again, it is assumed that the states are affine with respect to the controls and, at this point, the input-output linearization concerns a system with the same number m of outputs and inputs. This type of system can be represented by:

$$\begin{aligned} \dot{\underline{x}} &= \underline{f}(\underline{x}) + \underline{G}(\underline{x})\underline{u} = \underline{f}(\underline{x}) + \underline{g}_1(\underline{x})u_1 + ... + \underline{g}_m(\underline{x})u_m \\ \underline{y} &= \underline{h}(\underline{x}) = [h_1(\underline{x}) \ ... \ h_m(\underline{x})]^T \end{aligned} \tag{3-32}$$

Comparing with the previous case, the input $\underline{u}$ and the output $\underline{y}$ of the system are now vectors in $\mathbb{R}^m$, $\underline{h}$ is the nonlinear output vector function in $\mathbb{R}^m$ and $\underline{G}$ is a $n \times m$ input matrix. Once again, each component y_j of the output vector is differentiated with respect to time until an explicit dependence on one of the control inputs appears. The smallest number of differentiations needed for this to happen is r_j and, by analogy with the previous section, the result is:

$$y_j^{(r_j)} = L_f^{r_j} h_j(\underline{x}) + \left[L_{g_1} L_f^{r_j - 1} h_j(\underline{x}) \ ... \ L_{g_m} L_f^{r_j - 1} h_j(\underline{x}) \right] \begin{bmatrix} u_1 \\ \vdots \\ u_m \end{bmatrix} \tag{3-33}$$

Once again, r_j is the relative degree associated with the j-th component of the output vector and the total relative degree of the system is given by:

$$r = \sum_{j=1}^{m} r_j \tag{3-34}$$

Similarly to the SISO case, if the total relative degree of the system is inferior to its order, there are some degrees of internal dynamics that must be bounded to assure control effectiveness. Considering the influence of the m output variables, the total input-output linearization can be written in a compact form using the nonlinear vector field $\underline{a}$ and the input dependency matrix $\underline{B}$:

$$\underline{\nu} = \underline{a}(\underline{x}) + \underline{B}(\underline{x})\underline{u} \tag{3-35}$$

with:

$$\begin{bmatrix} \nu_1 \\ \vdots \\ \nu_m \end{bmatrix} = \begin{bmatrix} y_1^{(r_1)} \\ \vdots \\ y_m^{(r_m)} \end{bmatrix} \tag{3-36}$$

$$\underline{a}(\underline{x}) = \begin{bmatrix} L_f^{r_1} h_1(\underline{x}) \\ \vdots \\ L_f^{r_m} h_m(\underline{x}) \end{bmatrix} \tag{3-37}$$

$$\underline{B}(\underline{x}) = \begin{bmatrix} L_{g_1} L_f^{r_1 - 1} h_1(\underline{x}) & ... & L_{g_m} L_f^{r_1 - 1} h_1(\underline{x}) \\ \vdots & \vdots & \vdots \\ L_{g_1} L_f^{r_m - 1} h_m(\underline{x}) & ... & L_{g_m} L_f^{r_m - 1} h_m(\underline{x}) \end{bmatrix} \tag{3-38}$$

From this it can be understood why it was assumed that the number of outputs and inputs are the same: if they were not, matrix $\underline{B}$ would not be square and some sort of control allocation would be needed to invert the system. This issue will be further discussed in Chapter 5. If $\underline{B}$ is invertible for all $\underline{x}$ in the region of interest, the relation between the physical and virtual controls is given by:

$$\underline{u} = \underline{B}^{-1}(\underline{x})(\underline{\nu} - \underline{a}(\underline{x})) \tag{3-39}$$

and again a linear multiple integrator relation between the output $\underline{y}$ and the virtual control $\underline{\nu}$ is achieved from (3-36). From this equation it is also possible to verify that each y_j is only

affected by ν_j, meaning that the dynamics of each control channel j is completely independent and decoupled from the remaining system, as long as its model is accurately known. Therefore, all the channels can be controlled separately and the outer linear controller associated with each one can be designed based only on the desired performance for the corresponding response. This aspect is very useful for the development of flight control system since it enables a direct mapping of the desired flying qualities in the control laws. Moreover, since the system is linearized when all the nonlinearities are cancelled, the single linear controllers can be used for the complete flight envelope. For each control channel, the aspect of the closed-loop system is therefore similar to the one presented in Figure 3-1 for the SISO case.

For tracking problems, the outputs of the system are often selected to be the control variables. These control variables shall also be chosen such that the remaining internal dynamics are stable. Furthermore, when some control variables are physically related (for example, three attitude angles), the dynamic inversion can be performed using the complete control vector instead of individual variables. This is due to the fact that they are expected to have the same relative degree.

3-4 Time Scale Separation

Flight dynamics problems are nonlinear by nature, particularly in realistic representations that are appropriate for the development of guidance and control strategies. The existence of different time scales in a dynamical system can be used to greatly simplify its complexity by separating the fast and slow dynamics. This type of time scale separation exists naturally in many fields of applied mathematics, engineering and biological sciences and it is originated by the presence of some parasitic parameters. Time scales in dynamical systems are studied by the singular perturbations theory, of which (Naidu & Calise, 2001) is an important survey reference.

To more clearly understand the concept of singular perturbation, consider the nonlinear system:

$$\begin{aligned} \dot{\underline{x}}_s &= \underline{f}_s(\underline{x}_s, \underline{x}_f, \underline{u}, \epsilon) \\ \epsilon\dot{\underline{x}}_f &= \underline{f}_f(\underline{x}_s, \underline{x}_f, \underline{u}, \epsilon) \end{aligned} \tag{3-40}$$

where $\underline{x} = \begin{bmatrix} \underline{x}_s^T & \underline{x}_f^T \end{bmatrix}^T$ is the state vector, $\underline{u}$ is the control inputs vector, $\underline{f} = \begin{bmatrix} \underline{f}_s^T & \underline{f}_f^T \end{bmatrix}^T$ is a nonlinear vector field and the small parameter ϵ is known as singular perturbation. This system is labeled as singularly perturbed since the suppression of the perturbation ($\epsilon = 0$) results in the reduction of its order. When this happens, the fast dynamics are so rapid that the fast states $\underline{x}_f$ have reached a quasi-steady situation in the slow timescale. In this case, the evolution of the states is only described by the slow dynamics $\underline{x}_s$, subjected to $\underline{f}_f(\underline{x}_s, \underline{x}_f, \underline{u}, 0) = 0$. From this result, it can be concluded that the singular perturbation theory allows to represent a mathematical formulation of intuitive approaches in order to simplify the models via order reduction. This type of analysis can also be extended to systems with multiple time scales.

In general, a system with separated time scales does not need to be in the singularly perturbed structure since singularly perturbed systems are only a special representation of the general

class of time scale systems. Often, the small parameter ϵ does not appear in the desirable form or it may not be identifiable at all. It is also possible to know whether a system possesses slow and fast modes by physical insight and past experience. Several formal alternatives to select time scales are presented in (Naidu & Calise, 2001), complemented with examples regarding different aerospace systems.

The time scale separation principle can also be applied to simplify the design and analysis of control systems. In this case, fast dynamics are associated with variables with a higher control effectiveness, while slow dynamics correspond to the states that are more weakly affected by the control inputs. Typically, this principle is used for attitude control of an aircraft by separating the rotational dynamics (angular rates) from the slow dynamics, associated with the evolution of its orientation angles. This follows the assumption that the control effectors are primarily moment producing devices.

A very simple way to verify the existence of a difference in the time scale between attitude angles and angular rates is simply to introduce unit step signals in the control inputs of the helicopter in open loop and measure the time derivative of the responses in the transient instant. The results obtained when the referred step inputs are applied to the helicopter in hover are presented in Table 3-1.

Table 3-1: Verification of the time scale separation between attitude angles and rates.

Step in the lateral cyclic pitch	$\frac{\mathrm{d}\phi}{\mathrm{d}t} = 5.7$ deg/s	$\frac{\mathrm{d}p}{\mathrm{d}t} = 145.8$ deg/s^2
Step in the longitudinal cyclic pitch	$\frac{\mathrm{d}\theta}{\mathrm{d}t} = -2.5$ deg/s	$\frac{\mathrm{d}q}{\mathrm{d}t} = -60.1$ deg/s^2
Step in the collective of the tail rotor	$\frac{\mathrm{d}\psi}{\mathrm{d}t} = -0.7$ deg/s	$\frac{\mathrm{d}r}{\mathrm{d}t} = -16.5$ deg/s^2

From this table, it is possible to see that there is a substantial difference between the derivatives associated with the attitude angles and rates, showing that dynamics of the latter ones evolve considerably faster. Intuitively, it can also be understood that the dynamics of the angles are in fact slower than their rates, since the relation between these two types of variables involves an integration.

When the time scale separation principle is applied, the original differential equations are separated into two subsystems, each one controlled using a NDI approach. The dynamics of the angular rates correspond to an inner loop, where the physical control inputs are used to track references in terms of roll, pitch and yaw rates. Then, an outer loop is introduced to generate the latter references in order to control the desired angular orientation of the aircraft. This means that the fast variables are used as control inputs to the slow dynamics.

The application of the time scale separation principle to attitude control will be further developed later in this thesis. As already mentioned, the main advantage of this configuration is the simplification achieved in the development of a NDI-based control system. In this case, instead of inverting a system of sixth order directly, the control architecture is separated into two third order systems. The scale separation principle will also be used to separate the translational dynamics of the helicopter from its rotational motion. In this line of reasoning, it will be assumed that the evolution of the angular rates of the body is substantially faster than the attitude angles, which also evolve faster than the linear velocities of the helicopter.

When the time scale separation principle is applied, parameters associated with the slow dynamics are treated as constants in the inner loop (fast dynamics), since they evolve more slowly. Furthermore, the dynamic inversion of the outer loop (slow dynamics) is performed assuming that the states of the fast dynamics achieve their commanded values instantaneously, which is only valid if the time scales of the two loops are separated enough. Otherwise, if there is a weak separation between the different time scales, the performance of the overall controller may become severely degraded. It was however proven in (Schumacher, Khargonekar, & McClamroch, 1998) using Lyapunov theory that any system is exponentially stable about constant commanded values of the outer loop states if the inner loop gains are sufficiently large. This property was applied in practice for a missile control system in (Schumacher & Khargonekar, 1998). It can also be intuitively understood thar higher inner loop gains will impose faster responses in the corresponding states and thus improving the time scale separation with respect to those controller by the outer loop.

3-5 Model Uncertainties and Incremental NDI (INDI)

After deriving the NDI control theory, it is important to assess whether this kind of controller is robust to uncertainties and inaccuracies in the model of the system (Sieberling et al., 2010). For the sake of simplicity, this section concerns a generic MIMO system of m-th order, with $\underline{y} = \underline{x}$ and all the components of this vector have a unitary relative degree. As it was shown in Section 3-3, the extension to more complex systems is quite straightforward. Furthermore, it is still assumed that the system is affine in the control vector and that no internal dynamics exist after the dynamic inversion. Let (3-32) be reformulated such that the functions that describe the model are composed of a nominal part which is known ($\underline{f}_n$ and $\underline{G}_n$) plus an uncertain term ($\Delta\underline{f}$ and $\Delta\underline{G}$):

$$\dot{\underline{x}} = \underline{f}_n(\underline{x}) + \Delta\underline{f}(\underline{x}) + \left(\underline{G}_n(\underline{x}) + \Delta\underline{G}(\underline{x})\right)\underline{u} \tag{3-41}$$

In spite of the fact that this is the equation that describes the real system, the uncertain parts are not known when the dynamic inversion is performed, unless some kind of identification is applied onboard. As a consequence, the relation between the virtual and physical control inputs only accounts for the nominal part of the system. This yields:

$$\underline{u} = \underline{G}_n(\underline{x})^{-1}(\underline{\nu} - \underline{f}_n(\underline{x})) \tag{3-42}$$

where $\underline{\nu} = \dot{\underline{x}}$. However, when this input is applied to the system:

$$\begin{aligned} \dot{\underline{x}} &= \underline{f}_n(\underline{x}) + \Delta\underline{f}(\underline{x}) + \left(\underline{G}_n(\underline{x}) + \Delta\underline{G}(\underline{x})\right)\underline{G}_n(\underline{x})^{-1}(\underline{\nu} - \underline{f}_n(\underline{x})) = \\ &= \Delta\underline{f}(\underline{x}) - \Delta\underline{G}(\underline{x})\underline{G}_n(\underline{x})^{-1}\underline{f}_n(\underline{x}) + \left(\underline{I}_{n\times n} + \Delta\underline{G}(\underline{x})\underline{G}_n(\underline{x})^{-1}\right)\underline{\nu} \end{aligned} \tag{3-43}$$

where $\underline{I}_{n\times n}$ is the $n \times n$ identity matrix. As it can be seen, the linear relation $\dot{\underline{x}} = \underline{\nu}$ expected from Section 3-3 is only valid for $\Delta\underline{f}(\underline{x}) = \Delta\underline{G}(\underline{x}) = 0$. Otherwise, in the presence of uncertainties, the closed-loop system is not linearized anymore, causing the degradation of the performance of the overall controller and compromising the stability of the system. This high sensitivity of the NDI to model uncertainties is the main shortcoming of the standard version of this approach and the main motivation to develop a more robust version called

Incremental Nonlinear Dynamic Inversion (INDI), also known in the literature as Simplified or Modified NDI.

As the name indicates, the concept of the INDI is based on the incremental form of the dynamics of the system (Chen & Zhang, 2008). Instead of using the virtual input to compute the complete control vector, it is possible to determine only the required variation with respect to the previous input. To achieve this, consider the linearization of (3-32) in the same conditions as before, obtained from the first-order terms of its Taylor series expansion around the current solution of the system, denoted by $(\underline{x}_0, \underline{u}_0)$:

$$\begin{aligned}\dot{\underline{x}} &\approx \dot{\underline{x}}_0 + \frac{\partial}{\partial \underline{x}}\left[\underline{f}(\underline{x}) + \underline{G}(\underline{x})\underline{u}\right]_{\underline{x}_0,\underline{u}_0}(\underline{x}-\underline{x}_0) + \frac{\partial}{\partial \underline{u}}\left[\underline{f}(\underline{x}) + \underline{G}(\underline{x})\underline{u}\right]_{\underline{x}_0,\underline{u}_0}(\underline{u}-\underline{u}_0) = \\ &= \dot{\underline{x}}_0 + \frac{\partial}{\partial \underline{x}}\left[\underline{f}(\underline{x}) + \underline{G}(\underline{x})\underline{u}\right]_{\underline{x}_0,\underline{u}_0}(\underline{x}-\underline{x}_0) + \underline{G}(\underline{x}_0)(\underline{u}-\underline{u}_0)\end{aligned} \tag{3-44}$$

Note that this equation implies that $\dot{\underline{x}}_0$ is known, either by direct measurement or state estimation. Similarly, the current control vector $\underline{u}_0$ has also to be accurately known. Furthermore, for very small time increments, the variation $\underline{x} - \underline{x}_0$ can in principle be neglected, yielding:

$$\underline{\nu} = \dot{\underline{x}} \approx \dot{\underline{x}}_0 + \underline{G}(\underline{x}_0)(\underline{u}-\underline{u}_0) \tag{3-45}$$

The virtual control input is then directly related to the incremental command. As already mentioned, instead of computing the total control input directly, only the required increment relative to the previous input is necessary. Assuming that a demanded control input is achieved instantaneously (either by neglecting the actuator dynamics or by considering a difference in the time scales) and with no error, the corresponding control law is given by:

$$\underline{u} = \underline{G}(\underline{x}_0)^{-1}(\underline{\nu} - \dot{\underline{x}}_0) + \underline{u}_0 \tag{3-46}$$

As for the regular NDI, the virtual input $\underline{\nu}$ is generated by a linear control law, since its relation with the output of the system is linearized. At this point, a major advantage of the INDI can be identified: the linearization law does not depend on $\underline{f}$ anymore. This means that, in opposition to the regular NDI, it is not necessary to know this part of the model. Instead, this information is replaced by onboard measurements of $\dot{\underline{x}}_0$. This is why the INDI is sometimes referred to as a sensor-based approach while the NDI is mentioned as model-based. Nevertheless, both methods do require the description of the influence of the controls, contained in $\underline{G}$.

The insensitivity of the INDI to modelling errors that might be incorporated in $\underline{f}$ allows the implementation of simple and effective reconfigurable flight controllers, able to cope with structural damages or system failures without the need to perform real-time identification of the model. One example can be found in (Bacon, Ostroff, & Joshi, 2001), where the author also implements the technique known as Failure Detection and Isolation (FDI) to the inertial sensors.

The robustness of the linearizing control law for the INDI can also be evaluated following the same procedure used for the NDI. In this case, assuming ideal sensors, all the uncertainties will lie in $\underline{G} = \underline{G}_n + \Delta\underline{G}$. Note that this does not imply that changes and uncertainties in $\underline{f}$ are neglected, since they are still indirectly reflected in the construction of $\dot{\underline{x}}_0$. From (3-45):

$$\dot{\underline{x}} = \dot{\underline{x}}_0 + \left(\underline{G}_n(\underline{x}_0) + \Delta\underline{G}(\underline{x}_0)\right)(\underline{u}-\underline{u}_0) \tag{3-47}$$

and again, only the nominal part is known by the controller:

$$\underline{u} = \underline{G}_n(\underline{x}_0)^{-1}(\underline{\nu} - \dot{\underline{x}}_0) + \underline{u}_0 \tag{3-48}$$

Replacing this control law in (3-47) yields:

$$\begin{aligned} \dot{\underline{x}} &= \dot{\underline{x}}_0 + \left(\underline{G}_n(\underline{x}_0) + \Delta\underline{G}(\underline{x}_0)\right)\left(\underline{G}(\underline{x}_0)^{-1}(\underline{\nu} - \dot{\underline{x}}_0) + \underline{u}_0 - \underline{u}_0\right) = \\ &= -\Delta\underline{G}(\underline{x}_0)\underline{G}_n(\underline{x}_0)^{-1}\dot{\underline{x}}_0 + \left(\underline{I}_{n\times n} + \Delta\underline{G}(\underline{x}_0)\underline{G}_n(\underline{x}_0)^{-1}\right)\underline{\nu} = \\ &= -\underline{C}\dot{\underline{x}}_0 + (\underline{I}_{n\times n} + \underline{C})\underline{\nu} \end{aligned} \tag{3-49}$$

where $\underline{C} = \Delta\underline{G}(\underline{x}_0)\underline{G}_n(\underline{x}_0)^{-1}$. Also in this case, the relation $\dot{\underline{x}} = \underline{\nu}$ is only obtained when no model uncertainties exist ($\Delta\underline{G}(\underline{x}_0) = 0$). However, even in the presence of uncertainties, this equation is still linear and its components remain decoupled.

In addition, when a linear controller with a diagonal transfer matrix $\underline{K}(s)$ is applied to design the virtual control from the tracking error (in this case, $\underline{\nu} = -\underline{K}(s)(\underline{x} - \underline{x}_{com})$), taking into account that, as assumed before, $\underline{x}_0 \approx \underline{x}$ and, in the Laplace domain with zero initial conditions, $\dot{\underline{x}} = s\underline{x}$, it follows that:

$$s\underline{x} = -s\underline{C}\underline{x} + (\underline{I}_{n\times n} + \underline{C})\underline{K}(s)(\underline{x}_{com} - \underline{x}) \tag{3-50}$$

and the output of the closed-loop system is given by:

$$\underline{x} = \frac{\underline{K}(s)}{s\underline{I}_{n\times n} + \underline{K}(s)}\underline{x}_{com} \tag{3-51}$$

and, as it can be seen, the influence of the model uncertainties $\Delta\underline{G}(\underline{x}_0)$ contained in $\underline{C}$ have also disappeared. This means that, when closing the INDI-based feedback linearization loop, the applied control input eliminates the influence of the uncertainties that affect the model and the system can be linearized and decoupled as if no model uncertainties existed. The only limitation in this statement is associated with the dependence of the control laws on the sign of the control effectiveness matrix $\underline{G}$, as explained below.

Relative to both NDI and INDI, experience showed that an unknown reversal in the sign of the control effectiveness matrix leads to an unstable response (Kim, 2003). This can be intuitively understood since, if the sign of a component of the control effectiveness matrix is not correct ($\text{sign}\left(\underline{G}(\underline{x}_0)\right) \neq \text{sign}\left(\underline{G}_n(\underline{x}_0) + \Delta\underline{G}(\underline{x}_0)\right)$), instead of compensate for errors, the controller will tend to increase them. The effect of this uncertainty in the stability of the system can also be visualized by the sign of the entries of $\underline{C}$ in (3-49), for the INDI case. Note that the diagonal components of this matrix are equal to one when there are no model uncertainties, larger than the unity when there are uncertainties but the sign of the control effectiveness is correct and smaller than one when also the sign is wrong.

In summary, after this analysis, the following conclusions can be drawn:

- The implementation of the basic version of the NDI requires an accurate knowledge of the model of the system, which may not be possible in practice. Nevertheless, the incremental version allows to reduce significantly the dependence of the controller on the model available. In fact, with this type of approach, only the information about the influence of the controls is needed;

- With the application of INDI, even when there are uncertainties, the closed-loop system is still linearized and decoupled. Furthermore, as it was seen, the effect of those uncertainties is cancelled when the outer linear controller is applied to the linearized system. Hence, theoretically, the only information needed by an INDI-based controller to effectively control a nonlinear system is the sign of the control effectiveness matrix;
- The referred reduction of the model dependence is achieved by making use of information about the derivatives of the states and thus the efficiency of the controller depends on the accuracy of their measurements. It can also be the case that the required variables cannot be measured and thus they have to be estimated. This represents the main drawback of this type of controller. The measurements will not only contain biases, noise and delay, but also numeric errors may arise from the estimation processes. It is thus very important to minimize these influences in order not to degrade the control efficiency. Uncertainties in the form of biases can be compensated by outer loops. The remaining issues will be addressed in Chapter 8.

Chapter 4

Pseudo-Control Hedging (PCH)

In the previous chapter, the NDI theory was derived without any consideration of the dynamics of the actuators and therefore assuming them ideal. In fact, this type of controller is normally designed without making use of any information about the actuator limitations. As it will be seen, helicopter flight control easily involves inputs to the system with high values of magnitude and rate. If the referred limitations are not taken into account when developing the controller, the performance of the overall system may be severely degraded and its stability may even be put at risk.

Flight control saturation elements normally exist due to the physical limitations of the actuators or due to control limit implementation used to monitor the bound of a signal. These saturations can be related to the position and rate limits of the control actuators, as in the case of this thesis, but they can also involve dynamics of high orders. The overall system stability is dictated by the inputs of the control paths that contain these saturation elements. Saturation limits can normally be avoided by reducing the gains of the controller, but this option introduces conservatism into the system and its performance may become far from the desirable. On the other hand, saturation also implies controllability and invertibility issues, which may violate necessary conditions for the dynamic inversion.

The approaches adopted to avoid actuator saturations are normally developed based on adaptive control compensation. For adaptive control in general, modified adaptive laws have been proposed to modify the error signal in Model Reference Adaptive Control (MRAC) when some kind of saturation occurs (Wang & Sun, 1992). Nevertheless, as already mentioned, when it comes to flight certification, adaptive controllers are particularly troublesome in two aspects: it is not only difficult to show that the controller will never "learn" incorrectly and consequently cause harm to the vehicle, but it is also hard to prove that the adaptive element is able to recover from a failure in adaptation. These shortcomings were the main motivations for the development of an adaptive technique to deal with actuators dynamics while not in direct control of the plant: the Pseudo-Control Hedging (PCH). The present chapter starts with a description of the PCH technique in Section 4-1, followed by the derivation of NDI control loops with PCH in Section 4-2 and ends with a brief analysis of the tracking error dynamics in Section 4-3.

4-1 Description

The PCH design concept was firstly introduced in (E. N. Johnson & Calise, 2000), being further developed in (Lam, Hindman, Shell, & Ridgely, 2005). Successful applications of this technique can be found, for example, in (Lombaerts, 2010) to the model of a Boeing 747-100/200 aircraft and in (E. N. Johnson & Kannan, 2005) to a UAV helicopter. The purpose of the PCH is to prevent the overall control system from attempting to track a commanded reference when the effects of actuator saturation are present. This method also relies on modifying the error signal, but this modification is introduced in a reference model in such a way that the over-demanding control inputs are removed, rather than an adaptive law directly. This means that a pre-adaptation of the signal is made before handing it over to the control system.

A conventional controller computes the values of the commanded control deflections required to obtain the desired response of the system. PCH uses a model of the actuators with position and rate saturations to estimate their responses to the referred commands. The difference between the achievable and the commanded controls is used to adjust a Reference Model (RM), which will automatically reduce the saturation intensity and allow stabilization when it senses a command is too aggressive for the actuators.

The RM is used to impose the desired dynamics to the commanded variable handed to the remainder control system y_{rm}. Furthermore, this model is also very useful to provide the derivative of the command input, which can be used by the controller as a feedforward term ν_{rm}. Finally, this model can also include a saturation filter that keeps the desired references y_{com} from being physically unfeasible. The RM configuration with this element is also presented in the literature as a command filter. The desired references may be introduced directly by the pilot into the system or may be originated in an outer control loop. Figure 4-1 shows the aspect of a first-order RM where, for simplicity, the state to be controlled is a scalar.

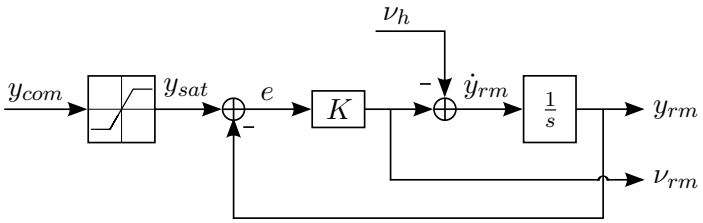

Figure 4-1: First-order reference model with saturation filter.

When no saturation of the actuators occurs, the pseudo-control hedge ν_h is zero and the RM behaves exactly like a Low-Pass Filter (LPF) with cutoff-frequency K. This value shall match the one imposed by the remainder control system so that the evolution of y_{rm} is not too aggressive for the actuators nor slower than the response capabilities of the controller. The existence of this filter is very important because, due to its action, the pilot does not have to be concerned on whether his commands are too demanding for the control system. The RM model will filter this commands so that they are as smooth as necessary to be tracked by the controller.

The magnitude of the pseudo-control hedge indicates how much less authority the controller system is getting due to saturations that what it desires. As soon as the system experiences saturations, the value of ν_h will no longer be zero and the RM starts attenuating the command such that saturations are no longer occurring. Note that this signal affects the derivative of y_{rm} and thus it only affects the RM state directly after a few instants.

In other words, as explained in (E. N. Johnson & Kannan, 2005), PCH moves (hedges) the RM in the opposite direction by an estimate of the amount the plant did not move due to the limitations of the actuators, preventing the continued demand to track the commanded references in this situation. The next section deals with the calculation of the pseudo-control hedge.

4-2 Architecture in a NDI Loop

Again considering a SISO system (which is coherent with the fact that the channel associated with each variable can be designed separately since the NDI decouples the responses), the NDI is used to determine a commanded input u_{com} from the inversion of the desired virtual control signal ν. However, due to the actuator dynamics, u_{com} may not be equal to the actual control u, which is assumed to be known based on a model or measurement. Using information of the system, it is also possible to estimate the value of a virtual control $\hat{\nu}$ corresponding to the physical control u. Recalling expression (3-4), deduced for the virtual control in the previous chapter, the pseudo-control hedge can then be defined as:

$$\begin{aligned} \nu_h &= \nu - \hat{\nu} = \\ &= [a(\underline{x}) + b(\underline{x})u_{com}] - [a(\underline{x}) + b(\underline{x})u] = \\ &= b(\underline{x})(u_{com} - u) \end{aligned} \tag{4-1}$$

The application of PCH to a NDI-based control loop is schematized in Figure 4-2, where the RM block corresponds to the one presented in the previous section, "Act." represents the dynamics of the actuators and the NDI was already discussed in Chapter 3.

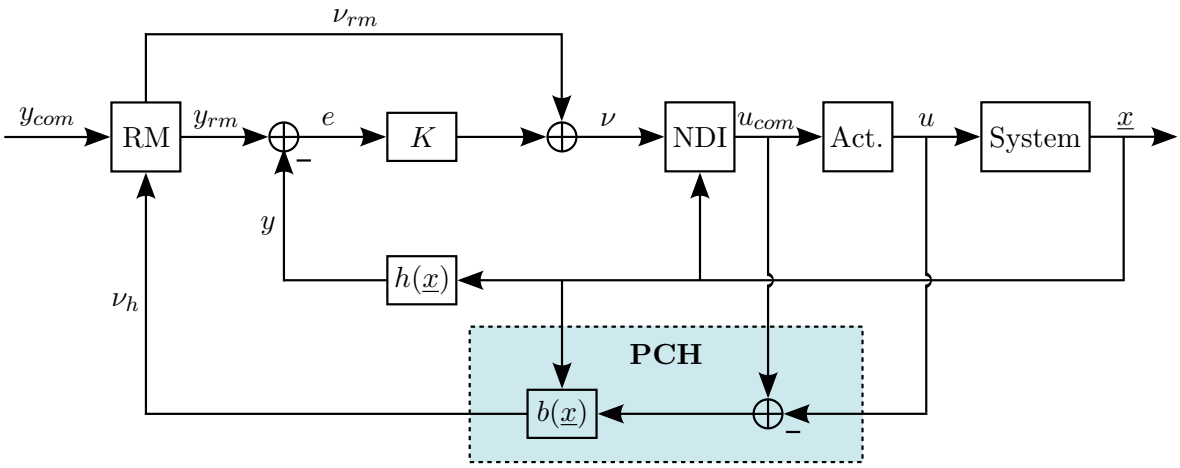

Figure 4-2: NDI controller with PCH compensation.

In this case, the linear controller of the NDI is assumed to be simply a proportional gain K plus the influence of the feedforward term from the RM. Recall that $b(\underline{x})$ is the scalar field that relates the physical input of the system with its state and $h(\underline{x})$ is the output function. In summary, from the analysis of the figure it is possible to conclude that the PCH subsystem monitors the control commands and scales (hedges) the RM such that the commanded references are within the system capabilities.

For the cases in which the incremental version of the NDI is chosen, the implementation of the PCH strategy comes straightforward from the previous situation. Applying (3-45) to a SISO system, the following relation is obtained for the pseudo-control hedge:

$$\begin{aligned} \nu_h &= \nu - \hat{\nu} = \\ &= [\dot{x}_0 + g(\underline{x}_0)(u_{com} - u_0)] - [\dot{x}_0 + g(\underline{x}_0)(u - u_0)] = \\ &= g(\underline{x}_0)(u_{com} - u) \end{aligned} \tag{4-2}$$

Moreover, if the control system presents a multi-loop design where the time scale separation principle (Section 3-4) was applied, it was assumed that the outer-loop bandwidth is much lower than that of the inner loop. As it will be seen in the next chapters, this assumption is alleviated with the adoption of PCH for the different loops, allowing to adjust the behavior of the outer loop when the bandwidth of the response of the inner loop is not separated enough. Note that the outer-loop "sees" the commanded references of the inner-loop as control inputs which, like real actuators, are characterized by practical limits and speed of response.

4-3 Error Dynamics

Finally, it is important to analyze what happens to the tracking error dynamics $e = y_{rm} - y$ when the PCH is introduced in the control system. From Figure 4-1, it can be seen that:

$$\dot{y}_{rm} = \nu_{rm} - \nu_h \tag{4-3}$$

where

$$\nu_h = \nu - \hat{\nu} \tag{4-4}$$

Furthermore, from the NDI theory it is known that:

$$\dot{y} = \nu \tag{4-5}$$

and, from Figure 4-2,

$$\nu = Ke + \nu_{rm} \tag{4-6}$$

The tracking error and its time derivative can hence be expressed as:

$$e = y_{rm} - y \Rightarrow \dot{e} = \dot{y}_{rm} - \dot{y} = [\nu_{rm} - (\nu - \hat{\nu})] - [Ke + \nu_{rm}] \tag{4-7}$$

or

$$\dot{e} = -Ke - (\nu - \hat{\nu}) \tag{4-8}$$

From the analysis of (4-8), some conclusions can be drawn. The first term of the right-hand side indicates that this dynamics is always stable as long as the proportional gain is positive

($K > 0$). The second term confirms that, as for ideal actuators the actual and commanded deflections are equal and thus $\nu = \hat{\nu}$, the addition of PCH has no effect on the system in this case. When they differ, the system response is as close to the commanded as permitted by the actuator model.

In the literature, PCH is often found associated with a controller based on an approximate dynamic inversion together with an adaptive element (normally a NN) to compensate for the approximation error. In this case, the knowledge of the tracking error dynamics is crucial to define the adaptation laws. As shown in (E. N. Johnson & Calise, 2000), some interactions may exist in this case that degrade the stability and tracking performance of the overall controller. In this thesis however, a more robust dynamic inversion, the INDI, was adopted, eliminating the need for the adaptive element. According to the explanation above, this is thus beneficial for the application of the PCH.

Chapter 5

Rate Controller

As the name indicates, the main objective of a rate controller is to automatically make the system's angular rates $\underline{\omega}$ track the desired values $\underline{\omega}_{com}$ commanded by a pilot or by an external control system while keeping the whole state vector $\underline{x}$ bounded. In a helicopter, this type of controller is used in the Rate Command/Attitude Hold (RCAH) mode.

As explained in Subsection 2-1-4, in a real helicopter, the controller developed in this chapter and in the next two is implemented in the flight computers onboard (recall Figure 2-5). These computers receive electric signals corresponding to the actions desired by the pilot and compute the required control inputs to perform those actions. These inputs are then sent to the control actuators, which are subjected to position saturations and rate limits. Mathematically, they are gathered in a vector $\underline{u}$ that contains the deflections of the collective pitch of the main rotor θ_0, the longitudinal θ_{1s} and lateral θ_{1c} cyclic pitches and the collective pitch of the tail rotor θ_{0tr}.

Recall also from Subsection 2-3-6 that the state vector is composed by the body-fixed linear velocities of the helicopter $\underline{v}$, the position of its CG relative to the Earth $\underline{p}$, the body-fixed angular rates $\underline{\omega}$, the angular attitude of the helicopter $\underline{\theta}$ and the inflow ratios of the rotors $\underline{\lambda}$.

The main theory necessary to design this control system has already been developed in the last two chapters, but the specific application to the rate control of a helicopter requires certain aspects to be considered more closely. This chapter presents then in detail the sequential development of the controller under analysis, showing simultaneously the results obtained from its simulation.

5-1 INDI Control Law

Firstly, a INDI-based control system is implemented to track the desired angular rates of the helicopter. The advantages brought by this kind of controller are especially a reduction in the required knowledge of the model to be controlled and an increased robustness to uncertainties existing in that model.

For this case, the output vector of the system contains the control variables, the three components of the angular rate of the helicopter:

$$\underline{y}_{rot} = \underline{h}_{rot}(\underline{x}) = \underline{\omega} = [p \; q \; r]^T \tag{5-1}$$

Since they are physically related, as mentioned in Section 3-3, the angular rates are expected to have the same relative degree and the dynamic inversion can be performed using the complete control vector instead of individual variables. To do so, following the procedure introduced in Chapter 3, the output of the system has to be differentiated until a dependence on the control inputs of the system appears. The first time derivative is given by (2-91), the EOM for the rotational dynamics of the helicopter:

$$\dot{\underline{y}}_{rot} = \dot{\underline{\omega}} = \underline{J}^{-1} \left[\underline{m} - \underline{\omega} \times \underline{J\omega} \right] \tag{5-2}$$

where $\underline{J}$ is the inertia matrix of the helicopter and $\underline{m}$ is the moment vector that results from the sum of the contributions of all its parts. Note that some of these components depend directly on the control deflections $\underline{u}$ of the actuators of the helicopter while others simply depend on the state vector $\underline{x}$. Figure 2-15 is very useful to identify these dependencies. It is now possible to divide the equation above into two terms, depending on whether they are influenced by the control inputs. This yields:

$$\dot{\underline{\omega}} = \underline{f}(\underline{x}) + \underline{g}(\underline{x}, \underline{u}) \tag{5-3}$$

in which:

$$\underline{f}(\underline{x}) = \underline{J}^{-1} \left[\underline{m}_{fus}(\underline{x}) + \underline{m}_{ht}(\underline{x}) + \underline{m}_{vt}(\underline{x}) - \underline{\omega} \times \underline{J\omega} \right] \tag{5-4}$$

$$\underline{g}(\underline{x}, \underline{u}) = \underline{J}^{-1} \left[\underline{m}_{mr}(\underline{x}, \underline{u}) + \underline{m}_{tr}(\underline{x}, \underline{u}) \right] \tag{5-5}$$

It can be noticed that a dependence on the control inputs has already appeared through the moments produced by the main and the tail rotors. This means that the relative degree of each component is one and the total relative degree of the output vector is three. The derivative of the angular rates corresponds then to the virtual control:

$$\underline{\nu}_{rot} = \dot{\underline{\omega}} \tag{5-6}$$

The desired dynamics for $\underline{\nu}_{rot}$ can be selected based on flying qualities requirements (Brinker & Wise, 1996). The procedure followed to deduce the INDI in Section 3-5 can now be applied to design the controller for the case under analysis. Nevertheless, some additional changes have to be made to overcome particular difficulties imposed by this system. The first one is related to the fact that, contrary to the assumption made in Chapter 3, the output of the system is not affine in the controls. In fact, these variables are related through the nonlinear functions used to compute the moments generated by the rotors. When the output vector is approximated by the first-order terms of its Taylor series expansion around the current solution of the system $(\underline{x}_0, \underline{u}_0)$, the influence of $\underline{g}(\underline{x}, \underline{u})$ is only taken into account with the information contained on its first derivative. More precisely:

$$\dot{\underline{\omega}} \approx \dot{\underline{\omega}}_0 + \frac{\partial}{\partial \underline{x}} \left[\underline{f}(\underline{x}) + \underline{g}(\underline{x}, \underline{u}) \right]_{\underline{x}_0, \underline{u}_0} (\underline{x} - \underline{x}_0) + \frac{\partial}{\partial \underline{u}} \left[\underline{f}(\underline{x}) + \underline{g}(\underline{x}, \underline{u}) \right]_{\underline{x}_0, \underline{u}_0} (\underline{u} - \underline{u}_0) \tag{5-7}$$

and, as already explained, $\underline{x} \approx \underline{x}_0$ for an incremental time step, yielding:

$$\begin{aligned}\underline{\nu}_{rot} &= \underline{\dot{\omega}} = \\ &= \underline{\dot{\omega}}_0 + \left.\frac{\partial \underline{g}(\underline{x},\underline{u})}{\partial \underline{u}}\right|_{\underline{x}_0,\underline{u}_0} (\underline{u}-\underline{u}_0) = \\ &= \underline{\dot{\omega}}_0 + \underline{J}^{-1}\frac{\partial}{\partial \underline{u}}\left[\underline{m}_{mr}(\underline{x},\underline{u}) + \underline{m}_{tr}(\underline{x},\underline{u})\right]_{\underline{x}_0,\underline{u}_0}(\underline{u}-\underline{u}_0)\end{aligned} \tag{5-8}$$

where the angular acceleration of the helicopter $\underline{\dot{\omega}}_0$, the control deflections $\underline{u}_0$ and the state vector $\underline{x}_0$ have to be known or estimated. The issues associated with the measurements of $\underline{\dot{\omega}}_0$ will be addressed is Section 5-5. The position of the control actuators can also be obtained in reality, as well as the major part of the state vector. The exception lies in the inflow ratios $\underline{\lambda}$ (the dimensionless velocities induced by the rotors), which cannot be directly sensed in flight are therefore have to be estimated.

The simplest way to estimate the inflow ratios is by applying the same theoretical equations used to model the helicopter behavior in this thesis. Note however that these equations are simplifications of the reality in which, for example, they assume a uniform distribution of the flow over the rotor disc. In alternative, more complex descriptions of the wake can obviously be adopted, but they involve measurements of different types of parameters. One possible approach was recently developed in (Houston & Thomson, 2009). In this reference, the required coefficients to define the induced velocity models are calculated based on online measurements of the blade flapping angles.

For the current inversion loop, it can be concluded that the only information needed about the helicopter model is its inertia property and the influence of the control inputs on the moments produced by the two rotors. The dependence on the model of the remaining components of the vehicle has been completely eliminated. More precisely, this dependence has been replaced by measurements or estimations of the angular accelerations and the performance of the controller is strongly depending on the accuracy of these measurements.

Comparing (5-8) to (3-45), it is possible to verify that, in the case of a system that is not affine in the controls, the information of matrix $\underline{G}(\underline{x})$ is simply replaced by the derivative of the control effectiveness $\underline{g}(\underline{x},\underline{u})$ with respect to the different control inputs.

As it can be seen, the Jacobian $\underline{D}(\underline{x}_0,\underline{u}_0) = \frac{\partial}{\partial \underline{u}}\left[\underline{m}_{mr}(\underline{x},\underline{u}) + \underline{m}_{tr}(\underline{x},\underline{u})\right]_{\underline{x}_0,\underline{u}_0}$ is composed by a component that depends on the dynamics of the main rotor and by another one that concerns the tail rotor. The second term can be obtained very easily from (2-69) to (2-71), especially because it is only influenced by the last component of the input vector:

$$\left.\frac{\partial \underline{m}_{tr}(\underline{x},\underline{u})}{\partial \underline{u}}\right|_{\underline{x}_0,\underline{u}_0} = \rho A_{tr}(\Omega_{tr}R_{tr})^2 F_{tr}\frac{\sigma_{tr}C_{L_{\alpha,tr}}}{2}\left(\frac{1}{3}+\frac{\mu_{x_{tr}}^2}{2}\right)\begin{bmatrix}0 & 0 & 0 & h_{tr}\\ 0 & 0 & 0 & 0\\ 0 & 0 & 0 & -l_{tr}\end{bmatrix} \tag{5-9}$$

However, the derivation of an analytical expression for the term concerning the main rotor is rather work intensive. As depicted in Figure 2-15, the influence of the first three control inputs on the moment generated is very complex. Not only do they influence the transformation of the forces generated by the rotor into the body frame of the helicopter but they are also crucial for these forces and for the determination of the blade flapping motion, which influences

directly the behavior of the rotor. These relations are described by complex equations, often involving trigonometric functions, as derived throughout Subsection 2-3-1. Therefore, central finite differences were used to compute the first term of the Jacobian, yielding:

$$\left.\frac{\partial \underline{m}_{mr}(\underline{x},\underline{u})}{\partial \underline{u}}\right|_{\underline{x}_0,\underline{u}_0} = \begin{bmatrix} \frac{\underline{m}_{mr}^T\left(\underline{x}_0,\underline{u}_0+[\tau_{\theta_0}\ 0\ 0\ 0]^T\right)-\underline{m}_{mr}^T\left(\underline{x}_0,\underline{u}_0-[\tau_{\theta_0}\ 0\ 0\ 0]^T\right)}{2\tau_{\theta_0}} \\ \frac{\underline{m}_{mr}^T\left(\underline{x}_0,\underline{u}_0+[0\ \tau_{\theta_{1s}}\ 0\ 0]^T\right)-\underline{m}_{mr}^T\left(\underline{x}_0,\underline{u}_0-[0\ \tau_{\theta_{1s}}\ 0\ 0]^T\right)}{2\tau_{\theta_{1s}}} \\ \frac{\underline{m}_{mr}^T\left(\underline{x}_0,\underline{u}_0+[0\ 0\ \tau_{\theta_{1c}}\ 0]^T\right)-\underline{m}_{mr}^T\left(\underline{x}_0,\underline{u}_0-[0\ 0\ \tau_{\theta_{1c}}\ 0]^T\right)}{2\tau_{\theta_{1c}}} \\ 0_{1\times 3} \end{bmatrix}^T \tag{5-10}$$

where $0_{1\times 3}$ is a 1×3 zero matrix. The value of the three perturbations $(\tau_{\theta_0}, \tau_{\theta_{1s}}, \tau_{\theta_{1c}})$ is chosen to be a small percentage of the absolute value of each variable or to a fixed infinitesimal quantity, if the unperturbed value is already too small.

In order to obtain the control law for the INDI loop, equation (5-8) has to be solved with respect to the input vector $\underline{u}$. However, since there are four actuators and only three rates to be controlled, a redundancy exists and the system is over-determined. As a consequence, the Jacobian matrix has more columns than rows and thus it cannot be inverted directly. This means that a control allocation strategy has to be used to solve this problem.

Control Allocation

Several algorithms exist to deal with the control allocation problem and the description of the ones that are most often adopted can be found, for example, in (Bodson, 2002) or (Bordignon & Bessolo, 2002). The simplest form of the referred allocation is by using the pseudo-inverse matrix. Given the Jacobian matrix $\underline{D}$, with more columns than rows, its pseudo-inverse corresponds to:

$$\underline{D}^+ = \underline{D}^T\left(\underline{D}\underline{D}^T\right)^{-1} \tag{5-11}$$

Control allocation using the pseudo-inverse method corresponds to the unconstrained minimization of the error between the desired effort produced by the actuators and its actual value. Since multiple solutions exist for an over-determined system, the calculation of the pseudo-inverse can also be affected by a diagonal weighting matrix $\underline{W}$ to prioritize the usage of the different actuators, yielding:

$$\underline{D}^+ = \underline{W}^{-1}\underline{D}^T\left(\underline{D}\underline{W}^{-1}\underline{D}^T\right)^{-1} \tag{5-12}$$

This method is very convenient, for example, to prevent the saturation of the actuators or to exclude a malfunctioning actuator by a proper choice of the weighting matrix. This matrix consists normally of a combination of the actuators rate and position limits (Bacon et al., 2001).

More optimal control allocations can be obtained when, besides the error between the desired and actual effort produced by the actuators, the demanded control actuation is also minimized. The methods used to achieve these objectives are normally based on linear, quadratic or nonlinear programming, as summarized in (Poonamallee & Doman, 2004).

At this point, only the pseudo-inverse method (5-11) was used to perform the dynamic inversion. According to this, at a given time instant (corresponding to the subscript 0), the required input vector for the next iteration to linearize and decouple the responses associated with the angular rates of the helicopter is given by:

$$\underline{u} = \underline{D}(\underline{x}_0, \underline{u}_0)^T \left(\underline{D}(\underline{x}_0, \underline{u}_0)\underline{D}(\underline{x}_0, \underline{u}_0)^T\right)^{-1} \underline{J}(\underline{\nu}_{rot} - \dot{\underline{\omega}}_0) + \underline{u}_0 \tag{5-13}$$

In the end of Chapter 3 it was shown that the loop based on INDI control laws assures the complete linearization and decoupling of the responses even in the presence of model uncertainties. However, in the derivation of the rate controller under analysis, two approximations were made: the control function $\underline{g}(\underline{x}, \underline{u})$ was only considered through its first derivative and some of its components were not obtained analytically, but using numerical differentiation instead. The consequences of these approximations in the accuracy of the control system obtained will be assessed in the next section.

At this point, assuming the relation $\underline{\nu}_{rot} = \dot{\underline{\omega}}$ holds when (5-13) is applied to the system, the channel i associated with each component of the angular rate of the helicopter becomes a single integrator and the three channels are completely decoupled and can be designed separately. Therefore, a simple linear control law (3-9) can be implemented to close the loop and allow the tracking of the desired references. The linear gains in this equation are determined using classical SISO control theory. To do so, it is convenient to analyze the open-loop response in the Laplace domain, by mean of its transfer function:

$$H_{i_{ol}}(s) = \frac{\omega_i(s)}{\nu_{rot_i}(s)} = \frac{1}{s} \tag{5-14}$$

If a linear controller $K_i(s)$ is applied with a negative feedback of the control variable and setting the feedforward term $\dot{\omega}_{i_{com}}$ to zero for now, the closed-loop transfer function associated with each channel is given by:

$$H_{i_{rot}}(s) = \frac{\omega_i(s)}{\omega_{i_{com}}(s)} = \frac{K_i(s)H_{i_{ol}}(s)}{1 + K_i(s)H_{i_{ol}}(s)} = \frac{K_i(s)}{s + K_i(s)} \tag{5-15}$$

where $\omega_{i_{com}}$ is the reference commanded to the angular rate of channel (axis) i. Note that the dynamics of sensors and actuators is neglected at this stage. The linear controller $K_i(s)$ to control the single-integrator open-loop may assume the form of a conventional Proportional (P) or Proportional-Integrative (PI) controller. In the first case, a first-order response is obtained for the closed-loop system, while the second one yields a second-order evolution. The decision made depends then on the desired flying qualities for the system. If a P controller with gain K_{1_i} is chosen to keep things simpler, the following transfer function is obtained:

$$H_{i_{rot}}(s) = \frac{K_{1_i}}{s + K_{1_i}} \tag{5-16}$$

The value of K_{1_i} corresponds to the bandwidth of channel i and to the inverse of the time constant imposed to its response. From this transfer function, it can be concluded that the closed-loop system is always stable for $K_{1_i} > 0$, since its pole is negative. Nevertheless, a higher gain implies a more demanding tracking and therefore more effort from the actuators. Furthermore, the steady-state gain ($s \to 0$) is unitary and thus the error for tracking the unit step reference is expected to be null when no disturbances affect the system.

The working principle of the controller developed so far is summarized in Figure 5-1. In this figure, $\underline{K}_1$ is a diagonal matrix with the proportional gains K_{1_i} and $\underline{h}_{rot}(\underline{x})$ is the output function to obtain the angular velocities from the state vector. Furthermore, recall that $\underline{x} \approx \underline{x}_0$ since the loop regarded here concerns only fast dynamics. The unit delay operator z^{-1} is used to access the current value of the control vector which, as already mentioned, is assumed to be known. Finally, the angular accelerations $\dot{\underline{\omega}}_0$ are also assumed to be known without any error. The result of the control system for a more realistic case in which this vector is not accurately estimated is evaluated in detail in Section 5-5.

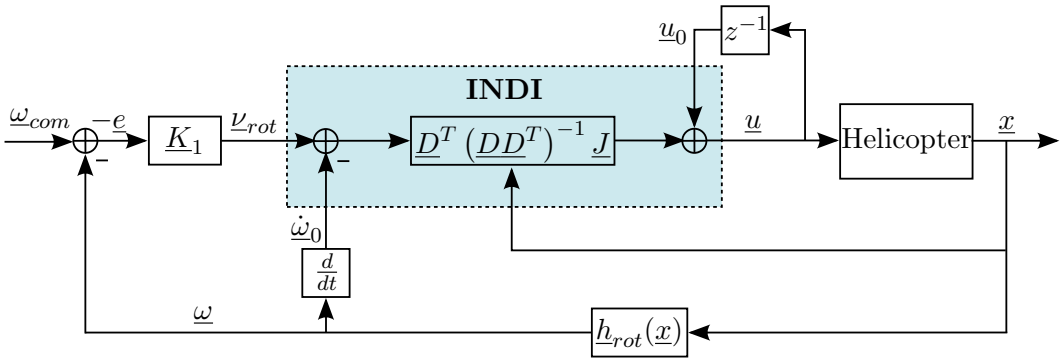

Figure 5-1: Schematic of the angular rate control system based on INDI.

5-2 Primary Tests

To test the control system developed so far, three simultaneous doublet inputs with an amplitude of 10 deg/s and duration of 2 s were commanded to the three components of the angular rate of the helicopter. The simulation was started with the helicopter in hovering flight at 1000 m of altitude. Both the model simulation and the controller calculations were sampled at 100 Hz. Moreover, the linear gains were chosen such that the responses of the three axes present a time constant of 0.09 s. The results obtained are depicted in Figure 5-2.

As it can be seen, the tracking of the references is achieved very efficiently, presenting the shape of a first-order response, as expected. The steady-state errors, despite being very small, are not exactly zero, as predicted theoretically. This can be explained from the fact that $\underline{\nu}_{rot} = \dot{\underline{\omega}}$ is not completely true due to the approximation $\underline{x} \approx \underline{x}_0$. Furthermore, the responses of the three axes were expected to be exactly equal. The difference observed for the z-axis is due to the different dynamics associated with the actuator that is mainly used to control the angular rates around this axis (the collective pitch of the tail rotor).

As already mentioned, the validity of the approximations made for the implementation of the INDI (considering the control function only through its first-order derivative and using numerical differentiation to determine some of its components) has still to be checked. To do that, a nonlinear solver is used to compute the control inputs required to perform the feedback linearization and assess the errors with respect to the previous simulation. In this case, no approximation based on the first-order terms of a Taylor series is used, but a numerical

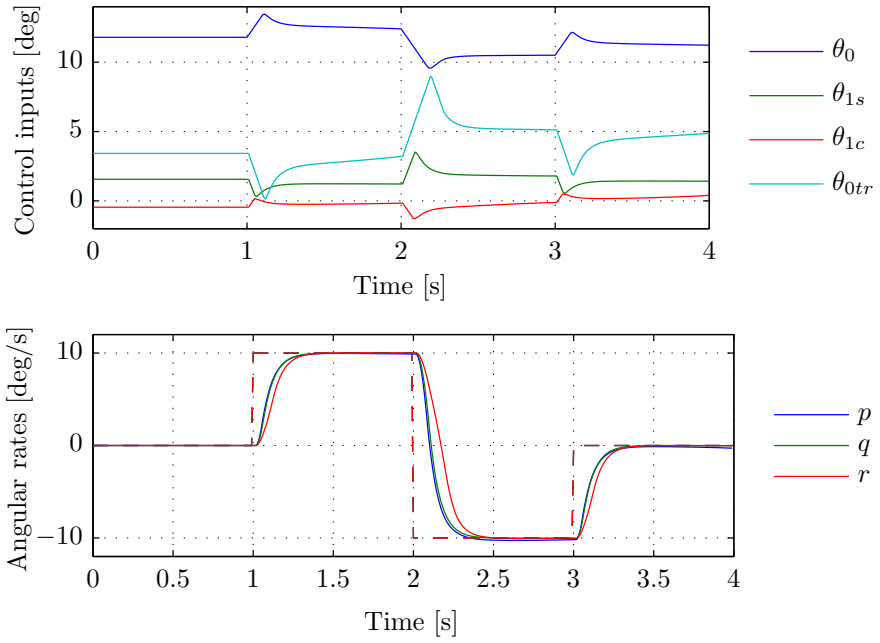

Figure 5-2: Doublet response of the INDI rate controller with control allocation. The dashed lines correspond to the references commanded while the solid lines represent the response of the helicopter.

optimization algorithm is implemented to invert the system. More precisely, consider again the EOM for the rotational dynamics of the helicopter, written as in (5-3):

$$\dot{\underline{\omega}} = \underline{f}(\underline{x}) + \underline{g}(\underline{x}, \underline{u})$$

At the current time instant (associated with the subscript 0), the same relation is expressed as:

$$\dot{\underline{\omega}}_0 = \underline{f}(\underline{x}_0) + \underline{g}(\underline{x}_0, \underline{u}_0) \tag{5-17}$$

Once again, assuming that $\underline{x} \approx \underline{x}_0$, the subtraction of the equations results in:

$$\dot{\underline{\omega}} - \dot{\underline{\omega}}_0 = \underline{g}(\underline{x}_0, \underline{u}) - \underline{g}(\underline{x}_0, \underline{u}_0) \tag{5-18}$$

where the angular acceleration corresponds to the virtual control $\underline{\nu}_{rot} = \dot{\underline{\omega}}$ and function $\underline{g}(\underline{x}, \underline{u})$ is given by (5-5). The required physical input $\underline{u}$ to generate the desired virtual control input is then obtained from the solution of:

$$\underline{g}(\underline{x}_0, \underline{u}) - \underline{g}(\underline{x}_0, \underline{u}_0) - \underline{\nu}_{rot} + \dot{\underline{\omega}}_0 = 0 \tag{5-19}$$

Note that this equation represents the error relative to the desired angular acceleration vector, which has to be minimized. An analytical solution cannot be obtained, since $\underline{u}$ is "hidden" in the nonlinear function $\underline{g}(\underline{x}, \underline{u})$ and thus a nonlinear solver has to be used. In this case, an optimization method was adopted to minimize the energy of the error, being $\underline{u}$ the solution of the problem:

$$\min_{\underline{u}} \left\| \underline{g}(\underline{x}_0, \underline{u}) - \underline{g}(\underline{x}_0, \underline{u}_0) - \underline{\nu}_{rot} + \dot{\underline{\omega}}_0 \right\|^2 \tag{5-20}$$

The most suitable method to solve this problem is based on nonlinear least squares. It is part of *MATLAB*'s Optimization Toolbox and makes use of the Levenberg-Marquardt algorithm to minimize the cost function above (MathWorks, n.d.-a), with a chosen tolerance of 10^{-6} rad^2/s^4. It is expected that this problem is convex so that it can be stated that when a minimum value of the cost function is found, it corresponds to a global minimum.

While it is not trivial to validate the procedure globally, a single simulation may be enough to identify potential problems. Under the same conditions as before, the evolution of the absolute differences between the simulation using the INDI approach and using the nonlinear solver is shown in Figure 5-3.

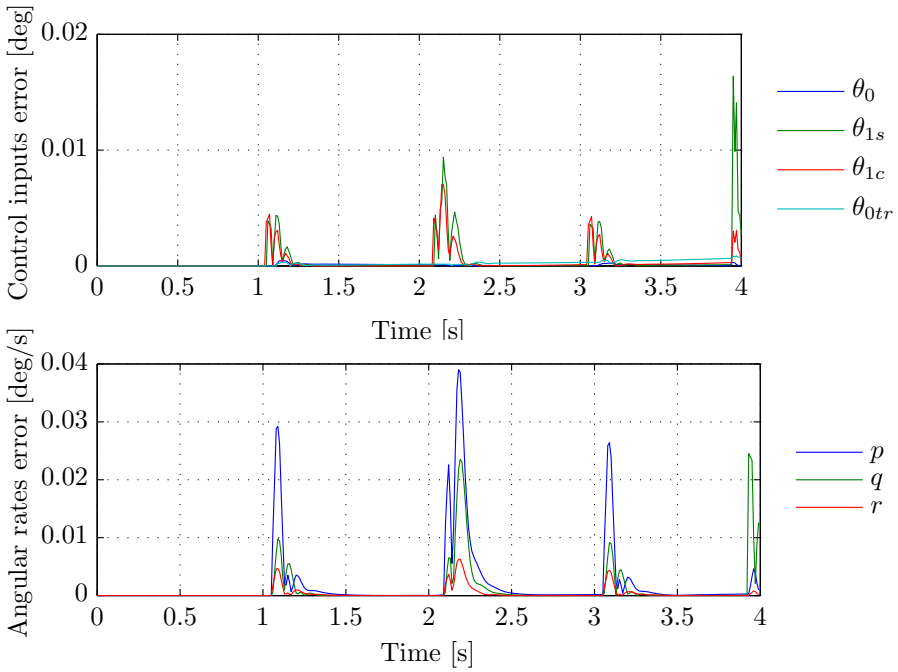

Figure 5-3: Validation of the approximations made for the INDI with a nonlinear solver. The dashed lines correspond to the references commanded while the solid lines represent the response of the helicopter.

As it can be seen, the differences in terms of the controls demanded and the angular rates obtained are always very small and only noticeable in the transient instances. These instances are when the nonlinear characteristics of the model are more noticeable and thus a linearized description of $\underline{g}(\underline{x}, \underline{u})$ is less accurate. Nevertheless, the approximation made to avoid the nonlinear solver is valid in general. Despite the verification made for this particular case, a generic validation for every possible condition would still be desirable. Note that the option of using the nonlinear solver to control the system is not feasible since it involves a more demanding computational load when compared to the INDI. In fact, the time necessary to simulate the same response was approximately eleven times higher with the nonlinear solver.

Finally, it was decided that the collective of the main rotor should not be used directly to control the angular rates of the helicopter. The reason for this choice is that this input will be needed to control the altitude (thus the vertical force) efficiently, as it will be seen in

Chapter 7. In fact, while θ_{1s}, θ_{1c}, θ_{0tr} are moment generators, the collective of the main rotor is primarily a force effector.

The command signal for the main rotor collective will therefore be supplied by an outer loop and, at this point, to control the angular rates, it is assumed constant and equal to its trim value. This has also the advantage of avoiding control allocation, simplifying the controller even further. After this change is applied, the performance of the control system was again simulated, leading to the results of Figure 5-4.

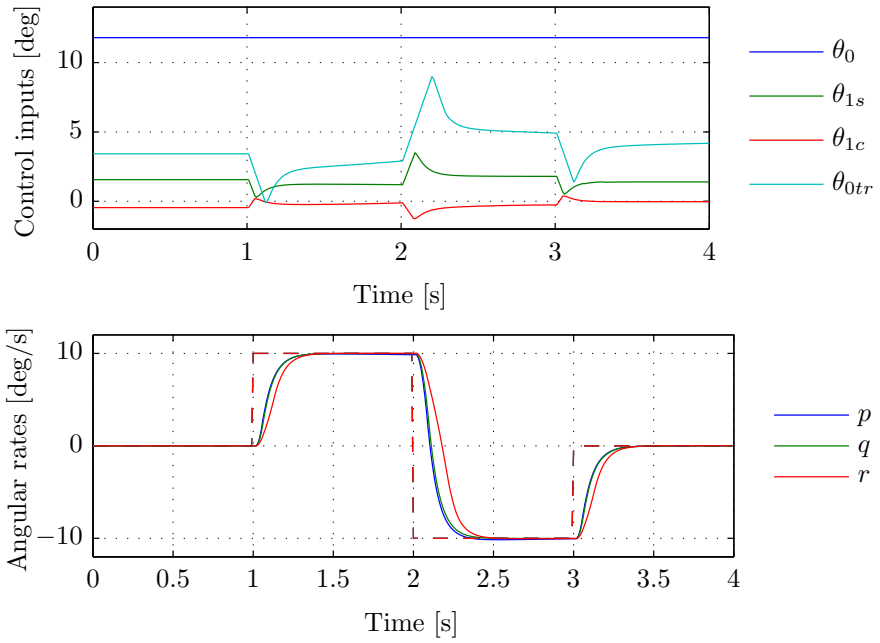

Figure 5-4: Doublet response of the INDI rate controller with the collective fixed. The dashed lines correspond to the references commanded while the solid lines represent the response of the helicopter.

From the analysis of this figure, it can be observed that even with the collective fixed, the control system is able to track the commanded references with no problem. No significant changes are observed when compared to Figure 5-2.

5-3 Controllability Analysis

As it was seen in Section 3-2, the performance of the controller is strongly dependent on the relative degree of the system. It was stated that if its value is inferior to the order of the system, internal dynamics still exist after the input-output linearization and, unless these hidden dynamics are stable, the controllability of the system is compromised. The present section aims to assess the effectiveness of the NDI-based control for the helicopter model under analysis by examining separately the degrees of internal dynamics that remain after the application of the INDI.

First, it has to be checked whether or not are internal dynamics present in the closed-loop system. As it was seen in Subsection 2-3-6, the helicopter system is of fourteenth order. The rate controller developed so far performs the inversion of (2-91) and is characterized by an input-output linearization with a total relative degree of three. This means therefore that the linearization produced eleven degrees of unobservable internal dynamics that may compromise the stability of the system. In fact, due to the existence of these dynamics, the closed-loop system with the rates controller is slightly unstable (note that the control signals are not steady when the angular rates of the helicopter are, in Figure 5-2, as well as the increased oscillations in the last seconds of Figure 5-3). This instability can be easily avoided by designing a simple control law (like a linear PID) for the collective of the main rotor that allows the helicopter to keep or to track a certain altitude reference.

Nevertheless, as already mentioned, the overall control system will contain two more loops to control the attitude angles of the helicopter and its velocity with respect to the Earth. The former one will perform the inversion of (2-92), increasing in three units the total relative degree of the controller. The last loop will carry out the linearization of the translational motion (2-89) (expressed in the NED reference frame instead), adding three more relative degrees to the system. Therefore the total relative degree of the closed-loop system is nine, while the nonlinear system is of fourteenth order, meaning that there are still five degrees of internal dynamics.

The stability of these dynamics has now to be evaluated. If they are stable (in the Bounded-Input Bounded-Output (BIBO) sense), no instabilities due to internal dynamics will arise in the complete control system. As mentioned above, this will be further facilitated when the input to the collective is not constant, but provided by an outer loop instead.

As already explained, stability evaluation is normally very difficult to be performed for non-linear systems. One way to investigate their stability is by using Lyapunov theory. However, methods based on this theory are not generally applicable due to the difficulty of finding a candidate Lyapunov function. In the current case, the stability of the internal dynamics can be easily assessed by a simple interpretation of the physical phenomena they describe.

Three degrees of internal dynamics correspond to the kinematic relations of the translational motion (2-90). The boundedness of these dynamics is however assured by the fact that they are related to the translational dynamics inverted in the outer loop through a simple rotation matrix, which is an orthonormal transformation. Therefore, only the dynamics relative to the quasi-dynamic inflow of the rotors still have to be investigated. According to (2-93), these are described by:

$$\tau_{\lambda_0}\dot{\lambda}_0 = C_T - C_T^{Gl}$$
$$\tau_{\lambda_{0,tr}}\dot{\lambda}_{0_{tr}} = C_{T_{tr}} - C_{T_{tr}}^{Gl}$$

As already explained, in steady operation, the thrust coefficient calculated by the blade element method tends to the one calculated from Glauert theory. As a consequence, it follows from the equations above that $\dot{\lambda}_0 \to 0$ and, similarly, $\dot{\lambda}_{0_{tr}} \to 0$. This proves the stability of the two remaining degrees of internal dynamics, corresponding to the behavior of λ_0 and $\lambda_{0_{tr}}$. It is also interesting to visualize the evolution of these two variables in the normal motion of the helicopter. The results obtained during the simulation performed for Figure 5-4 are depicted in Figure 5-5.

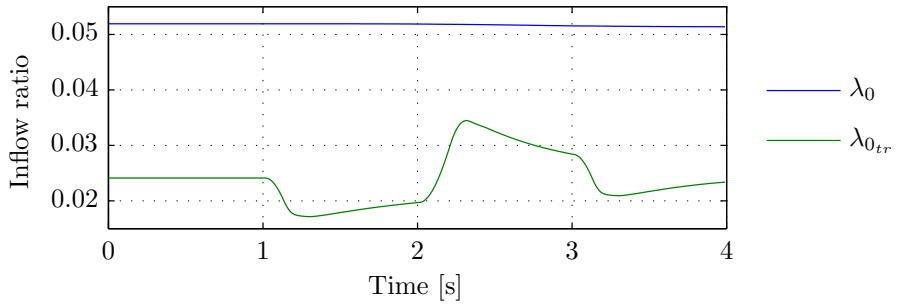

Figure 5-5: Inflow ratios for the previous simulation.

As it is possible to see, in this case, the responses of both inflow ratios are indeed bounded. It can also be verified that the inflow of the main rotor remained practically constant since the collective command was fixed, meaning that this is the main influence to the inflow of this rotor. Note also the fact that the signals are not completely steady by the end of the simulation is again justified by the small instabilities due to internal dynamics. As mentioned above, this situation will be automatically solved when the complete control law is designed and no remaining unstable internal dynamics exist after the dynamic inversion.

5-4 Introduction of PCH

The advantages of PCH in a system with sensitive actuator dynamics were already shown mathematically in Chapter 4. In order to protect the control system from degradations caused by saturation effects of the actuators, this technique is now applied to the rate controller of the helicopter developed so far. It makes use of a reference model exactly like the one presented in Figure 4-1 to filter the commanded angular rate and provide a feedforward term for each channel. The bandwidth of this filter corresponds to the one imposed by the INDI-based control loop. The limits allowed for the commanded angular rates were imposed after consulting (*ADS-33E-PRF*, 2000) and consist of 40 deg/s for the roll and pitch rates and 80 deg/s for the yaw rate.

The reference model is also adjusted by the pseudo-control hedge so that the demanded signal is within the system's capabilities. This value results from a constant monitoring of the system and the generic procedure to calculate it for a INDI-based loop is shown in (4-2). According to this and making use of (5-8) without considering θ_0 for the reasons explained before, the pseudo-control hedge is given by:

$$\underline{\nu}_{h_{rot}} = \underline{J}^{-1} \frac{\partial}{\partial \underline{u}'} \left[\underline{m}_{mr}(\underline{x}, \underline{u}) + \underline{m}_{tr}(\underline{x}, \underline{u}) \right]_{\underline{x}_0, \underline{u}_0} (\underline{u}'_{com} - \underline{u}') \tag{5-21}$$

where $\underline{u}'$ is the actual input vector without the collective of the main rotor and $\underline{u}'_{com}$ the corresponding commanded vector (neglecting the dynamics of the actuators). After implementing this, the overall control system is summarized in Figure 5-6.

In this figure, the block "Act." corresponds to the dynamics of the actuators and $\underline{h}_{rot}(\underline{x})$ is again used to obtain the angular velocities from the state vector. The block "RM" consists

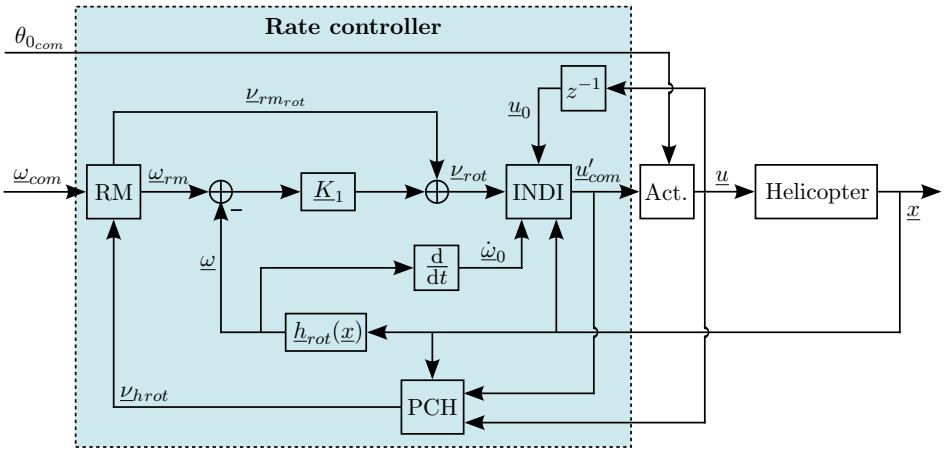

Figure 5-6: Schematic of the rate control system based on INDI and PCH.

of the subsystem represented in Figure 4-1 for each one of the three axes, "INDI" performs the dynamic inversion for the three control inputs used in this loop and "PCH" basically computes (5-21). As assumed, the collective of the main rotor $\theta_{0_{com}}$ is kept constant or provided by an external loop.

Since the doublet signal analyzed in this chapter is not too demanding for the system, the improvements brought by the PCH are still not identified at this moment. A detailed simulation presenting the benefits of the PCH to helicopter flight control will be carried out in Section 7-3 instead.

5-5 Angular Accelerations

Until now, it was assumed that the angular accelerations can be accurately measured and thus no error exists between the real acceleration of the helicopter and the value assumed by the control system. Despite they already exist (Klein & Morelli, 2006), angular acceleration sensors are still not common in practice and they are especially costly. This means that the angular accelerations have to be estimated using data that can be acquired with the Inertial Measurement Unit (IMU) onboard of the vehicle.

5-5-1 Finite differences

The most intuitive and simple method to estimate the angular accelerations is probably to use backward finite differences. From the information about the angular velocities of the helicopter, the accelerations at the time instant t are given by:

$$\dot{\underline{\omega}}(t) = \frac{\underline{\omega}(t) - \underline{\omega}(t - \Delta t)}{\Delta t} \tag{5-22}$$

where Δt is the sample time between two iterations, which should be as small as possible to obtain higher accuracy. When this strategy is applied to the control system, the required control deflections to perform the same maneuver as before are depicted in Figure 5-7.

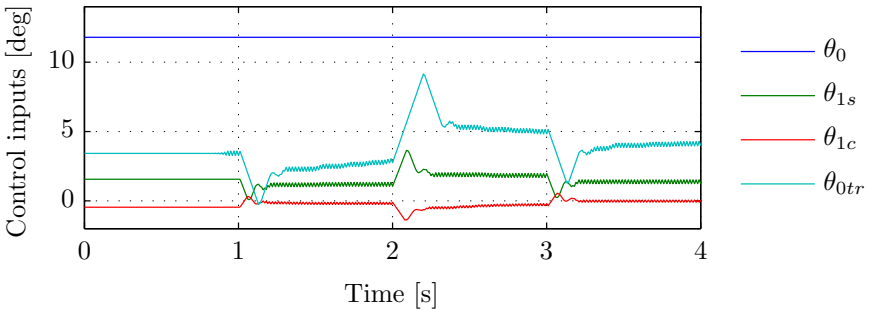

Figure 5-7: Control inputs when the angular accelerations are estimated by finite differentiation.

In this figure, it is possible to identify the appearance of oscillations with small amplitude and high frequency in the controls that result of the INDI law. These oscillations not only contribute to a degradation of the tracking performance of the controller, they affect especially the adequate operation of the control actuators.

This problem has been previously identified in (Sieberling et al., 2010). In this reference, it is explained that because in the INDI the demanded angular acceleration $\underline{\nu}_{rot} = \underline{\dot{\omega}}$ is considered to be one incremental time step from the measured angular acceleration $\underline{\dot{\omega}}_0$, any delay will violate this assumption, hence the system is not completely linearized, which causes a loss of performance. Because it is impossible to eliminate the time delay, the control system must be adjusted to anticipate upon it, which can be done using a predictive filter.

5-5-2 Predictive filter

In opposition to the predictive filters often found in the literature, based on multiple neural networks or extensive Kalman filtering, in (Sieberling et al., 2010) a very simple linear predictive filter is successfully implemented. This simplified filter only works in combination with the INDI, since the latter technique decouples the dynamics of the controlled model. This allows to use only information about one axis to estimate the angular acceleration of the helicopter around that axis. The combination of the predictive filter with the INDI is known as Predictive Incremental Nonlinear Dynamic Inversion (PINDI).

The current situation is however more complex than the one presented in the mentioned reference, since there the actuators were assumed ideal (without dynamics) and no PCH existed in the control loop. This means that the applicability of the filter in this case has still to be assessed.

Besides its simplicity, the main advantage of using a linear filter is that stability in the BIBO sense is guaranteed. To each axis i, a linear predictive filter is associated in order to predict the angular accelerations of the closed-loop system about that axis. The angular accelerations can then be represented by:

$$\dot{\omega}_i(t) = [\omega_i(t) \ \ldots \ \omega_i(t - 5\Delta t) \ \omega_{i_{com}}(t) \ \ldots \ \omega_{i_{com}}(t - 5\Delta t)] \, \underline{c}_i + \epsilon_i(t) \tag{5-23}$$

where $\underline{c}_i$ is a parameter vector with constant coefficients and $\epsilon_i(t)$ is the predictive error. Note that the left-hand side of the equation corresponds to the real value of the angular

acceleration. Vector $\underline{c}_i$ is determined from the minimization of the energy of the error $\epsilon_i(t)$, using least squares estimation.

To do so, the predictive filter has to be trained offline. Again, a doublet input with 10 deg/s of amplitude and 2 s of duration is applied to the model of the helicopter in closed-loop, the ideal angular accelerations are collected in a vector $\underline{z}_i$ and the commanded and actual values of angular rates are collected in the regressor function $\underline{H}_i$, yielding:

$$\underline{z}_i = \underline{H}_i \underline{c}_i + \underline{\epsilon}_i \tag{5-24}$$

In this case, $\underline{H}_i$ represents a linear mapping, but it could also assume a nonlinear model structure on the state and input variables of the system. For this kind of problem, it is however necessary that the model output $\underline{z}$ is linear in the unknown vector $\underline{c}$.

The cost function to be optimized is then selected as the sum of the squares of the predictive error:

$$J_i = \|\underline{\epsilon}_i\|^2 = (\underline{z}_i - \underline{H}_i \underline{c}_i)^T (\underline{z}_i - \underline{H}_i \underline{c}_i) \tag{5-25}$$

This corresponds to a quadratic optimization problem, in which a unique minimum exits for:

$$\frac{\partial J_i}{\partial \underline{c}_i} = \underline{H}_i^T (\underline{z}_i - \underline{H}_i \underline{c}_i) = 0 \tag{5-26}$$

from which follows:

$$\underline{c}_i = (\underline{H}_i^T \underline{H}_i)^{-1} \underline{H}_i^T \underline{z}_i \tag{5-27}$$

Once the vectors with the optimal coefficients $\underline{c}_i$ for $i = 1, 2, 3$ are determined, they can be applied online to predict the angular accelerations during the simulation. The result obtained from the training of the predictive filter to the roll axis ($i = 1$) is presented in Figure 5-8.

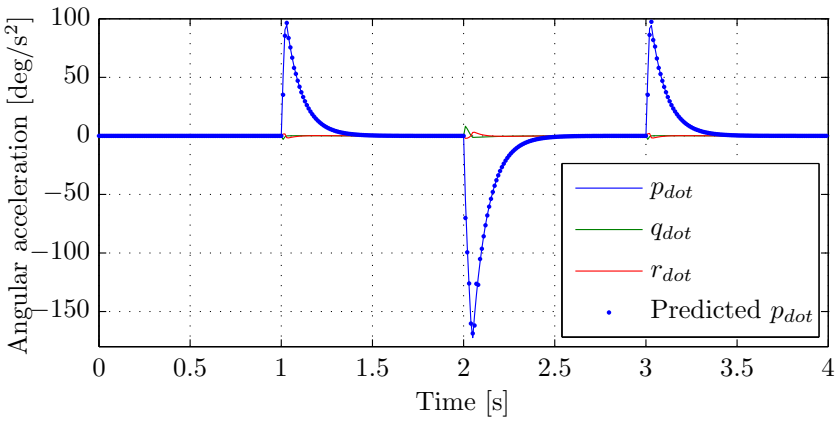

Figure 5-8: Training of the predictive filter for the roll axis.

It is possible to see that the predictive filter can estimate quite accurately the angular accelerations for this axis. Nevertheless, residual accelerations are verified for the remaining axes during the maneuver the responses could not be completely decoupled by the INDI. The conclusion on whether this is problematic for the application of the predictive filter will be drawn in a few moments.

5-5-3 Five points scheme

Finally, an intermediate estimation method was tested, based on a numerical scheme that makes use of five points. This method is also presented in (Sieberling et al., 2010) and, according to it, the angular accelerations are approximated by:

$$\dot{\underline{\omega}}(t) = \frac{1}{12\Delta t}\left[25\underline{\omega}(t) - 48\underline{\omega}(t-\Delta t) + 36\underline{\omega}(t-2\Delta t) - 16\underline{\omega}(t-3\Delta t) + 3\underline{\omega}(t-4\Delta t)\right] \quad (5\text{-}28)$$

When compared to the finite differences, this scheme is expected to be more accurate since it uses a higher number of points, but also more sensitive to noise because of the larger value of its coefficients. The comparative analysis between this method and the predictive filter (and also the finite differencies) has now to be carried out.

5-5-4 Choice of the method

In order to compare the three methods described above in this section, the same maneuver with which Figure 5-7 was obtained was repeated and the accelerations estimated were registered. Figure 5-9 shows a close-up of the results obtained for the x-axis.

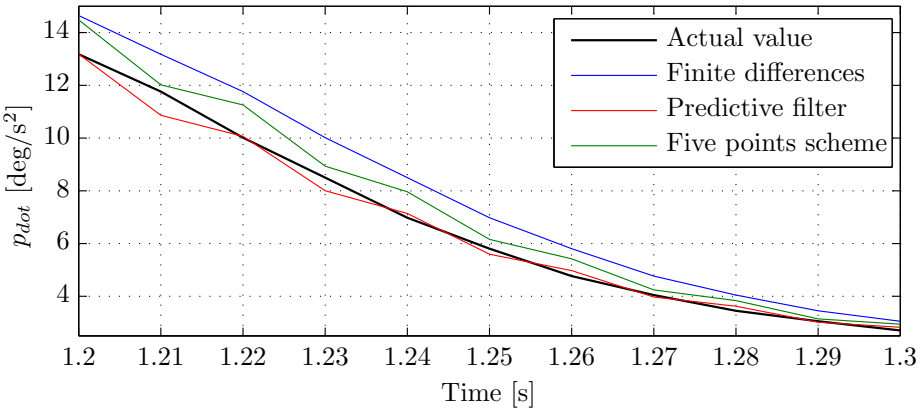

Figure 5-9: Comparison of the three estimation methods for the angular acceleration.

As expected, the largest error is associated with the estimations obtained by finite differentiation due to the delay that exists relatively to the real response. Furthermore, the predictive filter is the approach that is able to estimate the angular acceleration of the helicopter with the least error. Nevertheless, both the predictive filter and the five points scheme exhibit quite oscillatory responses. This indicates that they are very sensitive to variations in the angular rates, generating considerably noisy estimations that will not contribute to a reduction of the control oscillations shown in Figure 5-7.

Furthermore, note that the simulations used to train the predictive filter and obtain the optimal coefficients are started at a specific flight condition. The accuracy of the estimation may therefore become degraded when the helicopter moves away from the referred condition. This means that the predictive filter would have to be trained for several flight conditions, which is a quite unpractical task (that reminds of gain scheduling).

From the three methods presented here, despite the fact that the predictive filter is the one that estimates the angular accelerations more accurately, finite differentiation is expected to be the most suitable one to adopt for control purposes, since it is less affected by numerical noise (it shows less oscillations). It can be concluded that, in spite of the successful results obtained with the predictive filter for an ideal case in (Sieberling et al., 2010), its application is not worthy for real situations with actuator limitations and in which the closed-loop system is not fully decoupled as a consequence.

In order to eliminate the control oscillations that appear when finite differentiation is adopted, simple first-order low-pass filters (LPFs) with a bandwidth of 10 Hz were introduced before the three actuators. Obviously, this value has to be sufficiently higher than the bandwidth of the actuators in order not to degrade the performance of the system. The Bode diagram of these filters is depicted in Figure 5-11. The LPFs are not the ideal choice for the controller since they introduce a 90 deg phase delay around its cutoff frequency (the frequency for which the filter provides an attenuation of 3 dB). Nevertheless, the potential development of a more complex predictor for the angular accelerations is out of the scope of this thesis.

It is also very important to note that, in principle, for a potential practical implementation of the suggested control system, the introduction of the LPFs is not needed since the real actuators have already a dynamics normally modelled as a first or second order system, providing themselves the required filtering action.

The control inputs obtained from the simulation with finite differences plus the referred LPFs are illustrated in Figure 5-10.

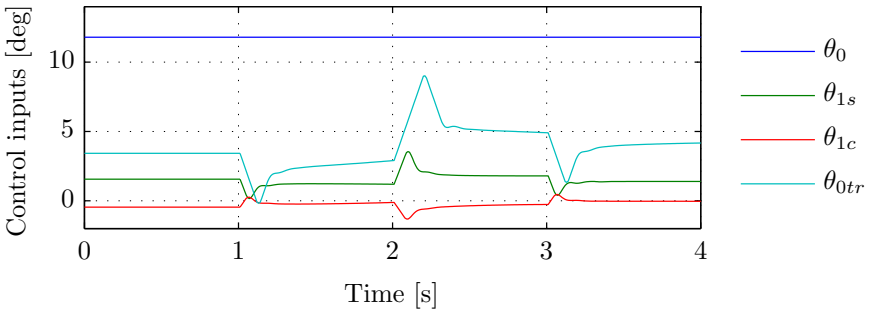

Figure 5-10: Control inputs when using finite differentiation and LPF before the actuators.

Comparing this figure with the ideal situation of Figure 5-4, it can be concluded that the results obtained with finite differentiation plus LPFs are very satisfactory. Furthermore, the tracking performance of the control system is roughly the same.

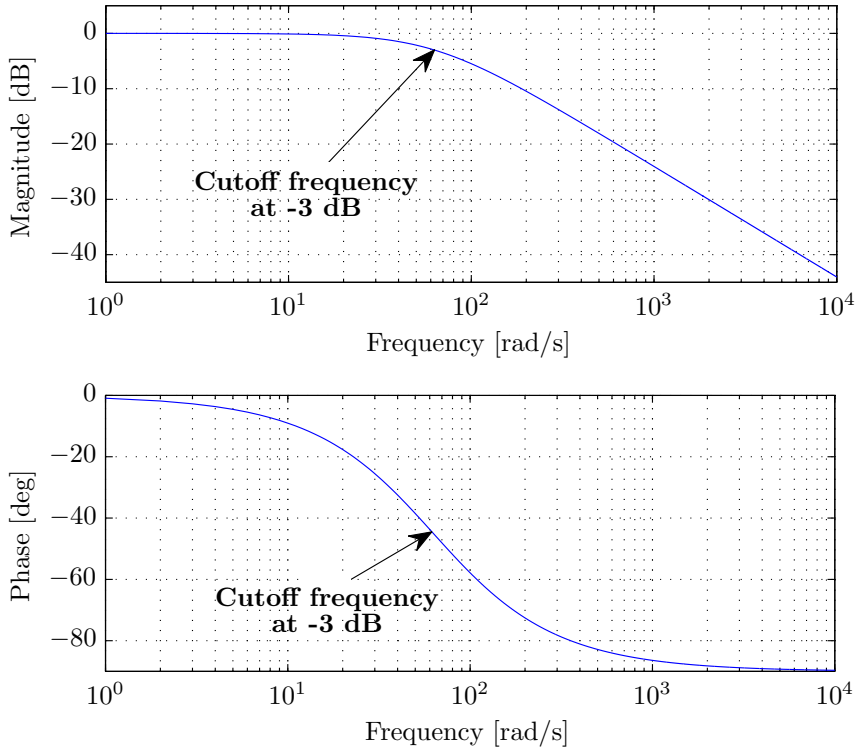

Figure 5-11: Bode diagram of the LPFs used to filter the control inputs.

Chapter 6

Attitude Controller

Now that the rate controller was implemented for the helicopter under analysis, the control system can be expanded such that commands in terms of attitude angles $\underline{\theta}_{com}$ are automatically tracked by the orientation of the rotorcraft $\underline{\theta}$. In a helicopter, this type of controller is used in the Attitude Command/Attitude Hold (ACAH) mode.

The implementation of this controller is mainly based on the time scale separation principle presented in Section 3-4. Since the evolution of the angular rates is assumed to be faster than the corresponding attitude angles, a loop to control the referred angles can be designed externally to the rate controller. In this line of reasoning, this loop (the slow dynamics) generates the commanded angular rates $\underline{\omega}_{com}$ to be tracked by the inner loop (the fast dynamics) in order to achieve the tracking of the desired attitude angles. This means that the angular rates are used as control inputs for the slow time scale loop. This assumes that the angular rates are always what they are commanded to be, just like the deflections of the actuators are assumed to be instantaneously what they are commanded to be.

The present chapter shows sequentially the development of the attitude controller for the helicopter, demonstrating also the improvement it brings when compared to simple linear controllers.

6-1 NDI Control Law with PCH

In this loop, the basic (non-incremental) version of the NDI is used to control the attitude angles of the helicopter. For this case, the output vector of the system contains the control variables, the three attitude angles that describe the orientation of the vehicle with respect to the Earth:

$$\underline{y}_{att} = \underline{h}_{att}(\underline{x}) = \underline{\theta} = [\phi \ \theta \ \psi]^T \tag{6-1}$$

Once again, as the three angles have the same physical meaning, they have the same relative degree and the dynamic inversion can be performed directly for the complete control vector. Following the procedure presented in Chapter 3, when the output of the system is

differentiated with respect to time, the differential equation for the rotational kinematics of the body (2-92) is obtained:

$$\underline{\dot{y}}_{att} = \underline{\dot{\theta}} = \underline{\Omega}_o^b \underline{\omega} \tag{6-2}$$

where matrix $\underline{\Omega}_o^b$ was derived in (A-9) and depends only on the attitude angles $\underline{\theta}$. Since this loop sees the angular rates $\underline{\omega}$ as control inputs and the direct dependence on them has already appeared, each one of the three components have a unitary relative degree, yielding the virtual control:

$$\underline{\nu}_{att} = \underline{\dot{\theta}} = \underline{\Omega}_o^b \underline{\omega} \tag{6-3}$$

At this point, it can be noticed that there is not a part of this system that does not depend on the control inputs (the angular rates). This means that the application of INDI would not bring any advantage in this case, since it would not result in the reduction of the required knowledge of the model. Furthermore, this mathematical model has practically no uncertainties associated with it since it corresponds to the well-known rotational kinematics of a rigid body in space and all the parameters it depends on (the attitude angles) can be measured very accurately by the helicopter's IMU.

If the time scale separation principle was not applied to simplify the design of the controller, the control inputs for the current loop would not be the angular rates of the helicopter, but its physical controls instead. Hence, the output vector would have to be differentiated twice until an explicit dependence on the these controls appears through $\underline{\dot{\omega}}$ (recall (5-3)). Mathematically:

$$\underline{\ddot{y}}_{att} = \underline{\ddot{\theta}} = \underline{\dot{\Omega}}_o^b \underline{\omega} + \underline{\Omega}_o^b \underline{\dot{\omega}} \tag{6-4}$$

Comparing this equation with (6-2), it can be concluded that the term $\underline{\dot{\Omega}}_o^b$ is never considered in the time scale separated approach. In fact, the time scale separation principle implies that $\underline{\dot{\Omega}}_o^b$ is neglected, which is consistent with the assumption that parameters associated with the slow dynamics (the attitude angles) are constant when seen by the inner loop (the fast dynamics). Obviously, this assumption is only valid if the two loops are separated enough.

The system to be inverted in the current loop has also the major advantage of being affine in the control inputs. Hence, the control law to generate the commanded angular rates comes straightforward:

$$\underline{\omega}_{com} = \underline{\Omega}_b^o \underline{\nu}_{att} = \begin{bmatrix} 1 & 0 & -\sin\theta \\ 0 & \cos\phi & \sin\phi\cos\theta \\ 0 & -\sin\phi & \cos\phi\cos\theta \end{bmatrix} \underline{\nu}_{att} \tag{6-5}$$

where $\underline{\Omega}_b^o$ is determined from (A-8). Since it corresponds to the inverse transformation of $\underline{\Omega}_o^b$, the dynamic inversion can only be performed when $\det \underline{\Omega}_o^b = \cos\theta \neq 0$. The controllability of this controller was already verified in Section 5-3.

Because of (6-3), this control loop is of first order and thus the linear control law for $\underline{\nu}_{att}$ can be designed exactly as in the previous chapter. Nevertheless, in order to alleviate the time scale separation requirements, allowing the bandwidths of the slow and fast dynamics to be closer, a combined analysis is performed to select the gains of the inner and outer loops appropriately. Assuming no PCH for now, when a linear controller $\underline{K}_2(s)$ is used to generate $\underline{\nu}_{att}$, the closed loop to control the attitude angles is schematized in Figure 6-1.

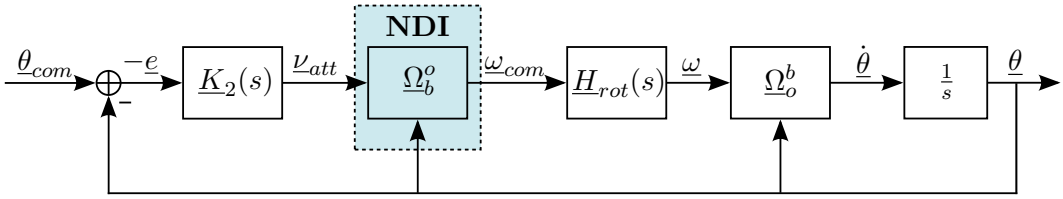

Figure 6-1: Time scale separated attitude controller based on NDI.

The transfer matrix associated with the full time scale separated system $\underline{H}_{att}(s)$ is then written as:

$$\underline{H}_{att}(s) = \frac{\underline{\theta}(s)}{\underline{\theta}_{com}(s)} = \frac{\underline{K}_2(s)\underline{\Omega}_b^o\underline{H}_{rot}(s)\underline{\Omega}_o^b}{s\underline{I}_{3\times3} + \underline{K}_2(s)\underline{\Omega}_b^o\underline{H}_{rot}(s)\underline{\Omega}_o^b} \tag{6-6}$$

where $\underline{I}_{3\times3}$ is the 3×3 identity matrix.

Since after the NDI is applied the channels associated with the three attitude angles become decoupled and again assuming a simple proportional gain for the linear controller, matrices $\underline{K}_2(s)$ and $\underline{H}_{rot}(s)$ are diagonal. Recalling that $\underline{\Omega}_o^b = \underline{\Omega}_b^{o^{-1}}$ and that the transfer function associated with the inner loop is given by (5-16) for each channel, the equation above can be further simplified into:

$$H_{i_{att}}(s) = \frac{K_{2_i}\frac{K_{1_i}}{s+K_{1_i}}}{s + K_{2_i}\frac{K_{1_i}}{s+K_{1_i}}} = \frac{K_{1_i}K_{2_i}}{s^2 + K_{1_i}s + K_{1_i}K_{2_i}} \tag{6-7}$$

Once again, it can be concluded that the steady-state gain ($s \to 0$) is unitary, meaning that the error for tracking the unit step reference is expected to be null in the absence of disturbances. Furthermore, according to the transfer function above, a second order evolution is now imposed to the attitude angles. Comparing its denominator with a conventional second order characteristic polynomial ($s^2+2\zeta\omega_n s+\omega_n^2 = 0$), the gains K_{1_i} and K_{2_i} can be determined such that the corresponding poles result in a response with the desired natural frequency ω_{n_i} and damping ratio ζ_i for each axis:

$$K_{1_i} = 2\zeta_i\omega_{n_i} \tag{6-8}$$

$$K_{2_i} = \frac{\omega_{n_i}^2}{K_{1_i}} = \frac{\omega_{n_i}}{2\zeta_i} \tag{6-9}$$

At this point, just like the INDI of the inner loop was performed assuming that the control deflections are instantaneously what they are commanded to be (neglecting the dynamics of the actuators), the time scale separated attitude controller based on NDI also assumes that the angular rates are exactly what they are commanded to be (discarding the dynamics of the inner loop). The validity of this assumption is reduced if these dynamics are not fast enough when compared to the evolution of the attitude angles, resulting in a decreased performance of the control system. To account for this limitation, another PCH layer can be introduced in the current loop to adjust the angular references to the capabilities of the rate controller in the inner loop. The current PCH layer prevents therefore undesired interactions between the loops.

The working principle of the PCH for the current loop is exactly the same as the one of the inner loop. Since the evolution of the control variables presents now a second order response, it would seem logical that the RM to be utilized was also of second order. Nevertheless, after several tests, it was verified that the performance of the system was clearly preferable with a first order RM, reason why this was the structure adopted. For further information on second order RMs, the reader is referred to (Farrell et al., 2005), where a very illustrative description is presented.

In this line of reasoning, the RM of Figure 4-1 was again implemented to perform a low-pass filtering of the commanded attitude angles with the bandwidth set by the NDI control and to provide a feedforward term to each control channel. The limits allowed for the attitude angles were again imposed after consulting (*ADS-33E-PRF*, 2000) and consist of 60 deg for the roll and pitch angles and 360 deg for the yaw.

The RM is adjusted by the pseudo-control hedge so that the demanded signal is within the capabilities of the inner loop. The calculation of this parameter was exemplified for a generic NDI-based control loop in (4-1) and, using (6-3) for this specific case, the pseudo-control hedge is defined as:

$$\underline{\nu}_{h_{att}} = \underline{\Omega}_o^b \left(\underline{\omega}_{com} - \underline{\omega}\right) \tag{6-10}$$

With this additional monitoring, the overall control system is depicted in Figure 6-2.

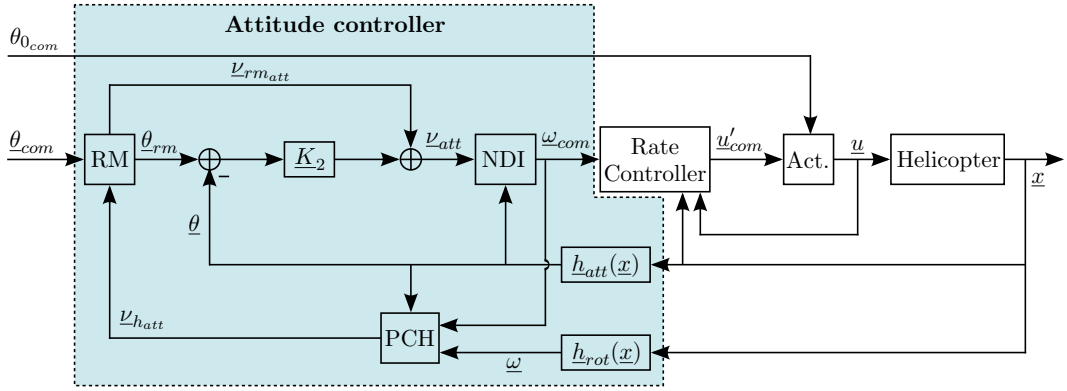

Figure 6-2: Schematic of the attitude control system based on NDI and PCH.

In this figure, the block "Act." corresponds again to the dynamics of the actuators and $\underline{h}_{rot}(\underline{x})$ and $\underline{h}_{att}(\underline{x})$ are the nonlinear functions that map respectively the angular rates and the attitude angles from the state vector. The block "RM" consists of the subsystem represented in Figure 4-1 for each one of the three axes, "NDI" performs simply the dynamic inversion (6-5) and "PCH" computes (6-10). The commanded angular rates $\underline{\omega}_{com}$ are supplied to the rate controller of Figure 5-6. At this point, the collective of the main rotor $\theta_{0_{com}}$ is still assumed to be constant or provided by an external loop.

6-2 Primary Tests

Once again, three simultaneous doublet inputs were used to test the control system developed up until now. These signals have an amplitude of 5 deg and a duration of 4 s. The helicopter has therefore to roll, pitch and yaw controllably and simultaneously in a very short time interval. This indicates that this maneuver is already quite demanding.

The overall system was again sampled at 100 Hz and the simulation started with the helicopter in hovering flight at 1000 m of altitude. The linear gains were chosen so that the responses associated with the three channels present a damping ratio of 0.9 and a natural frequency of 5 rad/s. It is possible to verify from (6-8) and (6-9) that a higher damping ratio contributes to a better separation between fast and slow dynamics since it simultaneously increases K_{1_i} and decreases K_{2_i}. According to this, the gain matrices $\underline{K}_1$ and $\underline{K}_2$ are, respectively:

$$\underline{K}_1 = \begin{bmatrix} 9.00 & 0 & 0 \\ 0 & 9.00 & 0 \\ 0 & 0 & 9.00 \end{bmatrix} \mathrm{s}^{-1}$$

$$\underline{K}_2 = \begin{bmatrix} 2.78 & 0 & 0 \\ 0 & 2.78 & 0 \\ 0 & 0 & 2.78 \end{bmatrix} \mathrm{s}^{-1}$$

The results of the simulation are depicted in Figure 6-3.

It can be seen that the tracking references are followed very efficiently, with a settling time of approximately 1 s and practically with no steady-state error. As expected, the responses of the different attitude angles are completely decoupled and the small differences between their evolution is only due to different control limitations associated with each axis. The last plot shows the response in terms of angular rates. Recall that the commands for these rates are provided by the outer loop associated with the slow dynamics and tracked by the control system developed and analyzed in the previous chapter. As it was seen, the tracking performance of this loop is also quite satisfactory.

In this case, small instabilities also exist due to internal dynamics. As explained in Section 5-3, these problems will be automatically solved when a new control loop is designed, allowing to invert all the unstable dynamic degrees. Nevertheless, the signal for the collective input will only be designed in the next chapter, as part of a controller for the translational motion of the helicopter.

Once again, the action of the PCH prevents undesirable effects due to the fact that the fast dynamics do not evolve instantaneously, as they would in the ideal situation. In the present case, the system tracks perfectly the states of the reference models associated with both control loops. To visualize the effects of the PCH layer in the rate controller, a close-up of the last plot is presented in Figure 6-4.

In this case, as no actuators experience saturation, the PCH simply filters the commanded references such that the system only tries to follow the response that is imposed by the NDI control law. In other words, the bandwidth of the referred filtering corresponds to the one demanded by the NDI. This means that the tracking of the state of the reference model has

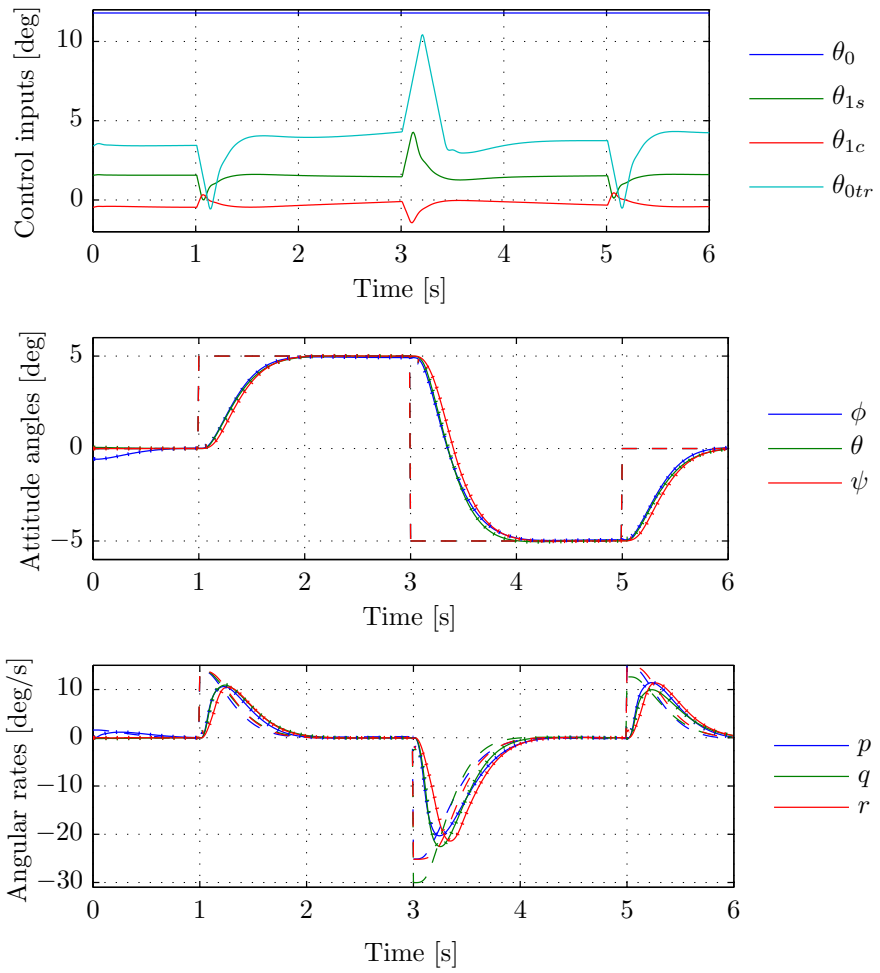

Figure 6-3: Doublet response of the time scale separated attitude controller based on NDI and PCH. The dashed lines correspond to the references commanded, the dotted lines to the state of the reference model and the solid lines to the actual response of the helicopter.

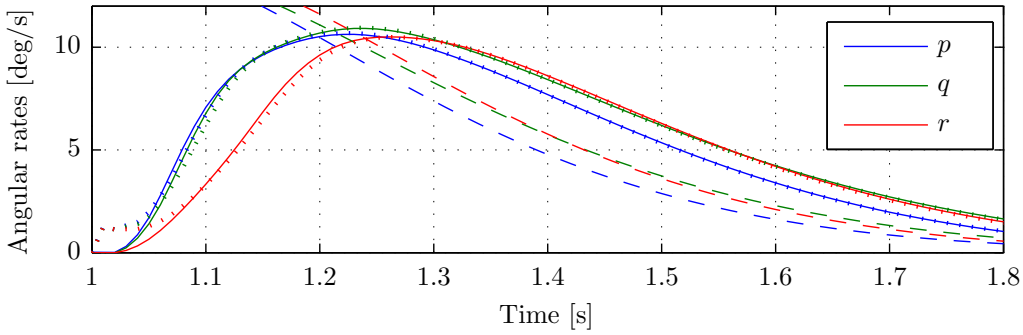

Figure 6-4: Close-up of the angular rate response for the previous simulation. The dashed lines correspond to the references commanded, the dotted lines to the state of the reference model and the solid lines to the actual response of the helicopter.

to be perfectly achieved by the system. This is indeed what happens, as it is indicated by the small mismatch between the dotted and the solid lines of Figure 6-4.

6-3 Linear Control Law

In order to assess the benefits of the controller developed so far using NDI and PCH, this section deals with the development of a linear control system to compare their performances with. To do so, the following steps had to be taken:

System linearization

As the name indicates, linear controllers are always designed based on linear systems. Since the system to be controlled in this case is highly nonlinear, it has to be firstly linearized around a pre-defined trim condition, but the linearization obtained is only valid near this point. The system is then described based on small deviations with respect to the trim solution. The theory behind this procedure can be found, for example, in (Olsder & Woude, 2006).

In summary, the linearization around the solution $(\underline{x}_0, \underline{u}_0)$ of a nonlinear system of the form:

$$\dot{\underline{x}} = \underline{f}(\underline{x}, \underline{u}) \tag{6-11}$$

corresponds to:

$$\dot{\underline{x}} = \underline{A}(\underline{x} - \underline{x}_0) + \underline{B}(\underline{u} - \underline{u}_0) \tag{6-12}$$

where matrices $\underline{A}$ and $\underline{B}$ are obtained from:

$$\underline{A} = \left.\frac{\partial \underline{f}(\underline{x}, \underline{u})}{\partial \underline{x}}\right|_{\underline{x}_0, \underline{u}_0} \tag{6-13}$$

$$\underline{B} = \left.\frac{\partial \underline{f}(\underline{x}, \underline{u})}{\partial \underline{u}}\right|_{\underline{x}_0, \underline{u}_0} \tag{6-14}$$

In this specific case, $\underline{x}$ and $\underline{u}$ are, respectively, the state and control vectors introduced in Subsection 2-3-6. To calculate the derivatives above, central finite differences were utilized. According to this, column i of matrix $\underline{A}$ (the same holds for matrix $\underline{B}$) is given by:

$$\underline{A}_i = \frac{\underline{f}(\underline{x}_0 + \underline{\tau}_i, \underline{u}_0) - \underline{f}(\underline{x}_0 - \underline{\tau}_i, \underline{u}_0)}{2\tau_i} \tag{6-15}$$

where $\underline{\tau}_i$ is a vector that introduces an infinitesimal perturbation τ_i in the component i of the state vector. Once again, the amplitude of this perturbation corresponds to a small percentage of the absolute value of each variable or to a fixed infinitesimal quantity, if the unperturbed value is already too small.

If the linear controller is to be applied to a wide range of flight conditions, several linearizations of the system have to be performed and the most adequate gains for each one determined. During flight, the gains are then selected according to the current flight condition of the helicopter. This strategy was already introduced in Chapter 1 as gain scheduling.

In the case presented here, the linear controller is however simplified to only one linearization because, since the main objective of its design is to compare its performance with that of the nonlinear control system developed so far, the flight conditions analyzed will be kept close to the trimming point. One of the advantages of the NDI-based controller is already implied in the latter statement: while several linear controllers have to be adopted for a wider flight envelope, only one nonlinear control system may have to be applied.

Open-loop analysis

The behavior of a system in open-loop (without the action of a controller) can be assessed by the eigenvalues of matrix $\underline{A}$, which characterizes the different modes of the helicopter motion. A detailed explanation of these eigenmotions is provided for general aircraft in (Etkin, 1972). A specific analysis for the case of rotorcraft can be found in (Pavel & Holten, 1997).

Basically, one mode is stable if its corresponding eigenvalue has a negative real part. Its position on the complex plane dictates the behavior of the response associated with it. If it is a real value, the associated response is of first order and its bandwidth is the absolute value. On the other hand, if it is associated with a complex conjugate pair, it yields a second order response with a natural frequency and damping ratio that depend on its real and imaginary parts.

The eigenmotions obtained for the linearization of the helicopter model for hovering flight at 1000 m are registered in Tables 6-1 and 6-2 together with the corresponding eigenvalues, for the decoupled longitudinal and lateral motion, respectively.

Table 6-1: Open-loop longitudinal eigenmotions of the Bö-105 for hovering flight at 1000 m.

Eigenmotion	Eigenvalue (rad/s)	Natural frequency/ /Bandwidth (rad/s)	Damping ratio
Phugoid	$0.036 \pm 0.487i$	0.488	-0.074
Short period	0.891	0.891	–
	-2.828	2.828	–

Table 6-2: Open-loop lateral eigenmotions of the Bö-105 for hovering flight at 1000 m.

Eigenmotion	Eigenvalue (rad/s)	Natural frequency/ /Bandwidth (rad/s)	Damping ratio
Dutch roll	$0.017 \pm 0.208i$	0.209	-0.083
Spiral	-0.879	0.879	–
Aperiodic roll	-11.62	11.62	–

Regarding the longitudinal case, it can be seen that the Phugoid mode is unstable and that the conventional Short period mode has degenerated into two aperiodic motions, one of them unstable. As for the lateral case, the only problematic eigenmotion is the Dutch roll, which is slightly unstable.

Control strategy

In order to stabilize the helicopter model and to provide the desired characteristics to its eigenmotions so that the tracking of commanded angular references is performed correctly, linear control laws have to be designed for its inputs, allowing to place the closed-loop eigenvalues in the required positions. With this objective, PID controllers were intuitively implemented for all the control inputs based on the attitude error associated with the axis that they control more efficiently:

$$\theta_{1s} = \theta_{1s_{trim}} + K_{P_2} e_\theta + K_{I_2} \int_0^t e_\theta \, \mathrm{d}\tau + K_{D_2} \frac{\mathrm{d}e_\theta}{\mathrm{d}t} \tag{6-16}$$

$$\theta_{1c} = \theta_{1c_{trim}} + K_{P_3} e_\phi + K_{I_3} \int_0^t e_\phi \, \mathrm{d}\tau + K_{D_3} \frac{\mathrm{d}e_\phi}{\mathrm{d}t} \tag{6-17}$$

$$\theta_{0tr} = \theta_{0tr_{trim}} + K_{P_4} e_\psi + K_{I_4} \int_0^t e_\psi \, \mathrm{d}\tau + K_{D_4} \frac{\mathrm{d}e_\psi}{\mathrm{d}t} \tag{6-18}$$

In these equations, $\theta_{1s_{trim}}$, $\theta_{1c_{trim}}$ and $\theta_{0tr_{trim}}$ are the trim values for the longitudinal and lateral cyclic and for the collective of the tail rotor and K_P, K_I and K_D are respectively the proportional, integrative and derivative gains. Furthermore, the attitude tracking errors are defined as: $e_\theta = \theta_{com} - \theta$, $e_\phi = \phi_{com} - \phi$ and $e_\psi = \psi_{com} - \psi$.

Additionally, as it was already explained for the NDI case, to assure the complete stabilization of the system, an altitude hold Proportional-Derivative (PD) controller had to be introduced for the collective of the main rotor:

$$\theta_0 = \theta_{0_{trim}} + K_{P_1} e_z + K_{D_1} \frac{\mathrm{d}e_z}{\mathrm{d}t} \tag{6-19}$$

where $e_z = z_{com} - z$. To keep the system causal, the required time derivatives were calculated by approximate derivative filters with transfer function $\frac{s}{1+Ts}$ and $T = 0.01$ s. This value is small when compared to the dynamics of the system (note that it corresponds to the conventional sample time of the controller) but big enough to avoid numerical problems.

Gains selection

In order to get a first approximation of the most adequate gains for this linear attitude control system, a SISO approach was adopted and the four relevant transfer functions (z/θ_0, θ/θ_{1s}, ϕ/θ_{1c} and ψ/θ_{0tr}) were obtained from the linear state-space system. For each one, a PD controller was designed using the root-locus tool. The derivative term is crucial to increase the speed of convergence of the response by providing anticipative action.

The root-locus of a transfer function is a plot of its poles when the loop is closed with a negative feedback of the tracking error affected with a proportional gain K_P. To understand how this tool can be used to define the position of the closed-loop poles when a PD controller is implemented, note that the transfer function of this controller, instead of being simply K_P, is given by:

$$K_P + K_D s = K_P \left(1 + \frac{K_D}{K_P} s\right) \tag{6-20}$$

Hence, this controller can be viewed as a normal proportional control loop but, in the open-loop, a transfer function with a zero placed at $s = -K_P/K_D$ exists now in cascade with the original system. Thus, the closed-loop poles are chosen by adjusting the position of the referred zero and the root-locus gain, allowing to determine unambiguously the values of K_P and K_D. Note here that the system will only be minimum-phase (with no unstable zeros) if both K_P and K_D have the same sign.

The initial gains obtained from this procedure were such that the complex poles of the closed-loop transfer functions had a damping ratio around 0.9 and a natural frequency around 5 rad/s (whenever as possible) and such that the real poles were faster than the complex conjugate pairs.

Recall that the SISO approach followed up until now to determine the gains only works as an approximation, since the overall system is highly coupled and described by a MIMO state-space. Therefore, after this analytical initialization of the gains, their values were manually adjusted so as to optimize the tracking performance of the response during the maneuver to be analyzed. Furthermore, small integrative terms K_I were introduced in order to minimize the static error that affects the responses.

Closed-loop analysis

Finally, after applying the linear control laws to the helicopter, the decoupled eigenmotions of the closed-loop system can now be evaluated. The referred eigenmotions for the same flight condition are shown in Tables 6-3 and 6-4, again separated into the longitudinal and the lateral motion.

Table 6-3: Closed-loop longitudinal eigenmotions of the Bö-105 for hovering flight at 1000 m.

Eigenmotion	Eigenvalue (rad/s)	Natural frequency/ /Bandwidth (rad/s)	Damping ratio
Phugoid	$-1.792 \pm 2.135i$	2.790	0.643
Short period	$-7.355 \pm 3.117i$	7.990	0.921

Table 6-4: Closed-loop lateral eigenmotions of the Bö-105 for hovering flight at 1000 m.

Eigenmotion	Eigenvalue (rad/s)	Natural frequency/ /Bandwidth (rad/s)	Damping ratio
Spiral	-0.079	0.079	–
Aperiodic roll	-1.704	1.704	–
Dutch roll	$-6.354 \pm 2.121i$	6.700	0.949

From the analysis of these tables, it can be seen that all the eigenmotions are now stable and their characteristics assume typical values. The bandwidth of the modes is high enough and the complex eigenmotions are well damped.

6-4 Comparative Results

The same maneuver executed in Section 6-2 is now demanded to the system with the linear attitude controller developed in the previous section in order to check if its behavior is too degraded in this case. As it was already mentioned, while a nonlinear controller can be used for a wide flight envelope, linear controllers have to be carefully adjusted according to the flight condition for which they are designed to operate. This already represents one major advantage of the NDI-based control system. Nevertheless, the gains of the linear controller in this section were already selected to optimize the performance of the maneuver to be analyzed. Using the notation introduced from (6-16) to (6-19), the gains adopted are:

$$\begin{array}{lll} K_{P_1} = -0.02 & K_{D_1} = -0.02 & \\ K_{P_2} = -0.1 & K_{D_2} = -0.01 & K_{I_2} = -0.001 \\ K_{P_3} = 0.2 & K_{D_3} = 0.01 & K_{I_3} = 0.01 \\ K_{P_4} = -2.5 & K_{D_4} = -0.6 & K_{I_4} = -0.1 \end{array}$$

and the results of the simulation when they are applied to the system are shown in Figure 6-5.

From this figure, it is clear that the tracking performance of the system is substantially degraded when compared to the response with the time scale separated controller based on NDI and PCH, in Figure 6-3, especially in terms of steady-state errors. Also, the responses present a more oscillatory behavior than with the nonlinear controller. These problems are mainly due to the fact that, in opposition to the NDI control laws, the linear controller is not able to decouple the responses associated with the three attitude angles. In this case, when one attitude angle is changed, the other two are also affected and their tracking response is degraded.

The difficulties experienced by the linear control system can also be identified by comparing the angular rate responses. In fact, the simulation with the nonlinear controller involves smaller angular velocities and less oscillatory evolutions when compared to the linear controller presented in this section.

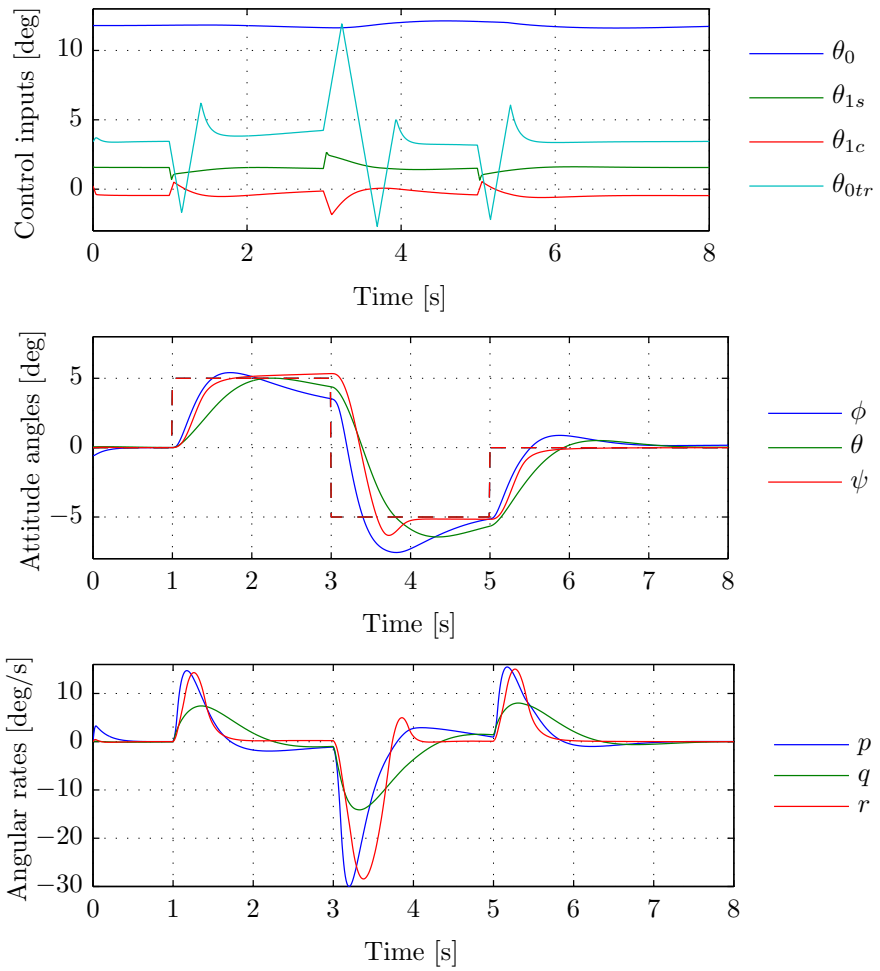

Figure 6-5: Doublet response of the linear attitude controller. The dashed lines correspond to the references commanded and the solid lines to the actual response of the helicopter.

Chapter 7

Navigational Controller

The control system developed so far is now able to follow commands in terms of attitude angles by generating references for the angular rates of the helicopter, which are then tracked by an inner loop. This type of architecture is based on the assumption that there is a considerable difference between the time scales associated with the dynamics of the two loops. In order to alleviate this assumption, to avoid problems associated with the saturation of the actuators and to filter the command references that are not smooth enough to be properly followed by the system, a PCH layer was also introduced in each loop.

It is however desirable to implement a control system that allows the helicopter to follow a specified velocity relative to the Earth, in the NED reference frame. This can be done by introducing an additional control loop such that the ground velocity vector of the helicopter $\underline{\dot{p}}$ tracks the commanded reference $\underline{\dot{p}}_{com}$. In rotorcraft, this type of controller is used in the Translational Rate Command/Position Hold (TRCPH) mode. For the sake of simplicity, from now on, the notation of these two vectors is changed to $\underline{v}_E$ and $\underline{v}_{E_{com}}$, respectively.

Once again, the time scale separation principle is applied in the implementation of this control loop. Basically, since the rotational dynamics of the helicopter evolve faster than its translational motion, this outer loop can be designed assuming that the components of the velocities are constant when compared to the attitude angles and, consequently, that the rotational kinematics occurs instantaneously when seen by the outer loop. This navigational control uses then the commanded attitude angles $\underline{\theta}_{com}$ as control inputs, computing the required values to be tracked in order to produce the desired ground velocities.

In this chapter, the navigational controller is developed for the helicopter and some intermediate results are presented to justify some of the design choices. In the end, the results obtained after performing three common rotorcraft maneuvers are also shown.

7-1 Approximate Dynamic Inversion

The dynamics associated with the translational motion of the vehicle are considerably less nonlinear than the rotational loops. Therefore, in principle, less accurate inversions may

be performed to control the corresponding variables, simplifying the design of this control loop. The hypothesis of applying linear controllers was discarded because their optimal gains depend strongly on the flight condition. The approach adopted here is the based on the suggestion presented in (Prasad & Lipp, 1993), which makes use of an Approximate Dynamic Inversion (ADI). The output vector of the system for this control loop is composed by the three components of the ground velocity of the helicopter:

$$\underline{y}_{nav} = \underline{h}_{nav}(\underline{x}) = \underline{v}_E = [V_x \; V_y \; V_z]^T \tag{7-1}$$

In order to obtain the differential equations for $\underline{v}_E$, a small change has to be made in the relation that describes the translational dynamics of the vehicle (2-89). For convenience, this equation is written in the body-fixed reference frame. However, it can also be expressed in the NED reference frame. In this case, the aerodynamic forces $\underline{f}$ produced by the helicopter have now to be rotated from the body-fixed reference frame, where the gravity is already alined with the vertical direction. The acceleration generated by these forces is then given by:

$$\dot{\underline{v}}_E = \frac{1}{m}\underline{T}_o^b \underline{f} + \begin{bmatrix} 0 \\ 0 \\ g \end{bmatrix} \tag{7-2}$$

where $\underline{T}_o^b$ was derived in Appendix A. Denoting $\cos\alpha$ and $\sin\alpha$ to c_α and s_α, respectively, the equation above can also be rearranged as:

$$\begin{bmatrix} \dot{V}_x \\ \dot{V}_y \\ \dot{V}_z - g \end{bmatrix} = \begin{bmatrix} c_\psi c_\theta & c_\psi s_\theta s_\phi - s_\psi c_\phi & c_\psi s_\theta c_\phi + s_\psi s_\phi \\ s_\psi c_\theta & s_\psi s_\theta s_\phi + c_\psi c_\phi & s_\psi s_\theta c_\phi - c_\psi s_\phi \\ -s_\theta & c_\theta s_\phi & c_\theta c_\phi \end{bmatrix} \begin{bmatrix} f_x/m \\ f_y/m \\ f_z/m \end{bmatrix} \tag{7-3}$$

Note that this equation contains the first time derivative of the output vector. As the dependence on the inputs for this loop (the attitude angles) has already appeared, each one of the three spatial components of the ground velocity has a relative degree of one and the virtual control for this loop corresponds to:

$$\underline{\nu}_{nav} = [\nu_x \; \nu_y \; \nu_z]^T = [\dot{V}_x \; \dot{V}_y \; \dot{V}_z]^T \tag{7-4}$$

The objective of this control loop is now to solve (7-3) in order to determine the commanded attitude angles $\underline{\theta}_{com}$ necessary to yield the required virtual control input $\underline{\nu}_{nav}$. Recall that, from the NDI theory, the virtual control is given by a linear control law based on the tracking error of the ground velocities. A nonlinear solver could be used for this purpose, but the required calculations would demand a substantial computational load. Nevertheless, the system can be inverted analytically if some approximations are taken in order to simplify it. To perform these approximations, the following assumptions have to be made:

- The commanded yaw angle ψ_{com} of the helicopter is already known, being directly supplied by the pilot or computed from kinematic relations involving the commanded ground velocities. Furthermore, from the time scale separation between translational and rotational dynamics, this outer loop assumes that the actual attitude angles are always exactly what they are commanded to be ($\underline{\theta} = \underline{\theta}_{com}$);

- The magnitude of the body Z force f_z is much larger than the remaining force components. It corresponds practically to the thrust produced by the main rotor, which has a considerably higher magnitude when compared to the other contributions to the global force vector acting on the helicopter. This indicates that, for the current inversion, f_x and f_y can be neglected.

According to these assumptions and taken into account that $\underline{T}_o^b$ is an orthonormal matrix, the norm of the acceleration of the helicopter is then approximated by:

$$\left\| \begin{bmatrix} \nu_x \\ \nu_y \\ \nu_z - g \end{bmatrix} \right\|^2 \approx \left(\frac{f_z}{m} \right)^2 \Rightarrow \frac{f_z}{m} \approx \pm \sqrt{\nu_x^2 + \nu_y^2 + (\nu_z - g)^2} \tag{7-5}$$

Note that only the negative sign makes physical sense since the thrust vector of the main rotor points upwards, in the opposite direction of the body z-axis.

When the assumptions above are applied and multiplying both sides of (7-3) by $\underline{T}_o^{b\,-1} = \underline{T}_b^o$, the following result is obtained:

$$\begin{bmatrix} 0 \\ 0 \\ f_z/m \end{bmatrix} \approx \begin{bmatrix} c_\psi c_\theta & s_\psi c_\theta & -s_\theta \\ c_\psi s_\theta s_\phi - s_\psi c_\phi & s_\psi s_\theta s_\phi + c_\psi c_\phi & c_\theta s_\phi \\ c_\psi s_\theta c_\phi + s_\psi s_\phi & s_\psi s_\theta c_\phi - c_\psi s_\phi & c_\theta c_\phi \end{bmatrix} \begin{bmatrix} \nu_x \\ \nu_y \\ \nu_z - g \end{bmatrix} \tag{7-6}$$

From the first equation of this system, it follows that:

$$(\nu_x \cos\psi_{com} + \nu_y \sin\psi_{com}) \cos\theta_{com} - (\nu_z - g) \sin\theta_{com} \approx 0 \tag{7-7}$$

and, solving (7-7) for the required pitch angle:

$$\theta_{com} \approx \arctan \frac{\nu_x \cos\psi_{com} + \nu_y \sin\psi_{com}}{\nu_z - g} \tag{7-8}$$

Furthermore, from the linear combination of the second row of (7-6) multiplied by $\cos\phi_{com}$ and the third row multiplied by $-\sin\phi_{com}$:

$$-\nu_x \sin\psi_{com} + \nu_y \cos\psi_{com} \approx -\frac{f_z}{m} \sin\phi_{com} \tag{7-9}$$

After substituting (7-5) in f_z/m, this equation can be solved with respect to the required roll angle:

$$\phi_{com} \approx \arcsin \frac{-\nu_x \sin\psi_{com} + \nu_y \cos\psi_{com}}{\sqrt{\nu_x^2 + \nu_y^2 + (\nu_z - g)^2}} \tag{7-10}$$

Note that when all the components of the virtual control are zero (for example, when the helicopter is maintaining hovering flight), the commanded attitude angles are also zero, but they should correspond to the required angles to trim the system. For this reason, the attitude angles obtained from the trim routine, θ_{trim} and ϕ_{trim}, have to be added to expressions (7-8) and (7-10), respectively.

Once again, assuming the dynamic inversion is accurate enough, the input-output relation is represented by single integrators (7-4) and, as these correspond to linear systems, a linear control law can be designed for $\underline{\nu}_{nav}$ based on the tracking error of the ground velocities $\underline{v}_E$. As it was done in the previous chapter, a combined analysis of the three loops is necessary to determine the linear gains appropriately in control systems where the time scale separation principle is adopted. At this point, no PCH layer is assumed and the procedure followed to choose the referred gains is exactly the same as presented in Section 6-1.

For convenience, define $\underline{T}^{\theta}_{\dot{v}_E}$ as the nonlinear mapping between the attitude angles of the helicopter and its linear accelerations relative to the Earth, given by (7-3). Due to its transcendental characteristics, the inverse mapping $\underline{T}^{\dot{v}_E}_{\theta}$ cannot be defined analytically. However, if the yaw angle ψ_{com} is known and applying (7-8) and (7-10) to determine the remaining two angles, an approximate inverse transformation can be obtained, yielding $\underline{T}^{\dot{v}_E}_{\theta}\underline{T}^{\theta}_{\dot{v}_E} \approx \underline{I}_{3\times 3}$.

Analogously to Section 6-1, the transfer function between the commanded and the actual ground velocities when a linear controller $\underline{K}_3(s)$ is applied to close the ADI loop can be written as:

$$\underline{H}_{nav}(s) = \frac{\underline{v}_E(s)}{\underline{v}_{E_{com}}(s)} = \frac{\underline{K}_3(s)\underline{T}^{\dot{v}_E}_{\theta}\underline{H}_{att}(s)\underline{T}^{\theta}_{\dot{v}_E}}{s\underline{I}_{3\times 3} + \underline{K}_3(s)\underline{T}^{\dot{v}_E}_{\theta}\underline{H}_{att}(s)\underline{T}^{\theta}_{\dot{v}_E}} \tag{7-11}$$

where $\underline{H}_{att}(s)$ is the diagonal transfer matrix given by (6-6). Again assuming the inversion law from the ADI is perfect, the channels associated with the three components of the ground velocity are decoupled and if the linear controller is composed by simple proportional gains, the transfer function for each control channel i becomes:

$$H_{i_{nav}}(s) = \frac{K_{3_i}\frac{K_{1_i}K_{2_i}}{s^2+K_{1_i}s+K_{1_i}K_{2_i}}}{s + K_{3_i}\frac{K_{1_i}K_{2_i}}{s^2+K_{1_i}s+K_{1_i}K_{2_i}}} = \frac{K_{1_i}K_{2_i}K_{3_i}}{s^3 + K_{1_i}s^2 + K_{1_i}K_{2_i}s + K_{1_i}K_{2_i}K_{3_i}} \tag{7-12}$$

As it can be seen, assuming a perfect inversion, this transfer function presents a third order response with no steady-state error, since the static gain ($s \to 0$) is unitary. The gains K_{1_i}, K_{2_i} and K_{3_i} can be established in order to place the poles according to a characteristic polynomial of third degree. This polynomial expression can be seen as a composition of a first order system with time constant τ_i and a second order system with natural frequency ω_{n_i} and damping ratio ζ_i. It is then given by:

$$\begin{aligned}(\tau_i s + 1)\left(s^2 + 2\zeta_i\omega_{n_i}s + \omega_{n_i}^2\right) = \\ = s^3 + \left(2\zeta_i\omega_{n_i} + \frac{1}{\tau_i}\right)s^2 + \left(\omega_{n_i}^2 + \frac{2\zeta_i\omega_{n_i}}{\tau_i}\right)s + \frac{\omega_{n_i}^2}{\tau_i} = 0\end{aligned} \tag{7-13}$$

and from its comparison with the denominator of (7-12), it follows immediately that:

$$K_{1_i} = 2\zeta_i\omega_{n_i} + \frac{1}{\tau_i} \tag{7-14}$$

$$K_{2_i} = \frac{1}{K_{1_i}}\left(\omega_{n_i}^2 + \frac{2\zeta_i\omega_{n_i}}{\tau_i}\right) \tag{7-15}$$

$$K_{3_i} = \frac{1}{K_{1_i}K_{2_i}}\frac{\omega_{n_i}^2}{\tau_i} \tag{7-16}$$

Note that, since the reference for the yaw angle ψ_{com} is not generated by the outer loop but instead provided externally by the pilot, this variable is only associated with a second order evolution and thus it does not make sense to account for the effect of the real pole in K_{2_3}. Therefore, this component of the gain matrix of the middle loop is still determined by (6-9). Substituting (7-14) in (7-15), the referred gain matrix is then given by:

$$\underline{K}_2 = \begin{bmatrix} \frac{\omega_{n_1}}{2\zeta_1} \frac{1+\frac{2\zeta_1}{\omega_{n_1}\tau_1}}{1+\frac{1}{2\zeta_1\omega_{n_1}\tau_1}} & 0 & 0 \\ 0 & \frac{\omega_{n_2}}{2\zeta_2} \frac{1+\frac{2\zeta_2}{\omega_{n_2}\tau_2}}{1+\frac{1}{2\zeta_2\omega_{n_2}\tau_2}} & 0 \\ 0 & 0 & \frac{\omega_{n_3}}{2\zeta_3} \end{bmatrix} \tag{7-17}$$

Note also that this control system requires information about the ground velocity vector $\underline{v}_E$. This measurement can be easily obtained with a Global Positioning System (GPS) receiver onboard, which uses the Doppler shift principle. Common receivers dedicated to velocity estimation operate at a maximum frequency considerably lower than that of the IMU. In the present case, the sampling frequency of the IMU is assumed to be 100 Hz, while the GPS operates five times slower, at 20 Hz.

With respect to this navigational controller, it is important to understand physically that the commanded ground velocities are effectively achieved by changing the attitude of the helicopter in such a way that the resultant z-axis force vector acting on the vehicle points in the required direction. Nevertheless, when this control system is applied, the tracking performance associated with the vertical velocity is far from the desirable. To overcome this problem, a different approach to control V_z is developed in the next section. Intuitively, this approach has to be based on the adjustment of the magnitude of the referred force vector produced by the helicopter.

7-2 Control Law for the Collective

As it might have already been anticipated, the most efficient way to change the magnitude of the force produced by the helicopter (which mainly depends on the thrust of the main rotor) passes through the variation of the collective pitch of the main rotor. Recall that, in the first control loop, the command signal for this control input was assumed to be provided by an external loop and, at this point, it was still fixed to its trim value. It is now very useful to allocate this input specifically to control the vertical velocity of the helicopter. In the present section, two different ways of defining a control law for the collective of the main rotor are explored, compared and, in the end, the most efficient one is selected.

7-2-1 Linearized force equation

The first strategy was suggested in (Lee et al., 2005) and makes use of a linearized equation for the body Z force. In principle this strategy is feasible since, as it was already mentioned, the navigational loop is associated with less intense nonlinearities. The linear equation allows to estimate the deviation of the third component of the aerodynamic force with respect to its

trim value based on the corresponding deviation of the states and control inputs, given the so-called stability derivatives for the flight condition under analysis.

In this section, the Z force, previously denoted as f_z, is simply denoted as Z, a more common notation when using linearized EOM. The stability derivatives Z_* are simply the derivatives of Z with respect to a certain variable here denoted by $*$. If the cross-couplings effects are neglected for the following development, the main contributions for the force on the body z-axis come from the states and control inputs associated with the longitudinal motion of the vehicle. If the remaining contributions are neglected and denoting $x - x_{trim}$ as Δx, the Z force can be approximated around a given trim condition as:

$$Z \approx Z_{trim} + Z_u \Delta u + Z_w \Delta w + Z_q \Delta q + Z_{\theta_0} \Delta\theta_0 + Z_{\theta_{1s}} \Delta\theta_{1s} \tag{7-18}$$

If the trim condition is chosen to be hovering flight, the Z force only has to balance the effects of gravity on the helicopter and thus:

$$Z_{trim} = -mg \cos\theta_{trim} \cos\phi_{trim} \tag{7-19}$$

Now consider the last equation of (7-3). If again f_x and f_y are assumed negligible when compared to f_z (here Z):

$$\dot{V}_z - g = \frac{\cos\theta \cos\phi}{m} Z \tag{7-20}$$

Using (7-18) and (7-19) to define Z and recalling that $\dot{V}_z = \nu_z$, the equation above can be recast as:

$$\begin{aligned} &\frac{m}{\cos\theta \cos\phi}(\nu_z - g) = \\ &\qquad = -mg \cos\theta_{trim} \cos\phi_{trim} + Z_u \Delta u + Z_w \Delta w + Z_q \Delta q + Z_{\theta_0} \Delta\theta_0 + Z_{\theta_{1s}} \Delta\theta_{1s} \end{aligned} \tag{7-21}$$

For the controller developed, the stability derivatives are determine before the simulation starts with central finite differences. The equation above can be solved in order to determine the required collective pitch:

$$\begin{aligned} &\theta_{0_{com}} = \\ &= \frac{\frac{m}{\cos\theta \cos\phi}(\nu_z - g) + mg \cos\theta_{trim} \cos\phi_{trim} - Z_u \Delta u - Z_w \Delta w - Z_q \Delta q - Z_{\theta_{1s}} \Delta\theta_{1s}}{Z_{\theta_0}} + \theta_{0_{trim}} \end{aligned} \tag{7-22}$$

The control law is not completely linear because of the trigonometric functions, but it is based on the linear approximation of the force. This method presents two major shortcomings:

- Being a linear approximation of the real (nonlinear) system, the performance of this control law may be severely degraded when the deviations relative to the trim conditions increase. To overcome this problem, several trim conditions would have to be defined and, for each one, the corresponding stability derivatives calculated;

- It requires a comprehensive knowledge of the helicopter model to be controlled through its stability derivatives. The amount of information needed was already reduced by neglecting the contributions of the remaining force components (f_x and f_z) and the cross-coupling terms (for example Z_v and $Z_{\theta_{1c}}$). This strong dependence on the model also makes the efficiency of the control system more vulnerable to modelling uncertainties.

Despite these disadvantages, the adoption of this control law may be convenient because it does not involve complex calculations nor the measurements from additional sensors. The results obtained when it is applied have still to be assessed.

7-2-2 INDI

The first shortcoming of the previous approach motivates the use of an exclusively nonlinear description to compute the control law for the collective. The second one suggests the adoption of an incremental approach in order to reduce the dependence of the controller on the model and to increase its robustness. For these reasons, a control law based on INDI is now derived.

To do so, the last equation of (7-3) can be recast as:

$$\dot{V}_z = \begin{bmatrix} -\sin\theta & \cos\theta\sin\phi & \cos\theta\cos\phi \end{bmatrix} \left(\frac{1}{m}\underline{f} + g \begin{bmatrix} -\sin\theta \\ \sin\phi\cos\theta \\ \cos\phi\cos\theta \end{bmatrix} \right) \tag{7-23}$$

The derivation of the control law based on INDI is made exactly as in Chapter 5. The equation above expresses already the influence of θ_0 on $\dot{V}_z$, since the force produced by the main rotor $\underline{f}_{mr}$ depends directly on it (as introduced in Subsection 2-3-6, $\underline{f}$ corresponds to the sum of the contributions of all the components to the overall force).

Once again, assuming that $\underline{x} \approx \underline{x}_0$ for an incremental time step and recalling that $\dot{V}_z = \nu_z$, the virtual control associated with the vertical acceleration can be represented as:

$$\nu_z = \dot{V}_z \approx \dot{V}_{z_0} + \frac{1}{m} \begin{bmatrix} -\sin\theta & \cos\theta\sin\phi & \cos\theta\cos\phi \end{bmatrix} \left. \frac{\partial \underline{f}_{mr}(\underline{x},\underline{u})}{\partial \theta_0} \right|_{\underline{x}_0,\underline{u}_0} (\theta_0 - \theta_{0_0}) \tag{7-24}$$

where the current state vector $\underline{x}_0$, the control inputs $\underline{u}_0$ (including the collective pitch of the main rotor θ_{0_0}) and the vertical acceleration $\dot{V}_{z_0}$ are assumed to be known. The latter however cannot be directly measured. One way to determine it would be with finite differences since V_{z_0} is known, but numerical differentiation often leads to problems associated with noise. Another hypothesis to compute the ground accelerations is by using information relative to the linear accelerations and attitude angles measured by the IMU onboard. The linear accelerations are sensed by the accelerometers and correspond to the specific force $\frac{1}{m}\underline{f}$ acting on the body. The orientation of the helicopter has also to be considered in order to account for the gravitational acceleration. Mathematically, according to the translational dynamics of the vehicle (2-89), the acceleration vector in the body-fixed reference frame $\underline{a}_B$ is given by:

$$\underline{a}_B = \dot{\underline{v}} + \underline{\omega} \times \underline{v} = \frac{1}{m}\underline{f} + g \begin{bmatrix} -\sin\theta \\ \sin\phi\cos\theta \\ \cos\phi\cos\theta \end{bmatrix} \tag{7-25}$$

This vector has now to be converted into the NED reference frame with $\underline{\underline{T}}_o^b$:

$$\underline{\dot{v}}_E = \begin{bmatrix} c_\psi c_\theta & c_\psi s_\theta s_\phi - s_\psi c_\phi & c_\psi s_\theta c_\phi + s_\psi s_\phi \\ s_\psi c_\theta & s_\psi s_\theta s_\phi + c_\psi c_\phi & s_\psi s_\theta c_\phi - c_\psi s_\phi \\ -s_\theta & c_\theta s_\phi & c_\theta c_\phi \end{bmatrix} \underline{a}_B \tag{7-26}$$

Noise problems are not expected from this computation since the IMU can estimate the translational accelerations and the attitude angles of the vehicle very accurately. Besides the referred measurements, the control system only needs the information relative to the mass of the helicopter and to the influence of the collective input on the forces generated by the main rotor. The dependence on the model of the remaining components of the vehicle has been replaced by the vertical acceleration measurement.

Due to the complex description of $\underline{f}_{mr}$, central finite differences were again used to determine its derivative with respect to θ_0. As in Chapter 5, the perturbation for this variable corresponds to a small percentage of its absolute value or to a fixed infinitesimal quantity, if it is too small. Finally, if (7-24) is invertible for a certain flight condition at a given instant, the required collective pitch for the next iteration is obtained from:

$$\theta_{0_{com}} = m \left(\begin{bmatrix} -\sin\theta & \cos\theta\sin\phi & \cos\theta\cos\phi \end{bmatrix} \left. \frac{\partial \underline{f}_{mr}(\underline{x},\underline{u})}{\partial \theta_0} \right|_{\underline{x}_0,\underline{u}_0} \right)^{-1} \left(\nu_z - \dot{V}_{z_0} \right) + \theta_{0_0} \tag{7-27}$$

In the literature, the INDI is not normally found in the inversion of the translational dynamics of aerospace vehicles but, as it will be seen in the following sections, it allows to obtain very good results.

7-2-3 Choice of the method

Before starting with the experimental comparison between the strategies presented in the two last subsections, an important remark has still to be made with respect to the linear gain $\underline{K}_3$, deduced in (7-16). The third component of this gain K_{3_3} is used to generate the virtual control ν_z, proportional to the error in the vertical velocity of the helicopter. This virtual control is then mainly used to define a control law for the collective pitch θ_0, either by using a linear approximation or INDI. Therefore, in opposition to the control laws established by ν_x and ν_y, which are applied to the internal control loops, the control law associated with ν_z is directly applied to the actuator. Because of this, the third channel of the navigational loop is of first order and thus K_{3_3} should only account for the desired time constant τ_3 associated with that response. Replacing (7-15) in (7-16), the gain matrix under analysis is given by:

$$\underline{K}_3 = \begin{bmatrix} \frac{1}{\tau_1} \frac{1}{1+\frac{2\zeta_1}{\omega_{n_1}\tau_1}} & 0 & 0 \\ 0 & \frac{1}{\tau_2} \frac{1}{1+\frac{2\zeta_2}{\omega_{n_2}\tau_2}} & 0 \\ 0 & 0 & \frac{1}{\tau_3} \end{bmatrix} \tag{7-28}$$

In order to compare the performances obtained with the two different approaches deduced to control the vertical velocity of the helicopter, a doublet input with an amplitude of 2 m/s and duration of 12 s was commanded in the corresponding control channel. The remaining

part of the navigational controller was already activated in order to keep the helicopter fixed horizontally and pointing North ($\psi_{com} = 0$ deg). The same gains were used for the trial with a linear approximation for the collective control law and with INDI. In particular, K_{3_3} was defined so that the response associated with the vertical velocity presents a time constant $\tau_3 = 0.2$ s in both cases. Starting the simulations in hovering fight at 1000 m, the results obtained are shown in Figure 7-1.

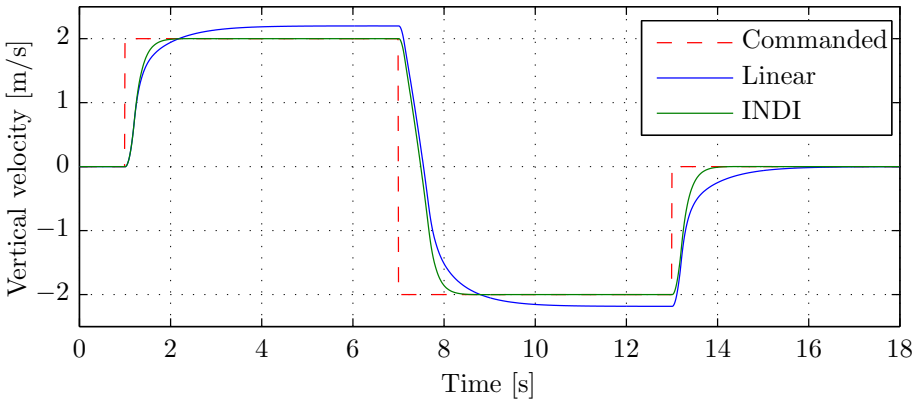

Figure 7-1: Comparison of vertical velocity responses with different control laws for the collective.

As it can be seen it this figure, the performance of the control law based on INDI is clearly the most well-suitable, either in terms of steady-state error and settling time. Note that in the first time instants the two evolutions coincide but, once the system moves away from the trim condition, the linear approximation for the Z force looses validity and the performance of the corresponding control law is degraded. The INDI-based approach is then the one selected to be implemented in the overall navigational control system.

According to this, the working principle of the overall navigational loop is as follows. It receives commands in terms of ground velocities $\underline{v}_{E_{com}}$ and yaw orientation ψ_{com}. The error relative to the first vector is used to generate the navigational virtual control $\underline{\nu}_{nav}$, multiplying it by $\underline{K}_3$, defined as in (7-28). The yaw command is used in this control loop and it is also sent to middle loop, to be tracked by the attitude controller. The virtual control $\underline{\nu}_{nav}$ is used by the current ADI loop to generate the required roll ϕ_{com} and pitch θ_{com} angles, as well as the command signal for the collective of the main rotor $\theta_{0_{com}}$. The equations behind these processes were already derived and are summarized below:

$$\phi_{com} = \arcsin \frac{-\nu_x \sin\psi_{com} + \nu_y \cos\psi_{com}}{\sqrt{\nu_x^2 + \nu_y^2 + (\nu_z - g)^2}} + \phi_{trim} \tag{7-29}$$

$$\theta_{com} = \arctan \frac{\nu_x \cos\psi_{com} + \nu_y \sin\psi_{com}}{\nu_z - g} + \theta_{trim} \tag{7-30}$$

$$\theta_{0_{com}} = m \left(\begin{bmatrix} -\sin\theta & \cos\theta\sin\phi & \cos\theta\cos\phi \end{bmatrix} \frac{\partial \underline{f}_{mr}(\underline{x},\underline{u})}{\partial \theta_0}\bigg|_{\underline{x}_0,\underline{u}_0} \right)^{-1} \left(\nu_z - \dot{V}_{z_0} \right) + \theta_{0_0} \tag{7-31}$$

7-3 Introduction of PCH

The dynamic inversion developed in the last two sections is performed assuming that the attitude angles of the helicopter and the collective pitch of its main rotor are instantaneously what they are commanded to be. In other words, the dynamics of the middle loop (which are assumed to be characterized by a faster time scale than the translational dynamics) and the dynamics of the collective pitch actuator are neglected in the formulation of the ADI and INDI, respectively.

Once again, a PCH layer can be introduced in the control system to account for the limitations imposed by the non-ideal dynamics mentioned above and to adjust the commanded references to the capabilities of the overall system. Exactly as in the two previous chapters, the current PCH layer uses the reference model of Figure 4-1 for each channel i with gain K_{3_i} and where the maximum velocities allowed were set to 80 m/s for the horizontal components and 20 m/s for the vertical speed.

With this improvement, the commanded references are subjected to an adaptive filtering, which is adjusted by the pseudo-control hedge $\underline{\nu}_{h_{nav}}$. This vector is composed by one part that monitors the capabilities of the middle loop and another one that accounts for the limitations of the collective pitch actuator. The control law for the latter one is obtained based on the INDI (see (7-24)), thus the equation for the third component of $\underline{\nu}_{h_{nav}}$ for this case comes directly from the generic expression (4-2):

$$\nu_{h_z} = \frac{1}{m}\begin{bmatrix}-\sin\theta & \cos\theta\sin\phi & \cos\theta\cos\phi\end{bmatrix}\left.\frac{\partial \underline{f}_{mr}(\underline{x},\underline{u})}{\partial\theta_0}\right|_{\underline{x}_0,\underline{u}_0}(\theta_{0_{com}}-\theta_0) \tag{7-32}$$

For the two remaining components, a different strategy has to be adopted to estimate the error associated with the virtual controls because their components are described by coupled transcendental equations. Nevertheless, in opposition to the PCH layers applied in the inner control loops, in the present case the actual virtual control is known. It corresponds simply to the ground accelerations of the helicopter, which can be accurately estimated with (7-26). Therefore, from the definition of pseudo-control hedge, the first two components of $\underline{\nu}_{h_{nav}}$ are given by:

$$\nu_{h_x} = \nu_x - \hat{\nu}_x = \nu_x - \dot{V}_x \tag{7-33}$$

$$\nu_{h_y} = \nu_y - \hat{\nu}_y = \nu_y - \dot{V}_y \tag{7-34}$$

A schematic of the complete control system developed for the helicopter model under analysis is depicted in Figure 7-2.

Once again, "Act." represents the dynamics of the actuators and $\underline{h}_{nav}(\underline{x})$ allows to obtain the ground velocities from the state-vector. The block "RM" is composed by the subsystem of Figure 4-1 for each component of the velocity vector. The ADI basically implements equations (7-29) and (7-30) and the INDI computes (7-31). Furthermore, the "PCH" block determines the pseudo-control hedges through (7-32) to (7-34). This control system makes use of the controllers presented in Figures 5-6 and 6-2. Note that, as already explained, the commanded yaw angle is needed in both the outer and middle control loops.

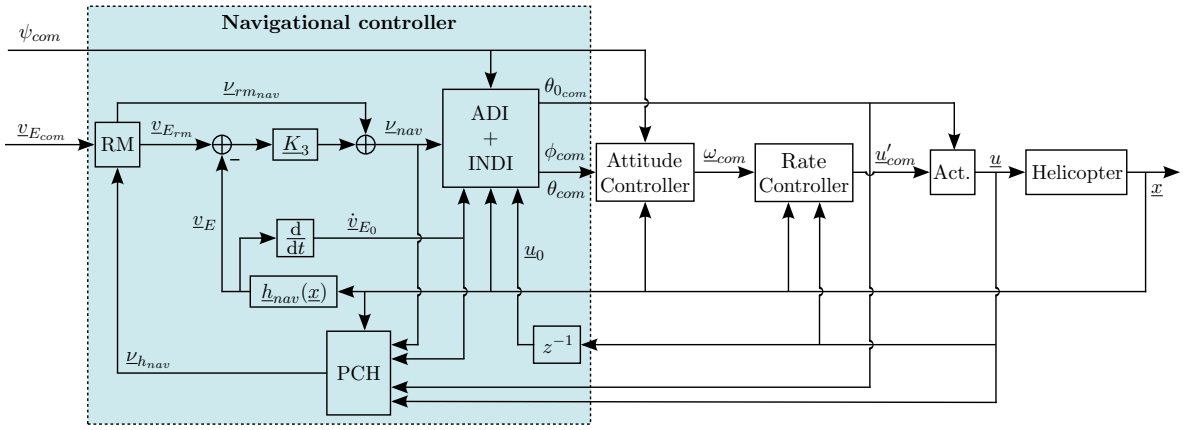

Figure 7-2: Schematic of the navigational control system based on ADI, INDI and PCH.

Benefits of the PCH

In order to verify the benefits of the PCH, a doublet signal was again demanded to the vertical velocity control channel using the INDI-based control law, with an amplitude of 2 m/s and a duration of 4 s. In order to visualize the effects of the PCH, the saturation of the actuator was forced by selecting a time constant $\tau_3 = 0.1$ s to the desired response. Since the referred control variable is directly controlled with the collective of the main rotor (MR), only the evolution of the variables that influence this channel has to be analyzed. The results obtained with and without PCH are presented in Figure 7-3.

As it can been seen, when there are no saturations (in this case in terms of rate), the response of both systems is exactly equal. Nevertheless, in the presence of saturations, the system with PCH is able to recover more quickly and without the overshoots that exist in the response without PCH. The introduction of the PCH clearly represents a significant improvement since only in this case it is possible to obtain the desired first order response for the vertical velocity of the helicopter. It is also interesting to visualize what happens with the auxiliar variables of the PCH architecture in this situation: the pseudo-control hedge ν_{h_z} and the feedforward term ν_{rm_z}, both shown in Figure 7-4.

The first one works like a detector of saturations. When this happens, its value is used to adjust the reference model so that the saturation is avoided, assuring a satisfactory response of the system. The second one is used to give the system an additional "push" when the derivative of the reference state is too large or, in other words, when a big variation in the conditions of the system is expected. Due to this feedforward action, the settling times of the response with PCH were even further reduced when compared to the baseline design.

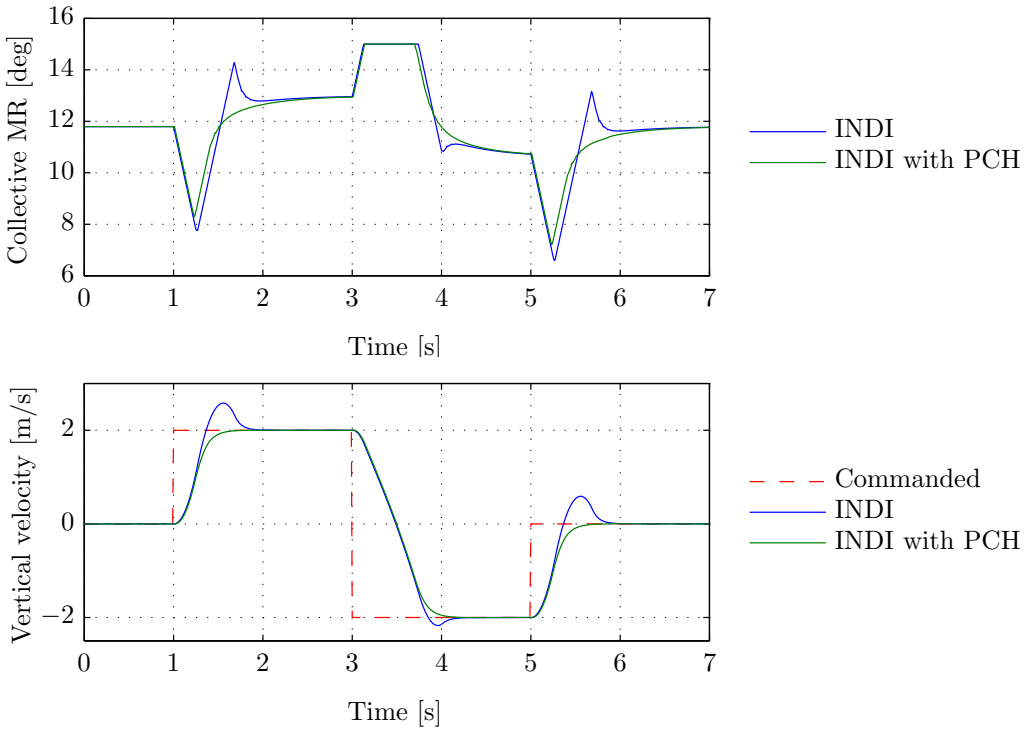

Figure 7-3: Benefits of the PCH in the control system.

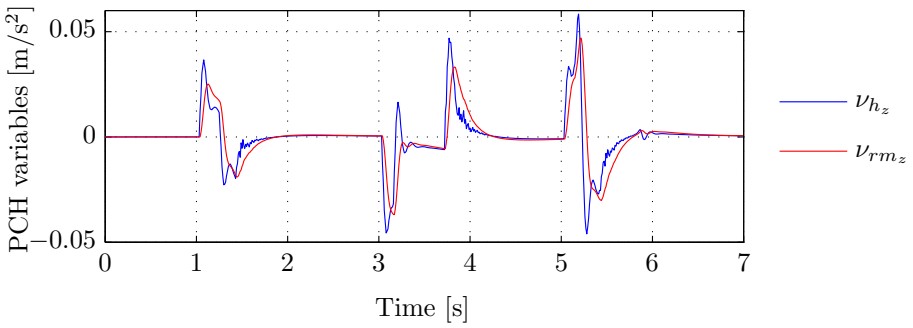

Figure 7-4: Pseudo-control hedge and feedforward term for the previous simulation.

7-4 Maneuvers Simulation

As stated in (Enns et al., 1994), the main job of a flight control system is to produce good responses for pilot commands. These good responses are well known from years of studies, piloted experiments and flight experience and are well documented in military specifications (*ADS-33E-PRF*, 2000). These requirements basically describe the rotorcraft response characteristics desired to complete various tasks. The main purpose of this section is to test the performance of the helicopter when the overall navigational controller is applied to fly three maneuvers commonly used to evaluate the referred flying qualities.

Before that, the gains associated with the three control loops have still to be defined. As it was already seen, the control system developed is able to track references in terms of

ground velocities (V_x, V_y, V_z) and yaw angle (ψ). To these variables, the desired response characteristics are imposed by the successive ADI/NDI/INDI loops. The parameters chosen for the remainder of this thesis are indicated in Table 7-1.

Table 7-1: Response characteristics selected for the overall control system.

Control variable	Rotational natural frequency (rad/s)	Rotational damping ratio	Translational time constant (s)
V_x	$\omega_{n_1} = 2.5$	$\zeta_1 = 0.8$	$\tau_1 = 0.2$
V_y	$\omega_{n_2} = 2.5$	$\zeta_2 = 0.8$	$\tau_2 = 0.2$
V_z	–	–	$\tau_3 = 0.4$
ψ	$\omega_{n_3} = 4.0$	$\zeta_3 = 0.8$	–

According to this table, the linear gains for the inner, middle and outer loop are obtained respectively from (7-14), (7-17) and (7-28), corresponding to:

$$\underline{K}_1 = \begin{bmatrix} 9.00 & 0 & 0 \\ 0 & 9.00 & 0 \\ 0 & 0 & 8.90 \end{bmatrix} \text{s}^{-1}$$

$$\underline{K}_2 = \begin{bmatrix} 2.92 & 0 & 0 \\ 0 & 2.92 & 0 \\ 0 & 0 & 2.50 \end{bmatrix} \text{s}^{-1}$$

$$\underline{K}_3 = \begin{bmatrix} 1.19 & 0 & 0 \\ 0 & 1.19 & 0 \\ 0 & 0 & 2.50 \end{bmatrix} \text{s}^{-1}$$

It is possible to verify that V_x and V_y are expected to present the same dynamics, with the three time scales as separated as the ratio between the gains of the corresponding loops. The yaw angle ψ has a second-order response with a weaker time scale separation, but with a faster evolution since it can be controlled very efficiently with the tail rotor. Independently of these variables, V_z presents a first-order response which is slower than V_x and V_y, due to the fact that the vertical velocity of the helicopter has to be controlled more smoothly than its horizontal components.

While the dynamics associated with ψ and V_z were inverted very accurately, the control of the horizontal velocities is subjected to a small error from the ADI due to the approximations made (see Section 7-1). To reduce this error, very small integrative terms were added to the first two channels of the navigational loop. In order to further reduce the referred error, the ideal strategy would be to adopt for the roll and pitch trim angles in (7-29) and (7-30) the values corresponding to the current flight condition, instead of using simply the ones obtained in the initial trim routine.

The integrative gains were adjusted manually based on step responses and correspond to 5×10^{-4} for both V_x and V_y. With this adjustment, the pole-zero plot of the transfer functions associated with the responses of V_x and V_y is depicted in Figure 7-5.

The transfer function under analysis is now of fourth order, but it can be approximated as a second order evolution, firstly because the natural frequency of the first order pole located

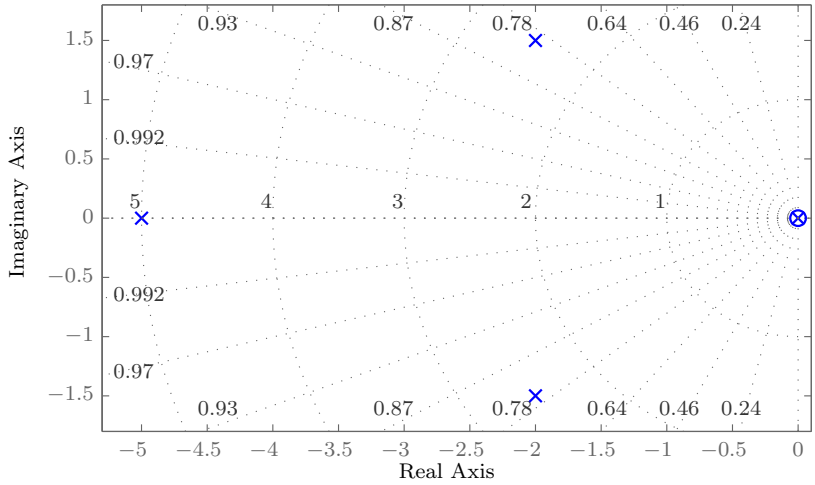

Figure 7-5: Pole-zero plot of the transfer function associated with V_x and V_y.

at -5 rad/s is higher than that of the complex conjugate pair and secondly because the remaining pole is practically cancelled by the real zero. The latter statement is only valid for infinitesimal integrative gains. For higher gains, the characteristics imposed in Table 7-1 as well as the stability of the system itself are compromised. On the other hand, the referred cancellation only occurs when no integrative action is adopted, being the closed-loop system of third order in this case. Note also that the real zero has always minimum-phase for positive values of the integrative gain.

Obviously, the integrative gains had also to be introduced in the RM of the PCH, despite their small influence. Furthermore, for this navigational layer, the proportional gain matrix of the RM was set to $0.8\underline{K}_3$, instead of simply $\underline{K}_3$, forcing the bandwidth of the filter to be 80% of that imposed to the responses associated with this control loop. The reason for this is simply to prevent high overshoots and intense efforts from the actuators and thus contributing to an increased performance of the system.

At this point, in order to further reduce some occasional oscillations in the control inputs, simple first order LPFs with a cutoff frequency of 10 Hz were also introduced to filter the output of the GPS sensor (recall that it is working at a lower frequency than the controller itself). The overall control system was then implemented in *Simulink* environment in order to simplify the implementation of the tests carried throughout the remainder of this thesis.

7-4-1 Limited agility: the bob-up and bob-down

The first maneuver performed by the helicopter is known as bob-up and bob-down and consists of a simple combination of horizontal and vertical flight path segments. This maneuver is very common in the primary tests of a flight control system for helicopters and some examples can be found in (Prasad & Lipp, 1993) and (Lee et al., 2005). The simulation setup is defined as follows:

The bob-up starts with the helicopter flying North at cruise, with a speed of 15 m/s (approx. 30 kt) and the vehicle is commanded to decelerate to hover at 610 m (approx. 2000 ft). After that, the helicopter is commanded to climb for 5 s at a constant rate of 5 m/s (approx. 15 ft/s), followed by hover at a higher altitude. It is then accelerated back to 15 m/s at constant altitude to prepare the bob-down maneuver.

Similarly, for the bob-down, the initial forward speed is of 15 m/s and the vehicle is again commanded to decelerate to hover. It is then commanded to descend for 5 s at a constant rate of 5 m/s and finish the maneuver in hovering flight approximately at the initial altitude.

During the entire maneuver, the helicopter is commanded to keep flying North with no sideslip angle by fixing $V_{y_{com}}$ and ψ_{com} to zero.

The results obtained from the simulation of the bob-up and bob-down maneuver with the overall navigational controller are presented in Figure 7-6.

As it can be seen, the commanded ground velocities are properly tracked, presenting fast evolutions, without oscillations and with a negligible steady-state error. Furthermore, couplings between the responses of the three components are practically inexistent. The most noticeable exceptions occur after around 2 and 22 s when the helicopter looses some altitude probably caused by the saturation of the collective pitch of the main rotor.

As expected, the response associated with the horizontal velocity V_x is controlled by directly changing the pitch of the helicopter, since it does not involve changes in the direction. The vehicle pitches down to accelerate and pitches up to loose speed. The collective of the main rotor is adjusted to track the desired vertical velocity, providing a first order response for V_z.

The remaining control inputs are only used to compensate the control moments and balance the rotorcraft. The yaw angle ψ is also tracked very efficiently with the collective of the tail rotor, since this actuator is only used to compensate the changes in the yaw moment introduced due to the adjustments of the collective pitch of the main rotor.

7-4-2 Moderate agility: the slalom maneuver

The slalom maneuver corresponds to a more demanding test since it involves a series of turns at constant speed and altitude. The simulation procedure is described in detail in (*ADS-33E-PRF*, 2000). The main objectives of this test are to check the ability to maneuver in moderately aggressive forward flight, to check the turn coordination and to identify objectionable inter-axis couplings during the maneuver. The simulation setup is as follows:

This maneuver is initiated with the helicopter flying North with no sideslip angle at a constant altitude of 31 m (approx. 100 ft) and at a constant speed of 31 m/s (approx. 60 kt). After 5 s, two doublet inputs are commanded to the lateral velocity $V_{y_{com}}$ with an amplitude of 8 m/s (approx. 15 kt) and a duration of 10 s.

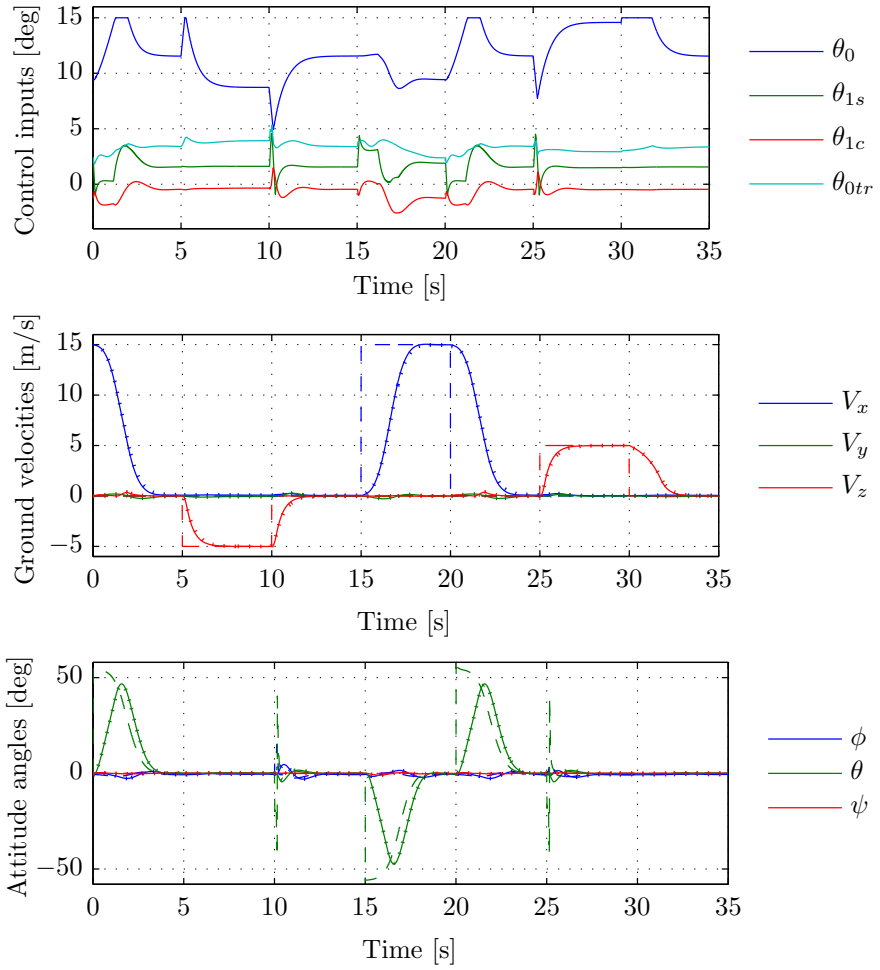

Figure 7-6: Results obtained from the simulation of the bob-up and bob-down. The dashed lines correspond to the references commanded, the dotted lines to the state of the reference model and the solid lines to the actual response of the helicopter.

Without sideslip, the yaw angle of the vehicle has also to be adjusted in order to cope with this variation. It is thus commanded to match its heading: $\psi_{com} = \arctan_2 V_{y_{com}}/V_{x_{com}}$. More information on this topic will be presented in the next section.

Finally, the commanded vertical velocity $V_{z_{com}}$ is set to zero to keep the altitude constant and, in the turns, $V_{x_{com}}$ is reduced to 30 m/s (approx. 58 kt) in order to keep the total airspeed constant.

The results obtained from the simulation of the slalom maneuver with the overall navigational controller are presented in Figure 7-7. Another example of a moderate agility maneuver, the pirouette, can be found in Appendix E.

From this figure, it can again be concluded that the commanded references are properly tracked by the helicopter. As expected, the lateral velocity V_y shows a second order shaped

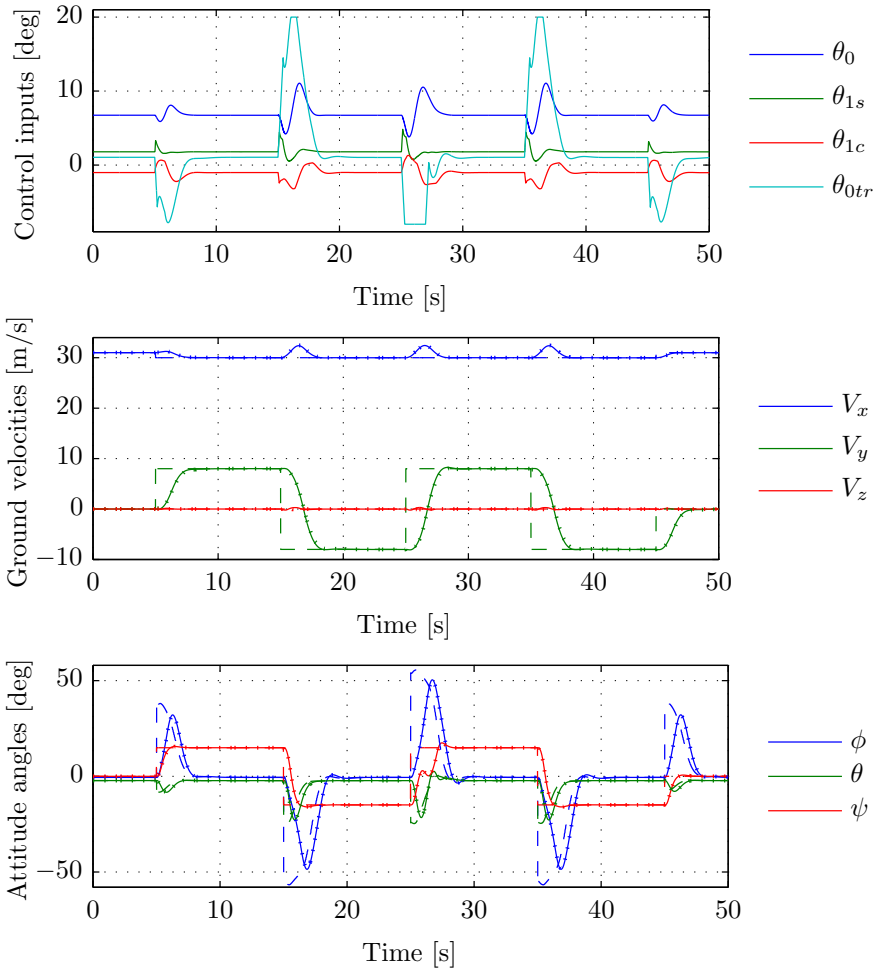

Figure 7-7: Results obtained from the simulation of the slalom maneuver. The dashed lines correspond to the references commanded, the dotted lines to the state of the reference model and the solid lines to the actual response of the helicopter.

response, with practically no steady-state error. The vertical velocity V_z is perfectly kept to zero, presenting only very slight oscillations around the transient instants of the horizontal velocity. This coupling is however more intense in the remaining component of the velocity, yielding overshoots of approximately 3 m/s around the referred moments.

The commanded velocities are now mainly tracked by changing the roll angle of the helicopter, becoming positive to turn right and negative to turn left. The pitch angle is also used to adjust the airspeed. Finally, the yaw angle is tracked very efficiently, presenting a quick response with no steady-state error. Some undesirable oscillations can however be identified around the second 26. These oscillations are certainly due to the saturation experienced by the collective of the tail rotor at the moment, but from which the system is able to recover immediately.

Besides the intense actuation associated with the collective pitch of the tail rotor, the commands to the remaining actuators throughout the maneuver are not too demanding.

7-4-3 Aggressive agility: the transient turn

The transient turn is a common robustness test for full authority controllers, since a wide range of sideslip angles and speed components are commanded during the maneuver. It is also well described in (*ADS-33E-PRF*, 2000). The main goals of this maneuver are to ensure that handling qualities do not degrade during aggressive maneuvering in all axes and to check for undesirable couplings between the three attitude angles. The simulation setup is as follows:

> The helicopter starts this test flying North with no sideslip angle at a constant altitude of 61 m (approx. 200 ft) and at a constant speed of 62 m/s (approx. 120 kt). In the next ten seconds, the vehicle is commanded to decelerate completely until hovering flight while accomplishing a 180 deg rotation about its vertical axis. In the end, the helicopter shall thus achieve wings-level attitude facing South.
>
> During the whole maneuver, the helicopter shall maintain the same altitude and a straight trajectory, hence $V_{y_{com}} = V_{z_{com}} = 0$ m/s.

The results obtained from the simulation of the transient turn with the overall navigational controller are presented in Figure 7-8.

As it can be seen, the commanded references are again followed but, due to the aggressivity of the maneuver, substantial tracking errors are verified in the transient responses of both V_x and ψ. The performance of these responses is also quite degraded in comparison to the theoretical predictions. The referred velocity exhibits a small steady-state error, finishing the maneuver with a residual forward speed. The yaw angle presents an overshoot of almost 20 deg before the settling of the response.

The altitude of the helicopter is perfectly kept by the controller, since its vertical velocity is always approximately null. The lateral component of the velocity shows however the existence of a substantial coupling, which is eliminated once the collective of the tail rotor becomes desaturated. The referred actuator is in fact saturated for practically the whole turn due to the required aggressivity. The actuation associated with the remaining control inputs is however far from demanding.

7-5 Additional Aspects

As it was seen, the navigational control system implemented for the helicopter model developed receives as references the three components of the desired velocity with respect to the Earth (V_x, V_y and V_z) and the commanded yaw angle of the vehicle (ψ). However, in practice, this combination of commands may not be the most adequate for the pilot to select. This section aims therefore to suggest three different sets of parameters that can be more conveniently chosen by the pilot and to introduce the required conversions between these types of references and the ones supported by the controller.

The referred conversions are mainly based on mathematical expressions presented in Appendix A. It is known that the ground velocities are conveniently expressed in the NED

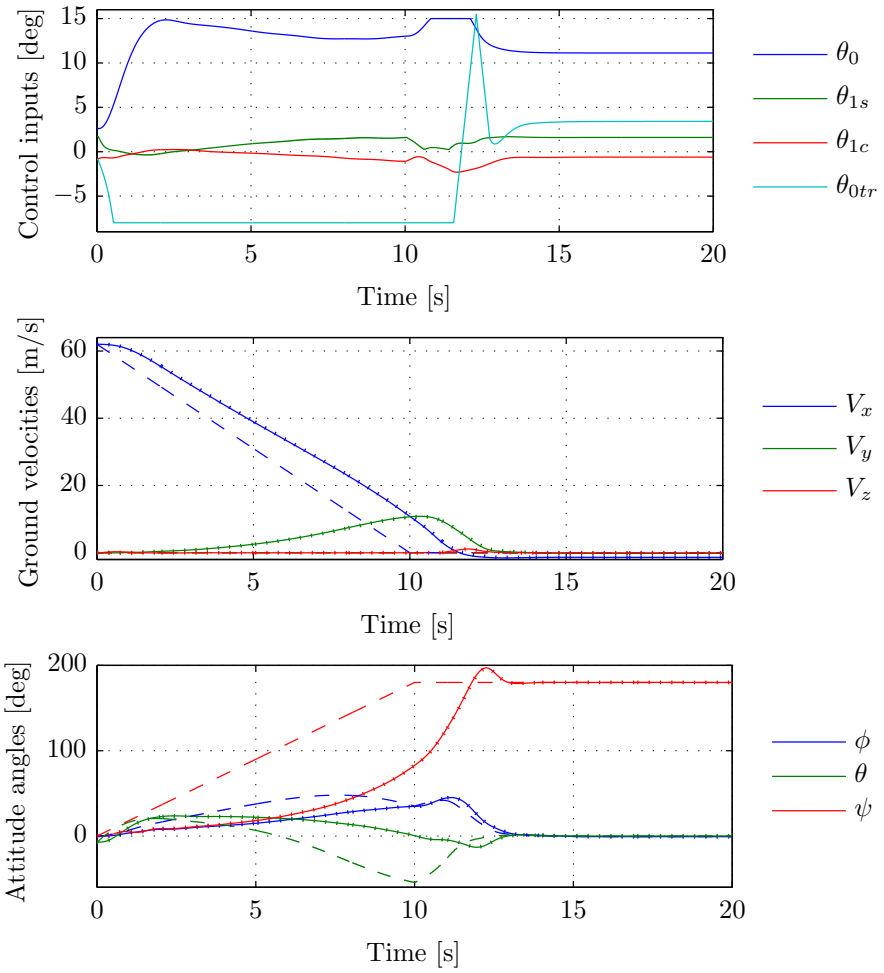

Figure 7-8: Results obtained from the simulation of the transient turn. The dashed lines correspond to the references commanded, the dotted lines to the state of the reference model and the solid lines to the actual response of the helicopter.

reference frame F_o as $[V_x\ V_y\ V_z]^T$. In the appendix mentioned above, it was stated that the velocity reference frame F_v is defined such that the velocity vector of helicopter is written in this coordinate system as $[V\ 0\ 0]^T$, where $V = \sqrt{V_x^2 + V_y^2 + V_z^2}$ is the airspeed of the vehicle. A relation between these two vectors can be established by means of the transformation from F_o to F_v, defined by (A-5) as $\underline{T}_v^o$. Using the inverse transformation, the following result is obtained:

$$\begin{bmatrix} V_x \\ V_y \\ V_z \end{bmatrix} = \underline{T}_o^v \begin{bmatrix} V \\ 0 \\ 0 \end{bmatrix} = V \begin{bmatrix} \cos\chi\cos\gamma \\ \sin\chi\cos\gamma \\ -\sin\gamma \end{bmatrix} \tag{7-35}$$

where γ is the flight path angle and χ is the heading. The yaw angle is related to the latter one through the sideslip $\beta = \chi - \psi$, which represents the angle between the longitudinal axis of the helicopter and the horizontal projection of its velocity vector (see Figure A-2).

From the desired ground velocities, the flight path angle can be directly determined using the

last component of (7-35):

$$\gamma = -\arcsin\frac{V_z}{V} \tag{7-36}$$

The heading can also be easily determined by dividing the first two rows of (7-35):

$$\chi = \arctan_2\frac{V_y}{V_x} \tag{7-37}$$

In this case, the two-argument arctangent function is adopted in order to distinguish the correct quadrant of the angle by taking into account the signs of the numerator and denominator of the fraction.

7-5-1 Autopilot

The first situation presented here concerns a conventional autopilot of an aircraft. This type of controller is mainly used during cruise flight and normally allows the pilot to select directly in the Mode Control Panel (MCP) the desired airspeed V_{com}, heading χ_{com} and climb rate $\dot{h}_{com}$ of the vehicle.

Knowing that the vertical velocity V_z is symmetrical to the climb rate $\dot{h}$, the flight path angle is given by:

$$\gamma_{com} = \arcsin\frac{\dot{h}_{com}}{V_{com}} \tag{7-38}$$

and since the airspeed and heading are both selected by the pilot, (7-35) can now be applied to determine the commanded ground velocities.

As in cruise flight it is desirable to fly with no sideslip for fuel efficiency and for passenger comfort, the yaw angle commanded shall yield $\beta_{com} = 0$ and thus:

$$\psi_{com} = \chi_{com} \tag{7-39}$$

This automatic turn coordination is also useful to reduce the pilot workload.

7-5-2 Fly-by-wire

The concept of FBW refers to a flight control system in which the movement of flight controls, instead of being directly transmitted to the actuators, is converted to electronic signals that serve as commanded references to be tracked by the flight control computer. Despite being normally used to give the references for a rate or attitude controller, this system could also be used to generate the commands for the navigational controller under analysis very quickly, making possible the use of this type of controller for precise maneuvering of the rotorcraft.

According to this, it would be useful that, when the three flight controls (the cyclic stick, the collective lever and the anti-torque pedals) are left free, the helicopter achieved a stabilized hover in the current orientation. This type of control provides an increased stability, but the agility is reduced. A possible arrangement of control deflection/references commanded is:

- The displacement and direction of the deflection of the stick would determine the horizontal components of the desired velocity $V_{x_{com}}$ and $V_{y_{com}}$: the translational ground speed would follow the stick;
- The position of the lever would control the climb rate $\dot{h}_{com} = -V_{z_{com}}$: when the pilot pulls it up or down, the helicopter would start climbing or descending, respectively.

When a helicopter is operating, it is useful to have the complete range of sideslip angles available and thus the condition $\beta_{com} = 0$ should not be imposed. Instead, the pilot could use the pedals to adjust the sideslip β_{com} of the rotorcraft: the left and right pedals would increase the sideslip angle in the respective direction. Knowing then the sideslip angle and using (7-37) to compute the desired heading, the commanded yaw angle is obtained directly from:

$$\psi_{com} = \chi_{com} - \beta_{com} = \arctan_2 \frac{V_{y_{com}}}{V_{x_{com}}} - \beta_{com} \tag{7-40}$$

7-5-3 Position control

The final suggestion of this section is based on the development of a position controller for the helicopter using the navigational controller already developed. This type of approach was already followed in (Moelans, 2008). The reason why a position controller was not developed in this thesis is simply because this kind of control system is normally implemented only for autonomous UAV helicopters, of which (E. N. Johnson & Kannan, 2005) is a good example.

Since the current navigational controller tracks commanded references in terms of ground velocities $\underline{v}_{E_{com}}$, position control can be easily achieved by introducing another external loop that generates these commands, proportionally to the errors in terms of position coordinates. A small integrative action shall also be introduced in order to eliminate steady-state tracking errors in the trajectory. Hence, the referred external loop consists simply of a PI controller applied to the position error:

$$\underline{v}_{E_{com}} = \underline{K}_P \left(\underline{p}_{com} - \underline{p} \right) + \underline{K}_I \int_0^t \left(\underline{p}_{com} - \underline{p} \right) \mathrm{d}\tau \tag{7-41}$$

where $\underline{p}_{com}$ is the desired position of the helicopter in NED coordinates at a given time instant and $\underline{p}$ is its actual position. The proportional and integrative gains can be chosen from the analysis of the closed-loop transfer function, similarly to what was done in the end of Section 7-1.

Finally, the commanded yaw angle can again be defined such that the helicopter flies with no sideslip, corresponding thus to its heading. According to (7-37) and since the commanded ground velocities are generated by the PI controller, this yields:

$$\psi_{com} = \arctan_2 \frac{V_{y_{com}}}{V_{x_{com}}} \tag{7-42}$$

Chapter 8

Robustness Tests

After implementing the complete control system designed throughout the previous chapters and simulating the performance of some maneuvers with the helicopter model, it is now important to assess whether the controller is robust to modifications on its nominal conditions. Therefore, in this chapter, several changes are introduced and, for each one, the response of the system is carefully analyzed. The referred changes considered in the following sections are: rotor aerodynamic uncertainties, inertia matrix mismatch, tail rotor malfunction, sensors noise and delay, actuator delays, wind effect and controller sampling frequency.

The nominal response of the system with which all the results will be compared corresponds to the moderate agility maneuver of Subsection 7-4-2, but with only one doublet input commanded to V_y, instead of two. A simplified block diagram of the multi-loop structure of the navigational controller is depicted in Figure 8-1. Figure 8-2 presents separately the nominal responses of the control inputs and control variables for the maneuver mentioned above. A detailed interpretation of these results was already carried out in Subsection 7-4-2.

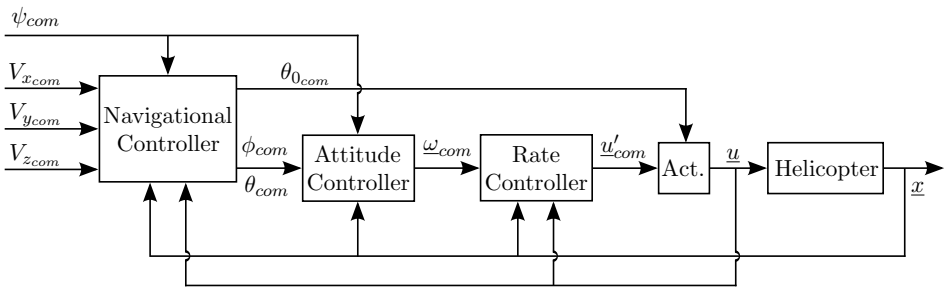

Figure 8-1: Simplified schematic of the overall flight control system.

Before proceeding with the robustness tests, it is important to mention that a comparison with the results obtained when a non-incremental NDI is used to control the inner loop of the overall controller and the control law for the collective of the main rotor would also be

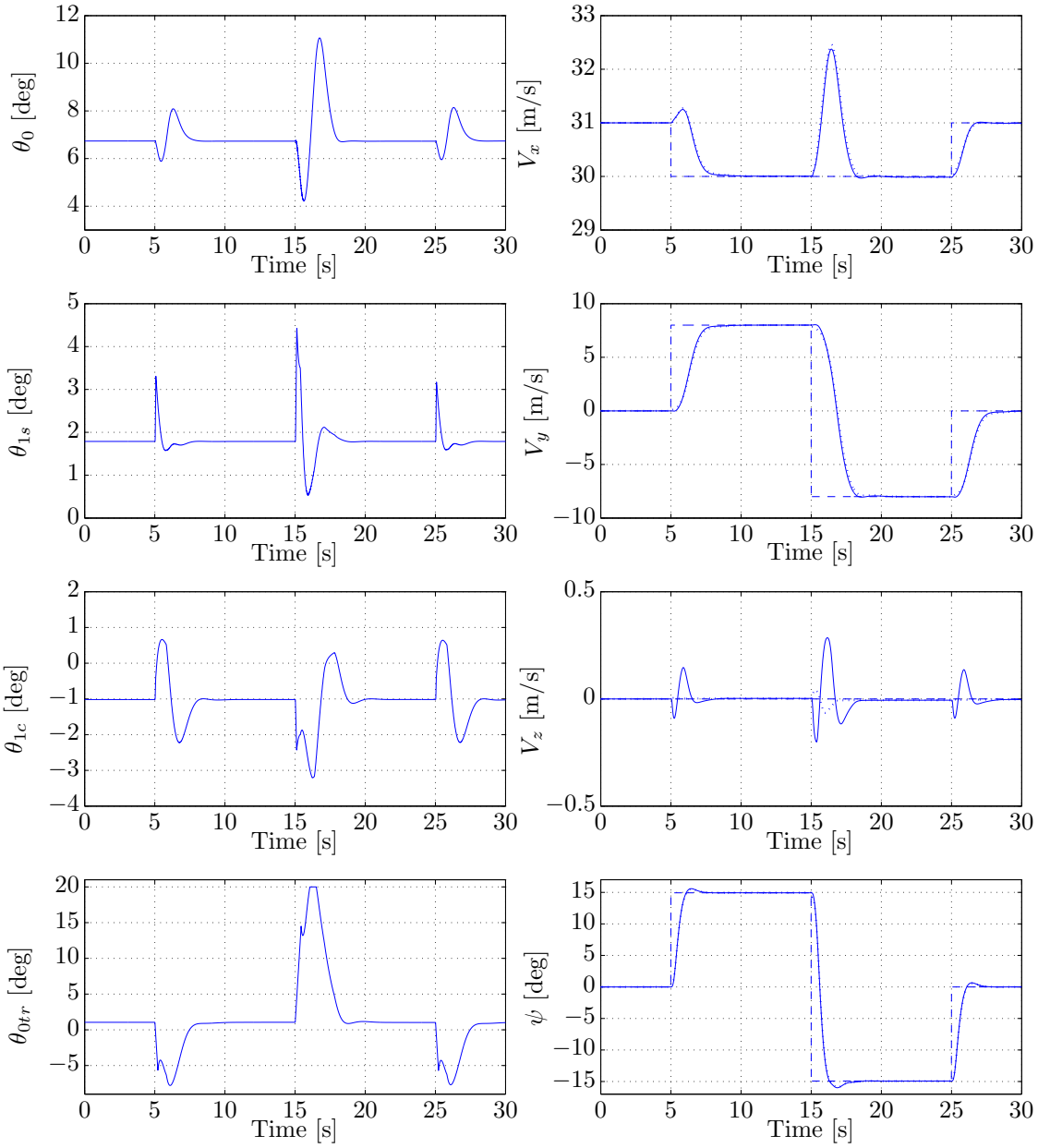

Figure 8-2: Nominal response of the system. The dashed lines correspond to the references commanded, the dotted lines to the state of the reference model and the solid lines to the actual response of the helicopter.

interesting. Nevertheless, the implementation of a NDI controller for a nonlinear helicopter model is computationally complex due to the need to invert numerically the highly nonlinear function $\underline{g}(\underline{x}, \underline{u})$, in (5-3). This type of controllers are therefore not suitable to apply as sole means to helicopter flight control. In fact, NDI-based helicopter controllers are normally designed using linearized versions of the system and a reasonable performance is only achieved when an adaptive approach is introduced to compensate for the inversion errors, as shown in (Moelans, 2008).

One of the main advantages of the INDI is that the function mentioned above is only considered through its first derivative with respect to u, which can be computed very easily using finite differences. Furthermore, it is already globally accepted that controllers based on INDI are substantially more robust to model uncertainties than the ones based on NDI since they do not depend on the accuracy of the control-independent part of the model. The issues associated with the differences between these two strategies were already analyzed in detail in (Sieberling, 2009) and (Wedershoven, 2010).

8-1 Aerodynamic Uncertainties

As it was seen in Section 3-5, theoretically, the control loops based on INDI are not sensitive to uncertainties in the control effectiveness function, as long as the signs of the derivatives of its components with respect to the control inputs are correctly known. Furthermore, by making use of angular or linear accelerations, they do not require any additional information about the helicopter model and thus they are not affected by the configuration of the fuselage nor the horizontal and vertical tails. This type of robustness is very important since it avoids the need for an extremely accurate model, which is very difficult and costly to obtain in practice. In addition, this property also allows the control system to cope with changes in configuration during flight. The behavior of the system in the presence of model inaccuracies is analyzed in this section, while the sensitivity to changes in the configuration will be assessed in the next two.

One of the main difficulties in helicopter modelling is to describe accurately the very complex processes in the rotor that generate the aerodynamic forces and moments. As shown in Subsection 2-3-1, expressions for these coefficients as well as for other parameters like the flapping angles or the rotor inflow always result from approximations to a certain extent. These approximations originate therefore discrepancies with respect to the real model of the helicopter and, when they are adopted in the control system, its performance may be compromised.

As already mentioned, theoretically the performance of INDI-based controllers is not affected by model uncertainties, as long as the sign of the derivatives of the control effectiveness is correctly known. Nevertheless, this conclusion may not be completely true for the particular case under analysis, since some additional approximations were made in the application of the INDI theory to invert the complex model of the helicopter. Namely, the influence of the control effectiveness function was only considered through its first order derivative and finite differences were used to determine some of its components. The validity of these approximations was already checked in Section 5-2 for the nominal condition of the system, but now the potential consequences in the presence of uncertainties have also to be evaluated. Besides the referred approximations, additional problems may also arise in the presence of model uncertainties due to the limitations associated with the actuators. These problems are however expected to be dealt by the PCH layers.

In this section, model uncertainties are simulated by introducing inaccuracies simultaneously in the values of $C_{T_{dp}}$, $C_{H_{dp}}$, $C_{S_{dp}}$ and $C_{Q_{dp}}$, associated with the main rotor and determined from equations (2-50) to (2-53). The coefficients adopted by the controller are thus given by:

$$\hat{C}_* = C_* \left(1 + \varepsilon\right) \tag{8-1}$$

where C_* is the real value of the aerodynamic coefficient, $*$ can assume each one of the rotor forces or moment and the error ε is generated randomly according to a normal distribution with zero mean and standard deviation σ. Its probability density function is represented by the Gaussian curve depicted in Figure 8-3.

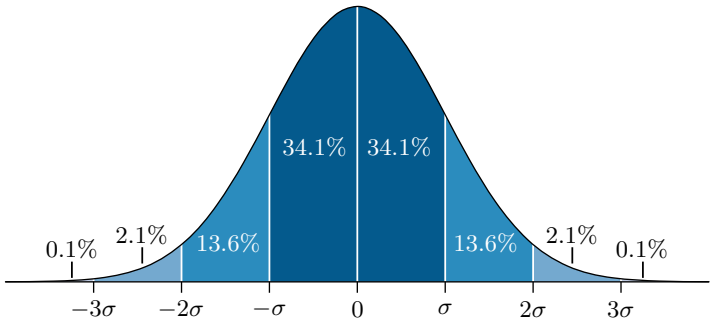

Figure 8-3: Probability density function of a normal distribution with zero mean. [adapted from Wikipedia]

From this figure, it can be understood that the value of ε has a probability of approximately 95.4% to be within the interval $[-2\sigma, 2\sigma]$ and thus 2σ can be viewed as the maximum relative uncertainty of the aerodynamic model known by the controller. Recall that the forces and moments produced by the main rotor are given by (2-54) to (2-55). Note also that only positive values make physical sense for the coefficients C_T and C_Q above, whereas the values generated by (8-1) may be negative. This is only allowed to analyze the response of the controller to substantial discrepancies in the aerodynamic model of the rotor.

The simulation of the nominal maneuver was then performed for different values of σ and, since the forces and moment coefficients are now given by a stochastic process, more than one trial shall be carried out for each magnitude of uncertainty. In this case, three different trials (I, II and III) were made for each value of σ and the results obtained are presented in Figure 8-4.

Several parameters can be used to compare the performance of a system when tracking a certain reference signal. Among these parameters are, for instance, the overshoots of the responses, the settling times or the steady-state errors. For simplicity, in the current chapter only the tracking Root-Mean-Square Error (RMSE) is analyzed for the referred comparison. The RMSE contains more information than a simple average of the error, since it also accounts for its variance. Physically, it would correspond to a continuous deviation of the variables with respect to their commanded reference. Defining the tracking error of a generic variable $x(t)$ as $e(t) = x_{com}(t) - x(t)$, its average over time as $\langle e(t) \rangle$ and its variance as $\text{var}\{e(t)\}$, the tracking RMSE of $x(t)$ is given by:

$$\text{RMSE}\{x(t)\} = \sqrt{\langle e(t) \rangle^2 + \text{var}\{e(t)\}} = \sqrt{\langle e(t)^2 \rangle} \tag{8-2}$$

It is important to note that, being a tracking error, it may happen in the following tests that a response affected with uncertainties presents smaller RMSE values than the nominal one if, by coincidence, it becomes closer to the commanded references. Table 8-1 shows the RMSE

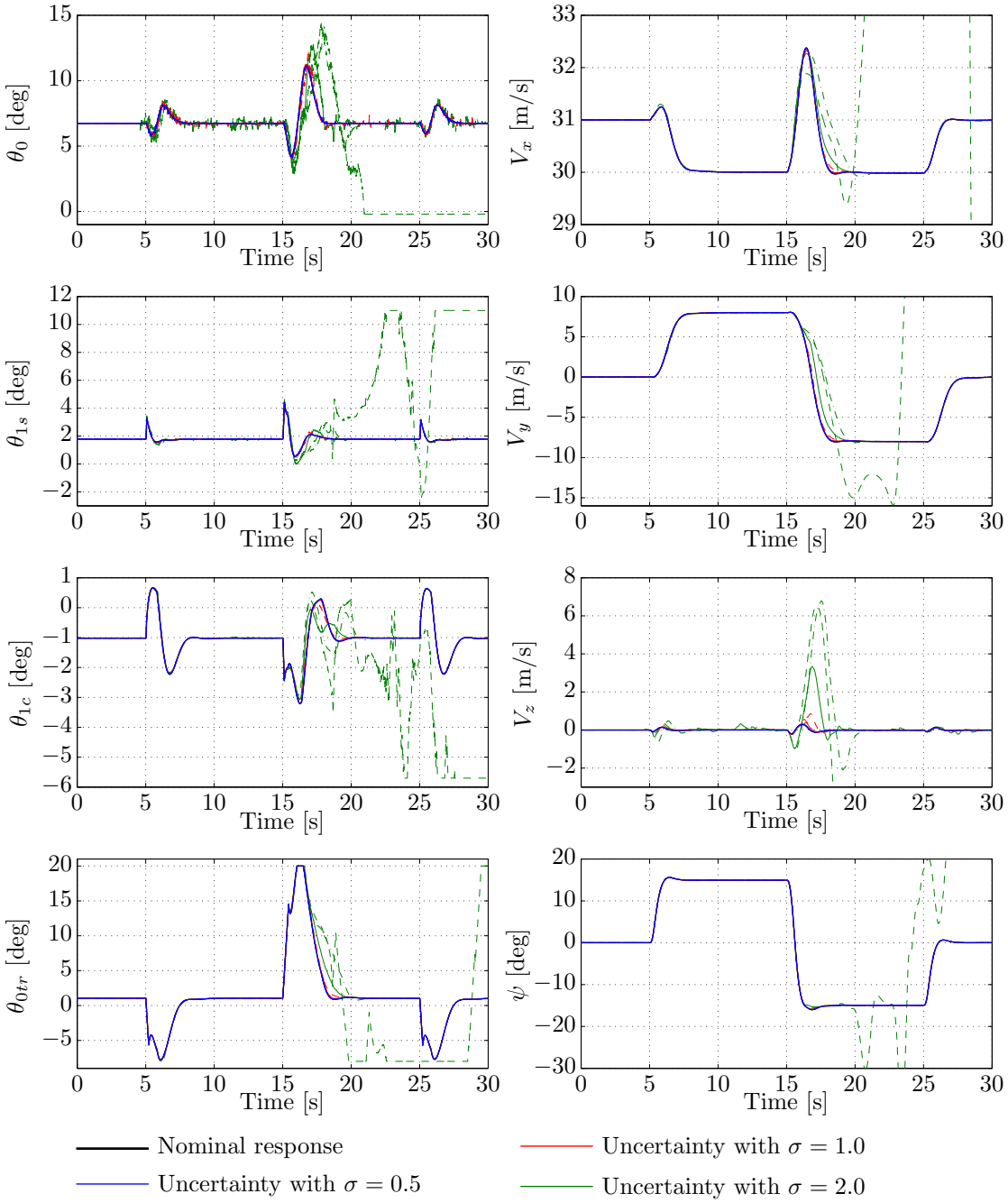

Figure 8-4: Response of the system with uncertainties in the aerodynamic model. The solid, dashed and dashdot lines correspond respectively to trials I, II and III.

for the four control variables of the helicopter system obtained from the simulations depicted in the previous figure. Besides the RMSE, a qualitative analysis of the control effort will also be taken into account for comparing the responses presented in the next sections.

From the joint analysis of Figure 8-4 and Table 8-1, the following observations can be made:

Table 8-1: Tracking RMSE for the simulations with uncertainties in the aerodynamic model.

Robustness test	Trial	V_x (m/s)	V_y (m/s)	V_z (m/s)	ψ (deg)
Uncertainty with $\sigma = 0.5$	I	0.535	4.174	0.054	4.511
	II	0.536	4.172	0.052	4.511
	III	0.535	4.173	0.054	4.511
Uncertainty with $\sigma = 1.0$	I	0.534	4.181	0.062	4.511
	II	0.535	4.217	0.122	4.511
	III	0.527	4.187	0.082	4.511
Uncertainty with $\sigma = 2.0$	I	0.559	4.433	0.531	4.513
	II		Helicopter	crashed	
	III	0.645	4.769	1.322	4.513
Nominal response	–	0.536	4.173	0.054	4.511

- For a maximum model inaccuracy of 100% ($\sigma = 0.5$), the performance of the system was not affected and all the trials were performed exactly as in the nominal conditions. For this case, the probability of occurring a reversal in the sign of the aerodynamic coefficients ($\varepsilon < -1$) is only of approximately 2.2%. Note however that a wrong sign of the aerodynamic coefficients does not necessarily imply a wrong sign in the derivative of the control effectiveness;

- For a maximum model inaccuracy of 200% ($\sigma = 1.0$), some very small alterations are already obtained, especially in the components of the velocity. In the collective of the main rotor, occasional oscillations can also be identified during the three trials, indicating that at some instances the controller tends to increase the errors, instead of compensating for them. This is clearly a result of an incorrect sign of the derivative of the control effectiveness (the probability of having $\varepsilon < -1$ is now of 15.9%). Nevertheless, if these extreme circumstances are not persistent, the controller is able to recover easily its nominal evolution;

- For a maximum model inaccuracy of 400% ($\sigma = 2.0$), the probability of $\varepsilon < -1$ is already of 30.9% and the performance of the system becomes severely degraded. Both the oscillations and the RMSE of the responses increased relatively to the nominal simulation and trial II was already unsuccessful since it resulted in the crash of the helicopter. As expected, control oscillations occur now more often and with higher amplitude. If the control actuation at those instances is not too demanding, the controller is able to recover from these disturbances very efficiently but, otherwise, the tracking performance is degraded and the stability of the helicopter compromised.

From this section it is then possible to conclude that the theoretical insensitivity of the control system to model inaccuracies holds for the design developed in this thesis, as long as the sign of the derivatives of the control effectiveness is not persistently wrong. Satisfactory good results were obtained for trials with relative uncertainties in the aerodynamic coefficients up to 200%. It must be noted that, in practice, only values considerably smaller than these are expectable.

8-2 Inertia Mismatch

As it was mentioned in the previous section, it is desirable to have a control system that shows some degree of insensitivity to changes in the model of the system during flight. In this section, the response of the helicopter when there is a mismatch between the inertia matrix known by the controller and the actual one is analyzed. Changes in the inertia property of a model can occur simply due to fuel consumption during flight but also in situations in which the load carried in the helicopter is rearranged.

Inaccuracies in the inertia property of the helicopter are introduced by adding a mismatch matrix $\Delta\underline{J}$ to the actual one $\underline{J}$, according to:

$$\hat{\underline{J}} = \underline{J} + \Delta\underline{J} \tag{8-3}$$

The responses obtained from the simulation of the system with three different values of $\Delta\underline{J}$ are depicted in Figure 8-5 and the corresponding tracking RMSE are registered in Table 8-2.

From the analysis of the plots, it is possible to see that both the tracking performance and the control actuation were affected by changes in the inertia matrix. Nevertheless, the tracking of the commanded references was always achieved and the system did not become unstable. Together with the RMSE of the responses, it is possible to conclude that, globally:

- The performance of the system is degraded when the components of the inertia matrix assumed by the controller are underestimated. While for $\Delta\underline{J} = -0.5\underline{J}$ the results are still quite reasonable, for $\Delta\underline{J} = -0.8\underline{J}$ the response is too oscillatory and the RMSE increase. Note however that the latter mismatch is already quite pessimistic and it is not likely that such discrepancies exist in reality;
- When the components of the matrix assumed by the controller are bigger than its actual values, the response of the system changes slightly, but its performance is enhanced. This can be explained from the fact that as the system "thinks" the helicopter has more inertia than it actually has, more intense control actuations are demanded and more efficient responses are achieved. These higher control efforts can be identified, for example, it the signal of the longitudinal cyclic. Obviously, this improvement is only achieved as long as it is supported by the actuators and PCH. Nevertheless, the successful simulation carried out here has already a mismatch of $\Delta\underline{J} = \underline{J}$, representing an inertia inaccuracy of 100%, which is not likely to find in reality.

From these results, it can be concluded that, despite being slightly sensitive to inertia mismatches, the performance of the controller is not severely degraded for the uncertainty values expected to find in practice.

8-3 Tail Rotor Malfunction

As it was mentioned in Section 3-5, the insensitivity of the INDI to modelling errors allows to use exactly the same controller developed in this thesis to control the helicopter in the presence

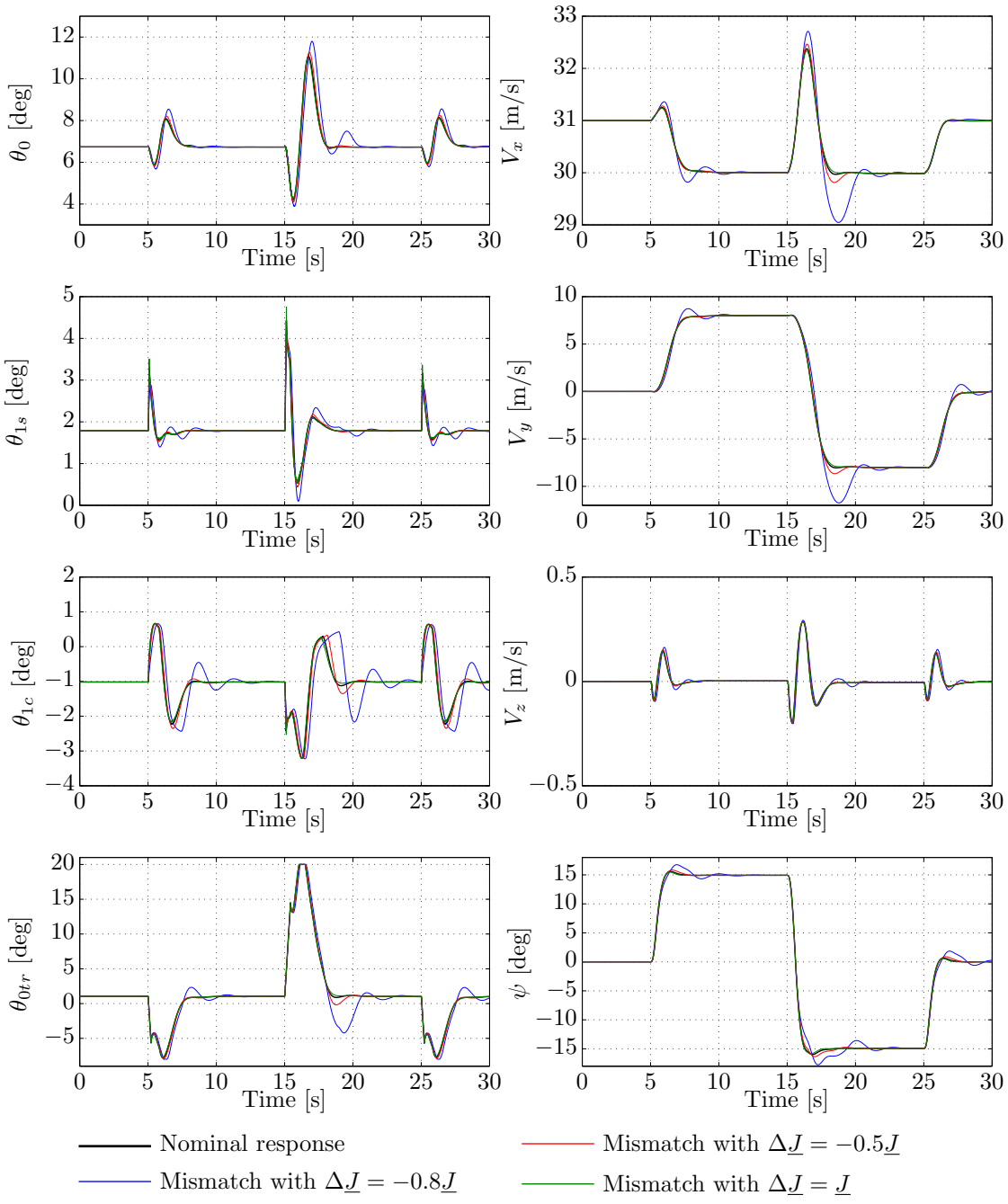

Figure 8-5: Response of the system with mismatches in the inertia matrix.

Table 8-2: Tracking RMSE for the simulations with mismatches in the inertia matrix.

Robustness test	V_x (m/s)	V_y (m/s)	V_z (m/s)	ψ (deg)
Mismatch with $\Delta\underline{J} = -0.8\underline{J}$	0.624	4.382	0.057	4.669
Mismatch with $\Delta\underline{J} = -0.5\underline{J}$	0.550	4.206	0.055	4.539
Mismatch with $\Delta\underline{J} = \underline{J}$	0.530	4.160	0.054	4.501
Nominal response	0.536	4.173	0.054	4.511

of structural damages or system failures without the need to perform real-time identification of its model. As explained in (Bacon et al., 2001), in a failure scenario, aerodynamic changes cause force and moment changes on the aircraft. The INDI approach exploits the fact that these changes are measured by accelerometers to regain control of the damaged vehicle.

In this section, the performance of the control system is evaluated when a malfunction in the tail rotor occurs. In order to simulate the referred malfunction, the collective pitch of the tail rotor is kept constant during the simulation and thus it is not possible for the control system to change this input. This would correspond to a situation in which the actuator got stuck at a certain position. The response of the system was tested for three fixed pitch angles of the collective of the tail rotor: -8 deg (lower limit), 0 deg and 20 deg (upper limit). The results obtained and the corresponding tracking RMSE are once again presented in a figure and a table, being in this case Figure 8-6 and Table 8-3.

It is possible to verify that the tracking of the velocities, despite being slightly degraded, can still be achieved quite efficiently for all the malfunctions tested. The responses associated with the yaw angle suffered however a more severe degradation, especially in terms of oscillations, settling time and steady-state error. This is explained by the simple fact that the yaw rate of the helicopter is directly influenced by the thrust produced by its tail rotor. Additionally, as it can be understood intuitively, the performance degradation due to the malfunction of the tail rotor is more intense when the difference between its fixed position and the values assumed in the nominal condition is larger.

8-4 Sensor Dynamics

As it was seen in Section 3-5, by replacing the knowledge of part of the helicopter model needed by the controller with linear or angular acceleration measurements, INDI-based control loops become more dependent on the accuracy with which these quantities are obtained. This problem is specially aggravated since a very simplistic process based on finite differentiation was assumed for the estimation of the angular accelerations. As it was already seen, for ideal sensors, it was possible to assure a very satisfactory response of the control system by low-pass filtering the signals demanded to the actuators.

In reality, sensors are not ideal but present a certain dynamic instead. They normally introduce noise, time delays and biases into the system. These uncertainties can be made very small by integrating state estimation processes like Kalman filtering. The design of this type of filter is however out of the scope of this thesis.

This section aims to analyze the changes introduced in the responses of the helicopter when non-ideal angular rate measurements are considered. These measurements are obtained by rate gyros in the IMU onboard of the aircraft. Since the sensor biases only yield steady-state errors that are, in principle, eliminated by the outer loops, only the influence of noise and time delays is discussed. The effect of noise is simulated by adding band-limited white noise, characterized by a bandwidth of 10 Hz and by a predefined standard deviation. In reality, time delays associated with sensors are very small and are especially noticeable if a filtering process is used to estimate some variables.

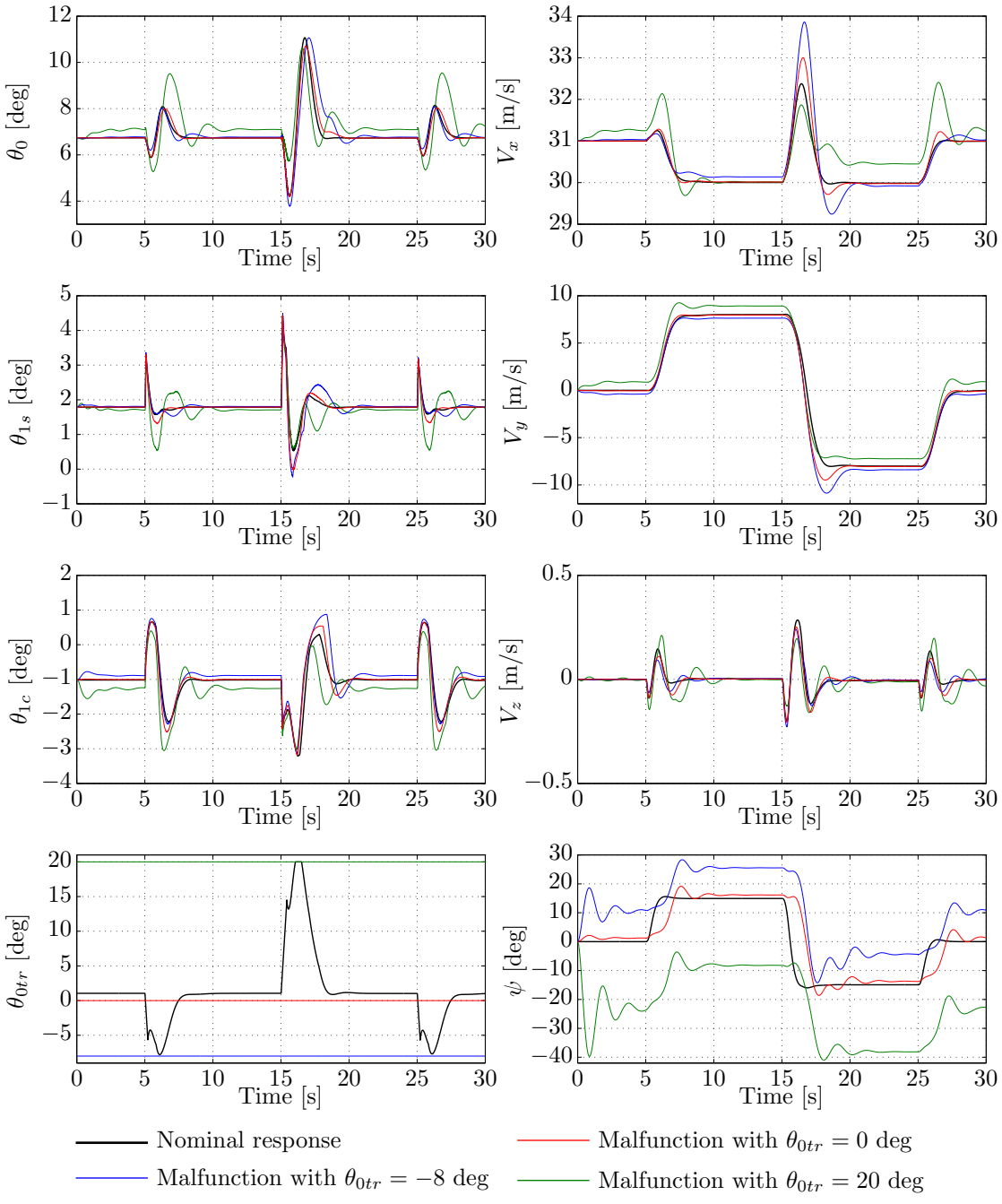

Figure 8-6: Response of the system with malfunctions in the tail rotor.

Table 8-3: Tracking RMSE for the simulations with malfunctions in the tail rotor.

Robustness test	V_x (m/s)	V_y (m/s)	V_z (m/s)	ψ (deg)
Malfunction with $\theta_{0tr} = -8$ deg	0.808	4.052	0.047	13.17
Malfunction with $\theta_{0tr} = 0$ deg	0.639	3.974	0.051	8.103
Malfunction with $\theta_{0tr} = 20$ deg	0.684	4.033	0.063	24.01
Nominal response	0.536	4.173	0.054	4.511

Figure 8-7 shows the results obtained when noise, time delay and both effects are considered in the angular rates measurements. The referred noise has a standard deviation of 0.1 deg/s and the time delay is of 20 ms. Usual values for these parameters were taken from (Sieberling, 2009), where a similar analysis is carried for a fixed-wing aircraft. The tracking RMSE for the distinct simulations are presented in Table 8-4.

As it can be seen, the responses of the system remain practically unchanged when noise or delay are introduced in the sensors. The control inputs are however slightly affected with additional undesired oscillations. In the case in which only noise was introduced, these oscillations are obviously due the oscillations in the angular rates measurements. When there exists a time delay, the oscillations are explained by the fact that the system is computing the control inputs for a situation that is already in the past and the controller is trying to compensate for an error that may have already been compensated. This effect is thus more noticeable in transient periods of the helicopter conditions. Note however that even when there are noise and time delay, the level of the referred oscillations is perfectly within an admissible range.

8-5 Actuators Delay

Another important aspect to consider when designing flight controllers is the existence of a time delay between the control system and the actuators of the aircraft. This delay is mainly due to the transmission time of the signal generated by the controller to the actuators themselves and, according to (Padfield, 1996), it assumes normally values around 100 ms. This means that, if the control system is operating at a frequency of 100 Hz, with a sampling time of 10 ms, there is a delay of ten samples between the computation of the demanded control deflections and the actual action of the actuators. Together with the rate limitations of the actuators, the overall delays can thus contribute severely to a degradation of the performance of the control system.

In this section, the behavior of the system is analyzed for time delays of 50 ms, 100 ms and 150 ms. The responses obtained are shown in Figure 8-8 and the tracking RMSE are summarized in Table 8-5.

As expected, when the delay of the actuators increases, the tracking performance of the system is degraded and the control effort required from the actuators also increases. With the controller developed in this thesis, a time delay of 50 ms still results in a quite satisfactory behavior of the helicopter, but the responses associated with delays of 100 ms and 150 ms have already considerable large overshoots and tracking RMSE.

8-6 Wind Effect

This section aims to analyze the influence of wind in the performance of the helicopter when describing the slalom maneuver. The wind was generated using a continuous turbulence model

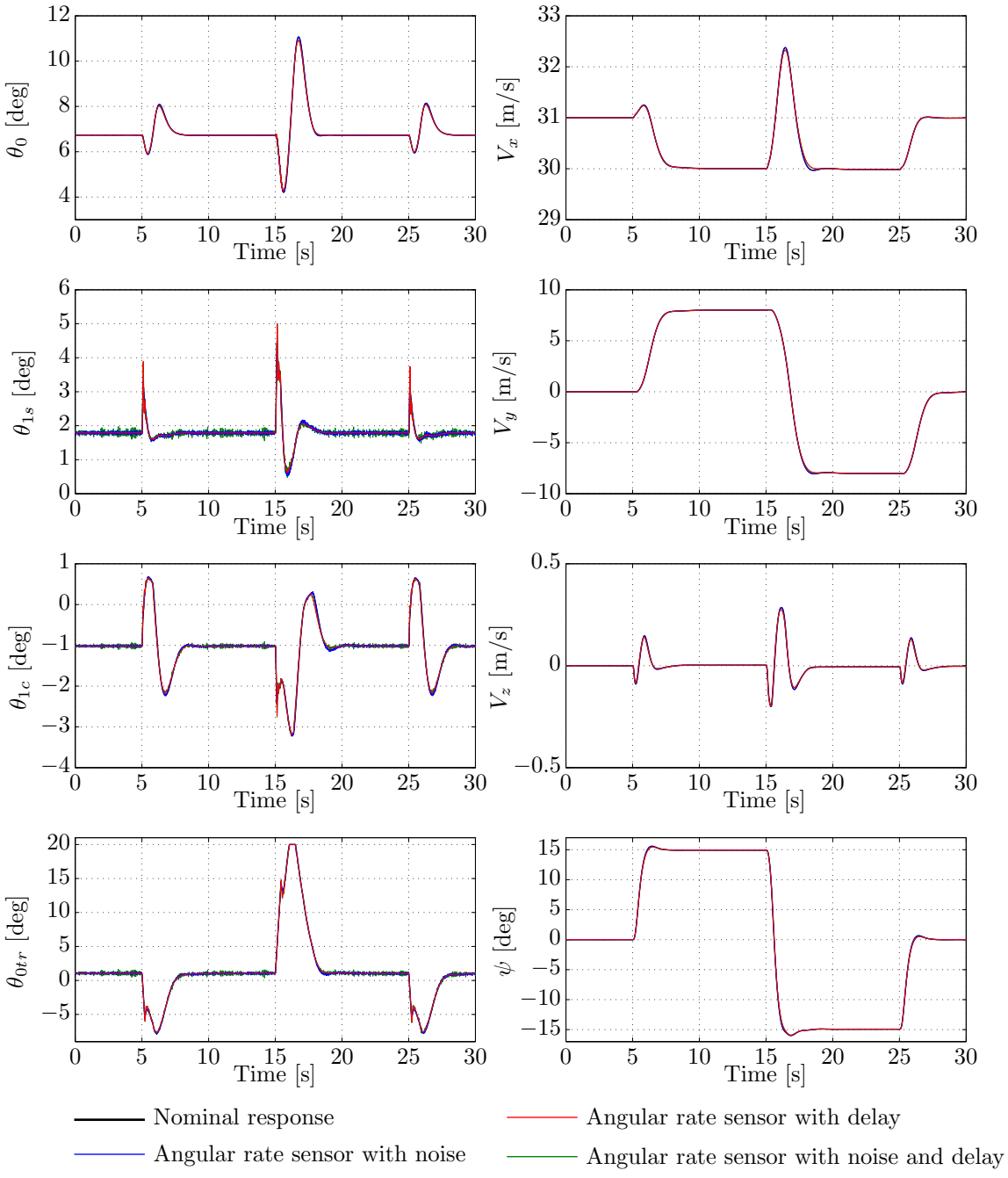

Figure 8-7: Response of the system with dynamics in the angular rates sensor.

Table 8-4: Tracking RMSE for the simulations with dynamics in the angular rates sensor.

Robustness test	V_x (m/s)	V_y (m/s)	V_z (m/s)	ψ (deg)
Angular rate sensor with noise	0.536	4.172	0.054	4.510
Angular rate sensor with delay	0.531	4.165	0.052	4.516
Angular rate sensor with noise and delay	0.531	4.165	0.052	4.494
Nominal response	0.536	4.173	0.054	4.511

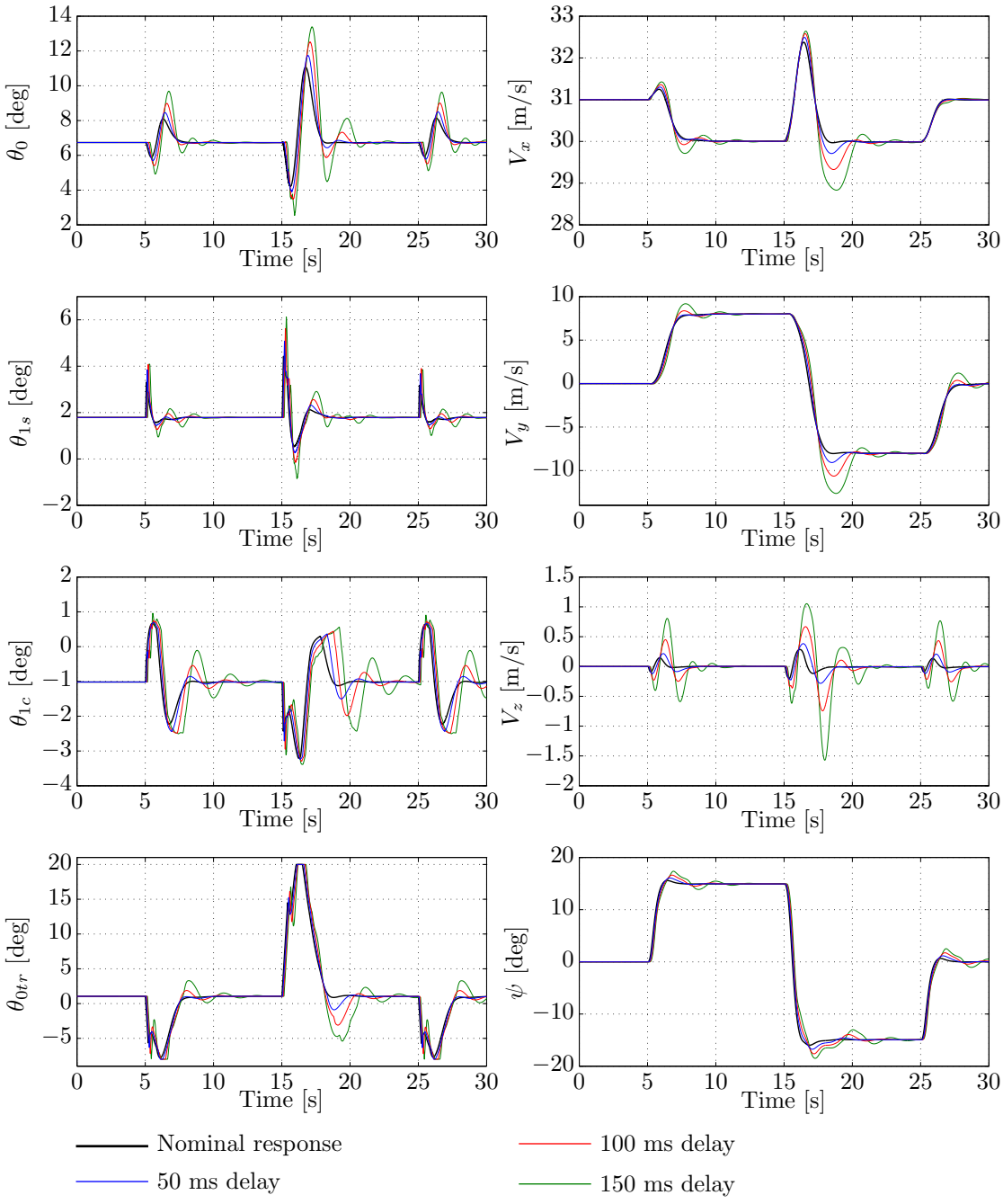

Figure 8-8: Response of the system with delay in the actuators.

Table 8-5: Tracking RMSE for the simulations with delay in the actuators.

Robustness test	V_x (m/s)	V_y (m/s)	V_z (m/s)	ψ (deg)
50 ms delay	0.556	4.275	0.089	4.765
100 ms delay	0.587	4.400	0.185	5.011
150 ms delay	0.646	4.586	0.347	5.270
Nominal response	0.536	4.173	0.054	4.511

available in *Simulink* based on the Dryden Spectral representation (MathWorks, n.d.-b). This type of model simulates the effect of continuous turbulence by passing a unit variance, band-limited white noise through appropriate forming filters, defined in military specifications.

According to these specifications, turbulence is a stochastic process defined by the wind velocity spectra. Its intensity and scale length are functions of altitude and introduce changes in the linear and angular velocity of aircraft. This turbulence model is valid when the mean-wind velocity is small relative to the aircraft ground speed since it assumes a frozen turbulence field. Furthermore, it describes an average of all conditions for clear air turbulence because factors like terrain roughness, wind shears and meteorological conditions are not considered.

The motion of the helicopter was simulated for three distinct turbulence intensities (light, moderate and severe) and the wind was kept blowing from the North. The distinct turbulence intensities are defined by a different probability of a gust that exceeds the high-altitude wind intensity. In order to be able to visualize the effect of the wind more clearly, the altitude of the simulation was also changed to 500 m. The results obtained are plotted in Figure 8-9 and the corresponding tracking RMSE calculated in Table 8-6.

As it can be seen from the analysis of the figure, additional oscillations appear in the motion of the helicopter when turbulence exists. The control system is however able to continue tracking the commanded references, but in this process, a considerable amount of oscillations also appear in the control inputs. As expected, the referred oscillations as well as the tracking errors presented in the table increase with the intensity of the turbulence.

8-7 Controller Sampling Frequency

Finally, it is important to analyze what happens when the helicopter control system is discretized at a lower frequency than the nominal 100 Hz. Lower controller frequencies require processing systems with less computational capabilities, which are therefore less costly. One the other hand, the INDI assumption $\underline{x} \approx \underline{x}_0$ is only valid for time steps small enough. Moreover, smaller time steps also contribute to more accurate estimations of the angular accelerations (which are calculated using finite differences) and thus improving the performance of the system. Note that, in this section, despite the sampling frequency of the controller is reduced, the rate of the simulation of the helicopter motion is kept at 100 Hz.

It is also important to note that, according to Nyquist theorem, the sampling time of the controller shall be at least two times smaller than the smallest time constant of the system in order to avoid aliasing phenomena. The smaller time constant imposed by the control loops is of 0.2 s, meaning that the controller shall always be sampled at a frequency higher than 10 Hz.

Additionally, it was also seen that the measurements of the ground velocities provided by the GPS receiver are obtained at a considerably lower frequency than the controller itself. Until now, it was assumed that the mentioned receiver is dedicated to the velocity estimation based on Doppler effect and possess high computational capabilities. Nevertheless, the consequences of using a cheaper receiver (operating at a lower frequency) to obtain the referred measurements have also to be investigated.

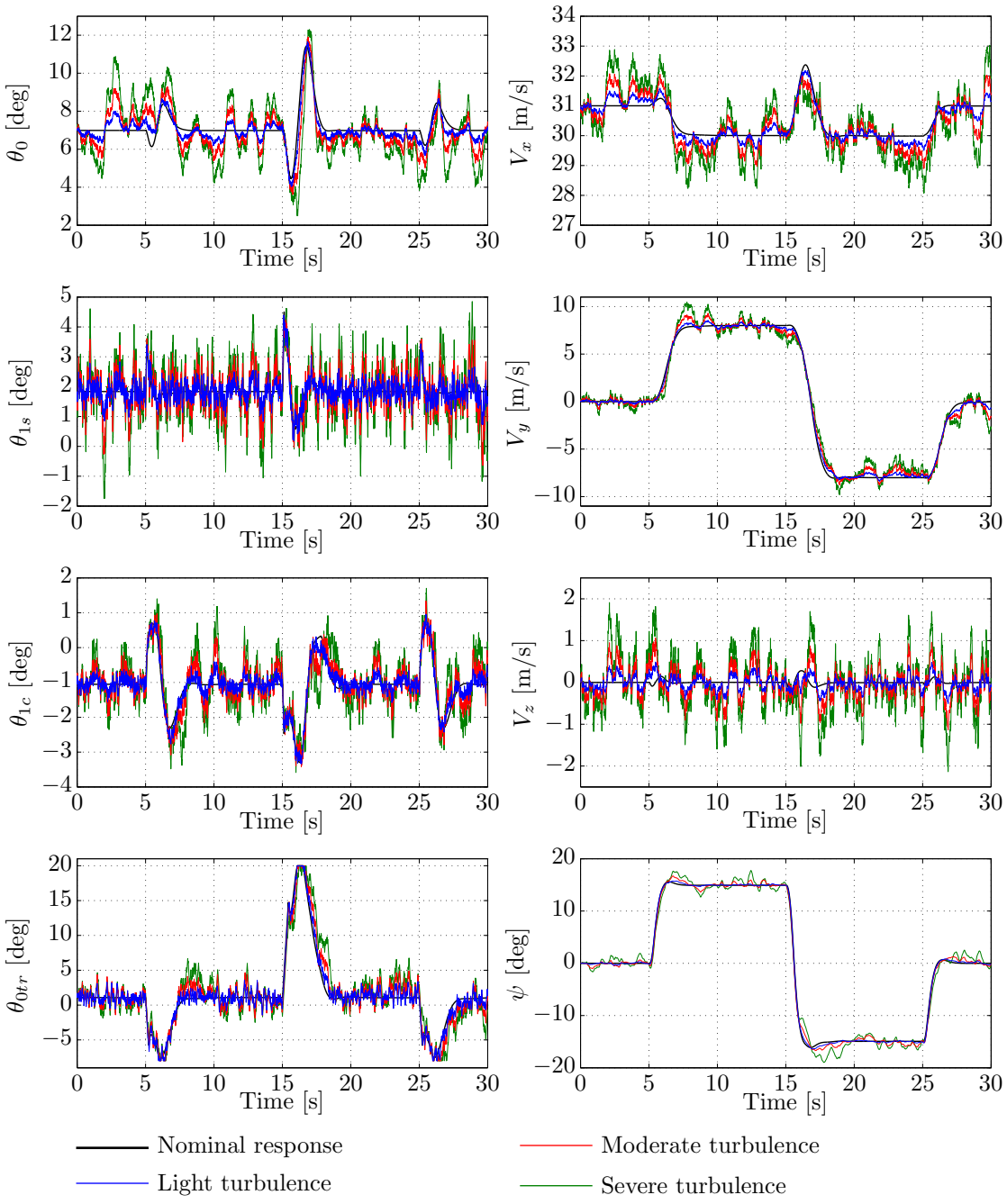

Figure 8-9: Response of the system in the presence of wind.

Table 8-6: Tracking RMSE for the simulations in the presence of wind.

Robustness test	V_x (m/s)	V_y (m/s)	V_z (m/s)	ψ (deg)
Light turbulence	0.566	4.152	0.165	4.526
Moderate turbulence	0.687	4.162	0.369	4.531
Severe turbulence	0.964	4.207	0.678	4.706
Nominal response	0.536	4.173	0.054	4.511

In this section, the system is simulated for three different combinations of the controller frequency $f_{control}$ and GPS sampling rate f_{GPS}. The results obtained and the tracking RMSE are available in Figure 8-10 and Table 8-7, respectively.

As it can be seen, when the GPS frequency is lowered to half its nominal value, the performance of the controller keeps practically unchanged. The corresponding responses match each other and the RMSE are barely affected.

With respect to the controller frequency, as expected, decreasing its value results in a degradation of the performance of the system. Despite this degradation being only slightly noticeable in the RMSE, some additional oscillations do exist in the responses of the helicopter, especially in terms of vertical velocity and heading angle. Nevertheless, the negative effects of a small processing frequency can be particularly identified in the control inputs, with the existence of substantial oscillations, characterized by a high frequency. This can be explained simply from the fact that, since the INDI is an incremental approach, higher frequencies allow to compute the required command deflections more often and therefore the corrections to achieve the desired tracking have a smaller magnitude, avoiding the introduction of oscillations. This type of oscillations is undesirable for the mechanical actuators.

8-8 Discussion of Results

As a summary, it was concluded that the flight control system designed is perfectly robust to model uncertainties due to aerodynamic inaccuracies and inertia mismatches for the range of values expected to find in reality. More robustness tests are recommended to be carried out in the future, namely to evaluate potential errors in the estimated flapping angles or rotor inflow, but the theory shows that the only requirement in terms of aerodynamic model to effectively control the helicopter is that the signs of the derivatives of the control effectiveness function are correct. It was also concluded that the robustness assured by the INDI-based control loops provide a very simple way to cope with system failures, namely with a malfunction in the tail rotor.

Afterwards, the potential degradation in the performance of the system caused by non-idealities in the sensors and actuators was also analyzed. It was concluded that, despite having a noticeable influence on the system, the degradations caused by both sensor dynamics and actuators delay still yield admissible results for the characteristics expected to find in reality.

Among all the factors studied in this chapter, the wind effect turned out to be the one that contributes more to the existence of oscillations in the control inputs and in the responses of the system. The controller sampling frequency, showed also some influence on the performance of the system, especially in terms of oscillatory control inputs.

Throughout this chapter, the effects of different factors in the performance of the system were analyzed separately. Obviously, when they are simultaneously present, their influence is summed up and the performance of the responses is further degraded. It is however expectable that, for the ranges of uncertainties encountered in reality, the present control system is able to assure asymptotic stability and tracking ability of the system.

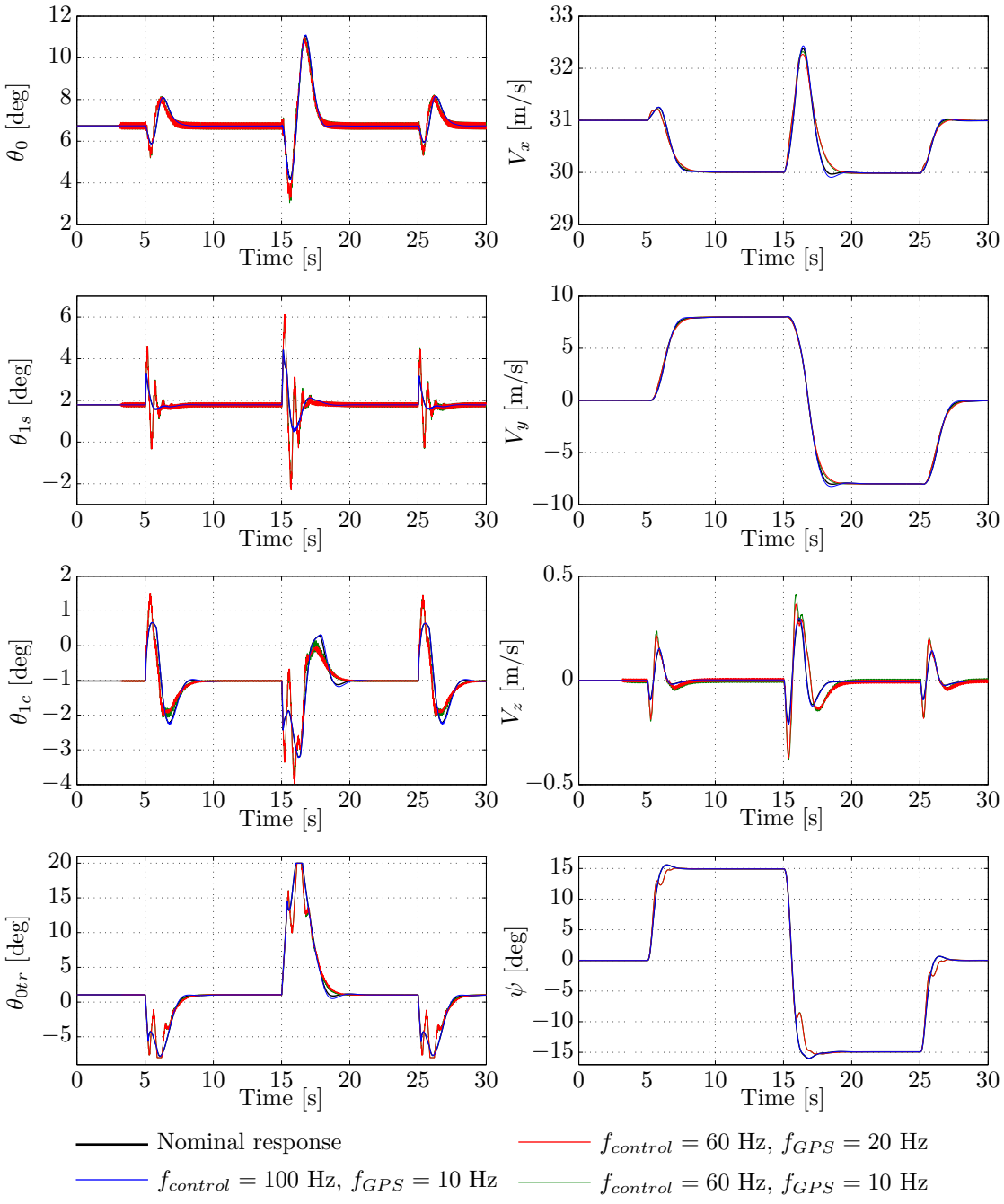

Figure 8-10: Response of the system with different controller frequencies.

Table 8-7: Tracking RMSE for the simulations with different controller frequencies.

Robustness test	V_x (m/s)	V_y (m/s)	V_z (m/s)	ψ (deg)
$f_{control} = 100$ Hz, $f_{GPS} = 10$ Hz	0.544	4.166	0.057	4.511
$f_{control} = 60$ Hz, $f_{GPS} = 20$ Hz	0.537	4.129	0.076	4.506
$f_{control} = 60$ Hz, $f_{GPS} = 10$ Hz	0.544	4.121	0.082	4.511
Nominal response	0.536	4.173	0.054	4.511

Chapter 9

Considerations on the Adopted Control Strategy

This chapter aims to present a very brief discussion mainly on the practical applicability of the overall navigational flight control system developed and on the differences regarding the application of INDI-based control loops to rotorcraft and fixed-wing aircraft.

As it was seen throughout this thesis, controllers based on the NDI technique require aircraft models stored onboard in order to invert the dynamics of the system. Nowadays, this does not represent a practical limitation of the technique since modern computer systems are perfectly capable of storing those amounts of data as well as computing the complex functions associated with them. Besides that, the NDI control loops also require information of the complete state vector of the system. Once again, this is not a prohibitive factor, because most modern aircraft carry a full complement of sensors, fused with efficient mathematical algorithms to improve the quality of the measurements and to estimate the necessary additional parameters (Enns et al., 1994). These factors justify the practical applicability of this kind of controllers.

It was however shown that the standard version of the NDI is very sensitive to model uncertainties, meaning that, if the model of the vehicle changes with respect to its nominal condition either due to modelling inaccuracies or changes in its configuration, the dynamic inversion will not be successfully attained and the system is not linearized nor its responses decoupled. To overcome this problem, an incremental version of the NDI was developed.

The proposed control system is less dependent on the onboard model than the conventional NDI, since only the control effectiveness (the influence of the control inputs in the states) is required and hence the information that does not depend on the control inputs is not needed for the implementation. Instead, the controller makes use of linear and angular acceleration measurements and actuator positions, meaning that it is more depending on sensor measurements. It was thus expected that the overall system would be very robust to model uncertainties but relatively affected by non-idealities (like delays and noise) associated with the sensor measurements or state estimation processes. These expectations were in fact corroborated by the results obtained in the previous chapter. As it was seen, the controller

showed great robustness to model changes and uncertainties, but it was weakly influenced by the sensor inaccuracies tested and likely to find in reality.

It is also important to understand that the flight control system developed here is not adaptive since no methods as online system identification or compensating NNs are included to adapt the controller in real-time. As already explained, this property is very useful when the potential certification of the flight control system is regarded. The INDI architecture allows to effectively replace the structure based on NDI plus an adaptive element to compensate for the inversion error, often encountered in the literature.

Besides the enhanced robustness already mentioned, the fact that INDI control loops require less information of the model also contributes to a considerable simplification of the control laws. Obviously, this simplification can be very useful, especially when the mathematical model of the system is rather complex, as in the case of a helicopter. Unfortunately, this issue is not as straightforward as it may seem on the first sight. In fact, the benefits brought by the INDI in terms of simplification depend on whether the most complexities and nonlinearities of the model lie in the control dependent or control independent part of the model. To illustrate this statement, consider the case of a fixed-wing aircraft, which is already well-know from recent research projects (Sieberling, 2009; Wedershoven, 2010).

The equation relative to the rotational dynamics of aircraft was already written in (5-3) as:

$$\dot{\underline{\omega}} = \underline{f}(\underline{x}) + \underline{g}(\underline{x}, \underline{u})$$

where $\underline{f}(\underline{x})$ is the control independent part of the model and $\underline{g}(\underline{x}, \underline{u})$ comprises moment terms that depend on the control inputs directly. As it was seen, the INDI eliminates the sensitivity of the control law to $\underline{f}(\underline{x})$, but the influence of $\underline{g}(\underline{x}, \underline{u})$ remains in the virtual control as its first order derivative with respect to $\underline{u}$:

$$\underline{\nu}_{rot} = \dot{\underline{\omega}}_0 + \left.\frac{\partial \underline{g}(\underline{x}, \underline{u})}{\partial \underline{u}}\right|_{\underline{x}_0, \underline{u}_0} (\underline{u} - \underline{u}_0) \tag{9-1}$$

This means that this approach is particularly effective when all the information of $\underline{g}(\underline{x}, \underline{u})$ can be constructed from its first order derivative. This only happens if the system under analysis is affine in the control inputs. Fixed-wing aircraft can normally be described by this type of systems. If the conventional control surfaces (ailerons (δ_a), elevator (δ_e) and rudder (δ_r)) are considered:

$$\underline{g}(\underline{x}, \underline{u}) = \underline{g}(\underline{u}) = \underline{J}^{-1} \begin{bmatrix} L_{\delta_a} & L_{\delta_e} & L_{\delta_r} \\ M_{\delta_a} & M_{\delta_e} & M_{\delta_r} \\ N_{\delta_a} & N_{\delta_e} & N_{\delta_r} \end{bmatrix} \begin{bmatrix} \delta_a \\ \delta_e \\ \delta_r \end{bmatrix} \tag{9-2}$$

and

$$\left.\frac{\partial \underline{g}(\underline{x}, \underline{u})}{\partial \underline{u}}\right|_{\underline{x}_0, \underline{u}_0} = \underline{J}^{-1} \begin{bmatrix} L_{\delta_a} & L_{\delta_e} & L_{\delta_r} \\ M_{\delta_a} & M_{\delta_e} & M_{\delta_r} \\ N_{\delta_a} & N_{\delta_e} & N_{\delta_r} \end{bmatrix} \tag{9-3}$$

where L_*, M_* and N_* are the control derivatives of the three components of the aircraft moment with respect to the generic variables denoted by $*$. The relation between the aircraft rotational dynamics and its control deflections is thus affine and the implementation of INDI for this system is very beneficial since no information about the influence of the control inputs is lost.

For the helicopter case however, the situation is already quite different since the most complex part of the model is contained in $\underline{g}(\underline{x},\underline{u})$. This is due to the fact that the inputs to the system are not proportional to the forces nor torques, but represent displacements of mechanical parts that enter in the rotor dynamics through complex aerodynamical phenomena. As it was presented in (5-5), this dependence is given by:

$$\underline{g}(\underline{x},\underline{u}) = \underline{J}^{-1}\left[\underline{m}_{mr}(\underline{x},\underline{u}) + \underline{m}_{tr}(\underline{x},\underline{u})\right]$$

in which $\underline{m}_{mr}(\underline{x},\underline{u})$ and $\underline{m}_{tr}(\underline{x},\underline{u})$ are complex nonlinear functions given by (2-55) and (2-71), respectively. This indicates that part of the information about the nonlinearities of $\underline{g}(\underline{x},\underline{u})$ is lost when only its first order derivative with respect to $\underline{u}$ is used to invert the system. Furthermore, due to its complexity, the Jacobian $\frac{\partial \underline{m}_{mr}(\underline{x},\underline{u})}{\partial \underline{u}}$ could not be calculated analytically and thus finite differences were used to estimate this matrix.

Despite the fact that the results obtained with the numerical method were corroborated with a nonlinear solver, the complex dependence on the controls that characterizes a helicopter seemed to impose a limitation to the application of the INDI to control these vehicles. This limitation was however not verified in practice due to the robustness that the INDI closed-loop systems present even when there are uncertainties in $\underline{g}(\underline{x},\underline{u})$ (recall (3-51)).

In conclusion, the same properties investigated in the previous chapter that grant the overall system robustness to aerodynamic uncertainties in the rotor model or changes in the inertia of the vehicle, also provide very good results when the influence of $\underline{g}(\underline{x},\underline{u})$ is poorly described. Consequently, neither an inaccurate description of $\underline{g}(\underline{x},\underline{u})$ nor the fact that the influence of this nonlinear function is only considered through its (approximated) first order derivative represent limitations to achieve an effective helicopter flight control. As already shown, the only requirement is that the signs of all the components of the derivative of the control effectiveness function $\frac{\partial \underline{g}(\underline{x},\underline{u})}{\partial \underline{u}}$ are well determined.

This property is notably useful since the accurate identification of helicopter high-fidelity models is extremely difficult and costly to obtain. If the control strategy developed in this thesis is adopted, only a simplified model as the one presented here may be enough to compute the signs of the derivative of the control effectiveness correctly and therefore assure an efficient control of the vehicle.

Chapter 10

Conclusions and Recommendations

This chapter concludes the research described in this thesis. The main conclusions drawn throughout its development are presented in Section 10-1. Section 10-2 contains the recommendations made for future work in the topic of Helicopter Nonlinear Flight Control.

10-1 Conclusions

This research thesis began with the development of a mathematical system to simulate the motion of a helicopter, presenting the basic configuration and working principle of common rotorcraft and modelling its dynamics by subdividing it into its main components and adding the contribution of each part to the general system of forces and moments. It was verified that rotorcraft dynamics are significantly nonlinear, cross-coupled, time varying and inherently unstable. A brief discussion was also carried out with respect to the required fidelity of the mathematical model, enforcing the idea that a trade-off has to be achieved between the complexity of the resulting system and its degree of accuracy. In the end, a 6-DOF model with two additional degrees to account for the quasi-dynamic inflow of the main and tail rotor was obtained.

Afterwards, the nonlinear control strategy known as Nonlinear Dynamic Inversion (NDI) was explored. Besides the theoretical formulation of this method, its robust version, the Incremental Nonlinear Dynamic Inversion (INDI), was also introduced. This type of approach is especially useful because, by using acceleration measurements and by computing a required incremental control input instead of the absolute value of the control deflections, great part of the model dependence is eliminated and the control system becomes much less sensitive to model uncertainties. This advantage is deeply associated with the three main objectives for this thesis listed in Section 1-3, since it is able to cope with the nonlinearities that characterize rotorcraft, while providing robustness in the presence of model inaccuracies and without the need for a complex control structure or an adaptive element.

It was seen that helicopter flight control can also be very problematic due to the limitations of its actuators. Their position and rate saturation levels are easily reached and, once this

happens, the performance of the helicopter is immediately degraded and its motion becomes highly unstable. In order to attenuate these problems, a technique named Pseudo-Control Hedging (PCH) was successfully applied to both NDI and INDI control loops. This technique turned out to be crucial for the system since it provides a dynamical filtering of the commanded references such that the demanded signals are within the capabilities of the system.

The practical implementation of the nonlinear control tools to the helicopter model developed started with the design of a system to provide tracking of the angular rates of the vehicle. This objective was efficiently achieved, using finite differences to deal with the fact that the model is not affine in the control inputs. It was also verified that, at this point, the system was still slightly unstable due to the existence of internal dynamics in the system. This is not problematic since those dynamics are eliminated with outer control loops. In addition, a brief investigation was carried out to determine the most adequate method to estimate the angular accelerations and, from the algorithms tested, finite differentiation turned out to be the most suited one for this case.

Once the rate controller was working properly, a middle loop was introduced into the system, allowing it to control the attitude angles of the helicopter. This task was again achieved very efficiently. The controller gains were defined based on expressions for the poles of the combined control loops, alleviating the bandwidth separation requirements imposed by the time scale separation design and thus leading to a better overall tracking performance. In addition, simple linear control laws were implemented to assess the benefits brought by the nonlinear control system. It was possible to verify that the tracking performance is substantially inferior for the linear controller, especially because it is not able to decouple the responses associated with the different axes.

Finally, an outer loop was designed to provide the tracking of the desired ground velocities. The horizontal components are controlled by changes in the attitude angles, calculated from an Approximate Dynamic Inversion (ADI). The vertical speed is controlled directly with the collective pitch of the main rotor, according to an appropriate INDI-based control law. To analyze the performance of the overall navigational system, several maneuvers commonly used for helicopter handling qualities analysis with different agility levels were simulated. The results obtained showed that the controller developed is able to stabilize the system and to track the commanded references as expected theoretically.

It was still necessary to evaluate whether or not the control system developed is robust to model uncertainties (due to mathematical inaccuracies or changes in the configuration of the vehicle), and external influences like sensor dynamics, actuator delay or wind effect. The conclusions of these tests are summarized in the end of Section 8-8. The most relevant observation is related to the fact that the system is perfectly robust to model uncertainties within the range of inaccuracies expected to find in reality. This seems to support the theoretical prediction that only the correct sign of the derivatives of the control effectiveness with respect to the control inputs is needed to control an INDI-based loop. With respect to the influence of sensor dynamics and actuator delay, it was verified that, despite degrading slightly the performance of the system, their effects are still admissible in reality.

Taking into account all the considerations made, the overall control system developed in this thesis seems to be adequate for helicopter flight control. Some additional conclusions concerning specifically the applicability of the adopted control strategy to rotorcraft flight control are presented in Chapter 9.

10-2 Recommendations

Being just the first step in the development of helicopter advanced control laws for the joint project with the Boeing Company and the first attempt to apply INDI-based strategies to helicopter flight control, several improvements/alternatives could not be developed in this thesis. These topics are listed below as recommendations for future research in Helicopter Nonlinear Flight Control:

- Since only a limited number of robustness tests was performed in this thesis, it is suggested that an additional variety of scenarios is analyzed so as to prove more convincingly that the INDI is in fact insensitive to almost all the uncertainties that may occur in a real flight. It would be also interesting to relate those uncertainties with the sign of the derivative of the control effectiveness and to prove that a correct sign is all that is needed to provide incremental control of a system. Furthermore, the commanded references used to test the control system were typically doublet signals which, even with the action of the PCH, result in an inadequate response of the helicopter for substantially high demands. It is therefore recommended to introduce additional command filters to smooth aggressive signals, guaranteeing the versatility of the controller to all kinds of inputs without compromising the agility of the system;
- It is also important to enhance the fidelity of the helicopter model developed to design and test control systems. This can be done by increasing its DOF, expanding the current model in the different areas suggested in Section 2-3. Besides this, several other expansions can be introduced to enhance the fidelity of the simulation: implement changes of the helicopter mass and inertia during flight (caused, for example, by fuel consumption), use a Quaternion-based representation of the rotational kinematics (avoiding numerical and singularity problems associated with Euler angles) and improve the accuracy of the actuators dynamics (modelling them as first or second order systems, instead of simply limiting them in terms of magnitude and rate);
- The linear gains associated with the nonlinear control loops in this thesis were set based on the required pole placement to enforce the desired handling qualities of the system. Nevertheless, the performance of the responses can be further improved if more complex strategies such as Lyapunov theory or multi-objective optimization are applied to design the referred gains. The first one can be used to provide a formal stability analysis for the closed-loop system, whereas the second one is useful to impose certain characteristics to the response of the system like maximum allowable values for the overshoot, settling time, etc. On the other hand, techniques like optimal or robust control seem not be adequate to apply within NDI control systems. These techniques are especially based on the cost of the control efforts and on the sensitivity to predefined plant disturbances. Regarding the NDI control loops, the control inputs seen by the linear controller correspond actually to a virtual control (not the actuators efforts) and the plant of the system corresponds to the cascade of integrators resulting from the feedback linearization. For these reasons, the physical meaning of the disturbances and the control inputs is lost;
- In this thesis, finite differences of the angular rates were used to compute the angular accelerations. Despite the satisfactory results obtained with this approach even when

sensor dynamics are considered, it was seen that the estimation of the angular accelerations were affected by a certain lack of accuracy and low-pass filters had also to be introduced in order to cope with the numerical noise. In addition, the linear predictor developed in Section 5-5 was not adequate for the case under analysis. It is therefore recommended that more efficient methods are developed to estimate the angular accelerations more accurately (based, for example, on Kalman filtering) or even that the introduction of angular acceleration sensors in flight control systems is considered. Also regarding the estimation of the parameters necessary to perform the dynamic inversion, a deeper investigation is also recommended in order to implement realistic algorithms to estimate the inflow ratios of the rotors as accurately as possible;

- In terms of flight control, the most interesting development in the area of helicopters is probably the application of a different type of controller to the dynamical model in order to check its benefits and shortcomings when compared to the INDI. The most promising method for this task (and therefore the suggested one) is the Incremental Backstepping. As mentioned in Section 1-2, despite being more complex, this approach allows a more flexible design of the controller when compared to the NDI and may thus contribute even further to the increase of the rotorcraft flight envelope. It is crucial that its incremental version is considered in order to provide robustness in the presence of model inaccuracies without using any kind of adaptive strategy.

Bibliography

Aalst, R. van, & Pavel, M. D. (2002, September). On the Question of Adequate Modelling of Steady-State Rotor Disc-Tilt for Helicopter Manoeuvring Flight. In *The 28th European Rotorcraft Forum.* Bristol, UK.

ADS-33E-PRF. (2000, March). United States Army, Aviation and Missile Command. (Aeronautical Design Standard, Performance Specification and Handling Qualities Requirements for Military Rotorcraft)

Anderson, J. (2004). *Introduction to Flight.* McGraw-Hill.

Bacon, B. J., Ostroff, A. J., & Joshi, S. M. (2001). Reconfigurable NDI Controller using Inertial Sensor Failure Detection & Isolation. *IEEE Transactions on Aerospace and Electronic Systems*, *37*(4), 1373–1382.

Bijnens, B. (2005). *Adaptive Feedback Linearization Flight Control for a Helicopter UAV.* Master thesis, Delft University of Technology.

Bodson, M. (2002). Evaluation of Optimization Methods for Control Allocation. *Journal of Guidance, Control and Dynamics*, *25*(4), 703–711.

Bordignon, K., & Bessolo, J. (2002, November). Control Allocation for the X-35B. In *The 2002 Biennial International Powered Lift Conference and Exhibit.* Williamsburg, Virginia.

Bradley, R., & Thomson, D. G. (2005, September). Helicoter and Tilt-rotor Inverse Simulation: Methods, Features, Problems and Cures. In *The 31st European Rotorcraft Forum.* Florence, Italy.

Bramwell, A., Done, G., & Balmford, D. (2001). *Bramwell's Helicopter Dynamics.* Butterworth-Heinemann.

Brinker, J. S., & Wise, K. A. (1996). Stability and Flying Qualities Robustness of a Dynamic Inversion Aircraft Control Law. *Journal of Guidance, Control and Dynamics*, *19*(6), 1270–1277.

Brockett, R. W. (1978, June). Feedback Invariants for Nonlinear Systems. In *The 7th Triennial World Congress.* Helsinki, Finland.

Calise, A. J., & Rysdyk, R. T. (1998). Nonlinear Adaptive Flight Control using Neural Networks. *IEEE Control Systems Magazine*, *18*(6), 14–25.

Chen, H. B., & Zhang, S. G. (2008, December). Robust Dynamic Inversion Flight Control

Law Design. In *The 2nd International Symposium on Systems and Control in Aerospace and Astronautics.* Shenzhen, China.

Chu, Q. P. (2010, April). *Course Notes on Advanced Flight Control.* (Delft University of Technology)

Costa, R. R. da, Chu, Q. P., & Mulder, J. A. (2003). Reentry Flight Controller using Nonlinear Dynamic Inversion. *Journal of Spacecraft and Rockets*, *40*(1), 64–71.

Cunha, R., & Silvestre, C. (2003, June). SimModHeli: A Dynamic Simulator for Model-Scale Helicopters. In *The 11th Mediterranean Conference on Control and Automation.* Rhodes, Greece.

Curtiss, H. C. J. (1986, September). Stability and Helicopter Modelling. In *The 12th European Rotorcraft Forum.* Garmisch-Partenkirchen, Germany.

Deagel. (n.d.). *UH-60M Upgrade Black Hawk Helicopter Achieves First Flight.* `http://www.deagel.com/news/UH-60M-Upgrade-Black-Hawk-Helicopter-Achieves-First-Flight_n000004949.aspx`. (Accessed August 2011)

Enns, D., Bugajski, D., Hendrick, D., & Stein, G. (1994). Dynamic Inversion: an Evolving Methodology for Flight Control Design. *International Journal of Control*, *59*(1), 71–90.

Etkin, B. (1972). *Dynamics of Atmospheric Flight.* Dover Publications.

Eurocopter. (n.d.). *History of the Bö-105.* `http://www.eurocopter.com/site/en/ref/1967:-Bo105_460.html`. (Accessed July 2011)

Farrell, J., Sharma, M., & Polycarpou, M. (2005). Backstepping Based Flight Control with Adaptive Function Approximation. *Journal of Guidance, Control and Dynamics*, *28*(6), 1089–1102.

Goman, M. G., & Kolesnikov, E. N. (1998, August). Robust Nonlinear Dynamic Inversion Method for an Aircraft Motion Control. In *The AIAA Guidance, Navigation and Control Conference and Exhibit.* Boston, Massachusetts.

Hedrick, J. K., & Girard, A. (2010). *Control of Nonlinear Dynamic systems: Theory and Applications.* Course Notes on Control of Nonlinear Dynamic Systems, Berkeley University of California.

Hohenemser, K. H. (1974). *Hingeless Rotorcraft Flight Dynamics.* AGARD-AG-197.

Houston, S. S., & Thomson, D. G. (2009). Calculation of Rotorcraft Inflow Coefficients using Blade Flapping Measurements. *Journal of Aircraft*, *46*(5), 1569–1576.

Hovakimyan, N., Kim, N., Calise, A. J., Prasad, J. V. R., & Corban, E. (2001, August). Adaptive Output Feedback for High-Bandwidth Control of an Unmanned Helicopter. In *The AIAA Guidance, Navigation and Control Conference and Exhibit.* Montreal, Canada.

Howitt, J. (2005, June). Application of Nonlinear Dynamic Inversion to Rotorcraft Flight Control. In *The American Helicoter Society 61st Annual Forum.* Grapevine, Texas.

Isidori, A. (1995). *Nonlinear Control Systems.* Springer.

Johnson, E. N., & Calise, A. J. (2000, November). Pseudo-Control Hedging: A New Method for Adaptive Control. In *The Advances in Navigation and Control Technology Workshop.* Redstone Arsenal, Alabama.

Johnson, E. N., & Kannan, S. K. (2005). Adaptive Trajectory Control for Autonomous Helicopters. *Journal of Guidance, Control and Dynamics*, *28*(3), 524–538.

Johnson, W. (1980). *Helicopter Theory.* Dover Publications.

Jong, A. de. (2004). *Helicopter UAV Control using Classical Control.* Master thesis, Delft University of Technology.

Kim, N. (2003). *Improved Methods in Neural Network-based Adaptive Output Feedback Con-*

trol, with Applications to Flight Control. Doctoral thesis, Georgia Institute of Technology.

Klamer, J. (2007). *UAV Helicopter Nonlinear Flight Control using Constrained Adaptive Backstepping Control with Neural Networks.* Master thesis, Delft University of Technology.

Klein, V., & Morelli, E. A. (2006). *Aircraft System Identification: Theory and Practice.* AIAA Educational Series.

Lam, Q. M., Hindman, R., Shell, W. M., & Ridgely, D. B. (2005, August). Investigation and Preliminary Development of a Modified Pseudo-Control Hedging for Missile Performance Enhancement. In *The AIAA Guidance, Navigation and Control Conference and Exhibit.* San Francisco, California.

Lee, S., Ha, C., & Kim, B. S. (2005). Adaptive Nonlinear Control System Design for Helicopter Robust Command Augmentation. *Aerospace Science and Technology*, *9*(3), 241–251.

Leitner, J., Calise, A. J., & Prasad, J. V. R. (1998, August). A Full Authority Helicopter Adaptive Neuro-Controller. In *The 1998 Aerospace Conference.* Aspen, Colorado.

Lombaerts, T. J. J. (2010). *Fault Tolerant Flight Control.* Doctoral thesis, Delft University of Technology.

Marino, R. (1986). On the Largest Feedback Linearizable Subsystem. *Systems & Control Letters*, *6*(5), 345–351.

MathWorks. (n.d.-a). *Matlab's Optimization Toolbox Manual.* `http://www.mathworks.com/products/optimization`. (Accessed June 2011)

MathWorks. (n.d.-b). *Simulink's Dryden Wind Turbulence Model.* `http://www.mathworks.com/help/toolbox/aeroblks/drydenwindturbulencemodelcontinuous.html`. (Accessed July 2011)

Moelans, P. (2008). *Adaptive Helicopter Control using Feedback Linearization and Neural Networks.* Master thesis, Delft University of Technology.

Naidu, D. S., & Calise, A. J. (2001). Singular Perturbations and Time Scales in Guidance and Control of Aerospace Systems: A Survey. *Journal of Guidance, Control and Dynamics*, *24*(6), 1057–1078.

Njaka, C. E., Menon, P. K., & Cheng, V. H. L. (1994, August). Towards an Advanced Nonlinear Rotorcraft Flight Control System Design. In *The 13th Digital Avionics Systems Conference.* Phoenix, Arizona.

Olsder, G. J., & Woude, J. W. van der. (2006). *Mathematical Systems Theory.* VSSD.

Oort, E. R. van. (2011). *Adaptive Backstepping Control and Safety Analysis for Modern Fighter Aircraft.* Doctoral thesis, Delft University of Technology.

Padfield, G. D. (1996). *Helicopter Flight Dynamics: The Theory and Application of Flying Qualities and Simulation Modelling.* Blackwell Science.

Pavel, M. D. (1996, December). *Memorandum M-756: Six Degrees of Freedom Linear Model for Helicopter Trim and Stability Calculation.* (Delft University of Technology)

Pavel, M. D. (2001). *On the Necessary Degrees of Freedom for Helicopter and Wind Turbine Low-Frequecy Mode Modelling.* Doctoral thesis, Delft University of Technology.

Pavel, M. D., & Holten, T. van. (1997, September). On the Prediction of the Necessary Rotor Dynamics for Helicopter Flight Simulation. In *The 23rd European Rotorcraft Forum.* Dresden, Germany.

Pitt, D. M., & Peters, D. A. (1981). Theoretical Prediction of Dynamic Inflow Derivatives. *Vertica*, *5*(1), 21–34.

Poonamallee, V. L., & Doman, D. B. (2004, June). A Nonlinear Programming Approach for Control Allocation. In *The 2004 American Control Conference.* Boston, Massachusetts.

Prasad, J. V. R., & Lipp, A. M. (1993). Synthesis of a Helicopter Nonlinear Flight Controller using Approximate Model Inversion. *Mathematical and Computer Modelling*, *18*(3/4), 89–100.

Prouty, R. W. (1986). *Helicopter Performance, Stability and Control.* PWS Publications.

Prouty, R. W., & Curtiss, H. C. (2003). Helicopter Control Systems: A History. *Journal of Guidance, Control and Dynamics*, *26*(1), 12–18.

Rohlfs, M. (1998, September). Identification of System Parameters in a Nonlinear Helicopter Model. In *The 24th European Rotorcraft Forum.* Marseilles, France.

Schumacher, C. J., & Khargonekar, P. P. (1998). Stability Analysis of a Missile Control System with a Dynamic Inversion Controller. *Journal of Guidance, Control and Dynamics*, *21*(3), 508–515.

Schumacher, C. J., Khargonekar, P. P., & McClamroch, N. H. (1998, August). Stability Analysis of Dynamic Inversion Controllers using Time-Scale Separation. In *The AIAA Guidance, Navigation and Control Conference and Exhibit.* Boston, Massachusetts.

Sieberling, S. (2009). *Design of a Robust Generic Flight Control System using Incremental Nonlinear Dynamic Inversion.* Master thesis, Delft University of Technology.

Sieberling, S., Chu, Q. P., & Mulder, J. A. (2010). Robust Flight Control using Incremental Nonlinear Dynamic Inversion and Angular Acceleration Prediction. *Journal of Guidance, Control and Dynamics*, *33*(6), 1732–1742.

Slotine, J.-J. E., & Li, W. (1991). *Applied Nonlinear Control.* Prentice-Hall.

Sonneveldt, L., Oort, E. R. van, Chu, Q. P., & Mulder, J. A. (2009, December). Nonlinear Adaptive Flight Control Law Design and Handling Qualities Evaluation. In *The 48th IEEE Conference on Decision and Control.* Shanghai, China.

Stevens, B. L., & Lewis, F. L. (2003). *Aircraft Control and Simulation.* John Wiley & Sons.

Stiles, L. R., Mayo, J., Freisner, A. L., Landis, K. H., & Kothmann, B. D. (2004, June). Impossible to Resist: The Development of Rotorcraft Fly-By-Wire Technology. In *The American Helicoter Society 60th Annual Forum.* Baltimore, Maryland.

Vilchis, J. C. A., Brogliato, B., Dzul, A., & Lozano, R. (2003). Nonlinear Modelling and Control of Helicopters. *Automatica*, *39*, 1583–1596.

Voskuijl, M., Padfield, G. D., Walker, D. J., Manimala, B. J., & Gubbels, A. W. (2010). Simulation of Automatic Helicopter Deck Landings using Nature Inspired Flight Control. *The Aeronautical Journal*, *114*(1151), 25–34.

Voskuijl, M., Pavel, M. D., Walker, D. J., Gubbels, A. W., & Manimala, B. J. (2009, October). Analytical Prediction of Rotor Flapping Angles for use in Helicopter Rotor State Feedback Control Laws. In *The 3rd International Basic Research Conference on Rotorcraft Technology.* Nanjing, China.

Wang, H., & Sun, J. (1992, December). Modified Model Reference Adaptive Control with Saturated Inputs. In *The 31st IEEE Conference on Decision and Control.* Tucson, Arizona.

Wedershoven, J. A. (2010). *Analysis of Nonlinear Dynamic Inversion Based Control Law Designs.* Master thesis, Delft University of Technology.

Zeng, S., & Zhu, J. (2006, November). Adaptive Compensated Dynamic Inversion Control for a Helicopter with Approximate Mathematical Model. In *The International Conference on Computational Intelligence for Modelling, Control and Automation.* Sydney, Australia.

Appendix A

Reference Frames and Transformations

Besides the reference frames specific for the study of the rotor already presented in Chapter 2, a more common set of coordinate axes is needed to describe the motion of the helicopter in space. This appendix aims to present those reference frames as well as the transformations used to convert the coordinates of a vector between them. It is mainly based on (Etkin, 1972) and (Sieberling, 2009).

A-1 North-East-Down Reference Frame F_o

The origin of the North-East-Down (NED) reference frame is attached to the vehicle, usually at its Cnter of Gravity (CG). The z-axis is directed vertically downward, pointing in the direction of the local gravity vector. The x-axis points towards the North, as seen from the vehicle CG, and the y-axis to the East, completing a right-handed coordinate axes system. For many applications, more specifically, for small distances, the orientation of this reference frame remains practically unchanged with the displacement of the vehicle and its rotation can therefore be neglected. This corresponds to neglecting the curvature of the Earth during the analysis of the motion. Furthermore, considering the Earth non-rotating, F_o can be regarded as an inertial reference frame. Again, this assumption is only valid when dealing with control design and cannot be applied to guidance or navigation systems for flying over large distances.

A-2 Body-fixed Reference Frame F_b

As the name indicates, this frame is also fixed to the vehicle, with the origin placed at its CG. It is common to find a plane of symmetry (to a good approximation) in flight vehicles. In this plane are contained the x-axis and the z-axis, the first one pointing to the front and aligned with the fuselage centerline and the latter pointing down, perpendicular to the other. The y-axis is defined such that a right-handed reference system is obtained. This coordinate system is very useful to express the linear (u, v, w) and angular velocities (p, q, r) of the aircraft, respectively about its three axis.

A-3 Velocity Reference Frame F_v

Once again, this reference frame has its origin fixed at the vehicle CG. The x-axis is now aligned with the velocity vector, the y-axis is perpendicular to the x-axis and to the local gravity vector and the z-axis completes the right-handed coordinate system. The velocity vector expressed in this reference frame becomes simply $[V\ 0\ 0]^T$, where V is the airspeed of the vehicle.

A-4 Rotation Matrices

To proceed with the derivation of the transformations between the reference frames introduced above, it is convenient to present the so-called rotation matrices $\underline{R}$. These matrices allow to convert the coordinates of a vector between coordinate systems that are related through the rotation of a generic angle α around one of its axis. Depending on the axis around which the referred rotation took place, the following matrices are obtained:

$$\underline{R}_x(\alpha) = \begin{bmatrix} 1 & 0 & 0 \\ 0 & \cos\alpha & \sin\alpha \\ 0 & -\sin\alpha & \cos\alpha \end{bmatrix} \tag{A-1}$$

$$\underline{R}_y(\alpha) = \begin{bmatrix} \cos\alpha & 0 & -\sin\alpha \\ 0 & 1 & 0 \\ \sin\alpha & 0 & \cos\alpha \end{bmatrix} \tag{A-2}$$

$$\underline{R}_z(\alpha) = \begin{bmatrix} \cos\alpha & \sin\alpha & 0 \\ -\sin\alpha & \cos\alpha & 0 \\ 0 & 0 & 1 \end{bmatrix} \tag{A-3}$$

It is important to note that these matrices are orthogonal, meaning that $\underline{R}(\alpha)^{-1} = \underline{R}(\alpha)^T$. It can also be noticed that $\underline{R}(\alpha)^T = \underline{R}(-\alpha)$. Furthermore, all the transformations presented in the following sections can be decomposed in the multiplication of these three basic matrices and they also result in orthogonal matrices.

A-5 Transformation from F_o to F_b

The orientation of any reference frame relative to another one can be given by a sequence of three angles that describes the required rotations so that one frame is transformed into the other. These three angles are generally known as Euler angles and twelve different sequences exist to describe the referred transformation unambiguously. In flight dynamics, one of the most common sequences is defined as follows: first a rotation of the yaw angle ψ about the z-axis, then a rotation of the pitch angle θ about the intermediate y-axis and finally a rotation of the roll angle ϕ about the intermediate x-axis. According to this, the transformation from the NED to the body-fixed reference frame $\underline{T}_b^o$ corresponds to:

$$\underline{T}_b^o = \underline{R}_x(\phi)\underline{R}_y(\theta)\underline{R}_z(\psi) =$$

$$= \begin{bmatrix} \cos\psi\cos\theta & \sin\psi\cos\theta & -\sin\theta \\ \cos\psi\sin\theta\sin\phi - \sin\psi\cos\phi & \sin\psi\sin\theta\sin\phi + \cos\psi\cos\phi & \cos\theta\sin\phi \\ \cos\psi\sin\theta\cos\phi + \sin\psi\sin\phi & \sin\psi\sin\theta\cos\phi - \cos\psi\sin\phi & \cos\theta\cos\phi \end{bmatrix} \tag{A-4}$$

Furthermore, as already explained, the inverse transformation $\underline{T}_o^b$ (from the body-fixed to the NED reference frame) corresponds to $\underline{T}_b^{o^{-1}} = \underline{T}_b^{o^T}$. The relation between the two reference frames is depicted in Figure A-1.

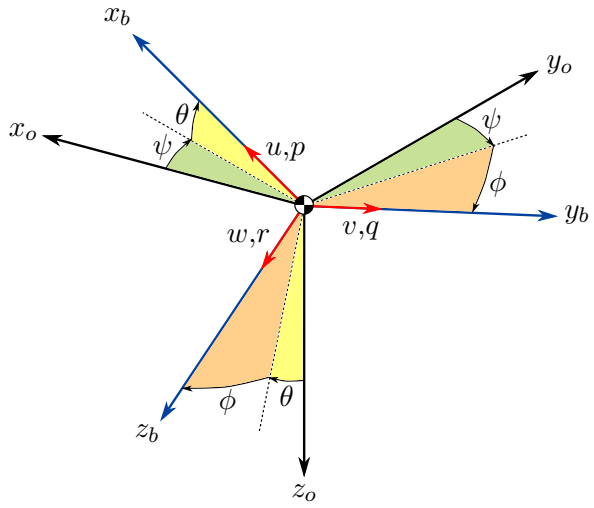

Figure A-1: Rotations between the NED and the body-fixed reference frames.

A-6 Transformation from F_o to F_v

Similarly to the previous case, another sequence of rotations $\underline{T}_v^o$ can be defined such that NED coordinates are converted into the velocity reference frame. This can be achieved only with two angles: the flight path angle γ and the heading χ. The first one is the angle between the velocity vector and the local horizon (the plane perpendicular to the local gravity vector) and the heading is the angle between the velocity and the North direction. The referred transformation is then given by:

$$\underline{T}_v^o = \underline{R}_y(\gamma)\underline{R}_z(\chi) = \begin{bmatrix} \cos\chi\cos\gamma & \sin\chi\cos\gamma & -\sin\gamma \\ -\sin\chi & \cos\chi & 0 \\ \cos\chi\sin\gamma & \sin\chi\sin\gamma & \cos\gamma \end{bmatrix} \tag{A-5}$$

and, once again, $\underline{T}_o^v = \underline{T}_v^{o^{-1}} = \underline{T}_v^{o^T}$. It is also possible to verify that when the fuselage centerline is aligned with the velocity vector, the pitch of the aircraft matches the flight path angle and the yaw angle corresponds to the heading. In a more general situation, two additional angles can be defined between the body-fixed and the velocity reference frames: the angle of attack $\alpha = \theta - \gamma$ and the sideslip angle $\beta = \chi - \psi$. All these relations are shown for the x-axis in Figure A-2.

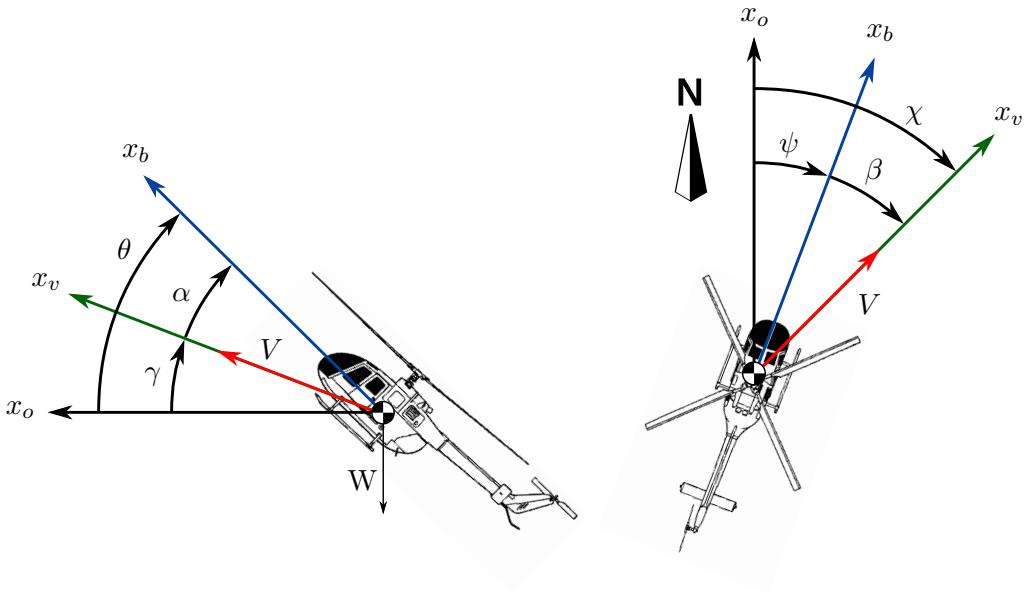

(a) Vertical plane. **(b)** Horizontal plane.

Figure A-2: Relations between the x-axes of the three coordinate systems analyzed.

A-7 Angular velocity of F_b

Finally, it is also useful to determine the angular velocity of the body $\underline{\omega} = [p\ q\ r]^T$ relative to F_o due to the change of orientation between the corresponding reference system and the NED reference frame $\underline{\dot{\theta}} = [\dot{\phi}\ \dot{\theta}\ \dot{\psi}]^T$. Firstly it is important to note that the rate of change of each Euler angle is written in different coordinate axes, which result from the existence of intermediate reference frames between the rotation from F_o to F_b (see Figure A-1). With this in mind, it can be concluded that:

$$\underline{\omega} = \begin{bmatrix} \dot{\phi} \\ 0 \\ 0 \end{bmatrix} + \underline{R}_x(\phi) \begin{bmatrix} 0 \\ \dot{\theta} \\ 0 \end{bmatrix} + \underline{R}_x(\phi)\underline{R}_y(\theta) \begin{bmatrix} 0 \\ 0 \\ \dot{\psi} \end{bmatrix} \tag{A-6}$$

This equation can be arranged in a more compact form using matrix $\underline{\Omega}$:

$$\underline{\omega} = \underline{\Omega}_b^o \underline{\dot{\theta}} \tag{A-7}$$

where

$$\underline{\Omega}_b^o = \begin{bmatrix} 1 & 0 & -\sin\theta \\ 0 & \cos\phi & \sin\phi\cos\theta \\ 0 & -\sin\phi & \cos\phi\cos\theta \end{bmatrix} \tag{A-8}$$

and

$$\underline{\Omega}_o^b = \underline{\Omega}_b^{o^{-1}} = \begin{bmatrix} 1 & \sin\phi\tan\theta & \cos\phi\tan\theta \\ 0 & \cos\phi & -\sin\phi \\ 0 & \sin\phi/\cos\theta & \cos\phi/\cos\theta \end{bmatrix} \tag{A-9}$$

Appendix B

Helicopter Parameters

This appendix presents the specific data of the helicopter Bölkow Bö-105 for the baseline configuration adopted for the simulations. These specifications are divided in several tables associated with the different parts of the helicopter for more clarity and they are available in (Pavel, 2001) and (Padfield, 1996). The last table shows the actuator limits of the Bö-105. The saturation limits can be found in (Prouty, 1986), but no information was found with respect to the rate limits. Therefore, in order to use values with physical meaning, the rate limits of the Bell 412 helicopter, found in (Voskuijl, Padfield, Walker, Manimala, & Gubbels, 2010), were adopted.

Table B-1: Main rotor parameters of the Bö-105.

Description	Symbol	Value	Unit
Rotational speed	Ω	44.4	rad/s
Rotor radius	R	4.91	m
Number of blades	N	4	–
Equivalent blade chord	c_e	0.27	m
Blade lift curve slope	C_{L_α}	6.11	rad^{-1}
Linear blade twist	θ_{tw}	-0.1396	rad
Blade mass	m_{bl}	27.3	kg
Blade moment of inertia about its flapping hinge	I_β	231.7	kg.m^2
Equivalent hinge offset ratio	ε_β	0.14	–
Rotor shaft tilt angle	γ_s	0.0524	rad
Time constant of the induced inflow	τ_{λ_0}	0.1	s
Longitudinal position with respect to the helicopter CG	l	-0.00761	m
Lateral position with respect to the helicopter CG	l_1	0.02995	m
Vertical position with respect to the helicopter CG	h	0.94468	m

Table B-2: Tail rotor parameters of the Bö-105.

Description	Symbol	Value	Unit
Rotational speed	Ω_{tr}	233.1	rad/s
Rotor radius	R_{tr}	0.95	m
Number of blades	N_{tr}	2	–
Equivalent blade chord	$c_{e_{tr}}$	0.18	m
Blade lift curve slope	$C_{L_{\alpha,tr}}$	5.70	rad^{-1}
Main rotor downwash factor at the tail rotor	K_{tr}	1	–
Time constant of the induced inflow	$\tau_{\lambda_{0,tr}}$	0.1	s
Longitudinal position with respect to the helicopter CG	l_{tr}	6.00965	m
Vertical position with respect to the helicopter CG	h_{tr}	1.05418	m

Table B-3: Fuselage parameters of the Bö-105.

Description	Symbol	Value	Unit
Parasite drag area	F_0	1.3	m^2
Eq. volume in the horizontal plane with only circular sections	V_{fus_M}	6.126	m^3
Eq. volume in the lateral plane with only circular sections	V_{fus_N}	25.525	m^3
Incidence angle for zero pitch moment	$\alpha_{fus_{M=0}}$	0	rad
Correction coefficient for moment calculation	K_{fus}	0.83	–

Table B-4: Horizontal tail parameters of the Bö-105.

Description	Symbol	Value	Unit
Surface area	S_{ht}	0.803	m^2
Surface lift curve slope	$C_{L_{\alpha,ht}}$	4.0	rad^{-1}
Built-in surface incidence	α_{ht_0}	0.0698	rad
Correction coefficient in the pitch moment	K_{ht}	1.5	–
Longitudinal position with respect to the helicopter CG	l_{ht}	4.548	m

Table B-5: Vertical tail parameters of the Bö-105.

Description	Symbol	Value	Unit
Surface area	S_{vt}	0.805	m^2
Surface lift curve slope	$C_{L_{\alpha,vt}}$	4.0	rad^{-1}
Built-in surface incidence	β_{vt_0}	-0.0812	rad
Longitudinal position with respect to the helicopter CG	l_{vt}	5.416	m
Vertical position with respect to the helicopter CG	h_{vt}	0.970	m

Table B-6: General properties of the Bö-105.

Description	Symbol	Value	Unit
Total mass	m	2200	kg
Inertia tensor	$\underline{J}$	$\begin{bmatrix} 1433 & 0 & -660 \\ 0 & 4973 & 0 \\ -660 & 0 & 4099 \end{bmatrix}$	$kg.m^2$

Table B-7: Actuator limits of the Bö-105.

Description	Symbol	Min. saturation limit (deg)	Max. saturation limit (deg)	Rate limit (deg/s)
Collective pitch MR	θ_0	-0.2	15.0	16.0
Longitudinal cyclic	θ_{1s}	-6.0	11.0	28.8
Lateral cyclic	θ_{1c}	-5.7	4.2	16.0
Collective pitch TR	θ_{0tr}	-8.0	20.0	32.0

Appendix C

Atmospheric Model

As for all vehicles that use the air as locomotive mean, the aerodynamics of rotorcraft is strongly influenced by the properties of the atmosphere, which are constantly changing in space and time. The International Standard Atmosphere (ISA) is an atmospheric model suggested in 1925 that allows to determine average values of temperature, pressure, density and other properties of the air as a function of the altitude. In this research thesis, the referred model was only needed to calculate the density of the air during the simulations. This appendix shows a summarized derivation of the evolution of this property with the altitude. For more detailed information, the reader is referred, for example, to (Anderson, 2004).

Assuming the atmosphere is composed of a homogeneous mean with uniform composition and that the air can be considered an ideal gas (in which the intermolecular forces can be neglected), the following law is verified:

$$p = \rho R T \tag{C-1}$$

where p is the atmospheric pressure in Pa, ρ is the density of the air in kg/m^3, R is a constant specific of the gas (287.05 J/(kg.K) for the air) and T is the absolute temperature in K.

Furthermore, from the balance of forces acting on an elementary volume of fluid in rest it is known that:

$$\mathrm{d}p = -\rho g \mathrm{d}h \tag{C-2}$$

in which g is the gravitational acceleration (normally assumed to have a constant value of 9.80665 m/s^2) and h is the altitude in m. Combining the two equations above, is it easy to obtain:

$$\frac{\mathrm{d}p}{p} = -\frac{g}{RT}\mathrm{d}h \tag{C-3}$$

The atmosphere is composed of several layers with different properties but, taking into account the maximum altitudes achieved by helicopters, only the lowest one is of relevance to analyze

their flight. It is known as troposphere and it holds up until an altitude of approximately 11 km. Experimentally, it was verified that the air temperature decreases linearly with the altitude in this layer according to the relation:

$$T = T_0 - ah \tag{C-4}$$

with $T_0 = 288.15$ K being the temperature at the sea level, $a = 0.0065$ K/m a constant and:

$$\frac{\mathrm{d}h}{\mathrm{d}T} = -\frac{1}{a} \tag{C-5}$$

Replacing this equation in (C-3) and integrating from the conditions at the sea level to a generic point in altitude, it is possible to obtain:

$$\int_{p_0}^{p} \frac{1}{p}\,\mathrm{d}p = \frac{g}{aR}\int_{T_0}^{T} \frac{1}{T}\,\mathrm{d}T \Leftrightarrow \frac{p}{p_0} = \left(\frac{T}{T_0}\right)^{\frac{g}{aR}} \tag{C-6}$$

Moreover, from (C-1) it is possible to see that:

$$\frac{p}{p_0} = \frac{\rho}{\rho_0}\frac{T}{T_0} \tag{C-7}$$

and, applying this relation together with (C-4) and (C-6), the following expression for the density of the air as a function of the altitude is obtained:

$$\rho = \rho_0 \left(\frac{T_0 - ah}{T_0}\right)^{\frac{g}{aR}-1} \tag{C-8}$$

This equation makes use of the density of the air at the sea level ($\rho_0 = 1.225$ kg/m^3) and, as already mentioned, it is only valid below 11 km of altitude, where the linear dependence between the altitude and the temperature is verified.

Appendix D

Trim Routine

Before any simulation is started, it is desirable that the helicopter is steady at a desired flight condition. This means that initially a combination of control inputs and state variables must be chosen such that the forces and moments acting on the helicopter are in equilibrium or, in other words, such that the translational $\underline{\dot{v}}$ and rotational $\underline{\dot{\omega}}$ accelerations are null. Furthermore, for a trimmed helicopter, the induced inflow of the rotors $\underline{\lambda}$ has also to be steady (recall the notation introduced in the end of Chapter 2). It was with the purpose of determining the referred combination of values that the trim routine discussed in this appendix was implemented.

The routine adopted for this thesis allows to determine the trim conditions of the helicopter given its airspeed V, flight path angle γ, heading χ and altitude h (the coordinates x and y of its initial position can also be specified, but they do not influence the motion). As it was already mentioned, in trim conditions: $\underline{\dot{v}} = \underline{\dot{\omega}} = \underline{\dot{\lambda}} = 0$. In addition, the ground velocity $\underline{\dot{p}}$ of the helicopter must match the desired flight condition $\underline{\dot{p}}_{des}$. According to the transformations presented in Appendix A, this corresponds to:

$$\underline{\dot{p}}_{des} = \underline{\underline{T}}_o^v \begin{bmatrix} V \\ 0 \\ 0 \end{bmatrix} = V \begin{bmatrix} \cos\chi\cos\gamma \\ \sin\chi\cos\gamma \\ -\sin\gamma \end{bmatrix} \tag{D-1}$$

Taking into account that the system under analysis is nonlinear, a solution for the conditions above cannot be found analytically, but it can be determined iteratively. To do that, the following cost vector is defined and its components must be minimized:

$$\underline{f} = \begin{bmatrix} \underline{\dot{v}} \\ \underline{\dot{p}} - \underline{\dot{p}}_{des} \\ \underline{\dot{\omega}} \\ \underline{\dot{\lambda}} \end{bmatrix} \tag{D-2}$$

Ideally, the value of its components should be zero in trimmed flight, but the minimization procedure only assures that their absolute value is inferior to a pre-established threshold that dictates when the iterative process stops.

The result of the trim routine is then the combination of control inputs $\underline{u}_{trim}$ and state variables that minimize the cost function above. Note that not all of the state variables are allowed to vary during the iterative process: the position of the helicopter $\underline{p}$ is fixed, the angular rates $\underline{\omega}$ are set to zero and the yaw angle is defined equal to the vehicle's heading ($\psi = \chi$), since it is assumed that it is flying with no sideslip angle. Thus, the vector that contains the variables that are allowed to vary is $\underline{x} = [\theta_0\ \theta_{1s}\ \theta_{1c}\ \theta_{0tr}\ u\ v\ w\ \phi\ \theta\ \lambda_0\ \lambda_{0_{tr}}]^T$.

The algorithm adopted to perform the minimization procedure is the Newton's method, which is known for its good commitment between complexity and quick convergence. Considering the first-order terms of the Taylor series expansion of the cost function around the current state variables:

$$\underline{f} \approx \underline{f}_0 + \left.\frac{\partial \underline{f}}{\partial \underline{x}}\right|_{\underline{x}=\underline{x}_0} (\underline{x} - \underline{x}_0) \tag{D-3}$$

and having in mind that ideally the cost function is to be zero ($\underline{f}$=0), the mentioned method updates the vector $\underline{x}$ in each iteration k according to:

$$\underline{x}_{k+1} = \underline{x}_k - \left.\frac{\partial \underline{f}}{\partial \underline{x}}\right|^{-1}_{\underline{x}=\underline{x}_k} \underline{f}_{\underline{x}_k} \tag{D-4}$$

To compute the Jacobian matrix of the cost function, forward finite differences were used. This approach involves the perturbation of all the components of $\underline{x}$ individually with a small quantity τ_i and the calculation of $\underline{f}$ for each case. The perturbation corresponds to a small percentage of the absolute value of each variable or to a fixed infinitesimal quantity, if the unperturbed value is already too small. The column of the Jacobian matrix corresponding to the i-th component of $\underline{x}$ is then approximated by:

$$\left.\frac{\partial \underline{f}}{\partial x_i}\right|_{\underline{x}=\underline{x}_k} \approx \frac{\underline{f}_{\underline{x}_k+\underline{\tau}_i} - \underline{f}_{\underline{x}_k}}{\tau_i} \tag{D-5}$$

where $\underline{\tau}_i$ is a vector that introduces the infinitesimal perturbation τ_i in the i-th component while the remaining ones are zero. Every iterative process needs a set of values to initialize the algorithm. These values correspond to initial guesses that shall be as close to the optimal solution as possible in order to assure a fast convergence of the method. The variables θ_0, θ_{1s}, θ_{1c}, θ_{0tr}, λ_0 and $\lambda_{0_{tr}}$ are initialized with physically meaningful values for a helicopter and the roll angle ϕ is assumed to be zero.

The pitch angle θ results from a simplified equilibrium of forces in the vertical plane of the rotorcraft: the thrust generated by the rotor T (assumed perpendicular to the xy plane of the body-fixed reference frame) has to balance the weight of the vehicle $W = mg$ (acting on the vertical direction) and the drag force which in mainly due to the fuselage $D = \rho V^2 F_0/2$ (aligned with the velocity vector). This situation corresponds to:

$$T \sin\theta = -D \cos\gamma \tag{D-6}$$

$$T \cos\theta = W + D \sin\gamma \tag{D-7}$$

Combining these equations, the initial estimate for the pitch angle is given by:

$$\theta = -\arctan\left(\frac{D\cos\gamma}{W + D\sin\gamma}\right) \tag{D-8}$$

where γ is the flight path angle.

Finally, the initial values of the body velocities can be determined using the transformation of the desired ground velocities into the body-fixed reference frame, as presented in Annex A: $\underline{v}_{trim} = \underline{\underline{T}}_b^o \underline{\dot{p}}_{des}$

Appendix E

Additional Maneuver: The Pirouette

The pirouette is another example of a moderate aggressivity maneuver often used to evaluate helicopter flight control systems. The purpose of this maneuver is to check the ability to accomplish precision control of simultaneous pitch, roll, yaw and heave motion and accurate control over a continuos heading change. The procedure to be followed is described in detail in (*ADS-33E-PRF*, 2000). The simulation setup is then as follows:

> This maneuver is initiated from a stabilized hover over a point on a circumference with a 30 m (approx. 100 ft) radius, with the nose pointed at its center and at an altitude of 3 m (approx. 10 ft).
>
> Then, a uniform lateral translation around the circumference has to be accomplished while keeping the nose of the rotorcraft pointing towards the trajectory center until returning to the starting position. If the complete circumference is to be flown in 40 s, a constant lateral velocity of approximately $V = 4.71$ m/s has to be maintained.
>
> To complete the pirouette maneuver, the same process described above is repeated in the reverse direction.

For this maneuver, the commanded references are generated according to the equations presented below. The results obtained from the simulation of the pirouette with the overall navigational controller are presented in Figure E-1.

$$
\begin{aligned}
V_{x_{com}}(t) &= 4.71 \sin\left(\frac{2\pi}{40}t\right) \text{ m/s} \\
V_{y_{com}}(t) &= \pm 4.71 \cos\left(\frac{2\pi}{40}t\right) \text{ m/s} \\
V_{z_{com}}(t) &= 0 \text{ m/s} \\
\psi_{com}(t) &= \mp\frac{360}{40}t \text{ deg}
\end{aligned}
$$

From this figure, it can be concluded that the commanded components of the velocity are followed very efficiently. In fact, the tracking error is always very small and the responses do not involve undesirable oscillations. Furthermore, it can be visualized that the vertical velocity is practically unaffected by the motion of the helicopter, indicating that the evolutions associated with the different axes are satisfactorily decoupled.

In terms of attitude angles, it is possible to see that the commanded yaw is perfectly tracked and that the roll is used to control the lateral velocity of the helicopter. The demanded responses of the three angles are very smooth, which allow the corresponding angular rates to be perfectly followed, as shown in the last plot.

The control actuation required to perform the maneuver is also quite simple. Basically, the yaw and the roll angles are controlled with the tail rotor and with the lateral cyclic pitch, respectively, being the remaining control inputs only used for small compensations. It is also interesting to note that the clockwise motion (second part of the maneuver) is slightly more demanding than the other one, as it is proven by a more intense activity of the collective and lateral cyclic of the main rotor. This part of the maneuver is also more risky since the collective of the tail rotor is operating closer to its saturation limits (-8 and 20 deg, as indicated in Appendix B). For a clearer view of the maneuver, the ideal and actual positions of the helicopter during the simulation are depicted in Figure E-2.

Reference (*ADS-33E-PRF*, 2000) also provides the adequate and desired performance standards for this maneuver, indicating some requirements that shall be met throughout the test. The referred criteria for a Good Visual Environment (GVE) (typically clear daylight) can be found in Table E-1, together with the results obtained in this particular simulation.

From the analysis of this table, it can be seen that all the errors obtained are considerably smaller than the limits allowed and that the maximum time to achieve a stabilized hover, despite being slightly higher than its desired value, is still within the adequate requirements. It is however important to note that the current simulation was performed under ideal conditions, without additional disturbances (namely ground and wind effects) that would certainly contribute to a performance degradation.

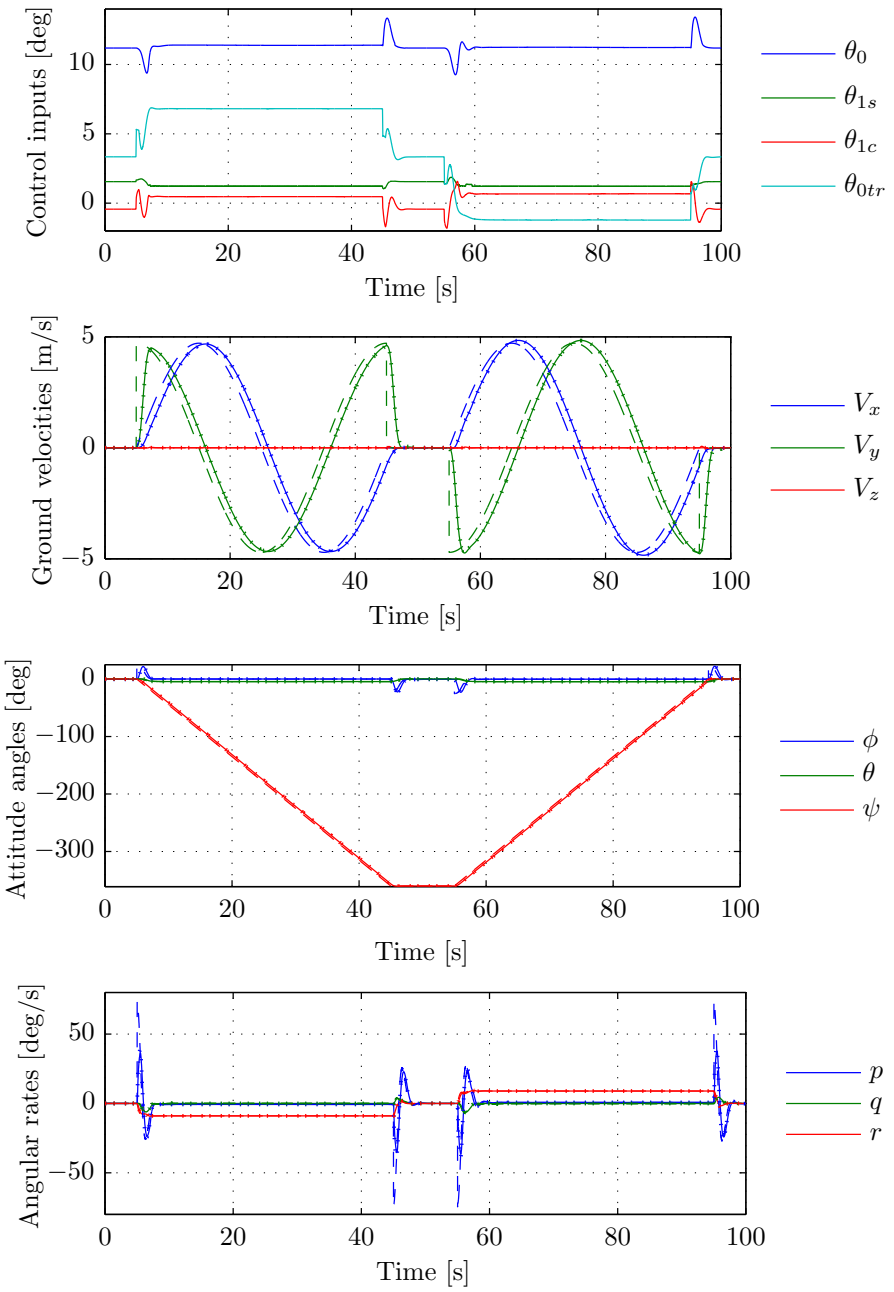

Figure E-1: Results obtained from the simulation of the pirouette. The dashed lines correspond to the references commanded, the dotted lines to the state of the reference model and the solid lines to the actual response of the helicopter.

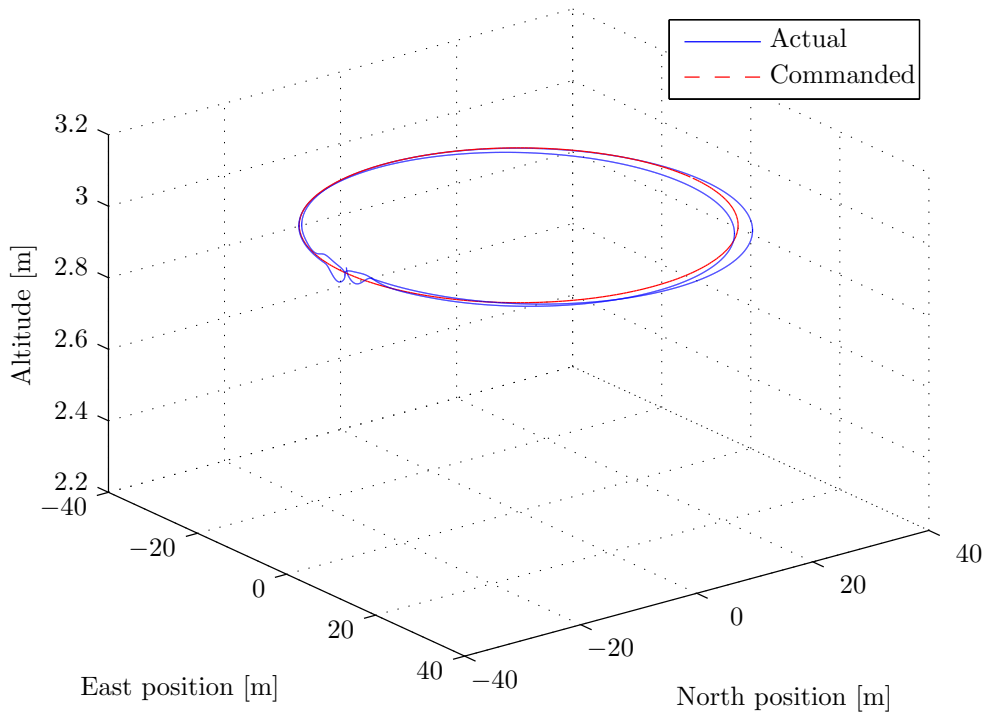

Figure E-2: Evolution of the position during the pirouette maneuver.

Table E-1: Performance evaluation of the pirouette maneuver.

Requirement	Adequate value	Desired value	Measured value
Max. absolute radial error	460 cm	300 cm	200 cm
Max. absolute altitude error	300 cm	90 cm	36 cm
Max. absolute angular error	15 deg	10 deg	4 deg
Max. time to achieve stabilized hover	10 s	5 s	7 s